Identifying Novel Strategies to Promote NK Cell-mediated Clearance of Senescent Cells

Virinder Singh Reen

Supervised by
Professor Jesús Gil

A thesis submitted to Imperial College London for the degree of Doctor of Philosophy

MRC London Institute of Medical Sciences
Faculty of Medicine
Imperial College London

September 2022

Statement of originality

I, Virinder Singh Reen, confirm that any work presented in this thesis is my own unless otherwise stated.

Copyright declaration

The copyright of this thesis rests with the author. Unless otherwise indicated, its contents are licensed under a Creative Commons Attribution-Non Commercial 4.0 International Licence (CC BY-NC). Under this licence, you may copy and redistribute the material in any medium or format. You may also create and distribute modified versions of the work. This is on the condition that: you credit the author and do not use it, or any derivative works, for a commercial purpose. When reusing or sharing this work, ensure you make the licence terms clear to others by naming the licence and linking to the licence text. Where a work has been adapted, you should indicate that the work has been changed and describe those changes. Please seek permission from the copyright holder for uses of this work that are not included in this licence or permitted under UK Copyright Law

Abstract

Cellular senescence is a stress-induced stable growth arrest programme that is accompanied by distinct phenotypic alterations including the production of a bioactive secretome, termed the senescence-associated secretory phenotype (SASP). Transient senescence induction can suppress cancer development, limit fibrosis, and promote wound repair. SASP-mediated activation of the host immune response triggers the clearance of senescent cells contributing to those phenotypes. However, with age and impaired immunity, senescence clearance is subdued, and lingering senescent cells paradoxically contribute to tumour progression and age-related disorders. Interventions that directly eliminate senescent cells such as senolytic compounds have shown to prolong survival and improve healthspan, but there are concerns regarding the safety and efficacy of these treatments. Consequently, strategies that target the SASP to reignite an anti-senescence immune response may provide an alternative therapeutic solution. Here, we carried out large-scale RNAi screens in search for perturbations that enhance an immunomodulatory SASP expression in oncogene-induced senescent cells. Based on our candidates, we screened for genes regulating natural killer (NK) cell effector function. We identified 9 targets whose knockdown preferentially sensitised senescent cells to NK cell-mediated elimination, without interfering with the viability of growing cells. Upon pharmacological inhibition of two of those targets, SMARCA4 and POLR1B, we observed a significant reinforcement of NK-mediated killing of cells that have undergone oncogene- or chemotherapy-induced senescence. Overall, our results indicate that the genetic or pharmacological inhibition of SMARCA4 and POLR1B enhanced NK cell surveillance of senescent cells and may represent novel senotherapeutic interventions for various senescence-associated diseases including cancer and fibrosis.

Dedicated to my mother, Jatinder; to my sister, Gurpreet; and my partner, Qingli; thank you all for your unconditional support.

Acknowledgements

First and foremost, I am incredibly grateful to my supervisor, Professor Jesús Gil. Your drive and passion for research are nothing short of inspirational to me and every member of our group, and I am exceptionally fortunate to have been your student. You have guided and supported me throughout my PhD and shaped my development from a naïve student to a scientist. Not only that, but you provided me with several research opportunities, from learning and performing single-cell analysis to visiting the University of Edinburgh to gain further research skills. Most importantly, you could somehow put up with me for several years, highlighting your incredible patience! I hope we can continue to work together and try to improve our understanding, even slightly, of the senescence-immune interaction.

I would like to thank Dr Tamir Chandra and Daniel Simpson at the University of Edinburgh. You both were mentors and friends that not only helped me to hone my skills in bioinformatics but made Edinburgh feel like a second home. I wish you both the greatest of success. Similarly, I want to thank Professor Juan Pedro Martinez-Barbera and Scott Haston for being such great collaborators and providing me with the opportunity to analyse your senescence datasets. Your research is fascinating, and I wish you great success with the paper!

I also would like to thank my PhD examiners, Professor Valery Krizhanovsky and Professor Iain McNeish, for your time in accepting to examine my work and for any constructive feedback in the future. Valery, your and your group's research has shaped the field of senescence and immune interaction, particularly with NK cells, which has been highly inspirational for my own work…And, of course, thank you for providing our group with the invaluable NK92-MI cell lines!
Iain, I am incredibly excited for the opportunity to collaborate with your group to try figure out new ways to eliminate these pesky yet resilient ID8 ovarian cancer cells!

Also, I want to thank my mentor Naveenan for always being up to discuss my work and life in the lab. Your words and advice have significantly impacted my scientific thinking more than you could imagine.

I cannot emphasise how grateful I am to all the members of my lab, past and present. I am so lucky to have had the opportunity to work alongside you all. To those who have left the group while I was here: Bin, Sandip, Aimee, Ana, Pia, Domhnall, Verena, and Andrew, I cannot describe how appreciative I am for your advice and guiding me throughout the academic world. Among the original group members when I first began that are still present: Jodie, Sharon, Joaquim (Joe); thank you for all your support throughout the years and for helping me settle in.

Jodie, it has been an absolute pleasure to have worked with you. I've always looked up to you, and your scientific curiosity and advice have helped push my own work further. Sharon, this lab would collapse without you! Your ability to keep the lab in tip-top shape yet always be so friendly and have time for a chat is remarkable! Joe, you are the most unique person I've ever met. Just pure entertainment. I have loved listening to your stories, raiding the stationary cupboard a million times with you, and, of course, discussing football. You never fail to bring a smile to everybody's face.

Among the newer members who joined after me: Mark, Matt, Imanol, Laura, Mariantonietta, and Carmen, you have all made coming to the lab a complete joy, even when experiments are failing! Mark, you somehow always manage to make me laugh. I wish you the best in your IL-11 and future clinical journey. Matt, despite being the only human who can catch Covid a thousand times, I was very lucky to have worked together without you (whenever you were not quarantining!) and learn all things chemistry. Your presence in the lab – like your immune system- is getting stronger! Imanol, my early-morning companion, thank you for all the brilliant conversations and jokes throughout our collective PhDs. You're a fantastic scientist and evidently our next lab manager too! Laura, thank you for being a brilliant office deskmate and for your invaluable questions and advice for my project. You are wiser beyond your years! Carmen, you bring so much positive energy every day. Thank you for sharing so many lunches, thank you for sharing many wonderful conversations, and thank you, most importantly, for sharing Colacao! Mariantonietta, despite only joining recently, it is clear that you were the missing piece of our group! Thank you for your ongoing hard work and never-give-up attitude. I could not have finished my PhD without your help. And thank you for working an incredible number of hours alongside me in TC without wanting to kill me (yet) - that is an honour you should be proud of.

You are all incredible researchers and humans. I would love to describe my gratitude for each one of you in more detail, but that would be a thesis in itself. Let's hope to celebrate together soon.

I want to thank all members of the LMS and, of course, my PhD year cohort: Ediem, Bea, Monica, Eliano, Sophia, Radina, Manos, Sijia, Alice, Julia, Macia, Eren, George, Katie, and Saul. We were undoubtedly all fortunate to be put together and I couldn't have asked for a better group of people. Saul, you are essentially my brother! From the very first day until the end of our PhD journey, I am so glad I shared this experience with you, and I am certain we will continue to be close beyond our studies.

Finally, and perhaps most importantly, I would love to provide my deepest appreciation for my family. I want to thank my late father who would have been incredibly proud to see me completing my PhD journey. For mum, I want to thank you for your tireless work and effort to provide for my sister and me, and for supporting me at times throughout this PhD when I struggled to manage. I want to thank my sister, Gurpreet, for being so supportive and helpful – for both personal and research matters- whenever I was down or stressed. You're experience and advice have guided me throughout both my PhD and in life.

And of course, I want to thank my partner and best friend, Qingli. To me, there is no doubt that I could've started this PhD journey without your support, let alone finish it. You have put up with so many challenges because of me, from being separated by over a thousand miles for several years, to the incredible time I devoted to the lab and being away. Yet you have always been so encouraging and my number one fan. I hope that one day I can return the favour. And finally, I want to thank our silly little pup, Latte. He has either led me to be more responsible, or crazier, and nothing in between.

Thank you.

Table of Contents

Statement of originality *2*

Abstract *3*

Acknowledgements *5*

Table of Contents *8*

List of figures *12*

List of tables *15*

Abbreviations *16*

Chapter 1 - Introduction *20*

1.1 What is cellular senescence? **20**

1.2 Types of senescence **20**

1.2.1 Replicative senescence 20

1.2.2 Oncogene-induced senescence 22

1.2.3 Therapy-induced senescence 23

1.2.4 Other forms of stress-induced senescence 24

1.3 The senescence phenotype **24**

1.4 Regulation of the senescence growth arrest **27**

1.4.1 DNA damage response 27

1.4.2 p53/p21^{CIP1} and p16^{INK4a}/pRb pathways 28

1.5 Physiological roles of senescence **30**

1.5.1 Role of senescence in ageing 30

1.5.2 Role of senescence in cancer 33

1.5.3 Role of senescence in biological processes 35

1.6 Senescence-associated secretory phenotype (SASP) **37**

1.6.1 Regulation of the SASP 38

1.6.2 Beneficial effects of the SASP 40

1.6.3 Harmful effects of the SASP 45

1.7 Strategies to target cellular senescence **48**

1.7.1 Why target senescent cells? 48

1.7.2 Targeting senescence with senolytics 50

1.7.3 Targeting senescence with senomorphics 52

1.7.4 Targeting senescence by potentiating their immune surveillance 54
1.7.5 Using TIS to promote SASP-mediated anti-senescence immunity 61

1.8 Project aims 63

Chapter 2 – Materials and Methods 64

2.1 Plasmid preparation 64

2.1.1 Plasmids 64
2.1.2 Bacterial transformation 64
2.1.3 DNA purification 65

2.2 Tissue Culture 65

2.2.1 Cell lines 65
2.2.2 Preservation and generation of cell stocks 66
2.2.3 Production of lentiviral or retroviral supernatants 67
2.2.4 Lentiviral and retroviral infection 68

2.3 Senescence induction 69

2.3.1 Oncogene-induced senescence (OIS) 69
2.3.2 Therapy-induced senescence (TIS) 69

2.4 Growth and survival assays 70

2.4.1 5-Bromo-2'-deoxyuridine (BrdU) incorporation assay 70
2.4.2. Crystal violet staining 71
2.4.3 Senescence associated β-Galactosidase (SA-β-Gal) assay 71

2.5 RNA processing and expression analysis 72

2.5.1 RNA isolation and purification 72
2.5.2 Complementary DNA (cDNA) synthesis 73
2.5.3 Quantitative RT-PCR (RT-qPCR) 73

2.6 Protein expression analysis 74

2.6.2 ELISA 76

2.7 NK cell-based assays 76

2.7.1 NK cell-mediated cytotoxicity assay 76
2.7.2 NK cell chemotaxis assay 78

2.8 siRNA screening for SASP reinforcers 80

2.8.1. siRNA genome library and transfection 80
2.8.2 Normalisation of the screen results 81

2.9 Screen for siRNAs enhancing NK-mediated killing of senescent cells 82

2.9.1 siRNA transfection for the screen for siRNAs enhancing NK-mmediated killing of senescent cells 82
2.9.2 Assays for drugs enhancing NK-mediated killing of senescent cells 82

2.10 RNA sequencing and analysis 83

Chapter 3 - Establishing a system to study senescence surveillance by Natural Killer cells 84

3.1 Introduction 84

3.2 Characterising a model of oncogene-induced senescence 84

3.3 Senescent cells upregulate an immunomodulatory SASP and NK activating ligands 87

3.4 Selective killing of senescent cells by NK cells 92

3.5 Characterising drugs that modulate the immunomodulatory SASP 97

3.6 Setting up the assay to identify factors modulating NK-mediated killing of senescent cells 102

3.7 Pilot screen using siRNAs targeting NK inhibitory ligands 109

3.8 Summary and Discussion 112

Chapter 4 - Screen for siRNAs potentiating the SASP 118

4.1 Introduction 118

4.2 Large-scale siRNA screen to identify SASP reinforcers 118

4.3 Secondary siRNA screen to validate hits potentiating SASP expression 122

4.4 Summary and discussion 129

Chapter 5 - Screen for siRNAs potentiating NK-mediated killing of senescent cells 135

5.1 Introduction 135

5.2 siRNA screen of selected SASP reinforcers to enhance NK-mediated killing of senescent cells 135

5.3 Validation of candidates that promote NK cell-mediated cytotoxicity of senescent cells 141

5.4 Summary and Discussion 146

Chapter 6 – FURIN, SMARCA4, and POLR1B can be targeted to potentiate NK-mediated killing of senescent cells 151

6.1 Introduction 151

6.2 Candidate drugs that promote NK-mediated killing of senescent cells 152

6.3 Characterising effect of inhibiting FURIN on NK-mediated killing of senescent cells 156

6.4 Characterising effect of inhibiting SMARCA4 on NK-mediated killing of senescent cells 159

6.5 Characterising effect of inhibiting POLR1B on NK-mediated killing of senescent cells 163

6.6 Summary and Discussion 167

Chapter 7 - General Discussion *177*

7.1. Overall summary and discussion of current work **177**

7.2 Future perspectives **183**

7.2.1 Investigating NK-mediated surveillance in KRAS mutant lung tumours 184

7.2.2 Investigating NK-mediated surveillance in ID8 ovarian cancer 191

8. Concluding remarks *198*

Bibliography *201*

Appendix *219*

List of figures

Figure 1.1 Hallmarks of senescence..... 26

Figure 1.2 Pathways regulating the senescence growth arrest..... 30

Figure 1.3 Different phases of the senescence response..... 37

Figure 1.4 Regulation of the SASP..... 40

Figure 3.1 Characterisation of OIS in IMR90 ER:RAS..... 86

Figure 3.2 Upregulation of a proinflammatory and chemoattractive SASP during OIS 90

Figure 3.3 OIS promotes NK cell activity..... 91

Figure 3.4 NK cells selectively kill cells undergoing OIS..... 94

Figure 3.5 Quantification of NK-mediated killing of senescent cells using nuclear-GFP..... 95

Figure 3.6 Adapting a high-throughput assay to monitor NK-mediated killing of senescent cells..... 96

Figure 3.7 Glucocorticoids strongly suppress SASP expression during OIS..... 99

Figure 3.8 Upregulation of a proinflammatory and chemoattractive SASP during OIS 100

Figure 3.9 Halofuginone strongly promotes SASP but does not affect $p16^{INK4a}$ expression during OIS..... 101

Figure 3.10 Indisulam modestly increases SASP expression without bypassing senescence..... 104

Figure 3.11 Halofuginone enhances NK cell-mediated killing of senescent IMR90 ER:RAS cells..... 105

Figure 3.12 Indisulam potentiates NK cell-mediated killing of senescent IMR90 ER:RAS cells..... 106

Figure 3.13 Characterisation of etoposide-induced senescence..... 107

Figure 3.14 Halofuginone and indisulam enhance NK cell-mediated killing of IMR90 cells undergoing TIS..... 108

Figure 3.15 Downregulation of NK cell inhibitory ligands promotes NK cell-mediated killing of senescent cells..... 111

Figure 4.1 Large scale siRNA screen identifies siRNAs enhancing SASP expression..... 120

Figure 4.2 Secondary siRNA screen validates hits upregulating IL6..... 123

Figure 4.3 Secondary siRNA screen validates hits upregulating IL8..... 124

Figure 4.4 Secondary siRNA screen validates hits upregulating IL1β..... 125

Figure 4.5 Secondary siRNA screen validates hits upregulating CCL2..... 126

Figure 4.6 Identifying siRNAs that upregulate the expression of several SASP factors..... 127

Figure 5.1 RNAi screen 1 identifies 22 targets whose knockdown potentiates NK-mediated killing of senescent cells..... 137

Figure 5.2 RNAi screen 2 uncovers 10 targets whose knockdown potentiates NK-mediated killing of senescent cells..... 138

Figure 5.3 Combined analysis of siRNA screens..... 139

Figure 5.4 RNAi screens discover 37 candidates whose knockdown potentiates NK cell-mediated killing of senescent cells..... 142

Figure 5.5 siRNAs against 9 genes potentiate NK-mediated killing of senescent cells 143

Figure 5.6 siRNAs against candidates do not cause NK-mediated killing of non-senescent cells 144

Supplementary Figure S5.1 Expression of the 37 hits from RNAi screens during senescence..... 149

Figure 6.1 Workflow summary of hit identification from multiple RNAi screens..... 153

Figure 6.2 FURIN, SMARCA4, and POLR1B show increased expression in cells undergoing OIS..... 154

Figure 6.3 siRNAs against FURIN specifically enhance NK-mediated killing of cells undergoing OIS..... 156

Figure 6.4 Inhibitors of FURIN increase NK-mediated killing of cells undergoing OIS..... 157

Figure 6.5 siRNAs against SMARCA4 selectively enhance NK-mediated killing exclusively of cells undergoing OIS..... 159

Figure 6.6 A SMARCA4 inhibitor enhances NK-mediated killing of cells undergoing OIS..... 160

Figure 6.7 Inhibitor of SMARCA4 enhances NK-mediated killing of cells undergoing TIS..... 161

Figure 6.8 siRNAs against POLR1B selectively promote NK-mediated killing of senescent cells..... 163

Figure 6.9 RNA Pol I inhibitors enhance NK-mediated killing of cells undergoing OIS..... 164

Figure 6.10 Inhibitors of RNA Pol I enhance NK-mediated killing of cells undergoing TIS..... 165

Supplementary Figure S6.1 Expression of the candidate genes in therapy-induced senescence.... 173

Supplementary Figure S6.2 SMARCA4 and RNA Pol I inhibitors enhance NK-mediated killing of cells undergoing OIS at low E:T ratios..... 174

Supplementary Figure S6.3 Inhibitors against EZH2 and FOSL1 modestly increase NK-mediated killing of cells undergoing OIS..... 175

Figure 7.1 Palbociclib synergises with trametinib to induce senescence in lung cancer cell..... 186

Figure 7.2 Palbociclib and trametinib combination promotes NK cell surveillance of senescent lung cancer cells..... 187

Figure 7.3 Combined palbociclib and halofuginone treatment promotes NK cell-mediated killing of lung cancer cells..... 188

Figure 7.4 Combined palbociclib and indisulam treatment promotes NK cell-mediated killing of lung cancer cells..... 189

Figure 7.5 Cisplatin treatment induces senescence in p53-null ID8 mouse ovarian cancer cells..... 193

Figure 7.6 Cisplatin treatment upregulates SASP and NK activating ligands in p53-null ID8 cells..... 194

Figure 7.7 Cisplatin treatment induces senescence in p53-null HR-deficient ID8 cells..... 195

Figure 7.8 Low dosage cisplatin treatment sufficiently upregulates SASP and NK activating ligands in p53-null HR-deficient ID8 cancer cells..... 196

List of tables

Table 1. Senescent cells contribute to several age-related diseases..... 33

Table A1. Plasmids..... 217

Table A2. Antibiotics..... 217

Table A3. RT-qPCR Primers (Human)..... 218

Table A4. RT-qPCR Primers (Mouse)..... 219

Table A5. Primary immunofluorescence antibodies..... 220

Table A6. Secondary immunofluorescence antibodies..... 220

Table A7. Chemical compounds..... 221

Table A8. siRNA sequences..... 222

Abbreviations

°C	degrees Celsius
4OHT	4-Hydroxytamoxifen
53BP1	p53-binding Protein 1
AD	Alzheimer's Disease
AP-1	Activator Protein 1
ATCC	American Type Culture Collection
ATM	Ataxia Telangiectasia Mutated
ATP	Adenosine Triphosphate
ATR	Ataxia Telangiectasia and Rad3 related protein
BCL2	B-Cell CLL/Lymphoma 2
BRAF	B-Raf Proto-Oncogene, Serine/Threonine Kinase
BrdU	5-Bromo-2'-deoxyuridine
BuBR1	BUB1 Mitotic Checkpoint Serine/Threonine Kinase B
C/EBPβ	CCAAT/enhancer binding protein beta
CCF	Chromatin Cytoplasmic Foci
CCL	C-C Motif Chemokine Ligand
CD	Cluster of Differentiation
CDK	Cyclin-Dependent Kinase
CDKi	CDK Inhibitor
cDNA	complementary DNA
cGAS	cyclic GMP–AMP synthase
CHK	Checkpoint Kinase
CM	Conditioned Media
CRISPR	Clustered Regularly Interspaced Short Palindromic Repeats
CV	Coefficient of Variance
CXCL	C-X-C Motif Chemokine Ligand
CXCR	C-X-C Motif Chemokine Receptor
DAMP	Damage-Associated Molecular Pattern
DAPI	4',6-diamidino-2-phenylindole
DDR	DNA Damage Response
DMEM	Dulbecco's modified Eagle's Medium
DMSO	Dimethyl sulfoxide
DNA	Deoxyribonucleic Acid
DNA-SCARS	DNA-Segments with Chromatin Alterations Reinforcing Senescence
dNTP	Deoxynucleoside Triphosphate
DPP4	Dipeptidyl Peptidase 4
DSB	Double-Strand Breaks
ECM	Extracellular Matrix
ELISA	Enzyme-linked immunosorbent assay
EMT	Epithelial to Mesenchymal Transition
EPRS	Glutamyl-Prolyl-TRNA Synthetase 1
ER	Endoplasmic Reticulum
ER	Oestrogen Receptor
E:T	Effector to Target

EV	Extracellular Vesicle
EZH2	Enhancer of Zeste Homolog 2
FBS	Fetal Bovine Serum
FCRL2	Fc Receptor-Like 2
FOSL1	FOS Like 1, AP-1 Transcription Factor Subunit
FOXH1	Forkhead Box H1
GFP	Green Fluorescent Protein
GO	Gene Ontology
GRO1α	melanoma growth stimulating activity alpha / C-X-C Motif Chemokine Ligand 1
GSEA	Gene Set Enrichment Analysis
H3K27ac	Histone 3 lysine 27 acetylation
H3K9me3	Histone 3 lysine 9 tri-methylation
HCA	High Content Analysis
HDAC	Histone Deacetylase
HDF	Human Diploid Fibroblast
HF	Halofuginone
HLA	Human Leukocyte Antigen
HMGB1	High Mobility Group Box 1
HRAS	Harvey Rat Sarcoma Viral Oncogene Homolog
HSC	Hepatic Stellate Cell
HTM	High-Throughput Microscopy
HTS	High-Throughput Screening
IF	Immunofluorescence
IFNγ	Interferon-gamma
IGF	Insulin Growth Factor
IGFBP7	Insulin Like Growth Factor Binding Protein 7
IL	Interleukin
IL1α	Interleukin 1 alpha
IL1β	Interleukin 1 beta
IL2	Interleukin 2
IL6	Interleukin 6
IL8	Interleukin 8
IL-1RA	IL-1 receptor antagonist
IL6R	Interleukin 6 Receptor
IPF	Idiopathic Pulmonary Fibrosis
IRF3	Interferon Regulatory Factor 3
Ind	Indisulam
JAK	Janus Kinase
KD	Knockdown
KEGG	Kyoto Encyclopedia of Genes and Genomes
KIR	Killer Cell Immunoglobulin-like Receptor
KRAS	Kirsten Rat Sarcoma Viral Oncogene Homolog
L3HYPDH	Trans-L-3-Hydroxyproline Dehydratase
LDH	Lactate Dehydrogenase
LMS	London Institute of Medical Sciences
LPAR2	Lysophosphatidic Acid Receptor 2

MAPK	Mitogen-Activated Protein Kinase
MAPKAPK2	MAPK-Activated Protein Kinase 2
MEK	Mitogen-Activated Protein Kinase Kinase
MEM	Minimum Essential Medium
MHC	Major Histocompatibility Complex
MICA	MHC class I polypeptide–related sequence A
MICB	MHC class I polypeptide–related sequence B
min.	minutes
MK2/ MAPKAPK2	Mitogen-Activated Protein Kinase-Activated Protein Kinase 2
MM	Multiple Myeloma
MMP	Matrix Metallopeptidase
MRC	Medical Research Council
mRNA	messenger RNA
mTOR	Mechanistic Target Of Rapamycin
MULT-1	Murine ULBP-like Transcript-1
Myc	V-Myc Avian Myelocytomatosis Viral Oncogene Homolog
NF-κB	NF-kappa B
NGS	Next-Generation Sequencing
NK	Natural Killer
NKG2A	Natural Killer Group 2 member A
NKG2D	Natural Killer Group 2 member D
NPA	Normalised Percent Activation
NRAS	Neuroblastoma RAS Viral Oncogene Homolog
nt	nucleotide
NT	Non-targeting
OIS	Oncogene-Induced Senescence
Palbo	Palbociclib
PBS	Phosphate-Buffered Saline
PCR	Polymerase Chain Reaction
PD1	Programmed cell Death protein 1
PD-L1	Programmed cell Death 1 Ligand 1
PD-L2/ PDCDLG1	Programmed cell Death 1 Ligand 2
PDGF-AA	Platelet Derived Growth Factor Subunit A
PDX	Patient Derived Xenograft
PFA	Paraformaldehyde
PGF	Placental Growth Factor
PI3K	Phosphoinositide 3-kinase inhibitor
POLR1B	RNA Polymerase I Subunit B
PPP4C	Protein Phosphatase 4 Catalytic subunit
PROTAC	Proteolysis Targeting Chimeras
PRC	Polycomb Repressive Complex
PTBP1	Py Tract Binding Protein 1
PTEN	Phosphatase and Tensin homolog
PTPN1	Protein Tyrosine Phosphatase Non-Receptor Type 1
qRT-PCR	quantitative Real-Time PCR
RAE-1	Retinoic Acid Early inducible protein-1

RAF	Raf-1 Proto-Oncogene, Serine/Threonine Kinase
Rb	Retinoblastoma
RIG-1	Retinoic acid-Inducible Gene I
RNA	Ribonucleic Acid
RNAi	RNA interference
RNA-Seq	RNA-Sequencing
ROS	Reactive Oxygen Species
rpm	revolutions per minute
RPMI	Roswell Park Memorial Institute medium
rRNA	ribosomal RNA
RT	Reverse Transcriptase
SA-β-Gal	Senescence-Associated β-Galactosidase
SAHF	Senescence-Associated Heterochromatin Foci
SASP	Senescence-Associate Secretory Phenotype
scRNA-Seq	Single Cell RNA-Sequencing
shRNA	short hairpin RNA
siRNA	small interfering RNA
SIRT1	Silent mating type Information Regulation 2 homolog 1
SMARCA4	SWI/SNF Related, Matrix Associated, Actin Dependent Regulator Of Chromatin, Subfamily A, Member 4
SMARCA4i	SMARCA4 inhibitor
STAT	Signal Transducer and Activator of Transcription
STING	Stimulator of Interferon Genes
T1D	Type 1 Diabetes
T2D	Type 2 Diabetes
TF	Transcription Factor
TGFβ	Transforming Growth Factor Beta
TIS	Therapy-Induced Senescence
TM	Transfection Mix
TNF-α	Tumour Necrosis Factor-Alpha
TP53/Trp53/p53	Tumour Protein P53
Tram	Trametinib
T_{reg}	Regulatory T cell
tRNA	Transfer RNA
TurboGFP	Turbo Green Fluorescent Protein
v/v	volume per volume
VEGF	Vascular Endothelial Growth Factor
w/v	weight per volume
WNT	Wingless-Type MMTV Integration Site Family
ɣH2AX	Phosphorylation of the Histone A2 Variant X at Ser139
µg/µm/µl/µM	microgram/micrometre/microlitre/micromolar

Chapter 1 - Introduction

1.1 What is cellular senescence?

Cellular senescence is a protective stress response whereby damaged, aged, or preneoplastic cells enter a state of permanent cell cycle arrest but maintain viability and metabolic functions (Sun et al., 2018). Senescent cells, therefore, differ from terminally differentiated cells that indefinitely exit the cell cycle due to their defined developmental programmed cues, and from quiescent cells, which are temporarily arrested and can re-enter the cell cycle in response to appropriate mitogenic signals (He and Sharpless, 2017).

Beyond the implementation of an irreversible growth arrest, senescent cells accumulate senescence-associated heterochromatin foci (SAHFs), secrete an inflammatory phenotype, undergo global chromatin reorganisation, and undergo metabolic reprogramming (Gorgoulis et al., 2019; Wiley and Campisi, 2016). Therefore, cellular senescence is a highly dynamic programme with wide-ranging repercussions on health, disease, and various biological processes. For instance, in the short-term, senescence is affiliated with suppressing tumours and ensuring homeostasis maintenance through tissue remodelling and repair (Campisi, 2005; Kumari and Jat, 2021; Tominaga and Suzuki, 2019). Yet, the prolonged existence of senescent cells may nurture the development of age-related diseases and cancer through both cell-autonomous and non-cell-autonomous mechanisms (Ou et al., 2021). The net outcome of senescence, however, is variable and context-dependent.

1.2 Types of senescence

Cells can undergo senescence in response to several intrinsic and extrinsic stressors. These stress signals can induce growth arrest engaging different signalling pathways (see Chapter 1.4).

1.2.1 Replicative senescence

Historically, the process of cellular senescence was a fortuitous discovery and was initially reported by Hayflick and Moorhead to define the limited number of cell divisions that human fibroblasts could

undergo in culture before reaching their finite proliferative lifespan and becoming permanently arrested (Hayflick and Moorhead, 1961). This state was initially referred to as the 'Hayflick limit' and was speculated to be associated with cellular ageing. However, there remained ambiguity regarding whether these findings represented a physiologically-relevant cellular milieu or were merely an artefact of cell culture. Eventually, this phenomenon was commonly accepted as 'replicative senescence' (RS) and was primarily attributed to gradual telomere shortening (Harley et al., 1990).

In accordance with the 'end-replication problem' during DNA replication, each successful cell division gradually shortens telomeric DNA that otherwise forms a protective cap at the ends of linear chromosomes to prevent chromosomal fusion. Telomeres are normally protected by a bound protein complex called shelterin, which conceals telomeric DNA from the DNA repair machinery, thereby guarding the chromosomal ends (De Lange, 2005). However, as cells continuously divide, attrition of telomeric DNA continues until telomeres eventually reach a minimal length whereby shelterin can no longer protect the chromosomal ends; the short telomeres uncap and begin to accumulate DNA damage foci and are eventually perceived as double-strand breaks (DSBs) by DNA repair proteins, leading to the activation of the DNA damage response (DDR) (D'Adda Di Fagagna et al., 2003). In addition to telomere shortening, the loss-of-function of shelterin components can result in the uncapping of telomeres, leaving the telomeric DNA vulnerable to end-to-end chromosomal fusion (Sfeir and De Lange, 2012). To prevent any risk of genome instability and cancer, the exposed telomeres trigger a DDR. Sustained DDR signalling can induce either cell death or cellular senescence, thereby curtailing any uncontrolled cell division. As individual human chromosomes possess telomeres with variable lengths within the same cells, it is important to appreciate that cellular lifespan and the rate of RS induction, may, in turn, be dictated by the length of the shortest telomeric DNA (Maciejowski and De Lange, 2017).

Therefore, telomere-dependent replicative senescence is justifiability an evolutionarily conserved mechanism critical to preserving genome stability and protecting against tumour development. However, over the past six decades, extensive research in this field and DDR signalling has

demonstrated that the senescence growth arrest can be driven prematurely in response to a diverse range of cellular stressors- both intrinsic and extracellular- independent of telomere length.

1.2.2 Oncogene-induced senescence

The aberrant activation of oncogenes, such as RAS or its downstream effectors, including RAF or MEK, are among the best-studied mechanisms that initiate a potent and sustained antiproliferative response termed oncogene-induced senescence (OIS) (Chandeck and Mooi, 2010). Generally, the abnormal overexpression of oncogenes is concomitant with tumorigenesis. For example, RAS is frequently mutated in adenocarcinomas of the lung, pancreas and colon (Li et al., 2018). However, oncogene activation can also induce genomic stress in cells to restrict cellular growth. OIS was first identified by Serrano and colleagues, who discovered that the constitutive activation of HRAS conferred by the G12V mutation ($HRAS^{V12}$) in primary fibroblasts could induce a cell cycle arrest near indistinguishable from replicative senescence (Serrano et al., 1997). Overexpression of oncogenic RAS activates the MAP kinase pathway and induces a brief hyperproliferative phase, resulting in excessive DNA replication (Hills and Diffley, 2014). Eventually, due to the increased burden on the DNA replication origins, the replication forks stall, and genomic damage accumulates, followed by a strong growth arrest associated with the activation of DDR and the p53 and $p16^{INK4a}$ tumour suppressor networks (Bartkova et al., 2006; Mallette et al., 2007).

Inhibiting the function of these tumour suppressors or DDR components can facilitate the bypass of senescence, highlighting the importance of these pathways in implementing OIS (Beauséjour et al., 2003; Ben-Porath and Weinberg, 2005). The biphasic response of OIS comprising of increased proliferation followed by a durable cell cycle arrest is not only limited to elevated oncogene expression but can apply to preneoplastic lesions in general, including the loss of tumour suppressor genes such as VHL or PTEN (Chen et al., 2005; Young et al., 2008). Although the significance of OIS in cell culture is apparent, the physiological relevance of this mechanism was initially met with scepticism. However, growing volumes of studies have shown that OIS occurs *in vivo*, mainly as several senescence markers have been detected in both human and mice preneoplastic cells but are lacking in the corresponding tumours (Braig et al., 2005; Dhomen et al., 2009; Kang et al., 2011; Michaloglou et al., 2005; Sarkisian

et al., 2007; Wu et al., 2007). Therefore, OIS is considered a powerful tumour suppressive mechanism activated by many oncogenes.

1.2.3 Therapy-induced senescence

Senescence can also be triggered by treatment with cytotoxic or cytostatic agents, referred to as therapy-induced senescence (TIS) (Ewald et al., 2010). Although TIS can be induced in normal cells to halt proliferation, TIS is more relevant for cancer therapy. Traditional cancer treatments such as conventional chemotherapy or radiotherapy have been shown to induce not only apoptosis but also senescence in malignant cells (Gewirtz et al., 2008; Prasanna et al., 2021; Schmitt et al., 2002; Wang et al., 2022b). Chemotherapeutic drugs include platinum-based agents such as cisplatin or carboplatin for the treatment of ovarian cancers, or DNA intercalating agents such as etoposide for treating small cell cancers, among many other drugs. Chemotherapy causes extensive DNA damage in rapidly dividing cancer cells. While this can trigger cell death (Wang et al., 2022b), DNA damage engages the p53 pathway causing a $p21^{CIP1}$-dependent cell cycle arrest and senescence (Ewald et al., 2010; Lakin and Jackson, 1999; Schmitt et al., 2002), which contributes to the positive outcomes of chemotherapy in tumours (Schmitt et al., 2002).

In addition to chemo- and radio-therapies, some targeted therapies (such as CDK4 or aurora kinase inhibitors) also act by inducing senescence (Finn et al., 2015, 2016; Toogood et al., 2005; Wang et al., 2017a). Cyclin-dependent kinase 4 and 6 (CDK4/6) inhibitors are commonly used in metastatic breast cancer patients who fail first-line endocrine therapy and are currently undergoing clinical trials for multiple tumour types for their cytostatic properties in driving a senescence growth arrest (Polk et al., 2016; Wagner and Gil, 2020). CDK4/6 inhibitors, such as palbociclib or abemaciclib, by inhibiting those CDKs, impair the phosphorylation of the retinoblastoma (Rb) protein to block cell cycle progression at the G1 phase (Rayess et al., 2012; Wagner and Gil, 2020). Malignant cells with deficiencies in core tumour suppressor pathways, such as p53, can still undergo senescence when treated with CDK4/6 inhibitors (Ruscetti et al., 2018, 2020; Wagner and Gil, 2020). Similarly, TIS can be highly effective in tumours with loss of apoptotic control where the effects of traditional chemotherapy may be hampered (Milczarek, 2020; Wang et al., 2022b).

Concerns regarding cancer cells escaping TIS exist, as cancer cells that have undergone senescence can acquire increased stemness properties that could favour tumour relapse (Demaria et al., 2017; Lee and Schmitt, 2019). However, combining different cytostatic drugs, or together with conventional immunotherapy or radiotherapy, might help promote a more robust anti-cancer response (Jerby-Arnon et al., 2018; Ruscetti et al., 2018; Wagner and Gil, 2020; Wyld et al., 2020). Thus, TIS offers a potent mechanism to inhibit the growth of cancer cells or cells undergoing neoplastic transformation.

1.2.4 Other forms of stress-induced senescence

Various other forms of cellular stress have come to light for their ability to induce senescence, often referred to as Stress-Induced Premature Senescence (SiPS). These include oxidative stress from the generation of reactive oxygen species (ROS) that can directly induce DNA damage to trigger DDR signalling (Passos et al., 2010); ionising radiation resulting in double-strand DNA breaks and accumulation of DNA damage foci (Fumagalli et al., 2012; Rodier et al., 2009); epigenomic alterations and chromosomal modification (Crouch et al., 2022; Martínez-Zamudio et al., 2020); and general changes to mitogenic or antiproliferative cytokine signalling to reinforce senescence (Kojima et al., 2013; Tominaga and Suzuki, 2019). TIS and OIS are also considered as part of SiPS. The different stress stimuli give rise to distinct senescence phenotypes and, as such, can have a highly diverse influence on the surrounding microenvironment.

1.3 The senescence phenotype

In addition to the loss of proliferative capacity, senescent cells display broad changes in morphology, cell metabolism, gene expression, and chromatin organisation (Hernandez-Segura et al., 2018). Senescence is a highly heterogenous phenomenon with varying phenotypes based on the cell or tissue type, species, and the senescence-inducing stressor. As a result, there are no universal biomarkers specifically for senescence but rather various hallmarks associated with senescent cells from which a combination can be used to assess senescence. As such, a three-step roadmap was recently proposed to more accurately identify senescent cells (Gorgoulis et al., 2019). These steps included detecting the presence of SA-β-gal activity, characterising changes in the expression of

tumour suppressor and proliferation genes, and validating context-specific markers such as the SASP (Gorgoulis et al., 2019).

Senescence is often characterised by a large flattened shape, usually displaying enlarged nuclei (Herranz et al., 2018). There is also an upregulation in lysosomal β-galactosidase activity, termed the senescence-associated β-galactosidase (SA-β-gal), which reflects the increased lysosomal mass of senescent cells (Kurz et al., 2000). As previously mentioned, senescence is typically associated with the activation of the DNA damage response. Therefore, there is accumulated deposition of DDR proteins, for example, ɣH2Ax or 53BP1 (Kuilman et al., 2010), and increased activity of the DDR-associated kinases ATM and ATR (D'Adda Di Fagagna et al., 2003) during senescence.

Senescent cells have high metabolic activity and show increased glycolysis and AMP/ATP ratios (Sabbatinelli et al., 2019), mitochondrial dysfunction (Miwa et al., 2022), and increased autophagy (Herranz et al., 2018; Kwon et al., 2017b). In addition, senescent cells undergo global reorganisation of the chromatin. The clearest example is the formation of senescence-associated heterochromatin foci (SAHFs), whereby specific chromatin regions are condensed, resulting in the silencing of genes associated with cell cycle progression, such as the E2F target genes (Narita et al., 2003, 2006; Zhang et al., 2007). However, transcriptionally active euchromatin remains susceptible to DNA damage (Adams, 2007). SAHFs, similar to general heterochromatin formation, are enriched for repressive marks such as the trimethylation of lysine residues on histone 3 proteins H3K9me3 and H3K27me3, in addition to histone macroH2A and heterochromatin protein 1 (HP1) accumulation (Adams, 2007; Chandra and Narita, 2013). Similarly, loss of Lamin B1 during senescence results in the deformation of the nuclear lamina resulting in the relocation of repressive heterochromatin marks, which can contribute to the formation of SAHFs (Camps et al., 2015; Freund et al., 2012; Salama et al., 2014).

During senescence, there is an upregulation in the expression of tumour suppressor genes, particularly the cyclin-dependent kinase (CDK) inhibitors $p16^{INK4a}$ and $p21^{CIP1}$, that suppress the expression of cell-cycle promoting genes and, therefore, are collectively responsible for the proliferative arrest (Rayess et al., 2012). As senescence and apoptosis are usually induced by similar cellular stressors, both

senescence and apoptosis are alternative sides of the same coin. Although we do not have a complete understanding of how the cell fate is decided, senescent cells are resistant to apoptosis, which may clarify, in part, why senescent cells accumulate with age (Ryu et al., 2007; Sasaki et al., 2001).

Perhaps one of the best-studied hallmarks of cellular senescence is its complex and multifunctional secretory response referred to as the senescence-associated secretory phenotype (SASP). Senescent cells undergo drastic transcriptomic changes associated with an altered and amplified secretome consisting of a vastly diverse assortment of soluble and insoluble factors (Coppé et al., 2010; Lujambio and Villanueva, 2015). These SASP proteins influence the tissue microenvironment (see Chapter 1.6). The SASP has multiple effects, including the propagation of the stress response and influencing neighbouring cells in a non-cell autonomous manner (see Figure 1.1 for different senescent markers).

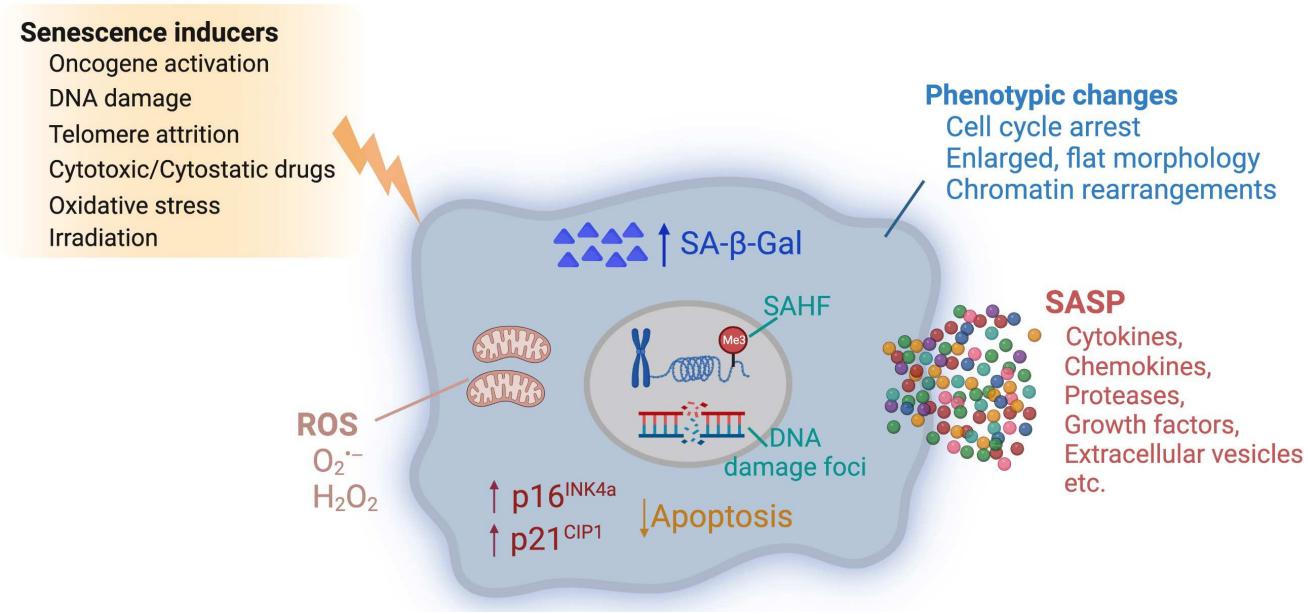


Figure 1.1 Hallmarks of senescence
Senescence can be induced in cells through a range of internal and external stressors. Although there is no exclusive phenotype to characterise senescence, senescent cells undergo several phenotypical, transcriptional, epigenetic, and metabolic changes in a context-dependent manner that can be used to define senescence. Presented here are some common hallmarks of senescent cells. Created on Biorender.com.

1.4 Regulation of the senescence growth arrest

A stable cell cycle arrest is a defining characteristic of senescent cells. The interplay between multiple genes, such as CDK inhibitors, across different pathways, regulate this process. Therefore, the increased activity of these genes is generally considered a senescence hallmark. However, it is important to consider that the specific pathway responsible for the cell cycle arrest is context-dependent and can differ according to the cell type and stressor.

1.4.1 DNA damage response

DNA Damage Response (DDR) is an evolutionarily conserved mechanism that acts as a safeguard to protect genome integrity (Mota et al., 2019). Upon detection of DNA lesions, the DDR mediates a transient growth arrest. At the same time, it initiates a cascade of events that activates various DNA repair pathways to correct any single- or double-stranded breaks, mismatches, or other forms of DNA damage, such as those associated with telomere attrition (Giglia-Mari et al., 2011). If repaired, the cell recommences its normal cycling state. However, if the genotoxic stress is irreparable, the damaged cells can undergo either apoptosis or cellular senescence. Short-term, severe DNA damage induces an apoptotic response. On the other hand, activating a chronic DDR, particularly at repair-resistant regions termed DNA-SCARS (DNA segments with chromatin alterations reinforcing senescence), such as telomeric sites, is crucial for committing to the senescent phenotype (Rodier et al., 2011).

DNA damage results in the phosphorylation and deposition of the histone γH2AX at the site of the damaged chromatin, colocalised with the tumour suppressor p53 binding protein 1 (53BP1) as well as the MRN complex (Lamarche et al., 2010; Rodier et al., 2011). This process is essential to recruit the critical players of the DDR pathway and trigger the DDR signalling cascade (D'Adda Di Fagagna et al., 2003). This cascade is orchestrated by the protein kinases ATM and ATR, which in turn regulate the activity of the downstream effector checkpoint kinases CHK1 and CHK2. These kinases can ultimately mediate the activation of the tumour suppressor protein p53 or the CDK activating CDC25 phosphatases, both of which are crucial regulators of the cell-cycle machinery.

1.4.2 p53/p21^{CIP1} and p16^{INK4a}/pRb pathways

The senescence growth arrest is typically regulated through the dialogue between two core tumour suppressor pathway axis: p53/p21^{CIP1} and p16^{INK4a}/pRb (Salama et al., 2014) **(Figure 1.2)**. Therefore, it is no surprise that components of both tumour suppressor protein axes are frequently mutated in various malignancies.

p53 mutations occur in almost all cancer types, with approximately 50% of human cancers expressing aberrant p53 (Olivier et al., 2010). The protein, encoded by the *TP53* gene in humans, is an essential transcriptional factor that governs the transcription of genes associated with a diverse biological functions, including the regulation of the cell cycle (Engeland, 2022), autophagy (Maiuri et al., 2010), DNA repair, cellular stress response, as well as protein synthesis through cross-talk with mTOR (Rufini et al., 2013). Ultimately, p53 is essential to maintain genome stability and suppress unwanted cell proliferation and is therefore regarded as the 'guardian of the genome' (Efeyan and Serrano, 2007; Lane, 1992).

p16^{INK4a} expression is strongly repressed in normal proliferating cells (Witkiewicz et al., 2011) and its overexpression can induce a senescence growth arrest (Dai and Enders, 2000). Accordingly, a complex regulatory program governs p16^{INK4a} expression. Primarily, p16^{INK4a} is regulated at the epigenetic level through the polycomb repressor complexes PRC1 and PRC2 (Rayess et al., 2012), which act in concert to silence the *INK4/ARF* locus of p16^{INK4a} through the deposition of repressive marks. For example, the PRC2 member protein EZH2 (Enhancer of zeste homolog 2) catalyses the trimethylation of lysine 27 on histone 3 (H3K27me3), inducing a heterochromatin structure and resulting in the transcriptional silencing of p16^{INK4a} (Bracken et al., 2007). On the other hand, different methylation marks can have opposing effects. For example, H3K4me3 deposition on the p16^{INK4a} locus by the methyltransferase MLL1 can promote senescence induction (Kotake et al., 2015). Similarly, the demethylation of H3K27me3 or the loss of PRC genes can induce premature senescence (Barradas et al., 2009). Additionally, with age, cells downregulate EZH2 expression which, in turn, promotes p16^{INK4a} expression (Sen et al., 2016), which may partly explain the increase in senescent cells observed during ageing (see Section 1.5.1). It is important to note that p16^{INK4a} expression can also be silenced through DNA

methylation of the *CDKN2A* gene (encoding $p16^{INK4a}$), which is evident during cancer (Herman et al., 1995).

Sustained activation of p53 can coordinate an antiproliferative program by inducing the transcription of the cyclin-dependent kinase (CDK) inhibitor $p21^{CIP1}$. $p21^{CIP1}$ primarily represses CDK2 from binding to Cyclin E, which results in the hypophosphorylation of the retinoblastoma protein, pRb. In parallel to $p21^{CIP1}$, the $p16^{INK4a}$ tumour suppressor protein inhibits both CDK4 and CDK6 interaction with Cyclin D (Rayess et al., 2012). The primary purpose of these CDKs is to phosphorylate pRb, to push cell cycle progression towards the S phase. The accumulation of both CDK inhibitors $p21^{CIP1}$ and $p16^{INK4a}$, therefore, inhibit the phosphorylation of the retinoblastoma protein. Hypophosphorylated pRb, can bind to E2F1 in a complex preventing its function. Repressing E2F1 transcription factor activity results in the downregulation of genes such as cyclins and *PCNA,* which are needed to promote DNA replication and cell cycle progression, thereby inducing cell cycle exit at the G1 phase (Sherr and McCormick, 2002). Upregulation of $p16^{INK4a}$ is deemed a broad senescence biomarker (Rodier and Campisi, 2011) and, in some contexts, has shown to contribute to senescence induction despite a deficient p53/$p21^{CIP1}$ response (Jacobs and de Lange, 2004). Interestingly, the expression of $p16^{INK4a}$ itself can also be regulated via a feedback loop with pRb; increased phosphorylation of pRb elevates $p16^{INK4a}$ expression, which then induces hypophosphorylation of pRb via CDK4/6 inhibition (Li et al., 1994).

It is important to note that the $p16^{INK4a}$ protein- encoded by the *CDKN2A* gene at the *INK4/ARF* locus- is not the only tumour suppressor to reside at this locus. *CDKN2A* also encodes $p14^{ARF}$, a protein that reinforces p53 activity by neutralising the function of *MDM2* ubiquitin ligase, which otherwise promotes the proteasome-mediated degradation of p53 (Kim and Sharpless, 2006). In addition, another gene at the INK4/ARF locus, *CDKN2B,* encodes the CDK inhibitor $p15^{INK4b}$. Active $p15^{INK4b}$ also blocks the formation of the CDK4/6-Cyclin D complex and contributes to the hypophosphorylation of pRb. In many forms of senescence, the derepression of the entire INK4/ARF locus is required to induce premature cell cycle arrest (Collins and Sedivy, 2003).

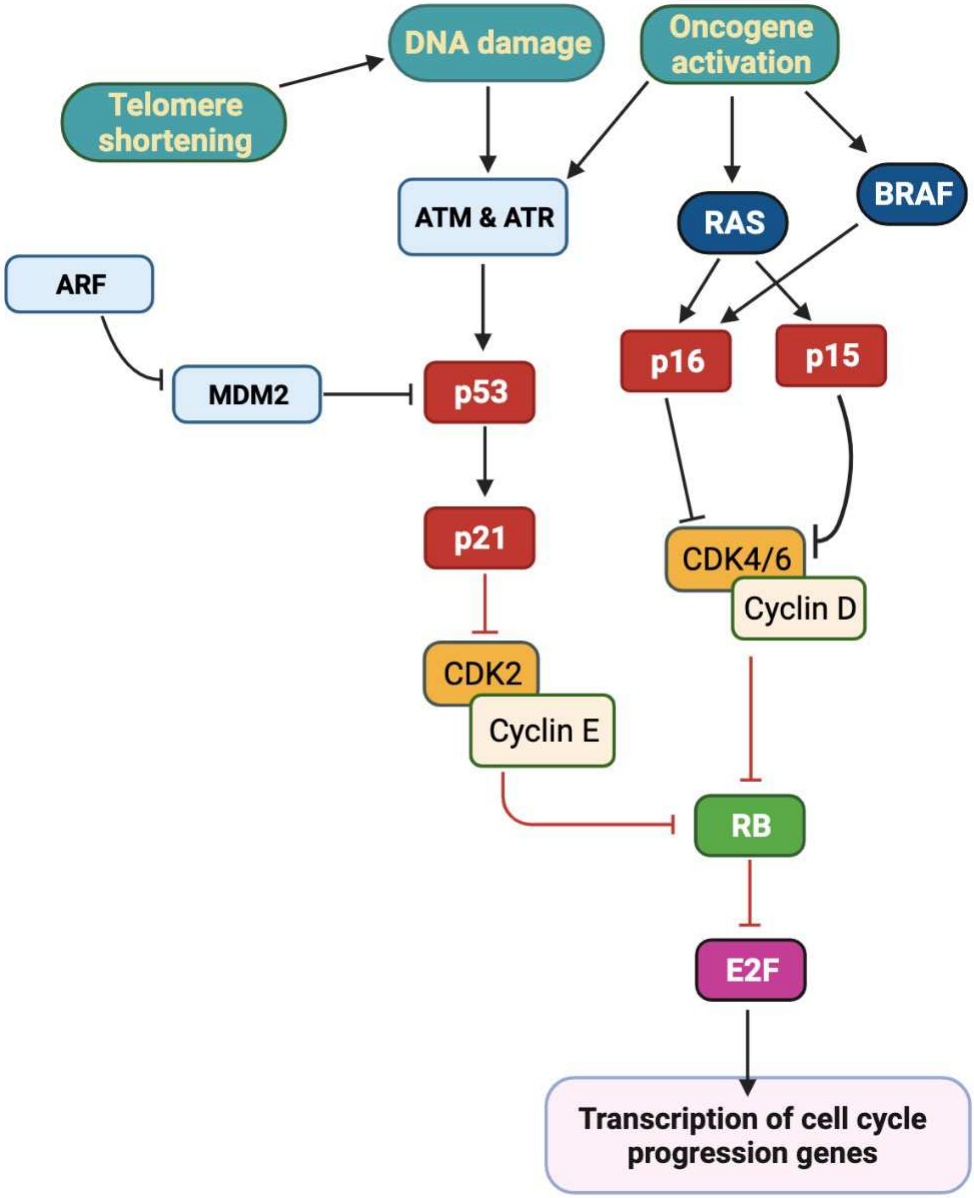


Figure 1.2 Pathways regulating the senescence growth arrest
Different stressors converge on the p53/p21^{CIP1} and p16^{INK4a}/Rb pathways to induce the senescence growth arrest. Created on Biorender.com.

1.5 Physiological roles of senescence

Senescent cells play a fundamental role in various physiological and pathological processes, including ageing and cancer.

1.5.1 Role of senescence in ageing

The opportune discovery by Hayflick and Moorhead that lung fibroblasts lose their proliferative potential after a limited number of population doublings was initially theorised as a model of senescence.

Additional experiments proved that adult lung fibroblasts have fewer cell division cycles than foetal lung fibroblasts, leading Hayflick to propose that this replicative senescence initiated 'ageing' at the cellular level (Hayflick, 1965). Although these findings and subsequent experiments investigating the association between telomere-dependent senescence and age demonstrated a strong correlation between the two phenomena, there was a paucity of evidence.

In recent years, however, mounting volumes of literature have implicated the senescence programme as a vital contributor to mammalian ageing, using $p16^{INKa}$ as a surrogate biomarker for senescence *in vivo* (Krishnamurthy et al., 2004). Initial experiments demonstrated that $p16^{INK4a}$ expression was elevated both during senescence and in aged mice (Zindy et al., 1997). These findings were later corroborated in multiple tissues validating that senescent cells tend to accumulate with age (Van Deursen, 2014; Jin et al., 2021). Using $p16^{INK4a}$ -luciferase mice models, two distinct groups have exhibited a striking increase in the accumulation of $p16^{INK4a}$-positive senescent cells during ageing (Burd et al., 2013; Yamakoshi et al., 2009). Similarly, by leveraging a $p16^{INK4a}$ -tomato reporter mouse model together with single-cell RNA-Sequencing (scRNA-Seq) analysis, Omori and colleagues deciphered the cell type compositions and gene expression changes that occurred with age in mice (Omori et al., 2020). They not only showed $p16^{INK4a}$ -positive cells to be associated with additional senescence hallmarks but also reported markedly high $p16^{INK4a}$ expression, and increased percentage of the senescent cell population, in multiple organ types of aged mice (~ 12 months) compared to that of young mice (~2 months). Intriguingly, quantifying the accumulated proportion of senescent cells in the liver and intestinal crypts of aged mice can also accurately predict their maximum lifespan (Jurk et al., 2014). Dysfunctional senescent cell burden during ageing has also been well documented in primates and human tissues (Van Deursen, 2014; Dimri et al., 1995; Herbig et al., 2006).

Senescence also promotes the attenuation of the adult stem cell pool resulting in the diminished regenerative capacity of progenitor cells needed to maintain tissue homeostasis and thereby reducing longevity, indicative of an ageing phenotype (Flores et al., 2006; Janzen et al., 2006; Krizhanovsky et al., 2008). Moreover, various cells of the immune system may undergo senescence during ageing, progressively impairing their ability to generate an immune response (Aw et al., 2007). This process is

commonly referred to as immunosenescence and may diminish the capacity of the immune system to remove senescent cells with age (Akbar et al., 2016; Ovadya et al., 2018). This, in turn, generates a loop whereby the reduced clearance of senescent cells, due to an immunosenescent effector response, can further drive senescent cell accumulation in multiple organ types during ageing (Yousefzadeh et al., 2021). These studies, however, do not directly address whether there is a clear causal link between senescence and ageing; much like the chicken-egg paradox, there remains uncertainty as to whether ageing contributes to senescent cell accumulation or vice versa.

Some of these concerns were alleviated through a pair of seminal studies by Darren Baker and colleagues. By employing a transgenic mouse model (known as *INK-ATTAC*), Baker et al. proved that the inducible elimination of $p16^{INK4a}$-positive senescent cells in young mice via drug-mediated apoptosis prolonged lifespan and directly hindered the onset of age-associated characteristics, for example, the loss of skeletal muscle or development of cataracts (Baker et al., 2011, 2016). Removal of these senescent cells in progeroid mice models (Baker et al., 2011) or naturally aged mice (Baker et al., 2016) produced a similar outcome with a reduced rate of progression in already established age-related disorders or the delayed onset of tissue dysfunction, and an improvement in organ viability and healthspan. These findings, to a great extent, provided evidence of the causal relationship between senescent cell accumulation and ageing. Additional studies have also validated the removal of $p16^{INK4a}$-expressing cells to investigate this causal relationship with age-associated disorders (Farr et al., 2017; Omori et al., 2020; Thompson et al., 2019). Although most research has investigated the connection between ageing and senescence, using $p16^{INK4a}$ as a surrogate of the senescence phenotype, it is important to point out that this field of study has been confounded by the limited availability of senescence biomarkers that can be detected *in vivo*, and warrants further exploration for an improved mechanistic understanding of the senescence-ageing relationship.

Finally, there is accumulating evidence of senescent cells present at sites of age-related pathologies, which can exacerbate these diseases, including osteoarthritis (Jeon et al., 2017), atherosclerosis (Childs et al., 2016), cardiovascular disease (Fyhrquist et al., 2013; Shimizu and Minamino, 2019), Parkinson's disease (Chinta et al., 2018), cognitive decline (Bussian et al., 2018), and hepatic steatosis

(Ogrodnik et al., 2017), among many others (Childs et al., 2017; Van Deursen, 2014). As such, the long-term existence of senescent cells is a major contributor to the development of chronic and often fatal age-associated diseases. Examples of studies reporting the role of senescence in ageing and age-related pathologies are presented in Table 1.

Disease	Senescent cells/tissues	References
Atherosclerosis	Endothelial cells Vascular smooth muscle cells Macrophages	Gevaert et al., 2017; Durik et al., 2012 Wang et al., 2015 Childs et al., 2016
Cardiac dysfunction	Cardiomyocytes Cardiac progenitors	Chimenti et al., 2003; Anderson et al., 2019 Lewis-McDougall et al., 2019
Fibrosis	Liver (Hepatic stellate cells, cholangiocytes) Cardiac (myofibroblasts) Lung (fibroblasts)	Krizhanovsky et al., 2008; Moncsek et al., 2018 Meyer et al., 2016 Shafer et al., 2017
Immune decline	T cells	Lanna et al., 2014; Akbar et al., 2016
Liver cirrhosis/steatosis	Hepatic stellate cells Liver sinusoid endothelial cells Hepatocytes	Krizhanovsky et al., 2008 Grosse et al., 2020 Ogrodnik et al., 2017
Neurodegenerative disorders	Astrocytes Microglia Neural progenitors	Kang et al., 2015; Chinta et al., 2018 Bussian et al., 2018 Nicaise et al., 2019
Osteoarthritis/ Osteoporosis	Articular cartilage Chondrocytes Osteocytes	Jeon et al., 2017 Sessions et al., 2019 Farr et al., 2017
Sarcopenia	Muscle stem cells	Chang et al., 2016; Sousa-Victor et al., 2014
Diabetes (Type I and II)	Pancreatic beta cells	Thompson et al., 2019a; Thompson et al., 2019b; Aguayo-Mazzucato et al., 2019; Di Micco et al., 2020

Table 1. Senescent cells contribute to several age-related diseases

1.5.2 Role of senescence in cancer

A prominent role of senescence is as a potent anticancer programme that can prevent tumorigenesis by curtailing the proliferation of dysfunctional and stressed cells. Senescence can suppress tumour initiation at an early stage to block incipient cancer cells from undergoing malignant transformation (Herranz et al., 2018; Kang et al., 2011). Senescent cells accumulate in multiple preneoplastic lesions but are absent in their malignant counterparts (Bartkova et al., 2006; Kang et al., 2011; Michaloglou et al., 2005; Suram et al., 2012). Given the critical role that the p53/$p21^{CIP1}$ and $p16^{INK4a}$/Rb pathways play in maintaining senescence, the loss of function of these key senescence effectors can trigger uncontrolled tumour growth, supporting the hypothesis of senescence as a cancer-controlling mechanism (Schmitt et al., 2002). In fact, cellular senescence can also be forced in established tumours

to inhibit further cancer progression, for example, following ionising radiation (Le et al., 2010) or through chemo- and targeted therapy (discussed earlier in section 1.2.3).

In addition, senescent induction in cancer cells can trigger anti-tumour immunity through non-cell autonomous effects. For example, the establishment of RAS-induced senescence in precancerous hepatocytes led to the secretion of immunomodulatory SASP components, which provoked immune cells to clear the senescent premalignant cells, thereby acting as a barrier to tumorigenesis (Kang et al., 2011). Similar findings have been reported in a range of studies, highlighting the fundamental role of senescence and the SASP in mitigating cancer (Prata et al., 2019) (see Chapter 1.7.5).

Senescence can also influence the prognosis of cancer patients. A proteomic screening of plasma membrane-associated proteins identified several candidates that were not only linked to senescence but strongly correlated with increased patient survival and favourable prognosis in multiple tumour types, particularly in breast cancer (Althubiti et al., 2014). In a different study focusing on TIS in lymphoma-bearing mice, the authors found that cyclophosphamide administration induced a p53 and $p16^{INK4a}$-dependent senescence system in the tumours, which was associated with a significantly better prognosis compared to chemotherapy-treated mice with deficiencies in senescence markers (Schmitt et al., 2002).

Contradictorily, the accumulation of senescent cells may be associated with tumorigenesis and worse survival outcome. In a retrospective study of breast cancer patient data over 11 years, the authors investigated the correlation between the expression of crucial senescence markers and cancer development**.** They identified increased expression of both $p14^{ARF}$ and $p16^{INK4a}$ as strongly associated with an elevated risk of disease recurrence and poor cancer prognosis (Pare et al., 2016). Similarly, enrichment of senescence-associated gene signatures, particularly proinflammatory SASP cytokines, in gliomas of aged patients correlated with a worse prognosis (Coppola et al., 2014). Following TIS, some cancers may undergo reprogramming leading to the acquisition of stemness characteristics that, upon bypass of senescence, can result in more aggressive proliferative potential (Milanovic et al., 2018). In addition, loss-of-function mutations in core tumour suppressor genes can drive genomic

instability in tumours and promote senescence escape (Georgakilas et al., 2017). These findings highlight the plasticity of tumours to evade therapy-induced senescence and survive in a dormant state with the capacity for self-renewal, contributing to therapy resistance and relapse.

Senescence of the immune system may also play a role in cancer development. For example, telomere-dependent T cell senescence increases the risk of tumorigenesis in elderly patients (Falci et al., 2013) Furthermore, a systematic analysis investigating the association between replicative senescence (via telomere length) and 13 different tumour types verified that telomere length inversely correlates with increased risk of cancer, with reduced telomere size in T- and B-lymphocytes and granulocytes, contributing to lymphoma development (Wentzensen et al., 2011; Widmann et al., 2007). Moreover, the immunosuppressive tumour microenvironment can also induce immunosenescence in both innate and adaptive immune cells to propagate further tumour growth (Ye et al., 2013).

However, one of the most common avenues linking senescence as a contributor to cancer is the SASP. An abundance of studies have reported that secretion of SASP components following TIS in cancers can recruit immunosuppressive cell types and that a chronic SASP can harbour an internal proinflammatory milieu that drives tumour progression (Eggert et al., 2016; Di Mitri et al., 2014) (discussed in detail in Chapter 1.6.3.1). As a whole, these studies point out the duality of senescence in having both pro- and anti-tumorigenic properties.

1.5.3 Role of senescence in biological processes

The role of senescence extends beyond ageing and cancer. For instance, $P21^{CIP1}$-mediated senescence growth arrest occurs at multiple stages and locations during embryonic development and is necessary for the proper formation of crucial anatomical structures, such as the gut endoderm, neural tube, and mesonephros (Muñoz-Espín et al., 2013; Storer et al., 2013). Mice deficient in $p21^{CIP1}$ suffer developmental abnormalities. Moreover, these studies highlighted the importance of senescence in tissue remodelling and patterning. In addition, senescence is implicated in wound healing and tissue repair in multiple organ models of fibrosis, including the liver (Krizhanovsky et al., 2008), the heart

(Meyer et al., 2016), and the lungs (Schafer et al., 2017). Senescent cells are also necessary for the maintenance of tissue homeostasis. For example, $p16^{INK4a}$-high expressing senescent vascular endothelial cells were found to be abundant in aged liver sinusoids and are essential for liver maintenance and structure. Eradication of these senescent endothelial cells abrogated tissue integrity and triggered a fibrotic response in the liver (Grosse et al., 2020). Likewise, in the setting of the brain, the elimination of senescent neuroblasts that arise with age in the dentate gyrus resulted in reduced cognitive function and defective neurogenesis, again suggesting the importance of the senescence phenotype for homeostasis preservation in specific tissue contexts (Jin et al., 2021). Cellular senescence has also been reported to promote tissue regeneration (Saito et al., 2020) and can regulate insulin secretion from pancreatic beta cells through its SASP (Helman et al., 2016). Overall, senescence is endorsed as a key player in various physiological processes and in maintaining tissue homeostasis (different phases of the senescence response depicted in Figure 1.3).

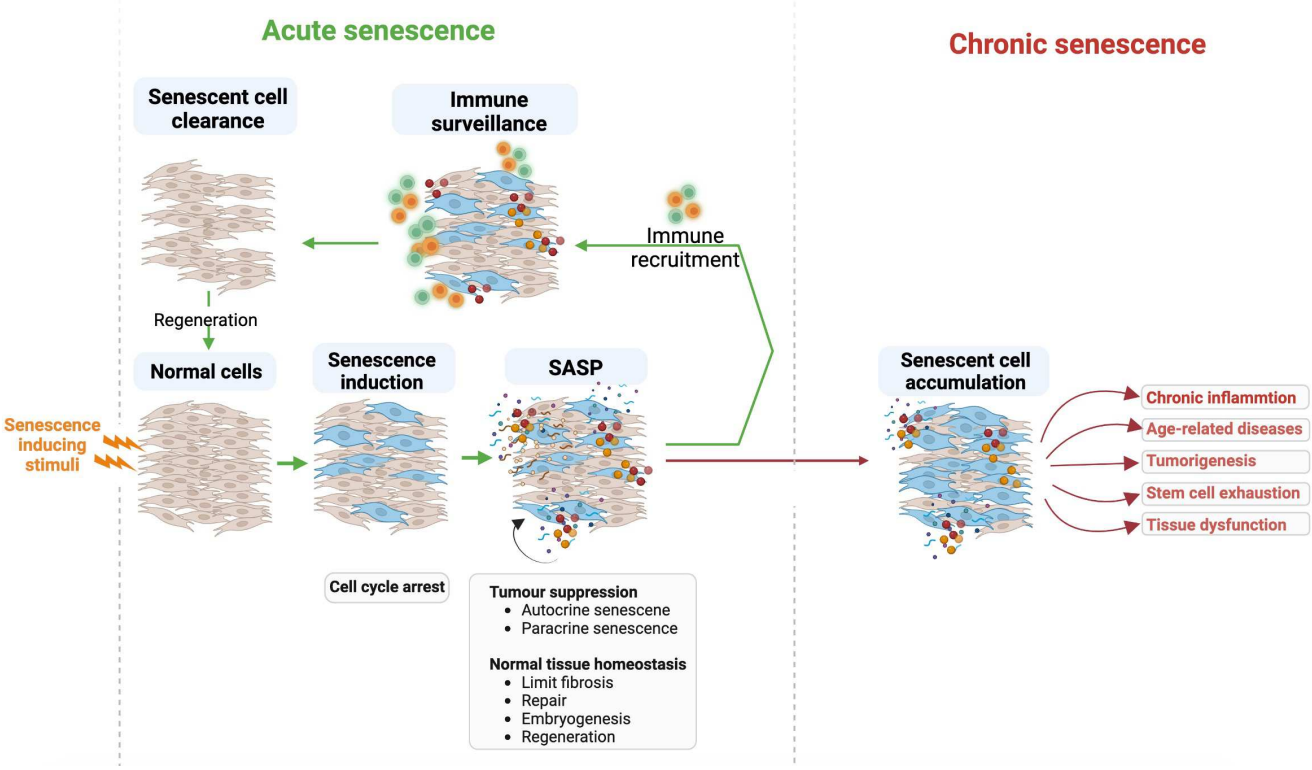


Figure 1.3 Different phases of the senescence response
Acute senescence induction results in a cell cycle arrest that is often associated with many beneficial effects including the maintenance of normal tissue homeostasis and suppression of tumorigenesis. Secreted SASP factors from these senescent cells can recruit and activate cells from the immune system to clear away the senescent cells. However, for various reasons including age, impaired immunity, infections, active immune evasion mechanisms, and persistent senescence, the immune-mediated clearance of senescent cells may be deficient or incomplete. This results in a chronic senescence state whereby senescent cells accumulate in tissues and over time the proinflammatory SASP can contribute to chronic inflammation, neoplastic transformation of cells, and several age-associated pathologies. Created on Biorender.com.

1.6 Senescence-associated secretory phenotype (SASP)

The SASP comprises a highly conserved secretome responsible for mediating many pathophysiological effects of senescent cells (Coppé et al., 2010). Among the plethora of extracellular factors secreted are proinflammatory cytokines and chemokines, proteases, angiogenic and growth factors, and signalling molecules (Kuilman and Peeper, 2009). Although the SASP composition varies between senescent cells, many of the prominent SASP factors, such as IL6 and IL8, as well as the critical transcriptional regulators of the SASP, such as NF-κB and CEBP/β, are shared (Acosta et al., 2008; Chien et al., 2011; Partridge et al., 2020). These secreted components enable senescent cells to communicate with neighbouring cells and modify the surrounding tissue microenvironment and exert pleiotropic effects. Whether the net effect of the SASP is beneficial or damaging is contingent upon

cellular context, the duration of the senescence response, the senescence inducer, and the specific SASP composition itself (Herranz et al., 2018). In line with this, scRNA-Seq analysis has shown that senescent cells possess a diverse secretome that, remarkably, not only exhibits substantial variation between individual cells of the same cell and senescence type but the composition of SASP factors in each cell are also associated with their gene proximity to each other in terms of their organisation on the chromosomes (Wiley et al., 2017). Therefore, it is essential to note that there is no 'one size fits all' impact of the SASP on the surrounding niche.

1.6.1 Regulation of the SASP

The SASP is regulated at both transcriptional and post-transcriptional levels. The NF-κB protein complex and the CCAAT/enhancer-binding protein-β (CEBP/β) transcriptional factor are commonly referred to as the master regulators of the SASP and are highly activated following the induction of senescence (Kuilman et al., 2008; Salminen et al., 2012). They can directly control the transcription of genes encoding multiple proinflammatory markers, including IL1α, IL6 and IL8, which in turn can form autocrine positive feedback loops with NF-κB and CEBP/β to further enhance the SASP programme (Lopes-Paciencia et al., 2019). IL1α is, in fact, a key regulator of the SASP, such that the ectopic expression of this cytokine alone is sufficient to partially phenocopy the proinflammatory SASP of cells undergoing OIS (Acosta et al., 2013). In addition, various signalling pathways, including a persistent DDR (Rodier et al., 2009), JAK/STAT (Toso et al., 2014), and cGAS/STING (Dou et al., 2017; Yang et al., 2017) are all associated with regulation of the secretory pathway, but nevertheless converge to trigger the activation of the NF-κB and CEBP/β signalling cascade (Herranz et al., 2018). Activation of p38, a mitogen-activated protein kinase (MAPK) family protein, is an important component of senescence and the SASP. Generally, the p38 signalling pathway is activated upon exogenous stress, including oxidative stress and radiation, or following the onset of inflammation or the DDR (Freund et al., 2011). p38MAPK signalling can induce a senescence growth arrest via the activation of the p53/$p21^{CIP1}$ and $p16^{INK4a}$/pRb pathways (Debacq-Chainiaux et al., 2010; Xu et al., 2014). p38MAPK expression can also regulate the SASP by activating the NF-κB and CEBP/β proteins (Freund et al., 2011).

The mechanistic target of rapamycin (mTOR) pathway is a critical SASP regulator. mTOR signalling regulates protein translation following senescence induction and SASP activation (Laberge et al., 2015). mTOR can promote NF-κB activation and the translation of IL-1α via phosphorylation of the 4EBP1 translational repressor protein (Laberge et al., 2015). Moreover, through 4EBP1 phosphorylation, mTOR differentially regulates the translation of the kinase MAPKAPK2, which, during senescence, inhibits ZFP36L1, an mRNA-binding protein that selectively targets the transcripts of various SASP components for degradation (Herranz et al., 2015). Thus, MAPKAPK2 activity indirectly regulates the SASP and stabilises the mRNA of the proinflammatory SASP components. Alongside mTOR signalling, the post-transcriptional regulation of the SASP can also be achieved through the alternative RNA splicing regulator PTBP1, whose inhibition can suppress the proinflammatory SASP during OIS without interfering with the growth arrest (Georgilis et al., 2018).

In addition, the SASP is also governed epigenetically. For example, BRD4, a member protein of the bromodomain and extra-terminal family, is involved in remodelling the enhancer landscape in senescent cells (Tasdemir et al., 2016). Specifically, BRD4 is recruited to super-enhancer elements in proximity of essential SASP genes and can regulate their transcription. Similarly, alterations to the chromatin, including the change in H3K9 histone methylation at SASP promoters (Takahashi et al., 2012) or via the localisation of epigenomic modulators such as HMGB2 following senescence (Aird et al., 2016), have been implicated in SASP regulation. Understanding the diverse range of avenues at play that regulate the SASP may unveil multiple approaches to target the secretory programme as a therapeutic intervention.

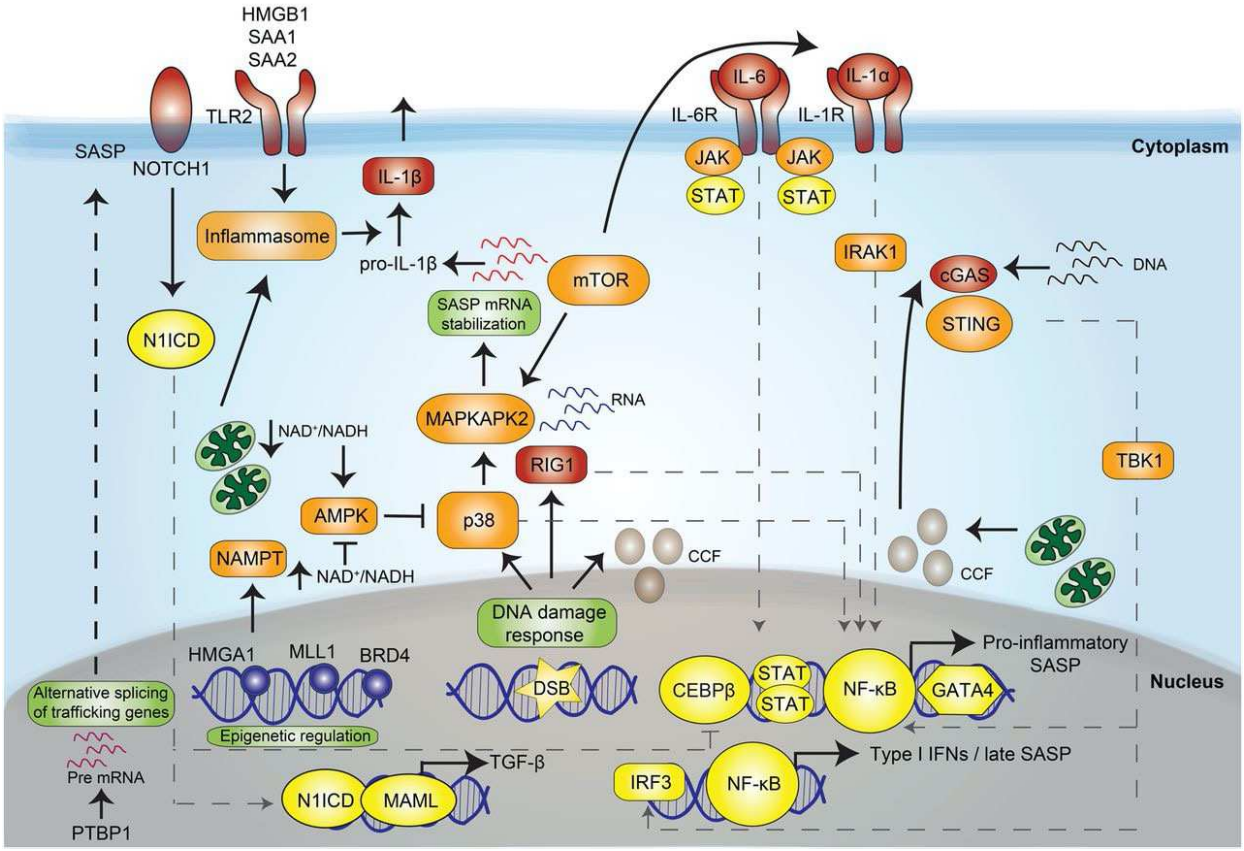


Figure 1.4 Regulation of the SASP
The SASP is a fundamental mediator for several pathophysiological roles of senescence. The SASP is regulated at different levels involving multiple receptors and ligands (red), signalling pathways (orange), and transcription factors (yellow). The interplay between these components is essential to regulate the transcription, translation, splicing, and secretion of different SASP factors.
DSB: Double-strand breaks; CCF: chromatin cytoplasmic foci.
Figure adapted from Birch & Gil. (2020).

1.6.2 Beneficial effects of the SASP

1.6.2.1 Reinforcement of senescence

The SASP is critical to reinforce the senescence growth arrest. For example, during cancer initiation, the transient expression of proinflammatory SASP factors from oncogene-activated senescent cells, such as IL-1α, IL-6, CXCR2, IGFBP7, or PAI-1, can reinforce a proliferative arrest via an autocrine positive feedback loop (Acosta et al., 2008; Kortlever et al., 2006; Kuilman et al., 2008; Wajapeyee et al., 2008). In these studies, depleting secreted components, such as IL6 or IGFBP7, resulted in SASP downregulation and enabled re-entry into the cell cycle (Kuilman et al., 2008; Wajapeyee et al., 2008). Similarly, gene silencing of the IL6 receptor promoted the bypass of senescence (Kuilman et al., 2008),

as did the knockdown of the chemokine CXCR2 receptor, which enabled senescence escape in both replicative and oncogene-induced senescence (Acosta et al., 2008). In addition, Orjalo and colleagues reported that IL1α signalling from senescent fibroblasts is a critical regulator for IL6 and IL8 secretion (Orjalo et al., 2009). Therefore, the SASP is fundamental for maintaining the senescence growth arrest through cell-autonomous mechanisms.

Indeed, the SASP can also act in a non-cell autonomous manner by inducing senescence in neighbouring cells in a paracrine fashion, thereby further amplifying the anticancer response. In a PTEN-deficient prostate tumour mouse model, Di Mitri and colleagues demonstrated that the onset of senescence triggers infiltration of immature myeloid cells that hinders the growth arrest of nearby proliferating tumour cells by secreting the interleukin-1 receptor antagonist (IL1RA), thereby sustaining tumour proliferation. Knocking out the IL1RA invigorated IL1α signalling from the senescent prostate tumours to induce paracrine senescence in surrounding cancer cells (Di Mitri et al., 2014). The SASP can also mediate paracrine senescence in normal cells. For example, during OIS, secretion of the vascular endothelial growth factor (VEGF), the chemokines CCL2 and CCL20, and TGF-β family ligands were all shown to contribute to spreading senescence to neighbouring fibroblasts in a $p15^{INK4b}$ and $p21^{CIP1}$-reliant manner (Acosta et al., 2013). Moreover, IL1 signalling is an upstream regulator of the SASP, and by inhibiting IL1 receptor (IL1R), the authors revealed that the senescence response was mitigated, resulting in fibroblast proliferation. Indeed, TGF-β ligand-mediated paracrine senescence has also been reported to blunt liver regeneration following injury and promote liver dysfunction (Bird et al., 2018). Among the bioactive molecules released from senescent cells, reactive oxygen species (ROS) are particularly intriguing (Passos et al., 2010). ROS are known to mediate cellular senescence and enhance oxidative stress that correlates with increased incidence of age-related diseases (Pole et al., 2016). ROS signalling from senescent fibroblasts has been shown to trigger DNA damage response and bystander senescence in neighbouring cells *in vitro* (Nelson et al., 2018).

Interestingly, the ability to induce paracrine senescence through SASP components extends beyond normal or precancerous senescent cells onto cells of the immune system. For instance, CD4+ T-helper-

1 ($CD4^+$ T_H1) cells secrete interferon-γ (IFN-γ) and tumour necrosis factor (TNF) cytokines whose combined signalling can directly induce senescence in pancreatic (β-cell) and breast cancer cells, both *in vitro* and *in vivo*, through the activation of $p16^{INK4a}$ (Braumüller et al., 2013). Likewise, secretion of factors from CD4+ T cells have also shown to be necessary to induce cellular senescence and promote tumour regressions in *MYC*-inactivated T cell acute lymphoblastic lymphomas (Rakhra et al., 2010). As a whole, the SASP and its components mediate and strengthen the tumour protective features of the growth arrest.

1.6.2.2 Regulation of physiological processes

As mentioned in chapter 1.5.3 regarding senescence, the SASP not only reinforces tumour suppression but can mediate a variety of essential biological processes. Some of these include insulin secretion (Helman et al., 2016), developmental senescence (Muñoz-Espín et al., 2013), and tissue remodelling (Mosteiro et al., 2016, 2018; Ritschka et al., 2017). During wound repair, initial deposition of collagen and extracellular matrix (ECM) are essential to maintain tissue integrity, but if unregulated, they can become over-deposited resulting in fibrotic response and scar formation (Wilkinson and Hardman, 2020). Therefore, wound healing requires extensive communication coordinated by extracellular SASP components, including cytokines, chemokines and growth factors, following the induction of senescence at the wound site. For example, following cutaneous injury in mice, the expression of the matricellular protein CCN1 at the site of injury induced senescence in fibroblasts through the activation of the $p16^{INK4a}$/Rb pathway. This process was necessary to suppress fibroblast proliferation and promote the expression of anti-fibrotic genes to limit the deposition of ECM components (Jun and Lau, 2010). Similarly, another study focusing on cutaneous injury reported an accumulation of senescent endothelial cells and fibroblasts at the wound site in p16-3MR transgenic mice models. Importantly, these senescent cells secreted platelet-derived growth factor AA (PDGF-AA), which was necessary to trigger myofibroblast differentiation required for complete wound closure. Moreover, topical application of recombinant PDGF-AA on the wound site following the inducible elimination of $p16^{INK4a}$-positive senescent cells from the mice was sufficient to reverse any delays in wound healing; however not to revert fibrosis, indicating the requirement of additional SASP factors, such as matrix metalloproteases (MMPs), for complete wound healing (Demaria et al., 2014).

An influential study by Krizhanovsky and colleagues highlighted the role of the SASP in limiting the fibrotic response (Krizhanovsky et al., 2008). In general, chronic liver damage resulting from an accumulation of tissue insults can amplify liver fibrosis and cause cirrhosis, which, if left unchecked, culminates in liver failure. Krizhanovsky et al. showed that following CCL_4-induced liver injury, the resident stellate cells undergo initial proliferation resulting in the secretion of ECM proteins essential for a fibrogenic response and scar formation. However, this is followed by the induction of senescence. These senescent hepatic stellate cells (HSCs) then facilitate the resolution of fibrosis through decreased ECM protein expression and upregulation in the secretion of anti-fibrotic SASP components, mainly MMPs required for the breakdown of the fibrotic deposition (Krizhanovsky et al., 2008). Nullifying the senescence response of HSCs corresponded with increased ECM deposition and liver fibrosis. Importantly, this SASP was also immunomodulatory and capable of activating natural killer (NK) cells from the immune system to clear away the senescent HSCs to complete the injury repair process. Likewise, additional alternative studies have shown the SASP of HSCs as a fundamental component of the wound resolution machinery following liver damage to restore tissue homeostasis (Kong et al., 2012; Lujambio et al., 2013). In particular, the latter study demonstrated that the SASP from senescent HSCs could drive macrophage polarisation towards a proinflammatory M1-phase that can hinder tumour proliferation and concurrently kill senescent cells. Therefore, both the studies by Krizhanovsky et al. and Lujambio et al. also highlight the importance of the SASP in alerting and modulating the immune system.

1.6.2.3 Immune clearance of senescent cells

The SASP is abundant in inflammatory cytokines and chemokines, adhesion molecules, and immune modulators and therefore is a key mediator of immune surveillance. The evolution of the SASP may have originated based on the need for senescent cells to communicate with the surrounding microenvironment and alert neighbouring populations of their compromised state, thereby sanctioning their removal. As mentioned previously, the SASP is highly heterogeneous and depending on the specific secreted composition, senescent cells may recruit distinctive immune cells, including but not limited to NK cells, CD4+ and CD8+ T cells, macrophages, and dendritic cells, which can interact with

senescent or damaged cells and promote their clearance (Saleh et al., 2018). This can be both a critical and a highly beneficial feature in the context of health and disease. As described in the previous section, senescent HSCs in the liver following CCL_4-induced injury can secrete SASP components to recruit NK cells (Krizhanovsky et al., 2008). In addition, these senescent cells also upregulate the expression of NK cell activating ligands on their surface, which can promote immune-mediated clearance of these HSCs from fibrotic tissue leading to the resolution of fibrosis (Krizhanovsky et al., 2008). On the other hand, p53-induced senescence in these hepatic stellate cells can induce a SASP profile resulting in the enrichment of cytokines such as Cxcl2, IL1α, IL1β, and IFN-γ that modulate macrophage polarisation to M1 and promote macrophage-mediated elimination of senescent HSCs (Lujambio et al., 2013). Thus, the distinction in senescence inducers between the two aforementioned studies in liver fibrosis, and consequently the SASP composition, alters the specific immune cell type recruited to mediate clearance.

In addition to fibrosis, immune clearance of senescence is fundamental for embryonic development. To prepare the endometrium for embryonic implantation following ovulation, endometrial stromal cells undergo senescence and secrete SASP components. IL-15 secretion from the SASP can activate uterine NK cells that target and kill senescent cells, thereby restoring tissue homeostasis as part of the normal cycling process of the endometrium (Brighton et al., 2017).

Many studies investigating SASP-dependent immune clearance of senescent cells have focused on cancer (Kale et al., 2020). In fact, the first reports of the interaction between senescence and the immune system *in* vivo were described in the p53-null model of hepatocellular carcinoma, whereby restoration of p53 expression in the tumours triggered a senescence response, resulting in the secretion of inflammatory cytokines (Xue et al., 2007). The SASP activated a potent immune response that eliminated senescent cancer cells to drive tumour regression. These findings were a significant discovery in the field and have led to other studies investigating senescence-mediated anti-tumour immunity in a wide range of tumour types, which will be discussed in depth in Chapter 1.7.4.

1.6.3 Harmful effects of the SASP

1.6.3.1 SASP contributes to tumorigenesis

To date, the senescent secretome has largely been examined from a pathological standpoint, with research primarily focused on the harmful effects of the SASP in age-associated disorders and cancer. Given the proinflammatory nature of the SASP, prolonged SASP expression from senescent cells can drive malignant transformation directly through paracrine signalling to established or incipient cancer cells or indirectly via the generation of an inflammatory tumour microenvironment (TME). Both criteria are not mutually exclusive; on the contrary, they are often coordinated to promote tumorigenesis. This was first evident in a pioneering study by Krtolica et al. whereby senescent human fibroblasts– irrespective of the senescence-inducing stimuli- were able to incite the proliferation and progression of cancerous and precancerous epithelial cells in co-culture through the secretion of SASP factors, but did not affect the growth of normal epithelial cells (Krtolica et al., 2001). Although the individual secretory components were not initially characterised, it has since become clear that the culpability lies with proinflammatory cytokines. For instance, in later studies, the persistent secretion of the inflammatory molecules IL6 and IL8 from replicative- and irradiation-induced senescent fibroblasts have shown to promote tumorigenesis in both premalignant and normal epithelial cells (Coppé et al., 2008). In another study, Yoshimoto and colleagues demonstrated that multiple inflammatory SASP factors secreted from senescent hepatic stellate cells in obese mice can stimulate the development of obesity-associated hepatocellular carcinoma (HCC) in surrounding liver cells (Yoshimoto et al., 2013). Another proinflammatory chemokine, CCL2, is also a chemoattractant SASP factor capable of recruiting different immune cells. In an intriguing study, Eggert and colleagues showed that the influence of SASP components such as CCL2 can be both pro- and anti-tumorigenic in a context-dependent manner. Following the establishment of senescence in premalignant hepatocytes, the secretion of CCL2 can recruit CCR2+ myeloid cells that may differentiate into macrophages and eliminate the senescent cells. However, if hepatocellular carcinoma (HCC) has developed, the senescent tumour cells impede myeloid cell differentiation into effector macrophages, thereby enhancing its own survival and furthering tumour growth following senescence escape (Eggert et al., 2016).

Persistent inflammation is a significant contributor to tumorigenesis and can trigger several classic hallmarks of cancer (Gonzalez et al., 2018; Hanahan and Weinberg, 2011). Secreted inflammatory mediators, such as those released from senescent cells, are frequently detected within the TME of patients and can promote angiogenesis, which is essential for sustainable tumour growth (Coppe et al., 2006; Watanabe et al., 2017). Depending on the SASP factors, they can also facilitate the epithelial-to-mesenchymal transition (EMT) to promote tumour migration, invasion, and, consequently, metastasis (Coppé et al., 2008; Kaur et al., 2016). There is evidence of altered expressions of EMT markers in the SASP of various senescent tumours, which may contribute to chemoresistance (Di Martino et al., 2018). For example, vimentin is a mesenchymal marker well known to organise cytoskeletal structure that has shown to be enriched in the SASP of senescent malignant cells (Canino et al., 2012). Various additional SASP factors contribute to EMT. Among these are VEGF and the matrix metalloproteases (MMPs), which are secreted from various senescent cells and can facilitate the remodelling of the ECM to stimulate tumour invasion and growth (Coppé et al., 2010; Paramos-de-Carvalho et al., 2021). MMPs have been described to promote breast cancer metastasis (Parrinello et al., 2005) and EMT induction during the development of adenocarcinomas (Kessenbrock et al., 2010). Upregulation of growth factors and amphiregulin from senescent prostate fibroblasts have been shown to nurture the growth of premalignant prostate epithelial cells (Bavik et al., 2006).

Despite its inflammatory properties, the SASP may also induce immunosuppressive effects, facilitating the unrestricted growth of tumours. As mentioned earlier, following the development of HCC, the SASP of senescent tumours can signal for the recruitment of immunosuppressive CCR2+ myeloid cells that are incapable of differentiating into effector cells. Rather, these immature myeloid cells accumulate in the tumour microenvironment and inhibit the activity of infiltrating NK cells to activate liver tumour proliferation (Eggert et al., 2016). Furthermore, in a different mouse model of PTEN-null prostate tumours, senescent induction also amplified the recruitment of tumour infiltrating myeloid-derived suppressor cells (MDSCs), which secreted IL1R antagonist into the TME, thereby preventing the activity of effector immune cells and impeding IL-1 signalling in tumours to restore tumour proliferation (Di Mitri et al., 2014).

Although direct evidence for the pro-tumorigenic effects of the SASP *in vivo* is limited, several lines of evidence report the tumour-promoting impact of the SASP following TIS (Prasanna et al., 2021). Of most concern are reports indicating the rise of cancer-stemness. Following the genotoxic stress of TIS, the SASP profile of senescent multiple myeloma or senescent melanoma tumours can induce reprogramming in preneoplastic cells to induce cancer stem-cell-like properties and trigger tumour proliferation (Cahu et al., 2012; Ohanna et al., 2011). These findings raise significant apprehensions regarding drug resistance and the potential of tumour relapse.

Extracellular vesicles (EVs) have gained recent interest as crucial components of the SASP of senescent cells that can also impact the surrounding senescent microenvironment, just as soluble cytokines and proteins do (Takasugi, 2018). The cargo protein encompassed within these EVs derives from the host senescent cell and, therefore, may exert cell-specific paracrine effects from cell to cell (Wallis et al., 2020). Takasugi and colleagues investigated doxorubicin-induced senescence in human epithelial cells and conducted a proteomic analysis of the secreted EVs, and reported their pro-tumorigenic properties (Takasugi et al., 2017). The authors characterised the protein EphA2, an Ephrin ligand which undergoes phosphorylation following senescence induction, as cargo for the EVs. Following secretion, EphA2 interacts with the Ephrin-1 receptor, which is highly expressed on the surface of multiple cancer types, to trigger the proliferation of breast cancer cells. These results highlight a novel approach for the SASP to amplify its pro-tumorigenic effects. However, these results focus on the cargo of just one of several proteins that may undergo packaging and secretion by EVs; a rising number of studies are currently investigating the implication of EVs in cancer and age-related diseases (Takasugi, 2018; Wallis et al., 2020).

1.6.3.2 SASP contributes to age-related pathologies

Similar to its effects in promoting tumorigenesis, the proinflammatory SASP can disrupt tissue architecture and cause chronic local and systemic inflammation (termed ‘inflammaging’) that is linked to several age-associated diseases (Franceschi and Campisi, 2014; Watanabe et al., 2017). Upon elimination of $p16^{INK4a}$-positive senescent cells from either premature- or naturally-aged mice, Baker

and colleagues observed a reduction in the expression of proinflammatory factors, including IL6, which may otherwise have, in some part, contributed to age-related diseases associated with senescence (Baker et al., 2011, 2016). Similarly, the deletion of $p16^{INK4a}$-expressing senescent cells in transgenic mouse models of non-alcoholic steatohepatitis (NASH) led to reduced tissue dysfunction (Omori et al., 2020). In fact, scRNA-seq analysis revealed that $p16^{INK4a}$-expressing senescent cells showed enrichment of IL6, and M1-like polarisation of macrophages, indicating increased SASP signalling in the livers of the NASH mice models compared to healthy mice. Importantly, removing the senescent cells reduced liver steatosis and inflammation, leading to decreased SASP in surrounding tissues. In the pancreas, senescent beta cells acquire a proinflammatory SASP which contributes to the immune-mediated destruction of the senescent cells and the development of insulin deficiencies and type-1 diabetes (T1D) (Thompson et al., 2019). Eliminating these senescent beta cells attenuated the SASP and prevented the onset of T1D, further highlighting the harmful contribution of the SASP in distinct age-related diseases.

Overall, the SASP has been regarded as a 'double-edged sword' (Coppé et al., 2010). While transient SASP induction brings substantial benefits in the form of tumour suppression, tissue regeneration, and wound healing, these are quickly upturned through the deleterious– and potentially fatal– consequences of a prolonged SASP secretion through increased tumour proliferation and metastasis, and chronic inflammation, which warrant targeting (discussed in the next chapter). These contradictory characteristics of the SASP are coherent with the notion of 'antagonistic pleiotropy'; therefore, any therapeutic interventions to control senescence or the SASP systems must consider the complete consequences, both rewarding and damaging.

1.7 Strategies to target cellular senescence

1.7.1 Why target senescent cells?

As described, the consequences of senescence and its secretory programme are paradoxical, although the reasoning behind these opposing effects requires a more mechanistic understanding. The

senescence growth arrest brings with it a myriad of physiological advantages. Senescence is necessary to maintain the structural integrity of tissues and organs (Grosse et al., 2020; Tominaga, 2015), facilitate wound healing following injuries (Wilkinson and Hardman, 2020), restore tissue function and homeostasis (Jin et al., 2021; Tominaga, 2015), and fundamentally to suppress the development of tumours (Birch and Gil, 2020). In theory, an acute SASP is sufficient to recruit immune cells from both the innate and adaptive immune systems which can eliminate senescent cells through their effector functions (Song et al., 2020). In physiology, however, the senescence clearance process is imperfect for multiple reasons: the immune response declines with age as immune cells may undergo senescence thereby impairing their ability to remove senescent cells (Akbar et al., 2016; Lanna et al., 2014; Ovadya et al., 2018); the rate of senescent cell accumulation outperforms that of immune-mediated clearance (Freund et al., 2010); and senescent cells evolve mechanisms to evade immunosurveillance (Muñoz et al., 2019; Pereira et al., 2019). As such, a chronic senescence response is established and bears unfavourable repercussions, attributed mainly to the SASP. The gradual yet persistent secretion of proinflammatory proteins from cells can disrupt the surrounding tissue architecture and function, generate a hostile microenvironment suitable for cancer growth, and contribute to the progress of ageing and age-related diseases (Faget et al., 2019).

The rationale to target senescent cells for destruction is inherently determined by the following aspects: (i) the risk of the detrimental effects from chronic senescence and SASP outweigh the temporary benefits achieved. (ii) the inducible ablation of $p16^{INK4a}$-positive senescent cells using transgenic mice models delivered a proof-of-principle of the remarkable benefits on health and lifespan (Baker et al., 2011, 2016; Jeon et al., 2017; Lujambio, 2016). (iii) Acute senescence induction can be beneficial, while lingering senescent cells may produce harmful effects. Therefore, the timely removal of senescent cells can prevent chronic senescence while maintaining the advantages associated with senescence induction.

Current strategies to combat senescence and its phenotypes can be grouped into three categories: senolytics, senomorphics, and immune surveillance.

1.7.2 Targeting senescence with senolytics

The inducible elimination of senescent cells in aged transgenic mice was a pioneering study that exhibited the range of anti-ageing and anti-tumorigenic health benefits that could be obtained *in vivo* (Baker et al., 2011, 2016). These findings spearheaded the discovery of numerous compounds that selectively eliminate senescent cells, referred to as senolytics.

Senolytic agents function by targeting pathways associated with vulnerabilities of senescent cells, but not necessarily in non-senescent cells (Zhu et al., 2015). A classic characteristic of senescent cells is their resistance to apoptosis. Therefore, Zhu and colleagues performed a transcriptomic analysis of senescent cells to discover an upregulation of pro-survival gene networks during senescence, including the anti-apoptotic BCL-2 family proteins (BCL-2, BCL-X_L, BCL-W) (Zhu et al., 2015). These findings ultimately led to the development of various pharmacological inhibitors of senescence-specific pro-survival gene pathways (Chang et al., 2016; Fuhrmann-Stroissnigg et al., 2017; Yosef et al., 2016; Zhu et al., 2015).

Among the most promising and well-characterised senolytic candidates available are the BCL-2 family inhibitors. One particular example is of ABT-263 (also termed navitoclax), which was successfully reported to kill senescent haematopoietic stem cells, and even senescent muscle stem cells in aged mice to mitigate the age-related deterioration of haematopoietic function (Chang et al., 2016). Furthermore, the same senolytic has been shown to reduce the onset of atherosclerotic plaque formation by inducing apoptosis of senescent foam cells in atherosclerotic lesions (Childs et al., 2016). Similarly, the administration of an alternative BCL-2 family inhibitor, ABT-737, rapidly eliminated DNA-damaged-induced senescent lung cells *in vivo* as well as senescent epidermal cells, leading to improved age-related phenotypes (Yosef et al., 2016).

Several alternative senolytic drugs have reported successful findings in treating age-related pathologies. The pan-tyrosine kinase inhibitor dasatinib (D) plus the flavonoid quercetin (Q) are two agents that are commonly paired (D+Q) for their combined senolytic properties to induce apoptosis in

senescent cells (Novais et al., 2021). D+Q treatment has shown to selectively eliminate senescent cells and, in turn, suppress the proinflammatory SASP of explanted human adipose tissues in mice (Xu et al., 2018). Moreover, D+Q therapy reduced tissue dysfunction and extended survival in naturally aged mice (Xu et al., 2018), improved age-dependent spinal disc degeneration (Novais et al., 2021), and has been shown to reduce bone loss with age (Farr et al., 2017). Seven new clinical trials using the D+Q senolytic cocktail are currently being conducted to treat a range of age-related pathologies, including Alzheimer's disease and skeletal disorders (Chaib et al., 2022). Other senolytic candidates that have garnered recent attention include inhibitors of FOXO4, a p53-forkhead box protein O4 (Baar et al., 2017), MDM2 inhibitors such as UBX0101 (Dolgin, 2020), as well as cardiac glycosides, such as Ouabain, that have broad senolytic activities over multiple senescence inducers suggesting a shared vulnerability between different senescent cell types (Guerrero et al., 2019; Triana-martínez et al., 2019).

The use of senolytics can also be strategically paired with anticancer drugs to promote tumour regression. The sequential treatment of a senescence-inducing agent in tumours followed by the administration of a senolytic drug can induce synthetic lethality in tumours to enhance cancer cell death, and this approach has been termed the "one-two punch approach" (Wang and Bernards, 2018). This strategy has witnessed success in a range of studies *in vitro* that have combined therapy-induced senescence typically with BCL-2 family inhibitors for the treatment of melanoma (Wang et al., 2017a), lung (Saleh et al., 2020), and breast cancer (Shahbandi et al., 2020; Whittle et al., 2020). However, the individual compound "punches" may produce distinct results. For example, for the treatment of melanoma in mice, Vilgelm et al. used a combination of targeted aurora kinase inhibitors to induce senescence, followed by the senolytic treatment of MDM2 inhibitors. Intriguingly, this combination synergistically mediated apoptotic-induced death in senescent melanoma. Moreover, these melanoma cells were capable of secreting an immunomodulatory SASP, including chemoattractive cytokines such as Ccl5 and Cxcl9 that triggered the infiltration of multiple effector immune cells into the tumour microenvironment (Vilgelm et al., 2015).

Despite the therapeutic promise of senolytics, including early phase trials, there remain several barriers to cross prior to large-scale clinical translation of these agents. Although senolytic target pathways

(such as pro-survival gene networks) are upregulated in senescent cells, these pathways are not exclusive to senescence and therefore raise concerns of potential toxicities. In fact, both ABT-263 and dasatinib administration have previously been reported to produce off-target adverse effects, including thrombocytopenia (Kaefer et al., 2014; Owens et al., 2021; Rudin et al., 2012). Additionally, there are concerns regarding even the on-target toxicities produced in response to senolytic therapy. For example, Grosse and colleagues have reported that the inducible ablation of senescent endothelial cells in liver sinusoids can deteriorate normal liver function and generate a fibrotic phenotype (Grosse et al., 2020). Similar to this study, in a physiological setting, senolytic treatment may selectively eliminate untargeted senescent cells, including senescent immune cells, thereby disrupting tissue homeostasis. In addition, it is also important to appreciate that in many cases, senolytic treatment can dampen an age-associated phenotype, and therefore it is likely that these agents will be administered to an elderly population. Thus, the development of senolytic candidates must consider any source of excessive senescent cell death that may occur in the tissues of aged individuals. Overall, senolytics offer incredible potential for the treatment of both senescent-mediated pathologies as well as tumours, yet there are still many qualms regarding the clinical translatability of these drugs, particularly associated with their toxicities. In addition, the complete elimination of senescent cells may revoke any potential initial benefits of the senescence phenotype. Perhaps gaining a more in-depth understanding of the assortment of senescent cell types in various disease contexts at the single cell level may guide the development of tailored senolytic cocktail treatments for specific tissues or tumour types.

1.7.3 Targeting senescence with senomorphics

To overcome some of the apprehensions associated with senolytics, an alternative strategy may be to modulate the chronic inflammation associated with the SASP without eliminating senescent cells (Di Micco et al., 2021). This can be achieved through senomorphic (sometimes senostatics) agents which aim to suppress or abolish an inflammatory SASP.

In most cases, senomorphics target regulators of the SASP. These include compounds interfering with the NF-κB pathway, such as metformin, which improves age-associated insulin sensitivity and can

extend lifespan (Anisimov et al., 2011; Moiseeva et al., 2013); compounds inhibiting BRD4, such as iBET-762, to suppress T1D development (Thompson et al., 2019); and compounds inhibiting the mTOR pathway using rapamycin or its analogues to limit a pro-tumorigenic SASP (Herranz et al., 2015) and to blunt an inflammatory TME (Zhang et al., 2018), among several others drugs. Indeed, in our lab, genetic inhibition of the alternative RNA-splicing factor regulator PTBP1 reduced pro-tumorigenic SASP signalling in senescent preneoplastic hepatocytes without bypassing the growth arrest (Georgilis et al., 2018). Furthermore, as PTBP1 is overexpressed in various cancers (Wang et al., 2017b; Zhu et al., 2020), its inhibition may suppress tumour progression and other inflammation-driven diseases. In line with this, there are a range of drugs that are currently in different stages of clinical trials for age-associated and inflammation-driven pathologies, including type 2 diabetes (Di Micco et al., 2021). From these trials, we can study the extent to which the beneficial effects associated with these compounds are due to senomorphic effects.

However, dampening the SASP, which comprises a plethora of immune recruiting and activating molecules, may also suppress an anti-senescence immune response. This could culminate in senescent cell accumulation and may require additional agents to eliminate the lingering senescent cells, including senolytics or immune-stimulating compounds. Furthermore, in cancer, a suppressed SASP can aggravate tumour growth which could drive drug resistance and tumour relapse (Jerby-Arnon et al., 2018). For example, NF-κB inhibition following TIS in lymphoma-bearing mice sufficiently abrogated the SASP and immune response, eventually leading to senescence bypass and chemoresistance in the p53-deficient tumour (Chien et al., 2011).

An alternative strategy is the direct inhibition of individual SASP molecules. Monoclonal antibodies and drugs inhibiting pro-tumorigenic cytokine signalling have been widely used in cancer therapy, including agents targeting TNFα (Klareskog et al., 2004) or the interaction between IL6-IL6 receptor (Emery et al., 2008) and IL1α/IL1β – IL1 receptors (Hoffman et al., 2008). However, early-phase clinical therapies using this approach have shown limited efficacies when combined with chemotherapy, particularly for treatments with solid tumours (Chibaya et al., 2022a). Furthermore, in the context of senescence and

age-related disorders, the obstruction of individual SASP components from an enriched SASP composition of hundreds of molecules poses questions regarding the feasibility of the treatment.

Senomorphics offer a promising, physiologically subtle alternative solution to the rapid destruction of senescent cells by senolytics. However, senomorphic therapies may require continuous administration to sustain SASP inhibition in a clinical setting, which may be logistically and physiologically challenging. In addition, senomorphic therapy may suppress immune surveillance of senescence, thereby indirectly promoting the accumulation of senescent cells. Whereas senolytic treatment eliminates the senescent cell and any possibility of pro-tumorigenic mutations, especially following TIS, senomorphics result in lingering senescent cells that may undergo mutations to bypass the growth arrest and promote proliferation. Therefore, regardless of senomorphic administration, any persistent senescent cells would require eradication either by means of senolytics or through immune modulators, which may be a caveat of senomorphic therapy.

1.7.4 Targeting senescence by potentiating their immune surveillance

An additional strategy for targeting senescent cells is to sensitise these cells to immune-mediated clearance. Although senolytic therapy can mediate senescent cell death through apoptosis, the immune response will still be required to clear the apoptotic cellular debris, suggesting that directly targeting senescence using the immune system may be a more efficient process. In addition, senolytic activity is generally limited to targeting a few pro-survival pathways, as opposed to the complex regulation of the immune response. As previously described, senescent cell accumulation with age has been largely attributed to the compromised immune-mediated clearance due to both an age-associated decline in immune function (immunosenescence) as well as enhanced immune evasion mechanisms of senescent cells (Akbar et al., 2016; Muñoz et al., 2019; Ovadya et al., 2018; Pereira et al., 2019; Zingoni et al., 2015). As such, there is a critical need to investigate the senescence-immune interaction, through both the surfaceome and secretome of senescent cells, in order to re-establish an efficient anti-senescence immune response.

1.7.4.1 Immunosurveillance through interaction with senescent cell surface proteins

The immune system resembles an intrinsic natural senolytic programme. Several lines of evidence have revealed that the surveillance of senescent cells can be executed by cells from both the innate and adaptive arms of the immune response, including natural killer (NK) cells (Krizhanovsky et al., 2008), CD4+ and CD8+ T cells (Kang et al., 2011; Pereira et al., 2019), and macrophages (Lujambio et al., 2013), among others. Furthermore, senescent cells can communicate directly with most of these immune cells by modulating the expression of immunostimulatory cell surface proteins. For instance, both senescent fibroblasts and senescent tumour cells have been reported to upregulate the expression of MHC molecules to evade T-cell-mediated killing (Pereira et al., 2019; Ruscetti et al., 2020). Also, similar to tumours, senescent cells can elevate the surface expression of immune checkpoint ligands, such as HLA-E and GD3, to escape T cell and NK cell surveillance (Pereira et al., 2019; Iltis et al., 2021).

Depending on the cellular context, various senescence-specific cell surface proteins have been identified that can be targeted using antibodies. These include, but are not limited to, dipeptidyl peptidase DPP4, a marker selectively upregulated during senescence and ageing (Kim et al., 2017), SCAMP4 (Kim et al., 2018; Li et al., 2018), NOTCH1 and NOTCH3 (Cui et al., 2013; Hoare et al., 2016), oxidised and membrane-bound vimentin (Frescas et al., 2017), CD36 (Chong et al., 2018), CD1d (Arora et al., 2021), and uPAR, a urokinase-type plasminogen activator receptor that is broadly expressed in senescent cells (Amor et al., 2020). Exploiting these interactions could offer a direct strategy to target senescence through immunity. For example, targeting CD1d presented on the surface of senescent preadipocytes or lung fibroblasts can trigger invariant natural killer T (iNKT) cell-mediated elimination of senescent cells, resulting in improved glucose regulation and reduced lung fibrosis, respectively (Arora et al., 2021). Targeting senescent cell surface markers was also the rationale behind an innovative study in which Amor and colleagues designed chimeric antigen receptor (CAR)- T cells with specificities towards the uPAR protein in mice. uPAR-specific CAR-T therapy enabled T cell-mediated ablation of senescent lung tumour cells and senescent fibrotic liver cells leading to significant improvements in survival and healthspan (Amor et al., 2020). Consistently, another study has shown

the use of engineered CAR-T cells to alleviate cardiac fibrosis (Aghajanian et al., 2019). These results demonstrate the incredible senolytic potential of guiding immune cell effector functions towards unique senescence markers, and raise questions as to what other senescent cell markers could be targeted and whether other immune cell types, such as NK cells, can be tailored to generate a potent anti-senescence immune response

NK cells are lymphocytes of the innate immune system that are part of the primary defence response against infections, malignant transformation, and induction of cellular stress (Di Vito et al., 2019a, 2019b). Unlike T or B lymphocytes, NK cell activity does not require priming through antigen recognition or through multiple co-activation receptor signalling (Lanier, 2005). Instead, as part of their maturation process, NK cells acquire both activating and inhibitory receptors enabling them to recognise self-cells and governing their cytolytic activity, which could be exploited for therapeutic purposes (Di Vito et al., 2019a, 2019b). Thus, NK cells are widely employed as part of the immune repertoire to rapidly target tumours and senescent cells. Senescent cells use a variety of mediums to communicate with and activate NK cells, including the secretion of SASP components (Antonangeli et al., 2019), senescent ligand interaction with NK receptors (Sagiv et al., 2016), and through the formation of cytoplasmic bridges (Biran et al., 2015). It has been shown that senescent cells elevate levels of activating NKG2D ligands on their surface in multiples modalities of senescence, thereby engaging NK cells to attack following recognition (Iannello et al., 2013; Sagiv et al., 2016). Indeed, active NK cells can generate a potent cytolytic response against senescent cells through the secretion of perforin and granzyme-containing granules via exocytosis (Sagiv et al., 2013).

NK cell-mediated cytotoxicity can be channelled to target senescent tumour cells by enhancing their interaction with senescent cell surface proteins through anticancer agents. For example, administration of low doses of doxorubicin and bortezomib induced senescence within multiple myeloma (MM) tumour cells and upregulated the expression of DNAM-1 and NKG2D activating ligands on their surface, which triggered NK cell-mediated elimination of senescent MM (Soriani et al., 2009). Similar findings have been witnessed in multiple tumour types *in vitro* and *in vivo* (Antonangeli et al., 2019; Gravett et al., 2019; Okita et al., 2016; Poggi et al., 2009; Zingoni et al., 2015). Interestingly, in some contexts, NKG2D

ligands can be cleaved from the surface of senescent tumours through the proteolytic action of metalloproteases as part of the SASP (Muñoz et al., 2019; Zingoni et al., 2015). This can blunt NK interaction with senescent cell ligands and generate chemo-resistant tumours. Therefore, inhibiting these metalloproteases offers a therapeutic opportunity to increase NK cell-mediated killing of senescent cells. Another mechanism of immune evasion by senescent cells is through the raised expression of NKG2A inhibitory ligands on their surface. Pereira and colleagues reported that senescent fibroblasts express HLA-E, a non-classical MHC molecule that can bind to NKG2A inhibitory receptors on NK cells to curtail their response. Knockdown of HLA-E disrupted this interaction and heightened NK cell cytotoxic activity against senescent cells (Pereira et al., 2019). Although it is not fully understood why senescent cells express markers to undergo immune escape, it opens up novel approaches to target senescence through their surface proteins. However, as ligands for NK cell inhibitory receptors are also present at a steady state in healthy cells to prevent self-elimination (Algarra et al., 2004; de Kruijf et al., 2010), albeit at a reduced level compared to senescent cells, the development of any clinical interventions blocking NKG2A receptor interaction with its ligands must be carefully considered and have high specificity for its target.

Novel immune-based strategies that are currently in development for cancer therapy could be redirected to target senescent cells. For example, recent developments in engineering CAR-NK cells (Liu et al., 2020), antibody-mediated blockade of NKG2A receptors as a checkpoint inhibitor (André et al., 2018; van Montfoort et al., 2018), or the development of vaccinations that stably express NKG2D activating ligands (Badrinath et al., 2022) may all bring extraordinary benefits as anti-senescence treatments. Alternatively, a more clear-cut mechanism to promote immune surveillance of senescent cells could be through reprogramming the SASP.

1.7.4.2 Targeting the SASP to potentiate immunosurveillance

The induction of the SASP arouses an immunogenic programme which functions to maintain tissue homeostasis. A significant advantage of adopting SASP-mediated immune surveillance is the high specificity for which senescent cells can be targeted, given that the SASP represents a broad-spectrum

senescence hallmark. In addition, unlike targeting cell surface proteins which stimulate the activity of limited immune cell types, the SASP can activate multiple immune cell populations from the innate and adaptive systems to eliminate senescent cells (Burton and Stolzing, 2018).

1.7.4.2.1 SASP can activate the innate immune response

The first evidence for immune surveillance of senescent cells emerged from Scott Lowe's group, in a pioneering study which demonstrated that the reactivation of endogenous p53 in p53-deficient mice models of hepatocellular carcinoma (HCC) induced a senescence phenotype (Xue et al., 2007). This resulted in elevated expression of SASP-mediated inflammatory cytokines and adhesion molecules, thus activating an immune response that remarkably resulted in tumour clearance and tumour regression *in vivo.* This response was achieved by cells of the innate branch of the immune system, primarily natural killer (NK) cells, macrophages, and neutrophils, which infiltrated the tumour following p53 restoration. Abrogating the expression of these immune cells individually delayed tumour regressions, suggesting that a coordinated response from the three immune cell types is required for rapid senescent tumour clearance. This study was the first of its kind to illustrate the interaction between cellular senescence and the innate immune system; it brought to light a novel function of the SASP in promoting anti-tumour immunity and indicated that the senescence response, as opposed to apoptosis, could pave the way as a powerful approach to target cancers.

Using a similar model of liver carcinoma and the inducible p53 expression system, members of the same group later demonstrated that NK cell recruitment was essential for successfully eliminating the senescent tumour cells (Iannello et al., 2013). The transformed liver cells expressed the ligand RAE1ε (retinoic acid early inducible 1ε), which was detected by NKG2D receptors on the NK cells to promote tumour clearance. Notably, p53 restoration further secreted various SASP chemokines, including CCL2, to facilitate NK cell recruitment and restrict tumour growth.

p53 induction in senescent cells can also drive other innate immune effectors, including macrophages and monocytes, to establish a tumour suppressive microenvironment. For example, Lujambio et al.

have shown that p53-expressing senescent hepatic stellate cells (HSCs) secrete SASP factors which promote polarisation of macrophages towards a tumour-suppressing M1-class capable of eliminating senescent cells. p53-deficient HSCs, on the other hand, did not secrete a SASP response and alternatively promoted M2-class macrophage polarisation, thereby amplifying the proliferation of premalignant hepatic cells (Lujambio et al., 2013). Therefore, secreted SASP components can modulate macrophage activity in HSCs, in a p53-dependent manner.

Indeed, the SASP-mediated immune clearance of senescent cells has been shown to go beyond its role in tumour suppression to facilitate fibrosis resolution (Krizhanovsky et al., 2008). Following liver injury, HSCs differentiate into proliferative fibrogenic myofibroblasts capable of driving liver fibrosis (Tsuchida and Friedman, 2017). However, the induction of senescence in HSCs upregulates the secretion of cytokines, matrix proteases, and NKG2D ligands (specifically ULBP2 and MICA), which promotes NK cell-mediated surveillance of senescent HSCs (Krizhanovsky et al., 2008; Sagiv et al., 2016). Consistent with these findings, the aforementioned study by Lujambio and colleagues also reported that the ablation of the senescence programme in HSCs exacerbates the fibrotic response, leading to the development of cirrhosis and hepatocellular carcinoma (Lujambio et al., 2013). Furthermore, premature senescence induction in liver cells through alternative means using oxidative stress has also been shown to elevate an immunostimulatory SASP that promotes macrophage recruitment (Irvine et al., 2014). All these studies highlight the need for a SASP-mediated innate immune surveillance programme to facilitate the resolution of liver fibrosis and prevent chronic liver diseases.

In a distinct setting, ionising radiation (IR) in osteoblasts can induce RB1-dependent senescence and the expression of a strong SASP, including IL6 (Kansara et al., 2013)**.** In this model, secreted factors were not only necessary for the infiltration of natural killer T (NKT) cells, which limited the development of osteosarcoma, but also to reinforce autocrine and paracrine senescence in bystander non-senescent tumour cells. More recently, investigating irradiation-induced senescence in human pancreatic tumour cells revealed an elevated SASP phenotype that redirects NK cell effector functions to restrict tumour growth (Walle et al., 2022). In fact, therapy-induced senescence is a critical strategy to promote SASP

and immune surveillance, particularly in impeding the development of malignant disorders, and will be discussed in the upcoming section (see Chapter 1.7.5).

1.7.4.2.2 SASP can activate the adaptive immune response

A pivotal study published by the Lars Zender group in 2011 reported that preneoplastic senescent hepatocytes undergo SASP-mediated clearance by the adaptive immune response (Kang et al., 2011). The researchers used an *in vivo* model of $Nras^{G12V}$ oncogene-induced senescence in murine livers to demonstrate that senescent premalignant liver cells secrete factors that orchestrate immune-mediated clearance by antigen-specific CD4+ T cells. However, the complete killing of the senescent cells also required the complementary action of monocytes and macrophages. Premalignant hepatocytes that were transduced with a mutant non-oncogenic form of *Nras* failed to undergo senescence or an immune surveillance programme, ultimately resulting in the development of hepatocellular carcinoma (Kang et al., 2011). Supporting this, another study suggested that the SASP of senescent primary human melanocytes, specifically IL-1β signalling, drives the expression of MHC-II, which can activate T-cell proliferation and suppress melanoma formation (van Tuyn et al., 2017).

Whereas senescent cells can promote T cell recruitment, T cells may equally regulate senescence in cancer cells. Rakhra et al. showed that effector cells of the adaptive immune response, notably CD4+ T cells, are required to sustain senescence growth arrest following *MYC* inactivation in mouse models of T cell acute lymphoblastic lymphoma and leukaemia. Importantly, these immune cells secreted cytokines, including IFNγ, TNFα, and IL-15, which were needed to remodel the tumour microenvironment and inhibit angiogenesis resulting in sustained tumour regressions and complete remission (Rakhra et al., 2010). These observations were critical in illustrating the importance of adaptive immune clearance of senescent cells as an anti-tumour barrier.

1.7.4.2.3 Summary

Collectively, these studies have shown the interplay between senescence, the SASP, and both arms of the immune system in propelling an anti-tumorigenic environment and restoring tissue homeostasis

in senescence-associated disease models. To complicate matters, this process may be disturbed during pathological conditions whereby senescence induction suppresses the immune response. For instance, Eggert and colleagues reported that secretion of SASP components by senescent hepatocytes also directed the recruitment of CCR2+ immature myeloid cells, generating an immunosuppressive environment (Eggert et al., 2016). Furthermore, loss of the *PTEN* tumour suppressor gene induces a senescence-mediated immunosuppressive SASP in prostate tumours (Toso et al., 2014). On a separate note, the cell-of-origin undergoing senescence may significantly impact the net effect of immune surveillance. This was evident in a recent study in which senescent neuroblasts, accumulated in pathological sites in the brains of aged mice, triggered a SASP-mediated NK cell surveillance programme. The clearance of senescent cells led to impaired neurogenesis and cognitive decline (Jin et al., 2021). For this reason, despite the immense therapeutic potential of immune surveillance of senescent cells, any senotherapeutic interventions must take into account the type of senescence induction and pathological state.

1.7.5 Using TIS to promote SASP-mediated anti-senescence immunity

Several anticancer therapies have emerged as strong contenders for inducing senescence and manipulating cancer cell immunogenicity. For instance, treatment with aurora-kinase inhibitors have repeatedly been shown to induce growth arrest and a SASP that can drive immune clearance of melanoma (Liu et al., 2013; Vilgelm et al., 2015). In a different study, PTEN-deficient senescent prostate tumours generated an immunosuppressive tumour microenvironment through JAK2/STAT3 signalling. Combining docetaxel with JAK2 inhibitors was shown to revert the SASP, from pro-senescence to anti-senescence, leading to recruitment of NK cells and immune surveillance of senescent tumours (Toso et al., 2014). This study revealed the scope of using TIS to pharmacologically reprogramme the SASP to favour senescence clearance.

Similar to the aforementioned ‘one-two’ punch approach for senolytic treatments of cancer, the combination of pro-senescence drugs, such as CDK4/6 inhibitors, with an immunomodulating agent offers an exciting strategy to target senescent cells. As described earlier (in Chapter 1.2.3), CDK 4 and 6 inhibitors (CDK4/6i), such as palbociclib, can drive a senescence growth arrest (Polk et al., 2016). In

addition, CDK4/6i can also participate in anti-tumour immunity (Goel et al., 2017). Pharmacological inhibition of CDK4/6 elevates breast cancer cell expression of endogenous retroviral elements, which sparks the production of type III interferons, thereby amplifying tumour antigen presentation (Goel et al., 2017). In addition, these drugs can enhance the vulnerability of target tumour cells to immune checkpoint blockade (ICB) (Burton and Stolzing, 2018). However, it is important to note that although tumours treated with CDK4/6i monotherapy undergo cell cycle arrest, it does not drive a strong inflammatory secretory response (Goel et al., 2017; Ruscetti et al., 2018; Wagner and Gil, 2020). Generally, a low SASP expression is associated with increased treatment resistance, in particular to immunotherapy (Jerby-Arnon et al., 2018). Consequently, this reflects the need for additional treatments synergising with CDK4/6i to upregulate a SASP-dependent immune response. In line with this, a remarkable study from Marcus Ruscetti and other members of Scott Lowe's group revealed that combining palbociclib with the MEK inhibitor trametinib (P+T) was sufficient to reduce cancer cell proliferation and invoke a potent SASP in *KRAS*-mutant lung tumours, capable of driving NK cell cytotoxicity of senescent cells and instigating tumour regressions *in vivo* (Ruscetti et al., 2018). Two follow-up studies in pancreatic adenocarcinomas revealed that P+T therapy combined with gemcitabine or EZH2 inhibition led to increased infiltration of cytotoxic T cells or both NK and T cells, respectively, as well as regressions of the senescent tumour and prolonged survival (Chibaya et al., 2022b; Ruscetti et al., 2020).

While the combination of MEK and CDK4/6 inhibitors represents just one possible approach, it is imperative to identify additional therapeutic agents that sensitise different types of senescent tumours to immune surveillance. For instance, it was recently shown that ovarian high-grade serous carcinoma (HGSC) with p53 deficiencies treated with cisplatin alone produced only a mild senescence and SASP response. The same treatment in p53- and *BRCA1*-mutant ovarian tumours potentiated the senescence and SASP phenotype as well as the recruitment of NK and T cell infiltration but did not increase the killing of senescent cells (Paffenholz et al., 2022). Although genotypic distinctions in the same tumour type may alter the immunomodulatory SASP composition, the subsequent immune response must show cytotoxic activity, and, most importantly, be sustained for tumour regression. As HGSC is among the tumour types with the highest incidences of chemoresistance and recurrence (Wang and Bernards,

2018), cisplatin monotherapy may fail to maintain a durable anti-tumour response. Alternatively, combining cisplatin with immunostimulatory agents could help overcome resistance and produce immune clearance of the senescent tumour. Overall, therapy-induced senescence confers a highly physiologically relevant mechanism to induce a growth arrest in different disease states, particularly cancer, and represents a medium by which the genetic or pharmacological inhibition of fundamental pathways associated with the SASP can stimulate immune effector functions to kill senescent cells. In addition to cancer therapy, whether these strategies can be applied to stimulate an anti-senescence immune response in specific age-associated pathologies would be fascinating to uncover.

1.8 Project aims

Prolonged senescence and its SASP can contribute to chronic inflammation, tumorigenesis, immune decline, and ageing. Mounting evidence has shown that eliminating senescent cells through senolytics can be beneficial in alleviating these disease phenotypes. However, senolytic compounds are limited in their target pathways and have also raised concerns regarding adverse side effects. On the other hand, recent years have witnessed a surge of studies focusing on SASP modulation as a strategy to harness an anti-senescence immune response. NK cells, in particular, have demonstrated potent cytotoxic activity against senescent cells in different tumours or fibrosis models. However, there are limitations to our mechanistic understanding of how senescence interacts with NK cells in different pathological contexts.

With this in mind, the aims of my project are to **identify and characterise novel strategies to potentiate NK-mediated killing of senescent cells**. The approach we are taking is to:

- Perform RNAi screens to identify novel perturbations that reinforce the SASP.
- Based on these hits, perform RNAi screens to identify strategies to potentiate NK-mediated killing of senescent cells.
- Identify candidates that promote NK cell surveillance of different senescent cells.

Chapter 2 – Materials and Methods

2.1 Plasmid preparation

2.1.1 Plasmids

The inducible IMR90 RAS^{G12V} cell line (hereinafter referred to as IMR90 ER:RAS) was produced through the retroviral infection of the pLNC ER:RAS-neo retroviral vector (Young et al., 2009). The generation of this vector has been described in detail in work published by our lab (Innes & Gil., 2019). The construct comprises an ER:RAS fusion protein inducible with 4-hydroxytamoxifen (4-OHT; from herein simply 4OHT) in addition to the neomycin resistance selection marker. The pLXSN retroviral vector was used as an empty vector control.

For generation of IMR90 ER:RASpGIPZ cells, IMR90 ER:RAS cells were stably infected with the lentiviral pGIPZ shRNA vector constitutively expressing TurboGFP (pGIPZ-EV-Puro). The pGIPZ-EV-Puro vector is readily available in our lab and was retrieved from the MRC LMS Genomics core facility library. Infected IMR90 ER:RAS cells were selected by treatment with 1μg/ml puromycin and maintained at a working concentration of 0.5μg/ml.

For generation of IMR90 ER:RAS H2B-GFP cells, IMR90 ER:RAS cells were stably infected with the lentiviral FU-H2B-GFP-IRES-Puro vector (AddGene, #69550) for constitutive expression of a nuclear GFP signal. Infected IMR90 ER:RAS cells were selected by treatment with 1μg/ml puromycin (InvivoGen) and maintained at a working concentration of 0.5μg/ml.

2.1.2 Bacterial transformation

Chemically competent bacteria, either *E. coli* DH5α (for general plasmid amplification) (Invitrogen™) or One Shot™ TOP10 *E. coli* (for transformation of ligation reactions) (Invitrogen™), were defrosted from -80°C and kept on ice to thaw. Next, 100ng of plasmid DNA was mixed with 25μl of bacteria. This mixture was kept on ice for 30 minutes before being subjected to heat shock at 42 °C for 45 seconds, followed again by recovery of bacterial cells on ice for an additional 2 minutes. 175μl of pre-warmed LB broth was then added to the heat-shocked bacterial cells, and the entire mixture was placed on a

shaking incubator for 1 hour at 37^{O}C at 400 rotations per minute (rpm) to allow bacterial transformation. 50µl of plasmid transformation mixture was then spread onto the pre-warmed LB agar plates containing the appropriate antibiotic and streaked carefully across the plate to generate optimal colonies. The plates were then incubated at 37^{o}C overnight for ~18 hours.

2.1.3 DNA purification

Single bacterial colonies were selected and inoculated with 50ml of LB broth with the required antibiotics and incubated on a shaking platform at 37^{O}C for 18 hours at 180rpm. Plasmid DNA was purified using the HiSpeed® Plasmid Midi kit (Qiagen), and the protocol was followed according to the manufacturer's guidelines. Purified plasmid DNA was eluted in 200µl of distilled water and stored at -20^{o}C**.** If larger volumes of DNA were required, bacterial colonies were inoculated with 200ml of LB broth containing antibiotics and the DNA was purified using HiSpeed® Plasmid Maxi kit (Qiagen).

2.2 Tissue Culture

2.2.1 Cell lines

IMR90 human lung diploid fibroblasts (ATCC CCL-186), Human Embryonic Kidney 293T (HEK293T) (ATCC CRL-3216), A549 lung adenocarcinoma (ATCC CCL-185) cell lines were obtained from the American Type Culture Collection (ATCC). IMR90 ER:RAS cells were generated from retroviral infection of IMR90 fibroblasts with pLNC-ER:RAS plasmid vector (see section 2.2.3 for further details on infection). All four cell lines mentioned were maintained in Dulbecco's Modified Eagle's Medium (DMEM, high glucose) (Gibco, 41965120), supplemented with 10% (v/v) foetal bovine serum (FBS) (Sigma) and 1% 100X Antibiotic-Antimycotic solution (Gibco, 15240062), hereafter referred to as 'D10 media'.

The NK92-MI lymphoma natural killer cell line (ATCC CRL-2408) was donated by Professor Valery Krizhanovsky's laboratory at the Weizmann Institute of Science, Rehovot, Israel. NK92-MI cells were maintained in 500ml Minimum Essential Medium (MEM) Alpha no nucleosides (Gibco, 22561054),

supplemented with 12.5% FBS (Sigma), 12.5% FBS Horse Serum (Gibco,16050130), 1% 100X Antibiotic-Antimycotic solution (Gibco), 0.6ml Inositol (Sigma, I7508) and 0.2M filter sterilised, 0.6ml Folic Acid (Sigma, F8758), prepared in 0.1M $NaHCO_3$ and 0.02M filter sterilised, and 4.1µl β-mercaptoethanol (Gibco, 21985023), hereafter referred to as 'NK92 media'.

The ID8 cell lines of either *Trp53*$^{-/-}$ or double *Trp53*$^{-/-}$;*Brca1*$^{-/-}$ genotype were generated and gifted by Professor Iain McNeish's laboratory at Imperial College London, UK. Both sets of ID8 cells were cultured in DMEM with high glucose and sodium pyruvate (Gibco, 11995073), supplemented with 4% FBS (Sigma), 1% 100X Antibiotic-Antimycotic solution (Gibco), 1% 100X Insulin-Transferrin-Selenium (ITS) (Gibco, 41400045), 1% 100X L-glutamine (Gibco, 25030081), hereafter referred to as 'ID8 media'.

All cell lines were maintained using standard tissue culture guidelines in a humid incubator with a temperature setting of 37°C and 5% CO_2 levels. Enzymatic detachment of adherent cell lines from tissue culture plates was accomplished by treatment with 0.05% trypsin-EDTA (Gibco, 25300096). Cell viability and cell quantification were performed by microcapillary flow cytometry using the Guava® Muse® Cell Analyzer (Luminex) or the Guava® easyCyte™ Flow Cytometer (Luminex), with cell suspension being diluted in the Guava® ViaCount™ reagent (Luminex) to allow quantification using the built-in software GuavaSoft™. This software was used to gate live cells and remove cell debris and dead cells from final quantification. For all experiments, all cell lines used had viability above 90%. All experiments using IMR90 and IMR90 ER:RAS cells were performed using cells between passages 10 and 15.

2.2.2 Preservation and generation of cell stocks

Cells were resuspended for cryopreservation and long-term storage in 'cryopreservation media' (D10 medium supplemented with DMSO). IMR90, IMR90 ER:RAS, A549, ID8 and HEK293T cells were detached, centrifuged, and resuspended in D10 medium supplemented with 10% DMSO. For NK92 cells, 5% DMSO was added to the D10 media. 1ml of cells suspended in cryopreservation medium were added to each CryoTube® (Nunc™, 377267) before being immediately transferred to a Nalgene® Mr. Frosty™ freezing container to be stored at -80°C. The freezing container allows gradual cooling at

a rate of 1°C per minute. After approximately 2-4 days, the cryotubes were transferred to liquid nitrogen storage tanks for long-standing cryopreservation.

Cryotubes were thawed in a 37°C water bath to revive cryopreserved cell lines. The cryopreservation medium containing the cells were diluted in the appropriate culture medium (D10, ID8, or NK92 media, depending on the cell line). This was followed by centrifugation and resuspension of the cell pellet in fresh culture medium to remove DMSO. 18-24 hours after thawing, the culture medium was replaced to remove any DMSO remnants, and the cells were then rested for at least 48 hours before passaging cells or plating for experiments.

2.2.3 Production of lentiviral or retroviral supernatants

For transfection, lentivirus and retrovirus were packaged and generated using HEK293T cells. 18-24 hours before transfection, HEK293T cells were quantified and split (at ~ 50% seeding density), so there would be ~80% confluency in 10cm dishes the following day for lentivirus production, or ~ 70% confluency for retrovirus production.

On the day of transfection, a transfection master-mix (TM) was produced. For lentivirus production, the TM comprised: 10µg of the lentiviral plasmid, 8µg of psPAX2 (Addgene), and 2µg of pVSV-G envelope protein plasmid; For retrovirus production, the TM comprised: 8µg of pGAG.pol packaging plasmid (Clonetech) and 2.5µg pVSV-G (Clontech). In both cases, the TM was supplemented with 75µg of 25kDa linear polyethyleneimine (PEI, 75µl of 1mg/ml stock (w/v), Polysciences) and made up to a final volume of 1mL using plain DMEM. The TM was immediately vortexed and incubated at room temperature for 30-45 minutes. During this incubation period, the medium for the HEK293T cells was replaced with 10ml of new D10 media. Following the 30-45 min incubation period, the TM was added to the HEK293T cells in the 10cm dish dropwise manner to prevent any cell disturbance. These cells were then incubated at 37°C for approximately 18 hours, after which the medium was replaced with 10ml of fresh D10 medium to remove any toxicities associated with the PEI. Following another 6 hours (approximately 24 hours after original transfection), 4ml of medium was removed from the HEK293T dish to leave 6ml medium (the reduced volume of D10 medium would increase the concentration of the

viral particles in the culture supernatant). These cells were then incubated again at 37^{O}C for approximately 18 hours. On the same day, target cells were quantified and seeded to prepare for infection at a concentration of 1x10^{6} per 10cm dish.

2.2.4 Lentiviral and retroviral infection

18 hours after changing medium (section 2.2.3), the viral supernatant produced in the medium of transfected HEK293T 10cm dishes was collected and filtered using 0.45µm cellulose acetate membrane filters (VWR International).

For lentiviral infections, this viral supernatant was diluted with D10 media, typically at a 1:4 dilution, to minimise toxicity (however, the dilution was dependent on the viral titre). 4µg/ml of Polybrene (hexadimethrine bromide, 8 mg/ml) (Sigma) was added to the dilute lentivirus to improve infection efficiency. The lentiviral medium then replaced the medium of the target cells, and the cells were then incubated at 37^{O}C for 3-6 hours, after which the dishes were washed with PBS and fresh D10 medium was added.

For retroviral infections, undiluted viral supernatant was complemented with polybrene (4µg/ml) and added to target cells, which were then incubated for 3 hours. During this time, the medium for the transfected HEK293T cells will be replaced with fresh D10 medium to generate more viral supernatant. This retroviral infection was repeated every 3 hours for three sequential rounds, using the viral supernatant continuously generated by the HEK293T cells. After a total of 9 hours of retroviral infection, the target cells were washed with PBS, and fresh D10 medium was added to help cells recover from the infection.

In both cases of lentivirus or retrovirus infection, the infected cells were incubated at 37^{O}C for 72 hours and were subsequently passaged into antibiotic selection, depending on the antibiotic selection marker. Successful antibiotic selection was achieved by comparing the viability of infected cells following

selection with an uninfected control plate. These methods have been described previously by literature published by our group (Georgilis et al., 2018; Guerrero et al., 2019).

2.3 Senescence induction

2.3.1 Oncogene-induced senescence (OIS)

A stock of the inducible stable IMR90 ER:RAS cell line required for the induction of oncogene-induced senescence (OIS) was generated through the retroviral infection of IMR90 fibroblasts with the pLNC-ER:RAS^{G12V}-neo plasmid vector, expressing the constitutively active RAS^{G12V} gene fused to the ligand binding domain of the oestrogen receptor (ER). IMR90 cells infected with the pLNC-ER:RAS^{G12V} vector were selected with 400 μg/ml neomycin. OIS was induced in IMR90 ER:RAS cells by treatment with 100nM 4-Hydroxytamoxifen (4OHT) reconstituted in DMSO (Sigma), which activates the ER:RAS fusion protein. IMR90 ER:RAS cells were typically treated with DMSO or 4OHT medium every 2-3 days, up to 7-8 days, depending on the experiment.

2.3.2 Therapy-induced senescence (TIS)

IMR90 cells underwent TIS upon treatment with 50μM Etoposide (Sigma-Aldrich, E1383) in D10 medium for 48 hours before being washed out with PBS. The medium was replaced with regular D10 medium for the remainder of the culture period.

In A549 cells, senescence was induced by treatment with Palbociclib HCl (Selleckchem, S1116), Trametinib (Selleckchem, S2673), or a combination of both drugs. In most cases, 500nM palbociclib and 25nM trametinib were used in combination. The cells were treated with the D10 medium containing the appropriate drug every 2-3 days for a total of 7-8 days, depending on the experimental settings.

In ID8 cells, senescence was induced by treatment of cisplatin (ApexBio, A8321) at different concentrations depending on the ID8 genotype and the experimental settings. Generally, for *Trp53*$^{-/-}$ ID8 cells, 1μM cisplatin was used; for *Trp53*$^{-/-}$*;Brca1*$^{-/-}$ ID8 cells, 375nM cisplatin was administered.

2.4 Growth and survival assays

2.4.1 5-Bromo-2'-deoxyuridine (BrdU) incorporation assay

5-Bromo-2'-deoxyuridine (BrdU) incorporation assay was used to assess cell proliferation, as cells incorporate 5-Bromo-2'-deoxyuridine as a thymidine analogue into the DNA if they are dividing. For IMR90 ER:RAS cell lines, $2x10^3$ and $3x10^3$ cells per well were seeded in triplicates into 96-well plates (Nunc™ MicroWell™, 167008) for DMSO (control) and 4OHT (OIS) conditions, respectively, and were left to adhere overnight. The following day, cells were treated with DMSO or 100nM 4OHT medium every 2-3 days according to their condition throughout the cell culture. 10μM BrdU was added to the cells 18 hours before the required fixation time point. After 18 hours, the wells of the 96-well plates were washed once in PBS and immediately fixed using 4% Paraformaldehyde (w/v, PBS) for approximately 45 minutes before removal and further three washes with PBS.

For A549 cells, $0.25x10^3$ cells per well (DMSO condition), $0.5x10^3$ cells per well (Palbociclib, 500nM), $1x10^3$ cells per well (Trametinib, 25nM), and $4x10^3$ cells per well (Palbociclib 500nM + Trametinib 25nM combination) were seeded in 96-well plates and allowed to adhere overnight. The next day, cells were treated with the appropriate drug according to each condition. 8 hours before the desired time point, 10μM BrdU was added. After this time, the A549 cells were fixed.

For both *Trp53*$^{-/-}$ and *Trp53*$^{-/-}$*;Brca1*$^{-/-}$ ID8 cells, $0.1x10^3$ cells per well (DMSO condition) and $0.5x10^3$ cells per well (Cisplatin, 1μM), were seeded in 96-well plates and allowed to adhere overnight. The next day, cells were treated with DMSO or cisplatin according to each condition. 16 hours before the desired time point, 10μM BrdU was added; after this time, the ID8 cells were fixed.

Wells from BrdU fixed plates were maintained in PBS and were either stored at 4^OC after fixation for up to 2 weeks or stained immediately via immunofluorescence. BrdU incorporation quantification and analysis were performed using the InCell Analyser 2500HS (GE Healthcare) high-throughput analysis system (see section 2.5).

2.4.2. Crystal violet staining

IMR90 ER:RAS cells were seeded at a low density of $1x10^5$ cells in 10cm dishes for this assay. Cells were then treated with DMSO or 100nM 4OHT (to induce oncogene-induced senescence) and cultured for approximately 14 days, or until the DMSO-treated control cells reached over 90% confluency.

For A549, cells were seeded at a density of $3x10^3$ per well in 6 well plates (**Nunc™, 140675)** and were treated with DMSO or to induce senescence with a combination of Palbociclib and Trametinib.

For ID8 cell lines, both *Trp53*$^{-/-}$ and *Trp53*$^{-/-}$*;Brca1*$^{-/-}$ cells were seeded at a density of $5x10^3$ (DMSO) and $1x10^4$ (Cisplatin) in 6 well plates and were treated with DMSO or to induce senescence with Cisplatin.

Regardless of the cell line, upon the experimental end-point, cells were fixed with 0.5% (w/v, PBS) glutaraldehyde (Sigma) for 1 hour. Cells were then washed three times with dH_2O and left to be air-dried for approximately 2 hours at room temperature. Dry plates were stained with 0.2% (w/v, PBS) crystal violet solution (Sigma, C6158) for 1 hour on a shaking platform before washing twice with dH_2O and left to be air-dried again overnight. Scanned images of plates were then taken using the HP Scanjet 4850 photo scanner.

2.4.3 Senescence associated β-Galactosidase (SA-β-Gal) assay

For OIS, IMR90 ER:RAS cells were seeded in 6 well plates at a density of $2x10^4$ and allowed to adhere overnight. The cells were treated with DMSO or 100nM 4OHT medium as appropriate and cultured for 8 days before being fixed with 0.5% glutaraldehyde (w/v, PBS) (Sigma) for 15 minutes.

For A549, cells were seeded in 6 well plates at a density of $1x10^3$ (DMSO), $1x10^4$ (Palbociclib or Trametinib), and $2x10^4$ (combination) and allowed to adhere overnight. The cells were treated with DMSO or the corresponding drug and cultured for 8 days before being fixed with 0.5% glutaraldehyde (w/v, PBS) (Sigma) for 15 minutes.

For both *Trp53*$^{-/-}$ and *Trp53*$^{-/-}$*;Brca1*$^{-/-}$ ID8 cell lines, cells were seeded in 6 well plates at a density of $5x10^3$ (DMSO), $1x10^4$ (Cisplatin) and allowed to adhere overnight. The cells were treated with DMSO or the corresponding drug and cultured for 8 days before being fixed with 0.5% glutaraldehyde (w/v, PBS) (Sigma) for 15 minutes.

In all cases, following fixation, cells were washed three times with 1mM $MgCl_2$ in PBS at pH 6.0 and then incubated with X-Gal staining solution (1mg/mL X-Gal (ThermoFisher Scientific™, R0402), K3[Fe(CN)6] and 5 mM K4[Fe(CN)6]) between 8 to 18 hours at 37°C. Following this incubation period, the cells were washed with dH_2O and imaged using a DP20 digital camera attached to an inverted light microscope (Olympus CKX41). All cell lines were imaged at a 10x objective, with the exception of ID8 cells that were imaged at a 4x objective. Quantification of percentage positive SA-β-gal cells was calculated by manually counting a minimum of 200 cells per condition per replicate using FIJI software.

2.5 RNA processing and expression analysis

2.5.1 RNA isolation and purification

For total RNA isolation, $0.8\text{-}2x10^5$ IMR90 ER:RAS cells were seeded in 6cm dishes cultured for the required duration in the presence or absence of 4OHT. Following this period, cells were dissociated using trypsin, centrifuged to obtain a pellet, and the supernatant was aspirated. The pellet was resuspended once with PBS for washing, and the cells were centrifuged again. PBS was then aspirated carefully to collect a cell pellet prior to lysis. Total RNA from the cell pellet was then isolated and purified using the RNAeasy® Mini Kit (Qiagen), starting from step 2 onwards, according to the manufacturer's protocol. Total RNA isolated was eluted in 30-50µl of RNAse-free water, and RNA concentration was quantified using the Nanodrop® ND-1000 UV-Vis spectrophotometer. RNA was stored at -80°C for long-term preservation. An identical protocol was performed for RNA extraction from A549 and ID8 cells with adjustments only to cell seeding densities and drug treatments.

2.5.2 Complementary DNA (cDNA) synthesis

For cDNA synthesis, 1-5µg of RNA was used and mixed with 2µl of 50 ng/µl Random Primers (Invitrogen™), 2µl of dNTP mix (10mmM, Bioline) and RNAse-free water to a final volume of 24µl (termed the RNA master mix). The RNA master mix was heated to 65°C for 5 minutes and rapidly cooled to 4°C. Next, a reverse transcription master mix was generated using 8µL of 5x First strand buffer, 4µL of 0.1M DTT, 2µL of RNaseOUT™ recombinant ribonuclease inhibitor (Invitrogen™, 10777019), 2µL of 200U/µL SuperScript® II RT reverse transcriptase, totalling 16µL. The reverse transcription master mix was then mixed with 24µL of the original RNA master mix to provide a total volume of 40µL. The complete mix was then treated under the following conditions: 25°C for 10 minutes, 42°C for 50 minutes, 70°C for 15 minutes, using the Dyad® Peltier Thermal cycler (Bio-Rad).

2.5.3 Quantitative RT-PCR (RT-qPCR)

For quantitative RT-qPCR, the cDNA samples were diluted to 10ng/µL according to the initial RNA concentration, and, if needed, the cDNA was stored at -20°C. mRNA expression analysis with RT-qPCR was performed using the CFX96TM Real-Time PCR Detection system (Bio-Rad). 4µl of diluted cDNA was mixed with 5µl of RNAse-free water, 0.5µl each of both forward and reverse primer (10 µM) and 10µl of SYBR® Green PCR Master Mix (Applied Biosystems) to a total volume of 20µl, and added in each well of a Hard-Shell® 96-Well PCR Plates, low profile, thin wall, skirted plates (Bio-Rad, HSP9655). Each RT-qPCR reaction was performed in triplicate. These plates were then cycled under the following conditions: 2 minutes at 52 °C (step 1), 5 minutes at 95 °C (step 2), 30 seconds at 95 °C (step 3), 30 seconds at 60 °C (step 4), 15 seconds at 72 °C (step 5). Following this, steps 3 to 5 were repeated an additional 39 times, and the fluorescence measurements and CT (cycling threshold) values were determined at the end of each cycle.

Forward and Reverse primers were designed using the online tools: PrimerBank or NCBI Primer-BLAST. To design optimal primer sequences, the primers must span exon-exon junctions, anneal to all splice variants of the gene of interest, and be less than 150bp in length. See Table A3 and A4 in the appendix for a complete list of RT-qPCR primers used in this thesis.

The delta-delta CT method ($2^{-\Delta\Delta Ct}$) was applied to the resulting CT values obtained during the amplification phase to calculate relative mRNA expression levels. RPS14 (human) and GAPDH (mouse) were used as the housekeeping control for normalisation, and an untreated sample was used as an internal relative control (DMSO).

The $2^{-\Delta\Delta Ct}$ method calculation is as follows:

$$\Delta\Delta Ct = \Delta Ct_{treated} - \Delta Ct_{control} \,/\, \Delta Ct = Ct_{target} - Ct_{housekeeping}$$

2.6 Protein expression analysis

2.6.1.1 Immunofluorescence (IF)

Prior to immunofluorescence (IF) staining, cells were seeded in 96-well plates (Nunc™ MicroWell™, 167008) and cultured, as required. At the desired timepoint, cells in the 96-well plates were washed once with PBS and then fixed using 4% PFA (w/v, in PBS) for 45 minutes, followed by three washes with PBS. For IF staining, fixed wells in 96 well plates were permeabilised using 0.2% Triton® X-100 (v/v, PBS) for 10 minutes while keeping the plate on a shaker platform at room temperature. Wells were then washed with PBS twice to stop further permeabilisation, and then the blocking solution was added to the wells for 1 hour. Plates were placed on a shaker platform. The blocking solution comprised of 1% BSA (w/v, PBS) supplemented with 0.2% Fish Skin Gelatin (v/v, PBS). Primary and secondary antibodies were diluted in the same blocking solution (see Table A5 and A6 for further details on antibodies, manufacturers, and dilutions). After 1 hour, the blocking solution was removed from the plates, and the wells were then incubated with primary antibody solution for 1 hour on a shaker platform. However, in the case of BrdU IF staining, the primary antibody solution comprised the Anti-BrdU antibody (Table A5) supplemented with 0.5U/ul DNase (Sigma) and 1mM $MgCl_2$; therefore, the primary antibody incubation time was only 30 minutes. For the primary and secondary SASP-reinforcer siRNA screens, the IF performed for the SASP readouts comprised a 2-hour primary antibody incubation period. Following primary antibody incubation, the wells were washed three times with PBS and then incubated with the secondary antibody solution for 1 hour in the dark. Secondary antibodies were conjugated to Alexa-594 (Red) or Alexa-488 (Green) fluorophores and were diluted in the blocking

solution. Plates incubated with the secondary antibody solution were wrapped in foil to limit exposure to light. Following incubation, secondary antibodies were removed, and the plates were washed three times with PBS. DAPI solution (1µg/mL DAPI; w/v, PBS) was added to the wells for 10 minutes for nuclei counterstaining, and the plates were again wrapped in foil to prevent light exposure during DAPI incubation. Next, the wells were washed three times with PBS. Wells were stored in PBS at 4°C until high-throughput imaging was performed.

2.6.1.2 High throughput microscopy and quantitative analysis

Images of wells from 96-well plates were acquired using the IN Cell Analyzer 2500HS high-throughput microscope and plate reader (Cytiva). For automated image acquisition of multiple 96-well, all plates were stacked into designated stack holders, which allowed the KiNEDx Robotic arm (PAA) operating the Overlord™ (PAA) software to collect each plate, load it into the In Cell Analyzer 2500HS apparatus, capture images of each plate, and remove each plate following image acquisition. For images of only DAPI (for example, for NK cell co-culture assays), images of wells were captured at a 10X objective. For all IF stainings, wells were imaged with a 20X objective with the exception of BrdU staining (imaged at 10X objective). Fluorescent images of fluorophores were captured based on the pre-set wavelength settings for 'DAPI' (for DAPI staining), 'Red' (for AlexaFluor® 594), and 'Green' (for AlexaFluor® 488) on the IN Cell microscope. In general, when using the 10X objective, the whole well was imaged by capturing 9 fields. When using the 20X objective, 16 fields per well were captured.

High content analysis (HCA) of acquired images was performed using the IN Cell Investigator 2.7.3 software (GE Healthcare®). DAPI nuclear staining was used as a nuclear mask to quantify of cells and allow segmentation of cells based on a Top-Hat method, according to the software guidelines. This method also allowed the detection of nuclear-localised antibody staining. Nuclear stainings were quantified by the average pixel intensity within the nuclear mask. Cytoplasmic staining was quantified after applying a collar of 6-9µm around the DAPI mask. Cytoplasmic-localised staining was quantified either by the average pixel intensity or by measuring the coefficient of variance (CV) pixel intensity within the cell collar. Detection of percentage positive cells was based on a threshold, typically set

according to the average pixel intensity of an internal negative control or an unstained secondary-antibody-only control sample, unless specified.

2.6.2 ELISA

2.6.2.1 Generation of Conditioned Medium (CM)

0.3 x 10^5 or 1.0x10^5 IMR90 ER:RAS cells were seeded in 6-well plates for the DMSO and 4OHT conditions, respectively. The following day DMSO and 4OHT treatments were administered as appropriate. Any compounds used were administered four days after DMSO/4OHT treatment. After seven days of DMSO/4OHT treatment, the D10 medium was replaced with serum-free D10 medium and maintained in culture for 48-72 hours to generate CM. After this timepoint, CM was collected, centrifuged to remove cellular debris, and aliquoted to be stored at -80^{o}C.

2.6.2.2 ELISA assays

To detect secreted cytokines from the CM, ELISAs were performed using kits for IL6 (DY206), IL8 (DY208), and CXCL10 (R&D Systems, DY266), according to the manufacturer's guidelines. For absorbance measurements, readings were taken using a SPECTRAmax® 340PC Microplate Spectrophotometer (Molecular Devices) at 450nm.

2.7 NK cell-based assays

2.7.1 NK cell-mediated cytotoxicity assay

Two methods were used to measure NK-mediated killing of senescent cells. The first used a live cell imaging and microscopy platform, and the second used high-throughput imaging and microscopy.

2.7.1.1 Live cell imaging and analysis of NK-mediated killing of senescent cells

IMR90 ER:RASpGIPZ and IMR90 ER:RAS H2B-GFP cells (see Section 2.1.1) were seeded in 96-well plates and allowed to adhere overnight (‘day -1’). An additional replicate plate was also seeded, labelled as ‘Time 0 plate’. The following day (‘day 0’), cells were treated with DMSO or 100nM 4OHT until the desired timepoint (7-8 days, depending on the experiment). Medium was replaced every 3-4 days. On the day of co-culture, ‘Time 0 plate’ was fixed with 4% Paraformaldehyde (w/v, PBS) for 20 minutes, followed by 10-minute incubation with DAPI solution (1µg/mL DAPI; w/v, PBS) to label the nuclei. Cell counts from the ‘Time 0 plate’ were quantified based on the number of stained nuclei to determine the correct effector to target cell (E:T) ratio of NK cells required, using the IN Cell Analyzer 2500HS (Cytiva). NK92-MI cells were stained red with 1µM CellTracker™ Red CMTPX Dye dye (Invitrogen, C34552) for 30-45 minutes, according to the manufacturer’s instructions. NK cells were then added to the 96-well plates containing IMR90 ER:RAS cells at the required effector to target cell (E:T) ratios in triplicates. Additional triplicate control wells received only medium alone without NK cells. For the duration of the co-culture, cells were maintained in regular D10 growth medium unless otherwise stated. Co-cultures were imaged every 2 hours using a 10X objective up to the end timepoint (usually around 48 hours) using the Incucyte® Live-Cell Analysis Systems (Sartorius). NK cell-mediated cytotoxicity was assessed by the percentage change in IMR90 ER:RAS cell confluency during the co-culture period using the built-in Incucyte® Zoom software (Essen Bioscience).

2.7.1.2 High-throughput imaging and analysis of NK-mediated killing of senescent cells

NK cell-mediated cytotoxicity was measured using the IN Cell Analyzer 2500HS high-throughput microscope and plate reader (Cytiva). The assay was performed similarly to that described above with, with a few adjustments. Fluorescent reporter expression in cells was not required. IMR90, IMR90 ER:RAS, or A549 cells were seeded in 96-well plates and allowed to adhere overnight (‘day -1’). At least one additional replicate plate was also seeded labelled as ‘Time 0 plate’. The following day (‘day 0’), cells were treated with the appropriate senescence inducer until the required timepoint (~7-8 days). Medium was replaced every 3-4 days. Any drugs tested to promote or inhibit NK-mediated cytotoxicity were added at ‘day 4,’ i.e. four days following senescence induction.

On the day of co-culture, cell numbers from the 'Time 0 plate' were quantified as described above. NK92-MI cells were then starved in plain DMEM lacking FBS for 30-45 minutes before being added to the 96-well plates cells in triplicates at the required effector to target cell (E:T) ratios. Additional triplicate wells received only medium alone without NK cells as a control. For the duration of the co-culture, cells were maintained in regular growth medium in the absence of drugs unless otherwise stated. Plates were incubated at 37^{o}C for the desired time (typically 48 hours). Plates were then fixed using 4% Paraformaldehyde (w/v, PBS) for 20 minutes, followed by 10-minute incubation with DAPI solution (1µg/mL DAPI; w/v, PBS) to label the nuclei. Following the co-culture, all plates were fixed, stained with DAPI, and imaged using the In Cell Analyzer 2500HS (Cytiva). NK cell-mediated cytotoxicity was assessed by the percentage change in DAPI-positive cell counts during the co-culture period using the InCell Investigator 2.7.3 software.

2.7.2 NK cell chemotaxis assay

2.7.2.1 Generation of Conditioned Medium (CM)

For IMR90 ER:RAS cells, 0.6 x 10^6 or 1.2x10^6 cells were seeded for DMSO control or 4OHT treatment, respectively, in 10cm dishes. The following day, medium was replaced with D10 medium containing DMSO or 100nM 4OHT as appropriate. After three days, the medium was replaced with serum-free DMEM, high glucose, no glutamine, no phenol red medium (Gibco, 31053028) containing DMSO or 4OHT, as appropriate to generate conditioned medium (CM). After an additional three days, the CM was collected from the 10cm plates and centrifuged (2000rpm, 4^{o}C, 15 minutes) to remove cellular debris. The supernatant (i.e. the CM) was then filtered through a 0.2µm pore size cellulose acetate membrane (Gilson) and concentrated by ultracentrifugation (2500rpm, 4^{o}C, 30 minutes) using Vivaspin 20 5kDA/10kDa MWCO columns (Sigma-Aldrich, GE28-9323-60). The concentrated CM was then aliquoted and was stored at -80^{o}C or directly used to perform the chemotaxis assay (below)

For A549 cells, 1.0 x 10^5 or 4.0x10^5 cells were seeded for DMSO control or drug-treatment conditions, respectively, in 10cm dishes. The following day, medium was replaced with D10 medium with the

presence or absence of drugs, as appropriate. The medium was replaced three days later ('day 3'). On 'day 5', the medium was replaced with DMEM (Gibco) supplemented with 0.5% FBS (Sigma), 1% antibiotic-antimycotic solution (Gibco), 1% 100X L-glutamine (Gibco), 1% 100X sodium pyruvate (Gibco), and 1% 100X MEM Non-Essential Amino Acids (Gibco). 72 hours later ('day 8'), the CM was collected from the 10cm dishes for each condition and centrifuged (2000rpm, 4^{o}C, 15 minutes) to remove cellular debris. The supernatant was then filtered through a 0.2µm pore size cellulose acetate membrane (Gilson), aliquoted, and either the chemotaxis assay was performed (described below) or the CM was stored at -80^{o}C.

2.7.2.2 Chemotaxis assay

The protocol for the chemotaxis assay was initially derived from Valery Krizhanovsky's lab (Weizmann Institute of Science, Israel) and was slightly adjusted. NK92-MI cells were starved for 4 hours in serum-free 'complete media' supplemented as described above but without FBS. After 4 hours, NK cells were centrifuged and replaced with 'complete media'.

For IMR90 ER:RAS cells, the concentrated CM was diluted to a final concentration of 162 ng/µl in 'complete media'. 600µl of CM from each condition was added in triplicates to the bottom chamber of a 6.5mm Transwell® apparatus with an 8.0µm pore polycarbonate membrane Insert (SLS, 3422). 200µl containing $2.0x10^5$ NK cells were added to the upper chamber. 600µl unconditioned medium was used as an internal negative control. As an additional control condition, NK cells were also treated with 1µM of the CXCR2 inhibitor SB225002 (ApexBio, B8200). As positive controls, 600µl unconditioned medium supplemented with 100ng/ml recombinant CXCL10 (R&D Systems, 266-IP-010/CF) or 100ng/ml CCL5 (R&D Systems, 278-RN-010/CF) were used.

For A549 cells, 600µl of undiluted CM from each condition was added in triplicates to the bottom chamber of a 6.5mm Transwell® apparatus. 200µl containing $2.0x10^5$ NK cells were added to the upper chamber. 600µl unconditioned medium was used as an internal negative control. 600µl unconditioned medium supplemented with 100ng/ml recombinant CXCL12 (R&D Systems, 350-NS) was used as a positive control.

The cells in the Transwell® apparatus were incubated for 21 hours at 37°C. For total cell calculation, 200µl of unconditioned medium containing 2.0x10^5 NK cells were incubated in separate tubes. After the incubation time, the number of cells at the bottom chamber were counted using Guava ViaCount® reagent (Millipore) and the associated GuavaSoft software. The following equation determined the percentage of NK cell migration:

$$\%\ NK\ cells\ migrated = \frac{(\text{Number of NK cells migrated towards CM} - \text{Number of NK cells migrated towards negative control})}{\text{Total NK cell count}} \text{ X } 100$$

2.8 siRNA screening for SASP reinforcers

2.8.1. siRNA genome library and transfection

Druggable genome siRNA libraries were purchased from Horizon Discovery (human siGENOME SMARTpool). Custom-designed siRNA library plates and individual siRNAs were purchased from the siGenome siRNA reagent-Human catalogue from Dharmacon (Horizon Discovery), and all plates arrived lyophilised coated onto 96-well plates (0.1nM) or in a tube (for individual siRNA orders). The siRNA 96-well plates (0.1nM) were reconstituted in 100µL of nuclease-free water and aliquoted appropriately in round bottom 96-well (Nunc™, 163320) daughter plates for storage at -20°C. For siRNA transfection, 3.6µL of aliquoted siRNA was added to new flat-bottom 96-well plates (Nunc™ MicroWell™, 167008). A 'transfection mix' was generated comprising 17.5µL of plain DMEM (Gibco) and 0.1µL DharmaFECT™1 transfection reagent per well (Horizon Discovery, T-2005-01). 17.6µL of the transfection mix was added to each well already containing 3.6µL siRNA (or for mock wells, containing 3.6µL water), and the mixture was incubated at room temperature for 30 minutes. For reverse transfection, IMR90 ER:RAS cells were first quantified, and 100µL of cell suspension (in D10 medium supplemented with only 10% FBS but no antibiotics) was added to the 96-well plates (containing siRNA and transfection mix) at the appropriate seeding density. This resulted in a final siRNA concentration of 30nM, and the plates were incubated at 37°C for 18 hours to allow cells to adhere and be reverse transfected (at 'day -1'). Following this period, the transfection medium was

discarded and replaced with fresh D10 medium supplemented with the presence of DMSO or 4OHT as appropriate (at 'day 0'). Four days following the initial DMSO/4OHT treatment ('day 4'), medium was replaced again. Seven days after the initial DMSO/4OHT treatment ('day 7'), cells were fixed in 4% PFA (w/v) for 45 minutes (for IF) and washed and stored in PBS at 4°C. For measuring SASP components, IF was performed (see Chapter 4).

2.8.2 Normalisation of the screen results

2.8.2.1 B score normalisation:

For the primary siRNA screens, B score normalisation was performed using the CellHTS2 package on R (Boutros et al., 2006). All data were assigned a normalised B-score using the plate-averaging method based on separate plate batches of transfection (see Chapter 4). A threshold was set to determine the hits.

2.8.2.2 Normalised Percent Activation (NPA):

For the analysis of smaller scale secondary siRNA screens (that are biased for hits), a distinct control-based normalisation method was used termed the Normalised Percent Activation (NPA), whereby the expression of SASP factors from each siRNA sample is normalised to the positive and negative controls within each 96-well plates. Each siRNA is then assigned an NPA score based on the following calculation:

$$NPA = \frac{(X_i - \bar{C}_{neg})}{(\bar{C}_{pos} - \bar{C}_{neg})}$$

where X_i is the percentage positive value of SASP for the sample measurement on the i^{th} siRNA, $\bar{C}_{neg}$ and $\bar{C}_{pos}$ are the means of the percentage positive SASP values of the negative and positive controls, respectively, in the SASP reinforcer screen.

2.9 Screen for siRNAs enhancing NK-mediated killing of senescent cells

2.9.1 siRNA transfection for the screen for siRNAs enhancing NK-mmediated killing of senescent cells

siRNA transfection for this screen followed an identical protocol to that of siRNA transfection of SASP reinforcers in section 2.6 with a few changes. Seven days following the initial DMSO/4OHT treatment ('day 7'), NK cell co-cultures were performed with the siRNA-transfected IMR90 ER:RAS cells following the protocol described in Section 2.6.1 using the high-throughput imaging method. NK cells were co-cultured with growing and senescent siRNA-transfected cells for 48 hours. Following this period, all plates were fixed with 4% PFA (w/v) for 20 minutes and stained with DAPI for 10 minutes before being imaged using the In Cell Analyzer 2500HS workstation (Cytiva). Cell quantification was performed using the IN Cell Investigator 2.7.3 software. Percentage change in cell counts was measured based on the change in IMR90 ER:RAS DAPI-positive cell numbers over 48 hours of co-culture in the presence or absence of NK cells. The normalised percent activation (NPA) criterion was used to normalise percentage change in cell counts between multiple plates, batches, and replicates.

2.9.2 Assays for drugs enhancing NK-mediated killing of senescent cells

Investigating the changes in NK-mediated killing of senescent cells following drug treatment followed the same protocol described in section 2.6.1, with a few adjustments. IMR90 ER:RAS cells were seeded at $2x10^3$ cells/well for DMSO condition and $3x10^3$ for 4OHT condition in 96-well plates and incubated at 37°C for 18 hours to allow cells to adhere ('day -1'). DMSO or 4OHT medium was added to maintain cell growth or induce senescence in cells, respectively ('day 0'). After four days ('day 4'), medium was replaced, but different concentrations of chemical inhibitors were added at the appropriate concentrations into the wells of the 96-well plates in triplicates. Three days after the addition of the inhibitors, the 96-well plates would undergo NK cell co-culture to assess NK-mediated killing of siRNA-transfected control or senescent IMR90 ER:RAS cells (section 2.6.1). The list of compounds investigated is presented in Table A7.

2.10 RNA sequencing and analysis

For OIS IMR90 ER:RAS cells or TIS IMR90 cells, RNA extraction was performed by another lab member, Verena Wagner. RNA-Sequencing was performed by the MRC LMS Genomics core facility. For OIS WI-38 cells, RNA-Seq datasets were retrieved from Casella et al (Casella et al., 2019).

Differential expression analyses of all datasets were performed using the DESeq2 package on R. For GSEA, differentially expressed genes were ranked according to their expression using the pre-ranked function on GSEA v4.0.3 (Broad Institute). Significant enrichment of gene sets was considered if the normalised enrichment score (NES) was >1.0, with a false discovery rate (FDR) lower than <0.25 (Subramanian et al., 2005). Gene sets used for GSEA were either obtained from built-in 'gene ontology' or 'curated' databases v7.5 (Broad Institute) or curated previously from our lab (Acosta et al., 2013).

Chapter 3 - Establishing a system to study senescence surveillance by Natural Killer cells

3.1 Introduction

Several lines of evidence have recently demonstrated that senescent cells are susceptible to innate and adaptive immune surveillance, typically driven by secreted immunomodulatory SASP factors (Kale et al., 2020). Immune-mediated removal of senescent cells, in particular by T cells and macrophages, is beneficial in the treatment of age-associated pathologies, to delay tissue dysfunction or as a cancer therapy (Kang et al., 2011; Lujambio et al., 2013; Rakhra et al., 2010; Sturmlechner et al., 2021; Xue et al., 2007). Recently, interest has emerged in Natural Killer (NK) cells as alternative immune candidates for senescence clearance. NK cells have been reported to directly eliminate senescent tumour cells (Chaturvedi et al., 2022; Paffenholz et al., 2022; Ruscetti et al., 2018) as well as regulate non-malignant senescent states, for instance, to limit fibrosis (Krizhanovsky et al., 2008) and to maintain tissue homeostasis (Brighton et al., 2017). In addition, NK cells, unlike T cells, do not require priming or prior activation and can kill senescent cells in an antigen-independent manner. Despite their promise, the ability of NK cells to effectively surveil different senescent cells- and whether this can be exploited therapeutically- requires further understanding.

The objective of this thesis is to identify novel strategies to potentiate an immunogenic SASP and an anti-senescence NK cell response. We postulate that an increased SASP would potentiate NK cell-mediated killing of senescent cells and can be exploited to treat malignancy and other pathophysiological conditions. Therefore, in this chapter, we aim to establish a co-culture system that can serve to quantify NK cell-mediated cytotoxicity of senescent cells and reflects suitable physiological conditions.

3.2 Characterising a model of oncogene-induced senescence

Cellular senescence can be induced in response to an array of cellular insults such as oncogene overexpression, replicative stress, and therapeutic drugs (Guillon et al., 2019). Among the different

senescence inducers, oncogene-induced senescence (OIS) has been used in our group to identify novel regulators of senescence and SASP (Acosta et al., 2013; Georgilis et al., 2018; Tordella et al., 2016) as well as novel senolytic candidates (Guerrero et al., 2019). Indeed, *in vivo* studies have also identified OIS as a tumour protective mechanism that prevents preneoplastic cells from developing malignant lesions through its growth arrest and immunomodulation properties (Iannello et al., 2013; Kang et al., 2011), making it an ideal mechanism for understanding the interplay between senescence and NK cells.

To model OIS *in vitro*, we used the well-established inducible IMR90 ER:RAS system (Innes and Gil, 2019), in which the oncogenic $HRAS^{G12V}$ transgene has been fused to the ligand binding domain of the oestrogen receptor to form the inducible ER:RAS construct. Administration of 4-hydroxytamoxifen (4OHT) to ER:RAS, but not endogenous oestrogen, activates the exogenous oestrogen receptor resulting in $HRAS^{G12V}$ activation and induces an arrest mediated by the $p53/p21^{CiP1}$ and $Rb/p16^{INK4a}$ tumour suppressor pathways (Young et al., 2009). Here, IMR90 primary foetal lung fibroblasts were retrovirally infected with the ER:RAS construct (pLNC-ER:RAS) or a plasmid vector control (pLXSN) (Figure 3.1A). Upon 4OHT treatment, IMR90 cells infected with ER:RAS (henceforth, IMR90 ER:RAS) exhibited several characteristics of senescence. Specifically, they underwent a stable growth arrest (Figure 3.1B) and a significant reduction in BrdU incorporation (Figure 3.1C). Furthermore, IMR90 ER:RAS cells undergoing OIS displayed an accumulation of ɣH2AX foci (Figure 3.1D). These cells also showed a significant increase in the expression of key tumour suppressor proteins $p16^{INK4a}$ and $p21^{CIP1}$ (Figure 3.1E & F), as well as elevated levels of senescence-associated β-galactosidase (SA-β-gal) activity (Figure 3.1G), corresponding to the increased lysosomal compartment associated with senescence (Dimri et al., 1995). At the RNA level, we validated the upregulation of *CDKN2A* and *CDKN1A* (encoding $p16^{INK4a}$ and $p21^{CIP1}$, respectively), as well as *PLAUR,* which has recently been reported as a senescence biomarker (Amor et al., 2020). We also observed a decline in *LMNB1* mRNA levels (encoding Nuclear lamin B1) (Figure 3.1H). Taken together, the above data shows that 4OHT treatment of IMR90 ER:RAS cells recapitulates OIS.

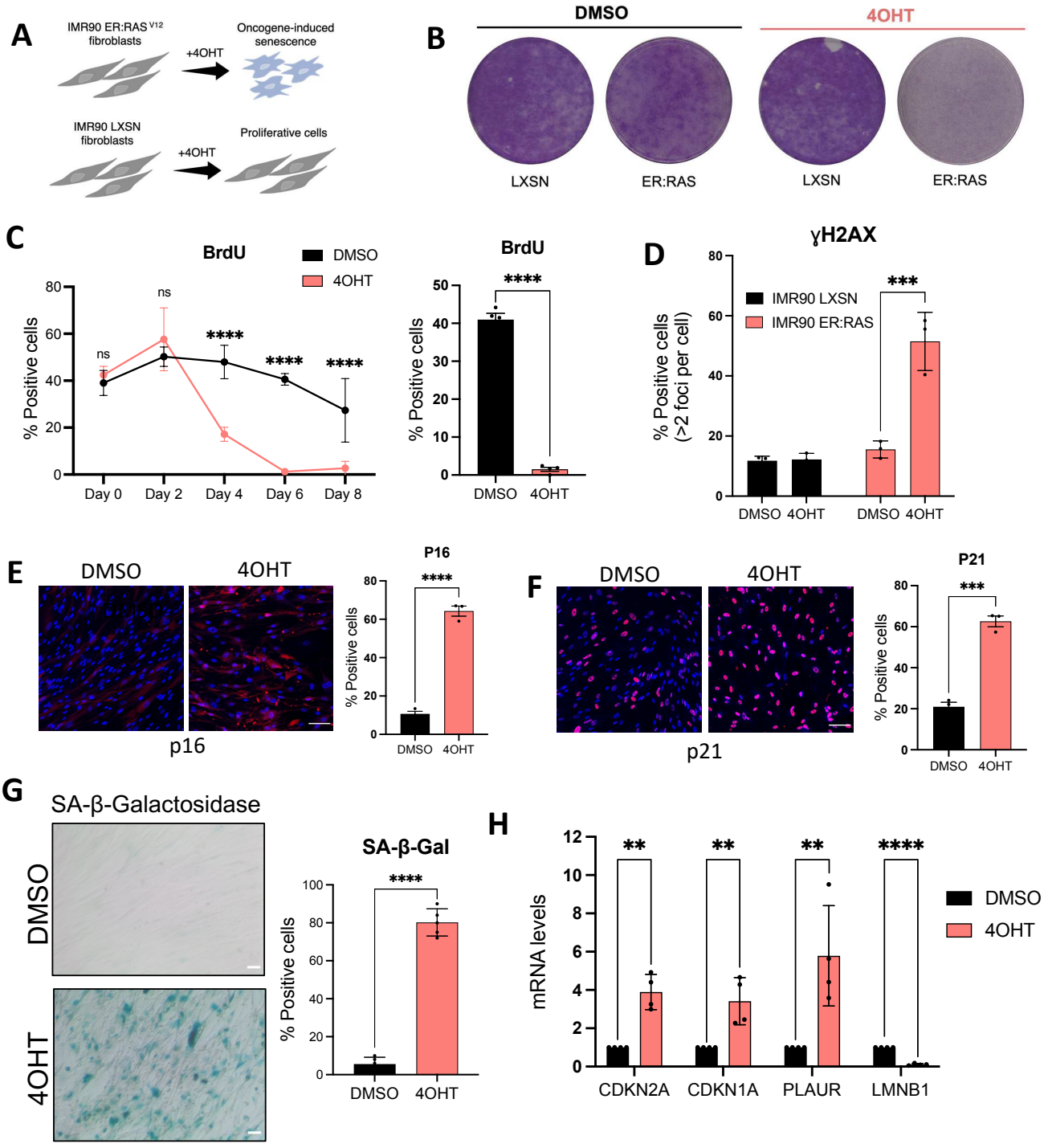


Figure 3.1 Characterisation of OIS in IMR90 ER:RAS

(A) Schematic of IMR90 ER:RAS system as a model of oncogene-induced senescence (OIS). IMR90 fibroblasts infected with the ER:RAS construct induce OIS upon addition of 4OHT, whereas IMR90 cells infected with the LXSN control plasmid continue to proliferate.

(B) Crystal violet staining of plates of IMR90 fibroblasts infected with LXSN or ER:RAS vectors and treated with either DMSO (vehicle) or 4OHT. Cells were fixed and stained 14 days after 4OHT treatment. Images display a representative experiment out of four.

(C) Quantification of immunofluorescence (IF) staining for BrdU incorporation in IMR90 ER:RAS cells. Left side shows a time course over 8 days with 'Day 0' representing day of 4OHT treatment (n = 5). Right side shows BrdU incorporation 8 days after treatment with DMSO or 4OHT (n = 4).

(D) Quantification of IF staining for γH2AX accumulation in IMR90 ER:RAS or IMR90 LXSN cells, 8 days following treatment with DMSO or 4OHT. Quantification represents the percentage of cells with at least 2 γH2AX foci (n = 3).

(E & F) Left side shows representative IF images for $p16^{INK4a}$ staining **(E)** and $p21^{CIP1}$ **(F)** in IMR90 ER:RAS cells 8 days following treatment with DMSO or 4OHT. Right side represents the quantification of percentage of cells staining positive for $p16^{INK4a}$ (n = 3) and $p21^{CIP1}$ (n = 3). Scale bar, 100μm.

(G) Left side shows representative brightfield images for SA-β-galactosidase (SA-β-gal) staining in IMR90 ER:RAS cells 7 days following treatment with DMSO or 4OHT. Right side represents the quantification of percentage of cells staining positive for SA-β-gal (n = 3). Scale bar, 100μm.

(H) qRT-PCR analysis of indicated senescence markers in IMR90 ER:RAS cells 8 days following treatment with DMSO or 4OHT (n = 3).

(C, E, F, G, & H) Unpaired two-tailed Student's t-tests. **(D)** Two-way ANOVA.

n signifies independent experiments. All error bars represent mean ± SD. *P < 0.05, **P < 0.01, ***P < 0.001, ****P < 0.0001; ns= not significant.

3.3 Senescent cells upregulate an immunomodulatory SASP and NK activating ligands

OIS is associated with a potent secretory programme (Herranz et al., 2018) that plays a significant role in NK cell activation and recruitment. To evaluate this, we analysed the upregulation of multiple SASP factors following senescence induction. IMR90 ER:RAS cells undergoing OIS displayed a substantial increase in the levels of the immunoregulatory cytokines IL6, IL8 and IL1β (Figure 3.2A). Secretion of CCL2, a chemokine known to mediate senescence surveillance by NK cells, was also significantly upregulated in senescent IMR90 ER:RAS cells (Figure 3.2A). Likewise, mRNA levels of various SASP factors were increased in 4OHT-treated IMR90 ER:RAS cells (Figure 3.2B). Among these included tumour necrosis factor-α (TNFα), a cytokine that regulates NK cell activation and proliferation. Gene Set Enrichment Analysis (GSEA) also revealed strong enrichment of a SASP signature in cells undergoing OIS (Figure 3.2C) (Original RNA-Seq data used for GSEA was collected by Verena Wagner, a previous member of our group).

To validate whether the RAS-induced senescence programme provoked the secretion of cytokines, ELISAs were performed on the conditioned medium (CM) collected from IMR90 ER:RAS cells. Secreted levels of IL6 and IL8 in 4OHT-treated CM were markedly higher than that of non-senescent control cells (Figure 3.2D & E). CXCL10 is an inflammatory cytokine that binds to CXCR3 receptors and can trigger the activation and recruitment of NK cells, as well as T cells and monocytes. We also observed a significant increase in CXCL10 secretion during OIS (Figure 3.2F).

As cells undergoing OIS secrete immunomodulatory cytokines, we next examined how this could affect NK cell-mediated surveillance. We, therefore, set up an *in vitro* chemotaxis assay to quantify the migration of NK92-MI cells towards medium conditioned by IMR90 ER:RAS cells. CM collected from cells undergoing OIS was placed in the bottom chamber of a transwell insert, separated from the NK92-MI cells by a microporous membrane (Figure 3.2G). CXCL10 and CCL5 are known chemoattractants of NK cells and were used as positive controls for the chemotaxis assay. The CM from senescent cells attracted significantly more NK cells than CM from control cells (Figure 3.2H). In fact, the increase in NK cell migration towards OIS CM resembled that observed by CXCL10. Conversely, a CXCR2

antagonist served as a control that successfully blocked NK cell migration even in the presence of 4OHT-induced CM, corroborating that CXCR2-binding chemokines are vital to activate NK cell receptor signalling (Figure 3.2H). Overall, these findings align with the crucial role that the SASP plays in recruiting NK cells for senescence surveillance.

NK cells express the NKG2D receptor on their surface that recognises activating ligands on stressed and senescent cells (Badrinath et al., 2022; Sagiv et al., 2016). In humans, these ligands include MICA, MICB, and the UL16-binding protein family (ULBPs) and are important regulators of NK cell function (Katlinskaya et al., 2015; López-Botet et al., 2000). We assessed whether our IMR90 ER:RAS cells undergoing OIS upregulated these NK activating ligands through RT-qPCR (Figure 3.3A). mRNA levels of MICA and all the ULBP ligands tested increased during OIS. These findings were consistent with those previously established in IMR90 fibroblasts (Sagiv et al., 2016). We also investigated the expression of the cell surface protein intercellular adhesion molecule-1 (ICAM1), which, although not an NKG2D ligand, is part of the SASP transcriptional module and implicated in NK cell cytotoxic activity (Chan et al., 2014; Morvan and Lanier, 2016). ICAM1 expression was increased over 10-fold in senescent IMR90 ER:RAS. RNA-Seq analysis of OIS IMR90 ER:RAS cells from our group (Wagner et al., unpublished data) and a published OIS dataset of WI-38 fibroblasts (Casella et al., 2019) confirmed our RT-qPCR findings. Differential expression analysis from both RNA-Seq datasets revealed an upregulation in several NK activating ligands following senescence induction (Figure 3.3B & C). Intriguingly, data from our group's IMR90 ER:RAS cells undergoing OIS demonstrated enrichment in GOBP and KEGG pathway signatures of NK cell activation and NK cell-mediated cytotoxicity, respectively (Figure 3.3D & E).

Senescent cells have been reported to develop mechanisms to escape NK-mediated clearance, for example, through upregulation of NK inhibitory ligand expression (Pereira et al., 2019). Therefore, we investigated the expression of NK cell inhibitory ligands in senescent IMR90 ER:RAS cells. We identified an upregulation of several NK cell inhibitory ligand genes, particularly HLA-A and PVR (Figure 3.3F). Although these findings juxtapose the upregulation of NK activating ligands previously observed, it also offers a potential therapeutic opportunity to modulate NK cell activity against senescent cells by

repressing NK cell inhibitory ligands. Overall, the data suggests that OIS not only induces a stable growth arrest in fibroblasts but can also promote NK cell surveillance of senescent cells through the induction of NK activating ligands and a complex SASP programme.

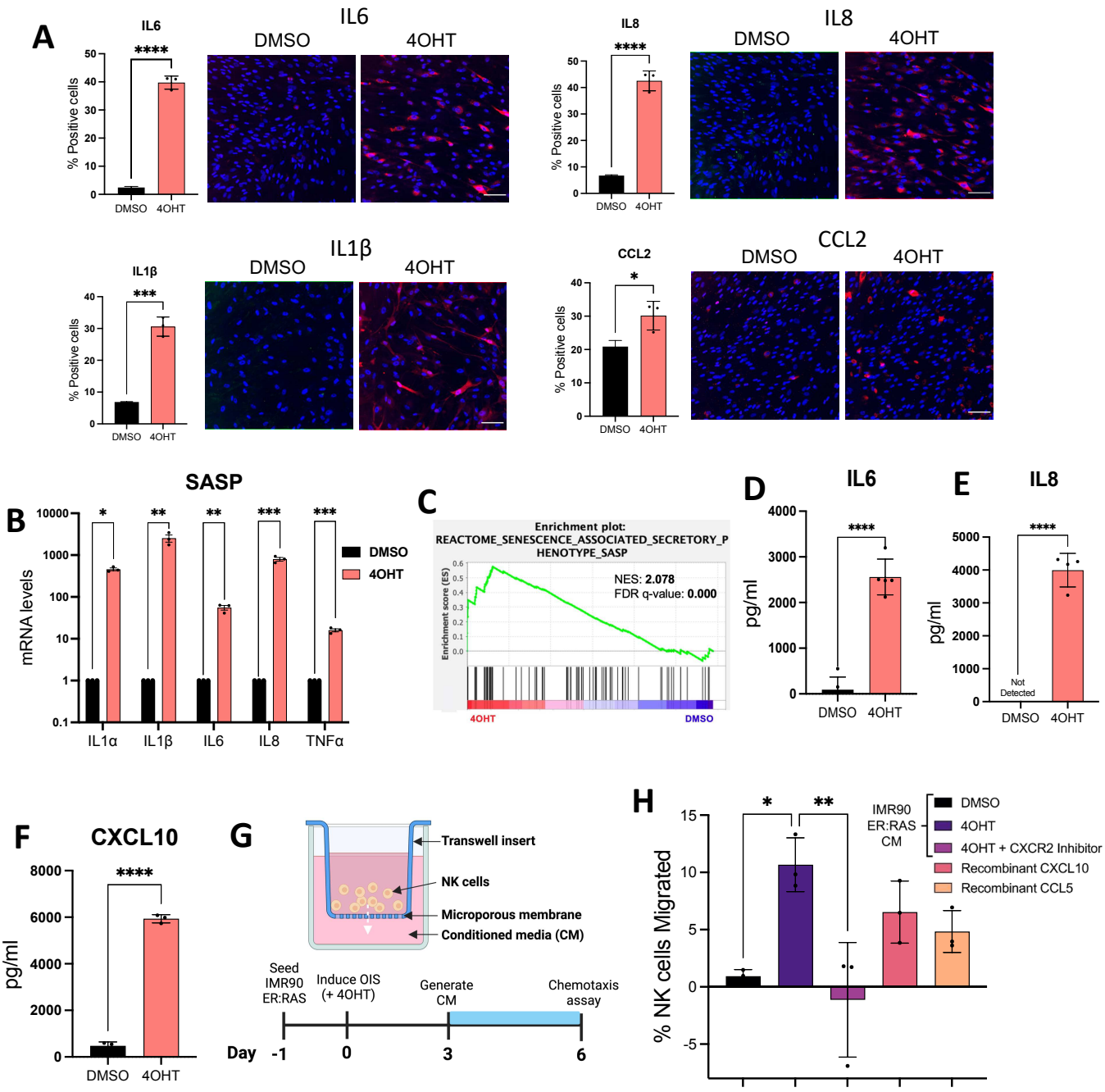


Figure 3.2 Upregulation of a proinflammatory and chemoattractive SASP during OIS

(A) Quantification of percentage of cells staining positive for the indicated senescence-associated secretory phenotype (SASP) markers and representative IF images in IMR90 ER:RAS cells 8 days following treatment with DMSO or 4OHT (*n* = 3). Scale bar, 100µm.
(B) qRT-PCR analysis of indicated SASP markers in IMR90 ER:RAS cells 8 days following treatment with DMSO or 4OHT (*n* = 3).
(C) Gene set enrichment analysis (GSEA) comparing transcriptomic data from IMR90 ER:RAS cells 8 days following DMSO or 4OHT-treatment showing an enrichment in the Reactome database SASP signature in senescent cells (*n* = 3). (Original RNA-Sequencing experiment performed by Verena Wagner, unpublished data).
(D-F) Quantification of levels of secreted cytokines from IMR90 ER:RAS cells 7 days following DMSO or 4OHT-treatment, as assessed by ELISA. Results shown for IL6 (*n* = 5) **(D)**, IL8 (*n* = 4) **(E)**, and CXCL10 (*n* = 3) **(F)**. For **(E)**, IL8 levels in DMSO-treated conditioned media was below detection limit.
(G) Schematic of the chemotaxis assay experimental setting.
(H) Quantification of the percentage of NK92-MI (NK) cells migrating of the lower chamber of the transwell insert after 21 hours of the chemotaxis assay. Lower chamber comprised of concentrated conditioned media (CM) generated from IMR90 ER:RAS cells treated with DMSO or 4OHT, or unconditioned media supplemented with recombinant proteins of CXCL10 or CCL5 (*n* = 3).
(A, D, E, & F) Unpaired two-tailed Student's *t*-tests. **(B)** Multiple *t*-tests. **(G)** Ordinary one-way ANOVA.
n signifies independent experiments. All error bars represent mean ± SD. *P < 0.05, **P < 0.01, ***P < 0.001, ****P < 0.0001; ns= not significant.

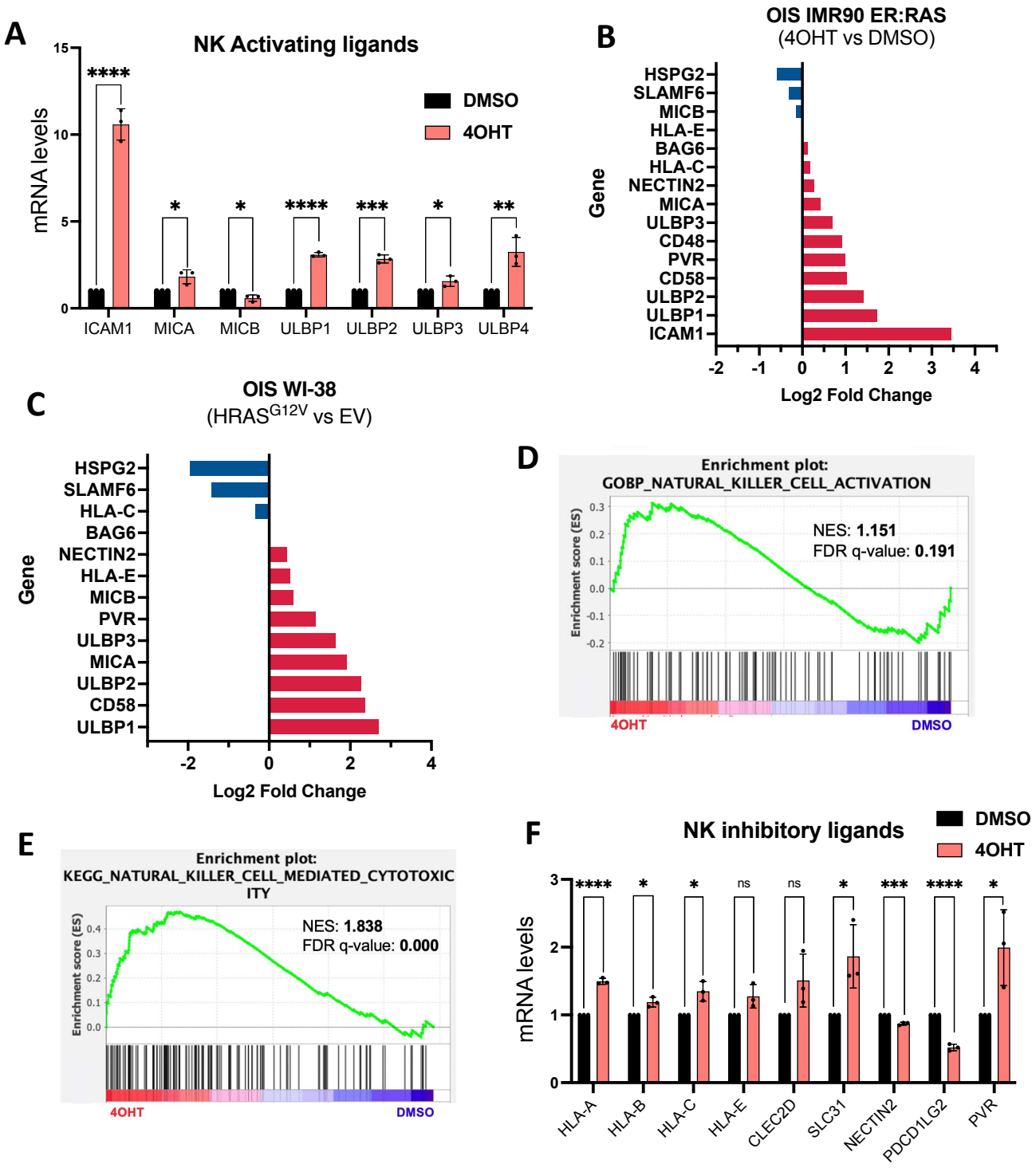


Figure 3.3 OIS promotes NK cell activity

(A) qRT-PCR analysis showing the expression of the indicated NK cell activating ligands and surface proteins in IMR90 ER:RAS cells 8 days following treatment with DMSO or 4OHT (*n* = 3).

(B & C) Results from differential gene expression analysis based on RNA-sequencing data for NK cell ligands and surface proteins between DMSO and 4OHT-treated IMR90 ER:RAS cells (B) or between constitutive HRAS^{G12V} vector expression and an empty vector (EV) in WI-38 fibroblasts. Both OIS cells show a significant upregulation in the expression of multiple NK cell activating ligands (*n* = 3). For (B), the original RNA-Sequencing experiment was performed by Verena Wagner, unpublished data. For (C), the raw RNA-Sequencing data was obtained from Casella et al., 2019.

(D & E) GSEA from the Gene Ontology Biological pathway (D) and KEGG (E) databases showing a significant enrichment in NK cell activation (D) and NK cell-mediated cytotoxicity (E) in IMR90 ER:RAS cells following treatment with 4OHT compared with treatment with DMSO. (Original RNA-Sequencing experiment performed by Verena Wagner, unpublished data).

(F) qRT-PCR analysis showing the expression of the indicated NK cell inhibitory ligands in IMR90 ER:RAS cells 7 days following treatment with DMSO or 4OHT (*n* = 3).

(A & F) Unpaired two-tailed Student's *t*-tests.

n signifies independent experiments. All error bars represent mean ± SD. *P < 0.05, **P < 0.01, ***P < 0.001, ****P < 0.0001; ns= not significant.

3.4 Selective killing of senescent cells by NK cells

We next examined the ability of NK cells to target and kill senescent IMR90 ER:RAS cells. In a previous study, Sagiv and colleagues reported that NK cells preferentially eliminate senescent cells by rapidly releasing cytolytic granules (Sagiv et al., 2013). To assess NK-mediated killing of cells undergoing OIS, we performed an *in vitro* co-culture assay whereby turboGFP-labelled proliferating or senescent IMR90 ER:RAS cells were co-cultured with NK92-MI cells that had been stained red by a fluorescent dye (Figure 3.4A). Control wells comprising IMR90 ER:RAS cells but lacking NK cells were also assessed. The co-culture was analysed using live cell microscopy (IncuCyte), and NK-mediated cytotoxicity was quantified by measuring the percentage change of green (IMR90 ER:RAS) cells 48 hours after adding NK cells. We initially optimised the effector-to-target (E:T) ratio of NK cells to senescent cells (Figure 3.4B). Consistent with previous literature (Krizhanovsky et al., 2008; Pereira et al., 2019), we noticed that NK cells preferentially attacked senescent cells over non-senescent; however, this effect was contingent on the E:T ratio of NK cells to IMR90 ER:RAS cells (Figure 3.4B). The lowest E:T ratio tested of 1:1 did not result in the killing of senescent cells. In contrast, an E:T of 10:1 resulted in the killing of both growing and senescent cells. An E:T of 5:1 produced a rapid and significant killing of senescent IMR90 ER:RAS by NK92-MI cells, yet the non-senescent (DMSO-treated) cells continued to proliferate in co-culture, albeit not at the same level as in the absence of NK cells (Figure 3.4C & D). Senescent IMR90 ER:RAS cells did not undergo cell death in the absence of NK cells, indicating that the NK cells were responsible for eliminating the senescent fibroblasts.

IMR90 ER:RAS cells undergo morphological alterations during senescence and develop a flattened and enlarged cell shape relative to growing cells. Consequently, despite the aforementioned co-culture assay demonstrating a discernible NK-mediated killing of senescent cells, quantification was not perfect due to inaccuracies of the IncuCyte software-defined cell masks bordering the DMSO and 4OHT treated IMR90 ER:RAS cells. To circumvent this issue, we used IMR90 ER:RAS cells infected with a nuclear GFP vector (IMR90 ER:RAS H2B-GFP cells) (see Methods and Materials, Chapter 2.7). Although there are nuclear morphology changes between growing and senescent cells, there is enough similarity to outline a nuclear border for a more accurate quantification using live cell microscopy. Therefore, NK cell-mediated cytotoxicity was evaluated based on the percentage change of the number of nuclei of

IMR90 ER:RAS cells following co-culture with NK cells. Again, we tested a range of E:T ratios (Figure 3.5A) and found similar results to the original co-culture experiment, whereby an E:T ratio of 5:1 showed a substantial killing of senescent cells by the NK cells (Figure 3.5B & C). We next analysed a reduced and more physiological E:T ratio of 2:1 (Figure 3.5D & E), which offers a larger dynamic range that can be exploited using siRNAs and compounds to promote NK-mediated senescence clearance. At this ratio, we observed NK cell-mediated killing of senescent fibroblasts but not in non-senescent cells.

Having validated NK-mediated removal of senescent cells at different E:T ratios, we next needed to establish a robust co-culture model system that is amenable for screening siRNAs and compounds that promote senescence surveillance. To fulfil these criteria, we established a high throughput system capable of quantifying NK-mediated cytotoxicity based on DAPI staining (Figure 3.6A). Nuclear counts of DMSO- or 4OHT-pretreated IMR90 ER:RAS cells were obtained before co-culture ('Timepoint 0 hours') (see Materials & Methods, Chapter 2.7). According to this value, the appropriate number of NK cells were seeded based on the required E:T ratio of the co-culture. IMR90 ER:RAS nuclear counts were then measured at the end of the co-culture ('Timepoint 48 hours'), and NK-mediated killing of senescent cells was calculated based on the percentage change in IMR90 ER:RAS cells following co-culture with NK cells. Using this system, we co-cultured NK cells with IMR90 ER:RAS cells at a 5:1 E:T ratio (Figure 3.6B & C) and a 2:1 E:T ratio (Figure 3.6D & E). In both cases, we observed that senescent (4OHT-treated) but not growing (DMSO-treated) IMR90 ER:RAS cells were killed by NK92-MI cells. The 2:1 E:T ratio caused a lower percentage of senescent cell death compared to the 5:1 E:T, providing greater leeway to measure an increase in NK-mediated cytotoxicity. Overall, these experiments set up a system to study factors affecting NK-mediated killing of senescent cells.

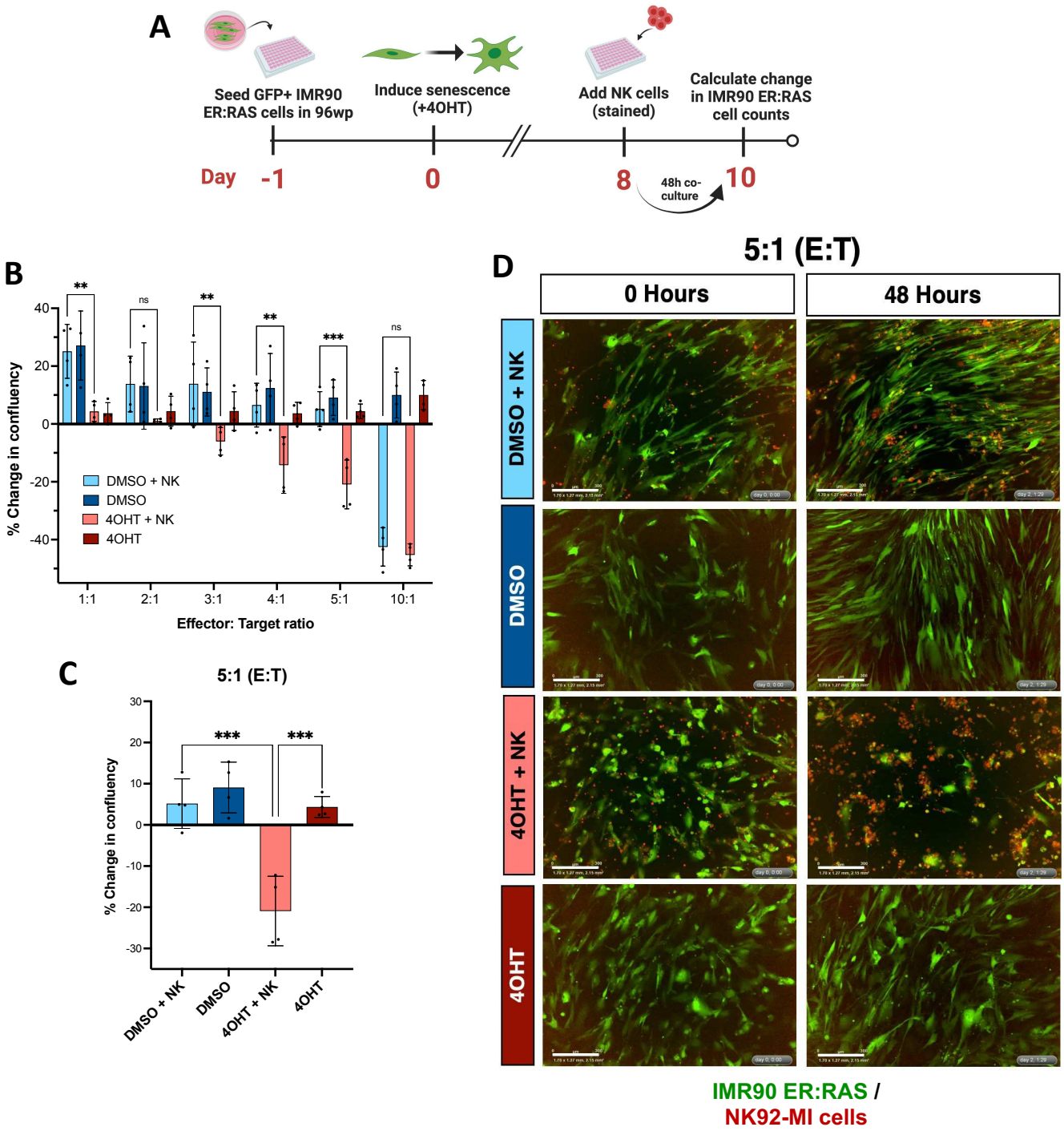


Figure 3.4 NK cells selectively kill cells undergoing OIS

(A) Schematic of the co-culture experimental setting between turboGFP-expressing IMR90 ER:RAS cells (IMR90 ER:RASpGIPZ) and red dye-stained NK92-MI cells using the IncuCyte live cell microscopy.

(B) Quantification of NK cell-mediated cytotoxicity of IMR90 ER:RAS cells 8 days following treatment with either DMSO or 4OHT and co-cultured with NK92-MI (NK) cells at different E:T ratios for 48 hours. Cytotoxicity was measured as the percentage change in green IMR90 ER:RAS cell confluency over 48 hours using live cell microscopy. Control wells contained DMSO or 4OHT-treated IMR90 ER:RAS cells in the absence of NK cells (n = 4).

(C) Quantification of NK cell-mediated cytotoxicity of IMR90 ER:RAS cells 8 days following treatment with either DMSO or 4OHT and co-cultured with NK92-MI cells at a 5:1 E:T ratio for 48 hours. Cytotoxicity was measured as in **(B)** (n = 4).

(D) Representative images of IMR90 ER:RAS cells with the indicated treatment and co-cultured with NK92 cells at a 5:1 E:T ratio, as quantified in (C) (n = 4). Scale bar, 300µm.

(B) Two-way ANOVA. **(C)** Ordinary one-way ANOVA.

n signifies independent experiments. All error bars represent mean ± SD. *P < 0.05, **P < 0.01, ***P < 0.001, ****P < 0.0001; ns= not significant.

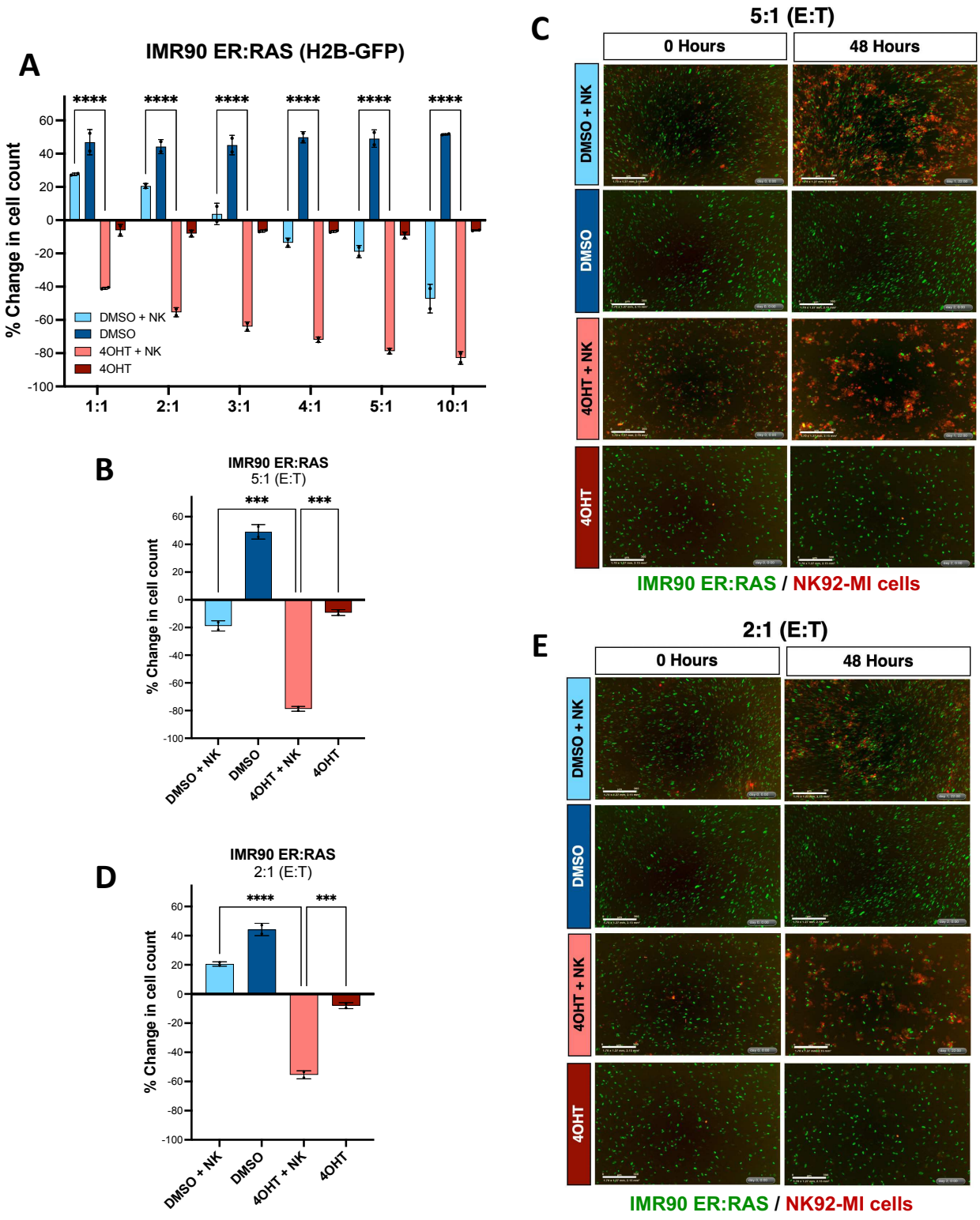


Figure 3.5 Quantification of NK-mediated killing of senescent cells using nuclear-GFP

(A) Quantification of NK cell-mediated cytotoxicity of nuclear-GFP+ IMR90 ER:RAS cells 8 days following treatment with either DMSO or 4OHT and co-cultured with NK92-MI cells at different E:T ratios for 48 hours. Percentage change in cell count was measured based on the change in green nuclei count of nuclear-GFP+ IMR90 ER:RAS cells over 48 hours of co-culture as detected by the IncuCyte™ Ilive cell microscopy. Control wells contained DMSO or 4OHT-treated IMR90 ER:RAS cells in the absence of NK cells (*n* = 2).

(B) Quantification of NK cell-mediated cytotoxicity of IMR90 ER:RAS cells 8 days following treatment with either DMSO or 4OHT and co-cultured with NK92-MI cells at a 5:1 E:T ratio for 48 hours. Cytotoxicity was measured as in **(A)** (*n* = 2).

(C) Representative images of the GFP+ nuclei of IMR90 ER:RAS cells with the indicated treatment and co-cultured with NK cells at a 5:1 E:T ratio, as quantified in (B) (*n* = 2). Scale bar, 300μm.

(D) Quantification of NK cell-mediated cytotoxicity of IMR90 ER:RAS cells 8 days following treatment with either DMSO or 4OHT and co-cultured with NK92-MI cells at a 2:1 E:T ratio for 48 hours. Cytotoxicity of IMR90 ER:RAS cells was measured as in **(A & B)** (*n* = 2).

(E) Representative images of the nuclei from IMR90 ER:RAS cells with the indicated treatment and co-cultured with NK cells at a 2:1 E:T ratio, as quantified in **(D)** (*n* = 2). Scale bar, 300μm.

(A-C) Ordinary one-way ANOVA.

n signifies independent experiments. All error bars represent mean ± SD. *P < 0.05, **P < 0.01, ***P < 0.001, ****P < 0.0001; ns= not significant.

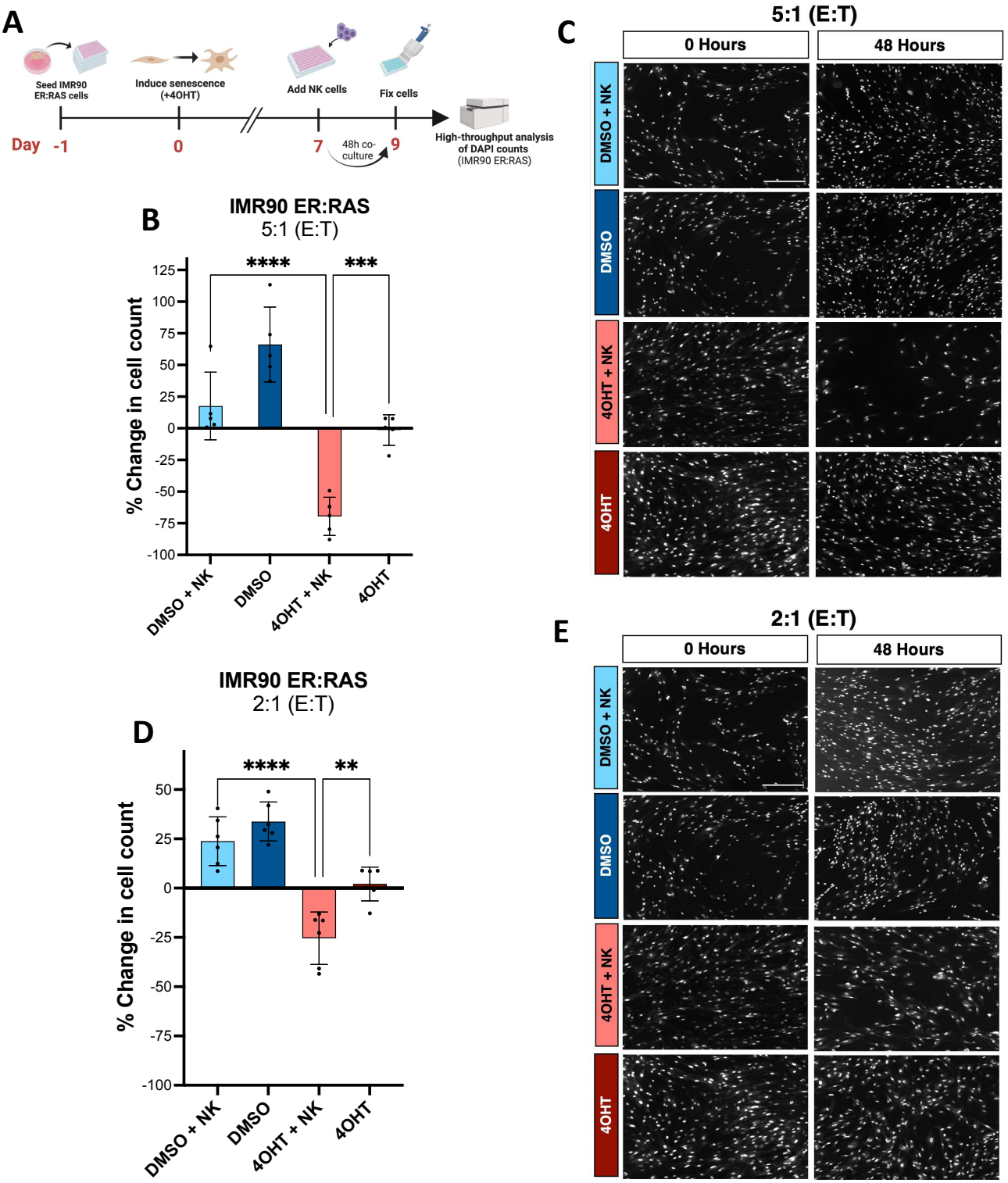


Figure 3.6 Adapting a high-throughput assay to monitor NK-mediated killing of senescent cells

(A) Schematic of the protocol for the co-culture experimental setting between growing or senescent IMR90 ER:RAS cells and NK92-MI cells using the InCell™ high-throughput imaging and analysis system.

(B) Quantification of NK cell-mediated cytotoxicity of IMR90 ER:RAS cells 7 days following treatment with either DMSO or 4OHT and co-cultured with NK92-MI (NK) cells at a 5:1 E:T ratio for 48 hours. Percentage change in cell count was measured based on the change in nuclei count (DAPI) of IMR90 ER:RAS cells over 48 hours of co-culture. Control wells contained DMSO or 4OHT-treated IMR90 ER:RAS cells in the absence of NK cells (n = 5).

(C) Representative images of IMR90 ER:RAS cells with the indicated treatment before and after co-culture with NK cells at a 5:1 E:T ratio, as described and quantified in (B) (n = 5). Scale bar, 300µm.

(D) Quantification of NK cell-mediated cytotoxicity of IMR90 ER:RAS cells 7 days following treatment with either DMSO or 4OHT and co-cultured with NK92-MI cells at a 2:1 E:T ratio for 48 hours. Cytotoxicity was measured as in **(B)**. Control wells contained DMSO or 4OHT-treated IMR90 ER:RAS cells in the absence of NK cells (n = 5).

(E) Representative images of IMR90 ER:RAS cells with the indicated treatment before and after co-culture with NK cells at a 2:1 E:T ratio, as described and quantified in (B) (n = 5). Scale bar, 300µm.

(B & D) Ordinary one-way ANOVA.

n signifies independent experiments. All error bars represent mean ± SD. *P < 0.05, **P < 0.01, ***P < 0.001, ****P < 0.0001; ns= not significant.

3.5 Characterising drugs that modulate the immunomodulatory SASP

Since mainly chemoattractive factors are part of the SASP, we theorised that modulating the expression of the SASP could impact NK cell surveillance of senescent cells. To investigate this, we first needed to assess different compounds that could regulate SASP activity (Figure 3.7a). Suitable drugs could then serve as controls for subsequent screens to identify SASP modulators and/or modulators of NK-mediated killing of senescent cells.

We initially explored compounds that would downregulate SASP secretion and identified two glucocorticoids which had previously been characterised as SASP repressors (Laberge et al., 2012). Treating senescent IMR90 ER:RAS cells with either beclomethasone or triamcinolone did not affect senescence induction (Figure 3.7B & C). However, treatment with both glucocorticoids reduced the levels of IL6 secreted by senescent fibroblasts (Figure 3.7D). In addition, administration of beclomethasone and triamcinolone resulted in a significant reduction in the expression of several SASP factors, including the immune-activating factor CCL2, to almost identical levels of the control cells (Figure 3.7E & F).

We next examined compounds that upregulate SASP expression. Previous lab members have internally tested siRNAs against EPRS, an aminoacyl-tRNA synthetase involved with attaching amino acids to their cognate tRNA, and reported that EPRS knockdown increases IL6 and IL8 expression in IMR90 ER:RAS cells. We tested two different concentrations of the EPRS inhibitor halofuginone (HF). Treatment with 20nM or 40nM HF did not influence the senescence phenotype (Figure 3.8A). However, treatment with HF significantly increased the expression of multiple SASP cytokines, including IL6, IL8, IL1β and CCL2, in senescent cells (Figure 3.8B- E). Finally, we tested the effect of indisulam, an anti-cancer agent that targets the degradation of the mRNA splicing factor RBM39 (Bussiere et al., 2020). Previously, a study by Pech and colleagues identified that low concentrations of indisulam inhibit DCAF15 function resulting in increased NK-mediated killing of leukaemia cells (Pech et al., 2019). Similar to HF, we found that indisulam treatment did not diminish the senescence phenotype (Figure 3.9A) while modestly increasing the expression of IL6 and IL8 (Figure 3.9B & C), with a significant increase in IL1β (Figure 3.9D). No significant change in CCL2 expression was observed (Figure 3.9E). Although indisulam does not extensively increase SASP expression, per se, it is reported to promote

NK cell effector function (Pech et al., 2019) and, therefore, may exert NK-stimulatory effects through other means.

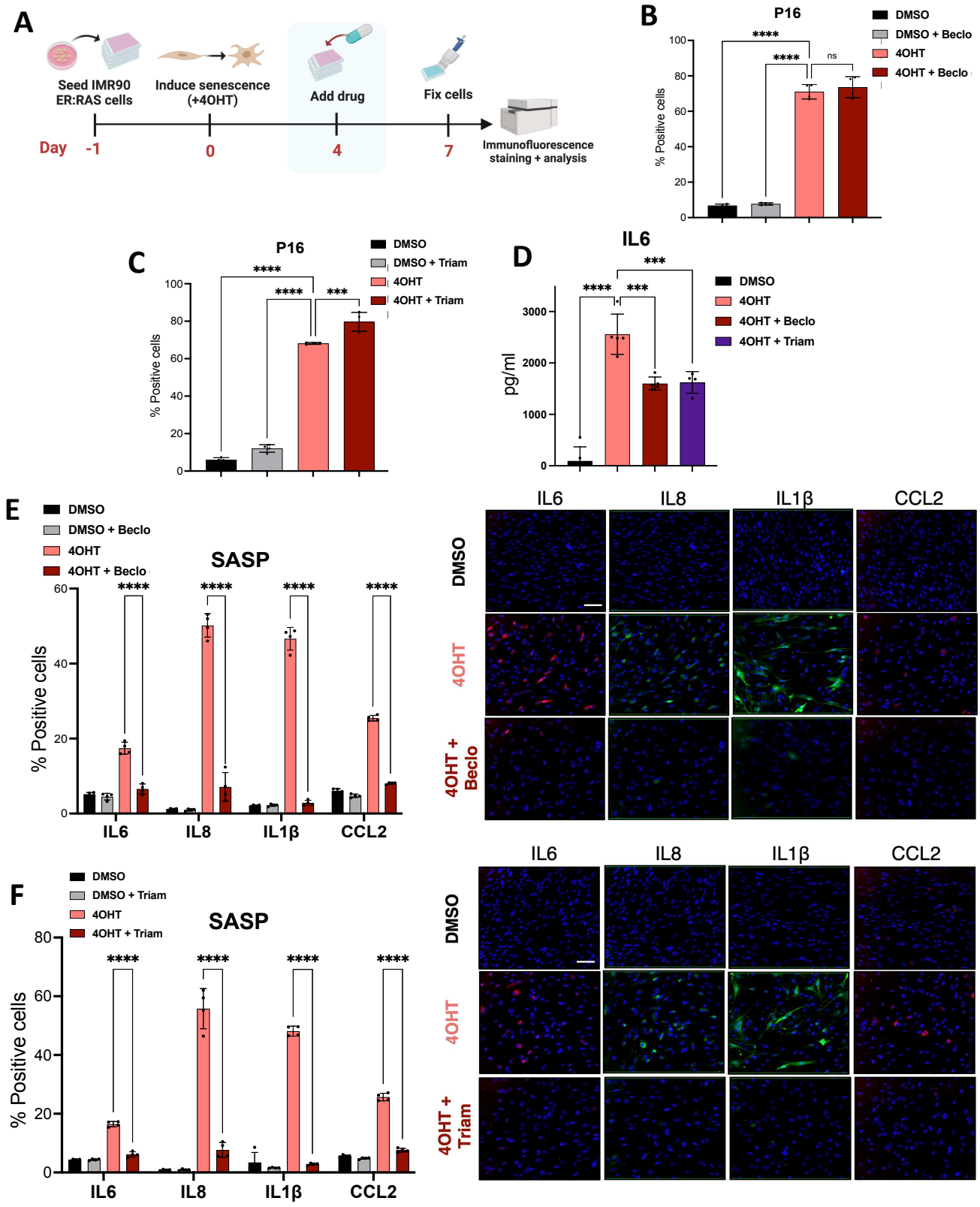


Figure 3.7 Glucocorticoids strongly suppress SASP expression during OIS

(A) Schematic of the protocol timeline to investigate the effect of drug administration on the SASP of OIS cells.
(B & C) Quantification of percentage of cells staining positive for $p16^{INK4a}$ in IMR90 ER:RAS cells treated with DMSO or 4OHT combined with beclomethasone (10μM) **(B)** or with triamcinolone (10μM) **(C)** following the treatment timeline from **(A)** (n = 4 for both **(B)** and **(C)**).
(D) Quantification of IL6 levels secreted from IMR90 ER:RAS cells 7 days following DMSO or 4OHT-treatment or with 4OHT treatment combined with beclomethasone (10μM) or triamcinolone (10μM), as assessed by ELISA (n = 5)
(E & F) Quantification of percentage of cells staining positive for the indicated SASP markers and representative IF images in IMR90 ER:RAS cells 7 days following treatment with DMSO or 4OHT alone, or in combination with beclomethasone (10μM) **(E)** or triamcinolone (10μM) **(F)** (n = 4). Scale bar, 100μm.
(B-D) Ordinary one-way ANOVA. **(E & F)** Two-way ANOVA.
n signifies independent experiments. All error bars represent mean ± SD. *P < 0.05, **P < 0.01, ***P < 0.001, ****P < 0.0001; ns= not significant.

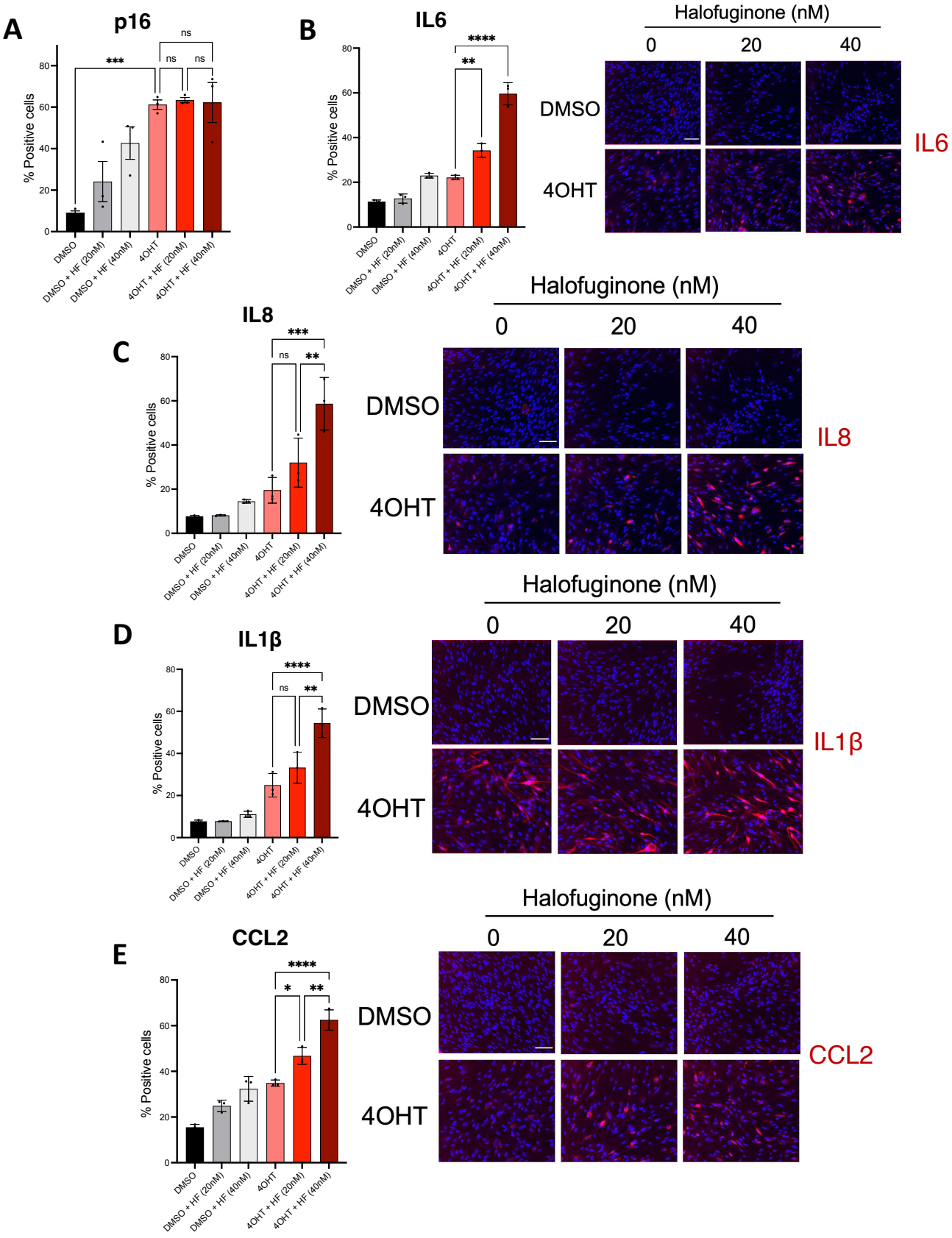


Figure 3.8 Halofuginone strongly promotes SASP but does not affect p16^{INK4a} expression during OIS

(A) Quantification of percentage of cells staining positive for p16^{INK4a} in IMR90 ER:RAS cells treated with DMSO or 4OHT combined with 20nM or 40nM of halofuginone (HF) following the treatment timeline from Figure 3.7A (*n* = 3).

(B-E) Quantification of percentage of cells staining positive for the indicated SASP markers and representative IF images in IMR90 ER:RAS cells 7 days following treatment with DMSO or 4OHT alone, or in combination with HF (20nM or 40nM) (*n* = 3). Scale bar, 100μm.

(A-E) Ordinary one-way ANOVA.

n signifies independent experiments. All error bars represent mean ± SD. *P < 0.05, **P < 0.01, ***P < 0.001, ****P < 0.0001; ns= not significant.

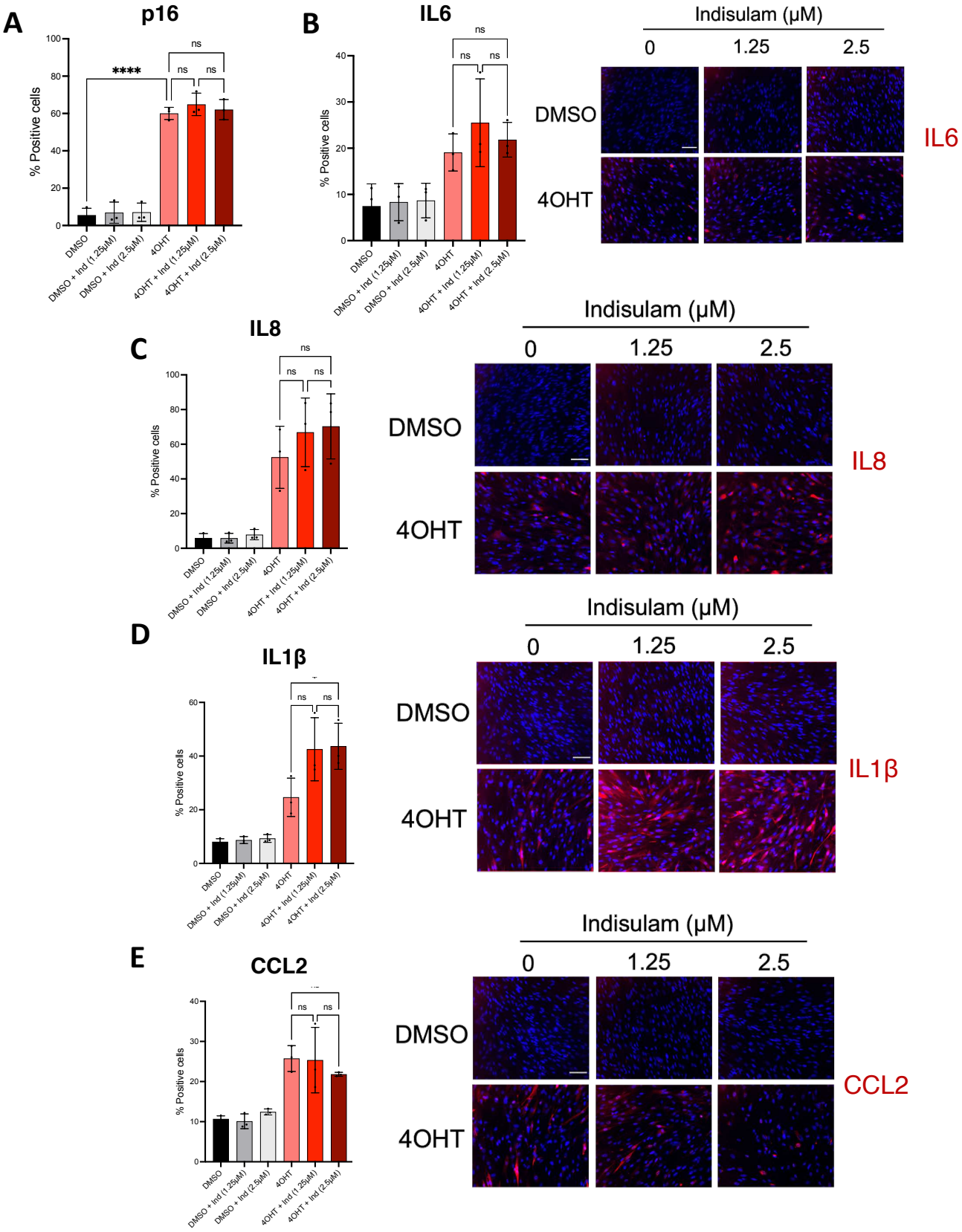


Figure 3.9 Indisulam modestly increases SASP expression without bypassing senescence
(A) Quantification of percentage of cells staining positive for p16^{INK4a} in IMR90 ER:RAS cells treated with DMSO or 4OHT combined with 1.25μM or 2.5μM of indisulam (Ind) following the treatment timeline from Figure 3.7A (*n* = 3).
(B-E) Quantification of percentage of cells staining positive for the indicated SASP markers and representative IF images in IMR90 ER:RAS cells 7 days following treatment with DMSO or 4OHT alone, or in combination with Ind (1.25μM or 2.5μM) (*n* = 3). Scale bar, 100μm.
(A-E) Ordinary one-way ANOVA.
n signifies independent experiments. All error bars represent mean ± SD. *P < 0.05, **P < 0.01, ***P < 0.001, ****P < 0.0001; ns= not significant.

3.6 Setting up the assay to identify factors modulating NK-mediated killing of senescent cells

Previously, we performed high throughput analysis to quantify NK cell-mediated cytotoxicity (Figure 3.6B-E). Using this system, we next aimed to evaluate whether different drugs could affect the NK-mediated killing of senescent cells. To test the glucocorticoids, DMSO- or 4OHT-treated IMR90 ER:RAS cells were pre-treated with either beclomethasone or triamcinolone before undergoing co-culture with NK92-MI cells plated at the desired effector-to-target ratios. Control wells lacking NK cells were also seeded for each condition. We analysed the 2:1 (Figure 3.10A) and the 5:1 (Figure 3.10B) E:T ratios for this assay. In both E:T ratios tested, beclomethasone treatment in senescent IMR90 ER:RAS cells significantly inhibited NK-mediated killing of senescent cells (Figure 3.10C). Triamcinolone treatment also noticeably impeded NK cell surveillance of senescent cells, although not significantly. These findings provide proof of concept for the importance of the SASP in regulating NK cell effector functions against senescent cells.

We next investigated the effect of HF in modulating NK-mediated killing of senescent cells. Both concentrations (20nM and 40nM) of HF tested increased NK-mediated killing of senescent IMR90 ER:RAS cells at the high 5:1 E:T ratio (Figure 3.11A). Surprisingly, at this E:T ratio, non-senescent DMSO cells treated with halofuginone were also killed by NK cells which may be attributable to the increased cytokine expression observed in non-senescent cells following HF administration (Figure 3.8B-E). At an E:T ratio of 2:1, HF treatment also significantly increased NK-mediated killing of senescent cells, almost 3-fold higher than that of 4OHT treatment alone (Figure 3.11B & C). However, unlike at the 5:1 E:T ratio, non-senescent fibroblasts treated with HF were not killed by NK cells at a 2:1 E:T ratio. Finally, we treated IMR90 ER:RAS cells with different concentrations of indisulam and observed an increase in NK-mediated elimination of senescent cells in all E:T ratios tested (Figure 3.12A, B, & C). However, indisulam treatment also strongly promoted NK-mediated killing of non-senescent cells. Despite its effect on non-senescent cells, indisulam can provoke a potent immunogenic response in senescent cells and, therefore, is an appropriate control for future siRNA screens. Ideally, any potential hits identified from future screens would potentiate a potent NK-mediated killing effect exclusively towards senescent cells without targeting non-senescent cells.

Keeping this in mind, we took advantage of our high-throughput co-culture system to investigate the effect of HF and indisulam in modulating NK surveillance in different types of senescence. In a clinical setting, for example, in cancer treatment, senescence may be induced therapeutically through the administration of cytostatic agents or chemotherapy drugs (termed therapy-induced senescence (TIS)). Therefore, we treated IMR90 cells with etoposide (Figure 3.13A). Etoposide treatment rapidly resulted in a stable growth arrest and reduction in BrdU incorporation (Figure 3.13B & C). We found a significant increase in the expression of the tumour suppressors $p16^{INK4a}$, $p21^{CIP1}$ and an induction of DNA damage observed by 53BP1 staining (Figure 3.13D-F). In addition, we detected a substantial upregulation of multiple immunomodulatory SASP factors, including CCL2 (Figure 3.13G).

NK-mediated elimination of etoposide-treated IMR90 cells has already been described (Kim et al., 2022; Krizhanovsky et al., 2008; Sagiv et al., 2013; Tasdemir et al., 2016). Therefore, we decided to exploit this model to assess whether HF or indisulam can promote NK-mediated clearance of cells undergoing TIS. We found that compared with the treatment of etoposide or HF alone, the sequential combination of the two drugs in IMR90 fibroblasts produced a considerable increase in NK-mediated killing of cells undergoing TIS (Figure 3.14A). Similarly, treatment of indisulam produced a significant increase in the elimination of cells undergoing TIS by NK cells that neither agent could produce alone (Figure 3.14B). These experiments accurately validated our NK cell co-culture system to quantify NK-mediated cytotoxicity of senescent cells using chemical compounds. Furthermore, based on these experiments, we identified positive control compounds that potentiate the SASP and NK-mediated killing of senescent cells.

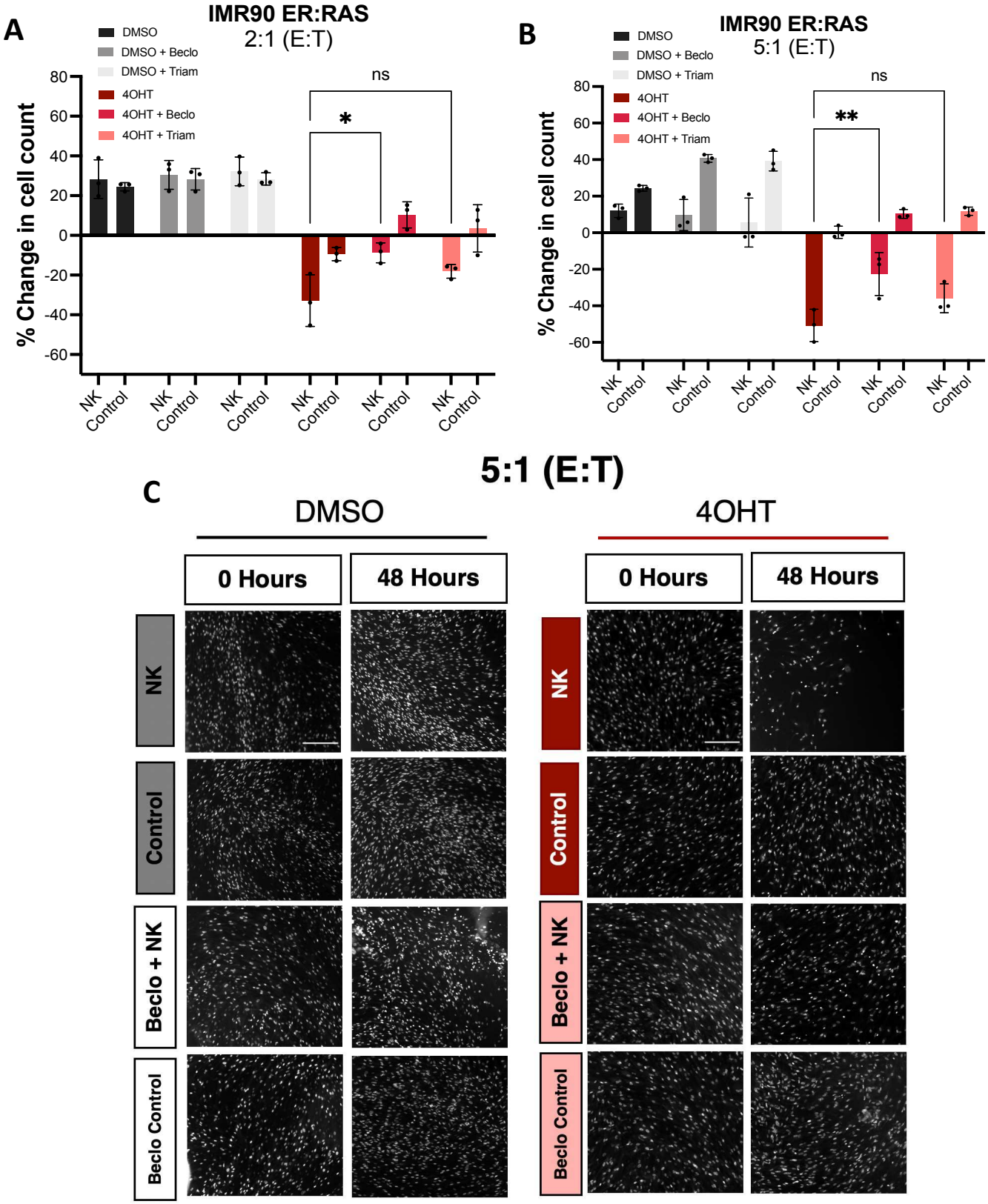


Figure 3.10 Glucocorticoids diminish NK-mediated surveillance of senescent IMR90 ER:RAS cells

(A & B) Quantification of NK cell-mediated cytotoxicity of IMR90 ER:RAS cells 8 days following treatment with either DMSO or 4OHT alone or in combination with beclomethasone (10μM) or triamcinolone (10μM). The glucocorticoid compounds were administered at day 4 following DMSO/4OHT induction. Experimental wells contained treated IMR90 ER:RAS cells co-cultured with NK92-MI cells at either a 2:1 E:T **(A)** or 5:1 E:T **(B)** ratio. Percentage change in cell count was measured based on the change in nuclei count (DAPI) of IMR90 ER:RAS cells over 48 hours of co-culture. Control wells contained treated IMR90 ER:RAS in the absence of NK cells (*n* = 3).

(C) Representative images of IMR90 ER:RAS cells treated with DMSO or 4OHT alone and in combination with beclomethasone (10μM) treatment before and after co-culture with NK cells at a 5:1 E:T ratio, as described in **(B)** (*n* = 3). Scale bar, 300μm.

(A & B) Ordinary one-way ANOVA.

n signifies independent experiments. All error bars represent mean ± SD. *P < 0.05, **P < 0.01, ***P < 0.001, ****P < 0.0001; ns= not significant.

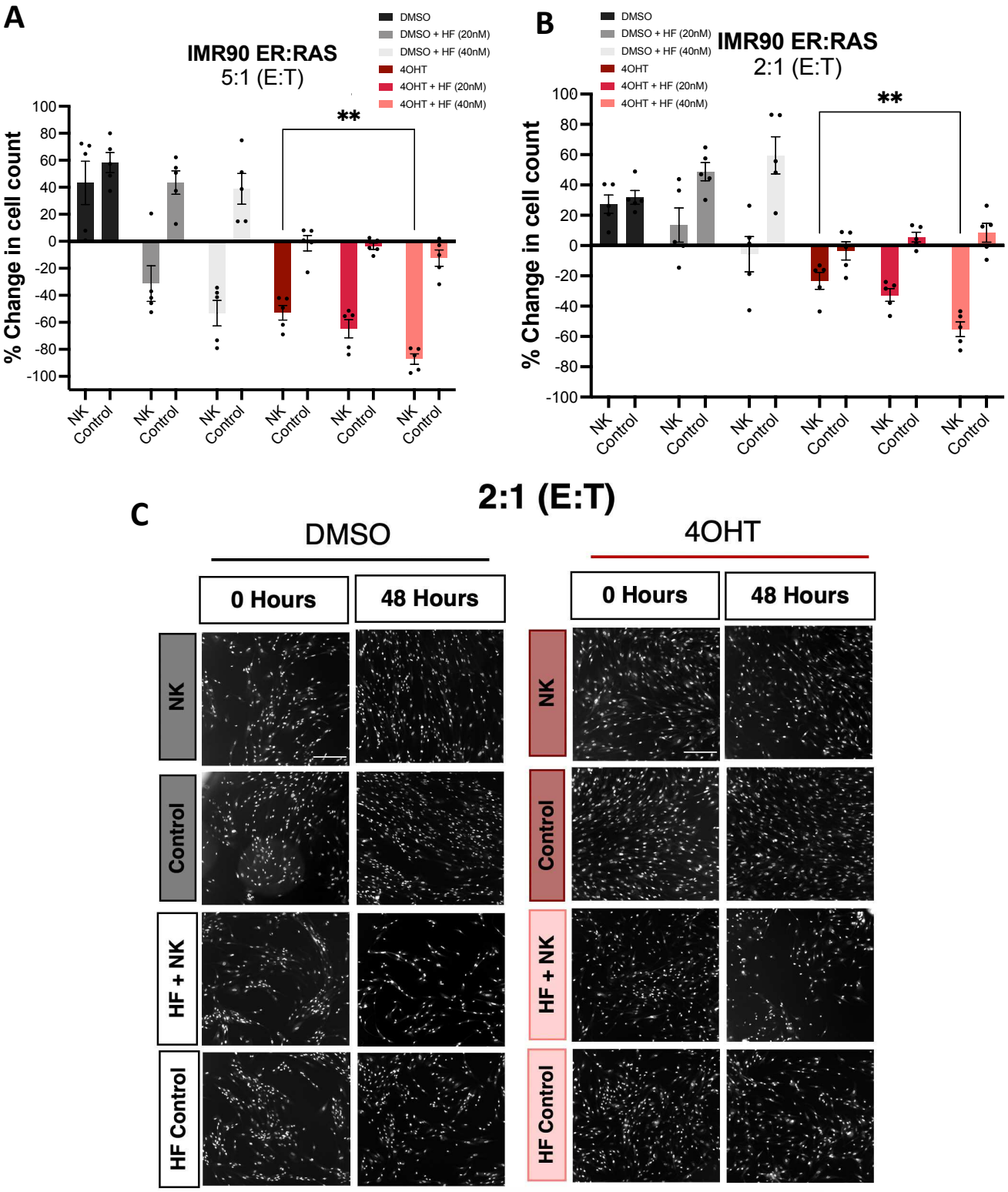


Figure 3.11 Halofuginone enhances NK cell-mediated killing of senescent IMR90 ER:RAS cells

(A & B) Quantification of NK cell-mediated cytotoxicity of IMR90 ER:RAS cells 8 days following treatment with either DMSO or 4OHT alone or in combination with halofuginone (20nM or 40nM). Halofuginone was administered at day 4 following DMSO/4OHT induction. Experimental wells contained treated IMR90 ER:RAS cells co-cultured with NK92-MI cells at either a 5:1 E:T **(A)** or 2:1 E:T **(B)** ratio. Percentage change in cell count was measured based on the change in nuclei count (DAPI) of IMR90 ER:RAS cells over 48 hours of co-culture. Control wells contained treated IMR90 ER:RAS in the absence of NK cells (*n* = 5).

(C) Representative images of IMR90 ER:RAS cells treated with DMSO or 4OHT alone and in combination with halofuginone (20nM or 40nM) treatment before and after co-culture with NK cells at a 2:1 E:T ratio, as described in **(B)** (*n* = 5). Scale bar, 300µm.

(A & B) Ordinary one-way ANOVA.

n signifies independent experiments. All error bars represent mean ± SD. *P < 0.05, **P < 0.01, ***P < 0.001, ****P < 0.0001; ns= not significant.

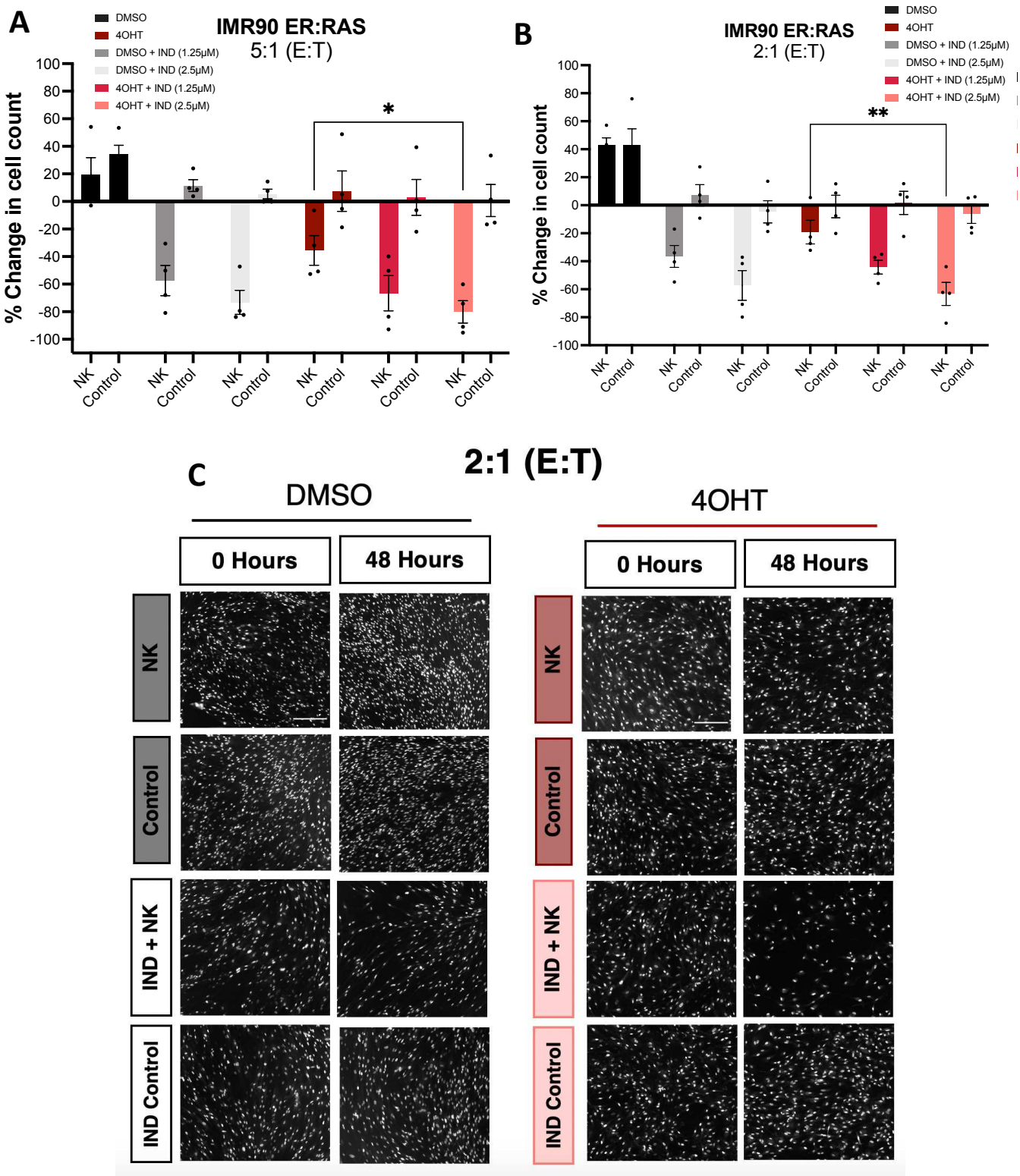


Figure 3.12 Indisulam potentiates NK cell-mediated killing of senescent IMR90 ER:RAS cells

(A & B) Quantification of NK cell-mediated cytotoxicity of IMR90 ER:RAS cells 8 days following treatment with either DMSO or 4OHT alone or in combination with indisulam (1.25μM or 2.5μM). Indisulam was administered at day 4 following DMSO/4OHT induction. Experimental wells contained treated IMR90 ER:RAS cells co-cultured with NK92-MI cells at either a 5:1 E:T (A) or 2:1 E:T (B) ratio. Percentage change in cell count was measured based on the change in nuclei count (DAPI) of IMR90 ER:RAS cells over 48 hours of co-culture. Control wells contained treated IMR90 ER:RAS in the absence of NK cells (*n* = 5).

(C) Representative images of IMR90 ER:RAS cells treated with DMSO or 4OHT alone and in combination with indisulam (1.25μM or 2.5μM) treatment before and after co-culture with NK cells at a 2:1 E:T ratio, as described in (B) (*n* = 5). Scale bar, 300μm.

(A & B) Ordinary one-way ANOVA.

n signifies independent experiments. All error bars represent mean ± SD. *P < 0.05, **P < 0.01, ***P < 0.001, ****P < 0.0001; ns= not significant.

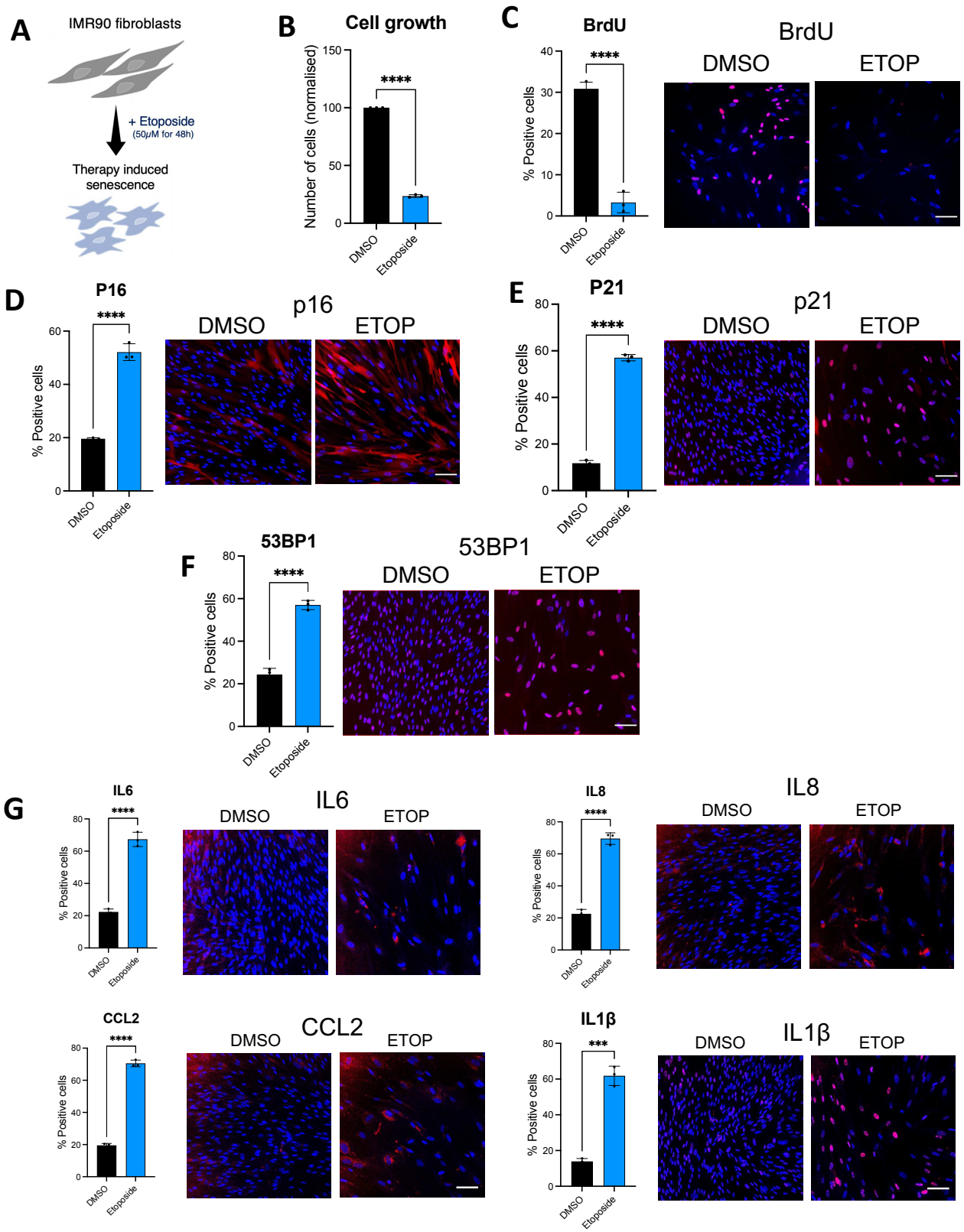


Figure 3.13 Characterisation of etoposide-induced senescence

(A) Schematic of etoposide treatment as a model of therapy-induced senescence (TIS) in IMR90 cells. Etoposide (50μM) was added for 48 hours to induce senescence.

(B) Quantification of the normalised cell growth in IMR90 cells 7 days following administration of DMSO or etoposide (*n* = 3).

(C) Quantification and representative images of IF staining for BrdU incorporation in IMR90 cells. BrdU incorporation was measured 4 days after administration of DMSO or etoposide (*n* = 3). Scale bar, 100μm.

(D-F) Quantification and representative images of IF staining for $p16^{INK4a}$ **(D)**, $p21^{CIP1}$ **(E)**, and 53BP1 **(F)** in IMR90 cells 7 days following administration of DMSO or etoposide (*n* = 3). Scale bar, 100μm.

(G) Quantification of percentage of cells staining positive for the indicated SASP markers and representative IF images in IMR90 cells 10 days following administration of DMSO or etoposide (*n* = 3). Scale bar, 100μm.

(B-G) Unpaired two-tailed Student's *t*-tests.

n signifies independent experiments. All error bars represent mean ± SD. *P < 0.05, **P < 0.01, ***P < 0.001, ****P < 0.0001; ns= not significant.

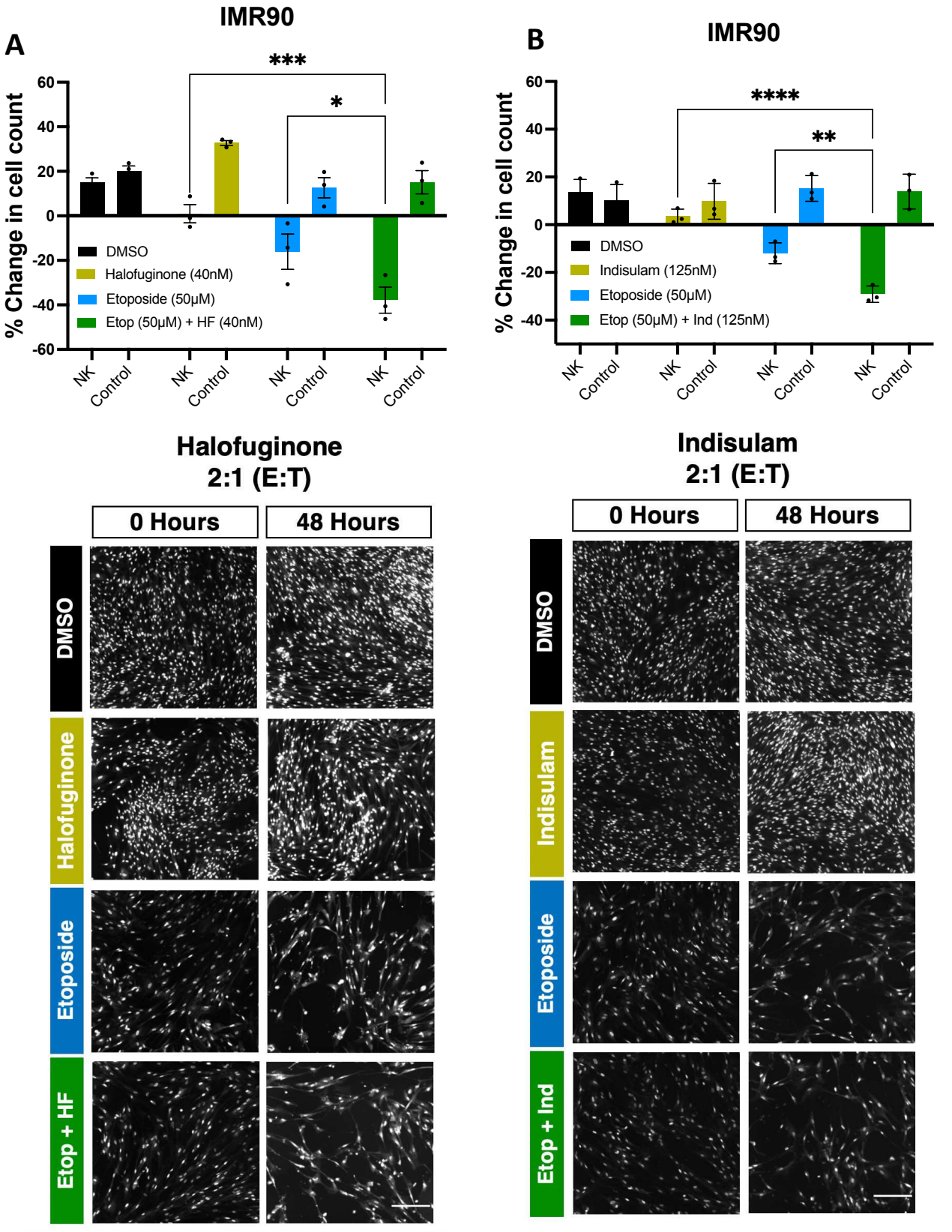


Figure 3.14 Halofuginone and indisulam enhance NK cell-mediated killing of IMR90 cells undergoing TIS

(A & B) Quantification and representative images of NK cell-mediated cytotoxicity of IMR90 cells 7 days following initial administration of either DMSO or etoposide. Halofuginone **(A)** or indisulam **(B)** were added at 4 days after DMSO/etoposide induction. Experimental wells contained treated IMR90 cells co-cultured with NK92-MI cells at a 2:1 E:T ratio. Control wells contained treated IMR90 in the absence of NK cells Percentage change in cell count was measured based on the change in nuclei count (DAPI) of IMR90 cells over 48 hours of co-culture (*n* = 3). Scale bar, 300μm.

(A & B) Two-way ANOVA.

n signifies independent experiments. All error bars represent mean ± SD. *P < 0.05, **P < 0.01, ***P < 0.001, ****P < 0.0001; ns= not significant.

3.7 Pilot screen using siRNAs targeting NK inhibitory ligands

Going forward, we aim to carry out a large-scale siRNA screen to identify genes that potentiate SASP expression and NK-mediated killing of senescent cells. Therefore, we first decided to conduct a pilot siRNA screen to optimise screening conditions and enable us to determine whether this assay could be feasible on a wide scale.

NK cell activity is finely regulated by a complex balance between activating and inhibitory receptor signalling (Kumar, 2018). Therefore, we investigated the knockdown of NK cell inhibitory ligands in OIS IMR90 ER:RAS cells to identify siRNAs increasing NK-mediated killing of senescent cells. We obtained a 96-well custom siRNA library plate (Dharmacon) comprising 4 individual siRNAs targeting 12 inhibitory ligand genes. The 96-well plate format was ideal for assessing NK-mediated cytotoxicity using our high-throughput analysis system. In addition to our target siRNAs, two negative control non-targeting siRNAs (siNT) were used for both growing and senescent cells. To ensure that any inhibitory ligand hits identified from this pilot study are reliable, we also tested five different positive control samples: 1) the inhibitor halofuginone, previously shown to increase NK-mediated killing of senescent cells (Figure 3.11B & C); and 2) four siRNA positive controls (siPTPN1, siSMARCA4, siL3HYPDH, siPGF) that were identified beforehand as reinforcers of NK-mediated killing of cells undergoing OIS through a small-scale trial experiment (data not shown).

Prior to conducting the screen, the transfection conditions were optimised by reverse transfection of the green fluorescent-labelled siRNA siGLO^{TM} (Dharmacon) into growing and senescent IMR90 ER:RAS cells using multiple different concentrations of the transfection reagent DharmaFECT 1. Ultimately, we used the same transfection conditions previously established in our group (reported in detail in Georgilis et al., 2018). For the pilot screen, IMR90 ER:RAS cells were reverse-transfected with the siRNA libraries (Figure 3.15A). Oncogene-induced senescence was subsequently induced by 4OHT treatment, and after a 7-day incubation period, NK cells were added at a 2:1 E:T ratio to the transfected senescent cells. Consistent with previous findings, we observed NK cells selectively killed senescent cells transfected with the non-targeting siRNA relative to the non-senescent cells. A stringent threshold was applied to identify hits set as the percentage change in IMR90 ER:RAS cell counts after co-culture

('Cytotoxicity Score') equal to 1 SD above the 'Cytotoxicity Score' of the senescent negative controls (4OHT siNT). Hits were identified according to this threshold. For each gene, at least 2 siRNAs (out of 4) must fall above this threshold in a minimum of 2 replicates (out of 3). Following this criterion, 5 out of the 12 NK cell inhibitory ligands tested were selected (Figure 3.15B & C). These included the MHC-I molecule HLA-E, consistent with the results from the literature (Pereira et al., 2019) (Figure 3.15C & E). PDCDLG1 encodes the immune checkpoint receptor ligand PD-L2 and is well known for inhibiting T cell activity by binding to the immunoinhibitory receptor PD-1 (Latchman et al., 2001). Interestingly, our results suggest that PD-L2 also negatively regulates NK-mediated cytotoxic activity in senescent cells as knockdown of PDCDLG1 significantly promoted NK-mediated clearance of senescent fibroblasts (Figure 3.15C & F). The remaining hits identified were the NK inhibitory ligands NECTIN2, CLEC2D, and SLC35A1.

To verify that the downregulation of NK inhibitory ligands is responsible for the increased NK-mediated killing of senescent cells, we measured IMR90 ER:RAS cell viability in the absence of NK cells (Figure 3.15D). With almost all samples, we did not observe IMR90 ER:RAS cell death from siRNA transfection alone, suggesting that the senescent cell death was dependent on NK cells. Overall, based on these experiments, we were able to set up a co-culture system to measure NK cell-mediated killing of senescent cells that is amenable to investigate the effects of drugs and siRNAs.

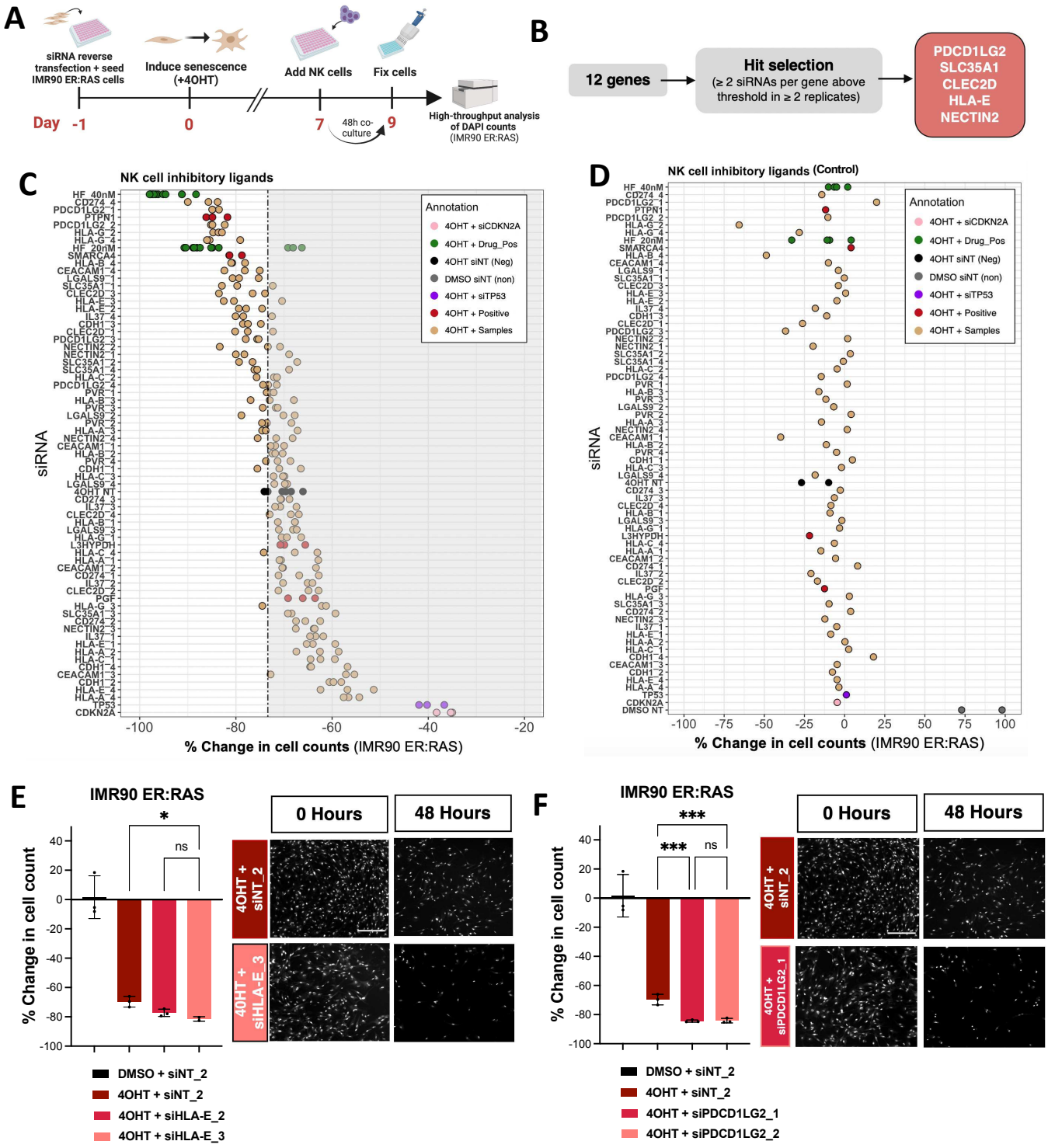


Figure 3.15 Downregulation of NK cell inhibitory ligands promotes NK cell-mediated killing of senescent cells

(A) Schematic of the experimental settings for siRNA knockdown of NK cell inhibitory ligands in IMR90 ER:RAS cells.

(B) Flowchart outlining the results of the pilot siRNA screen against 12 genes for NK cell inhibitory ligands. Following hit selection criteria, 5 genes listed were considered hits.

(C) Scatter plot displaying the quantification of NK cell-mediated cytotoxicity of siRNA-transfected IMR90 ER:RAS cells. IMR90 ER:RAS cells were transfected with either control siRNAs or 4 deconvoluted siRNAs each targeting an NK cell inhibitory ligand. 12 distinct genes for NK inhibitory ligands were examined. Following transfection, IMR90 ER:RAS cells were treated with DMSO or 4OHT as appropriate for 7 days and then co-cultured with NK92-MI cells at a 2:1 E:T ratio over 48 hours. Percentage change in cell count was measured based on the change in nuclei count (DAPI) of IMR90 ER:RAS cells over 48 hours of co-culture. Y axis lists all siRNAs. Each dot represents 1 biological replicate experiment for each siRNA (n = 3).

(D) Scatter plot for the control experiment as described in **(C)**. siRNA-transfected IMR90 ER:RAS cells were treated with DMSO or 4OHT as appropriate for 7 days but did not undergo not co-culture with NK92-MI cells. Experiment was performed in conjunction with **(C)** (n = 1).

(E & F) Quantification and representative images of NK cell-mediated cytotoxicity of IMR90 ER:RAS transfected with siRNAs against the genes HLA-E **(E)** or PDCD1LG2 **(F)**, both of which were hits identified from **(C)**. Percentage change in cell count was measured based on the change in nuclei count (DAPI) of IMR90 ER:RAS cells over 48 hours of co-culture (n = 3). Scale bar, 300μm.

(E & F) Ordinary one-way ANOVA.

n signifies independent experiments. All error bars represent mean ± SD. *P < 0.05, **P < 0.01, ***P < 0.001, ****P < 0.0001; ns= not significant.

3.8 Summary and Discussion

The immune system's involvement in the clearance of stressed or senescent cells has been well documented (Antonangeli et al., 2019; Kale et al., 2020) and has amassed significant interest as an alternative therapeutic approach to small-molecule senolytics for eliminating senescent cells. Furthermore, NK cells display vital effector functions against senescent cells and do not require initial priming but instead can be activated by signalling from secreted cytokines (Birch and Gil, 2020), making them ideal senotherapeutic candidates. In this current chapter, we aimed to set up the conditions to screen for novel regulators of NK-mediated killing of senescent cells.

We first established a model of OIS. In addition to upregulating various senescence markers, IMR90 ER:RAS cells undergoing OIS upregulated several proinflammatory cytokines (ranging from 50 to a 1,000-fold increase), as well as NK cell-activating factors, including CCL2 and TNF-α. Suppressing SASP expression through beclomethasone or triamcinolone treatment reduced the concentration of cytokines secreted from the senescent cells. Having observed elevated IL6 and IL8 secretion upon senescence induction, we also validated the enrichment of CXCL10, an important immunostimulatory SASP component. However, these findings do not exclude the possibility that other activation molecules within the SASP may be at play in recruiting NK cells. Therefore, it is important to investigate additional NK-attracting chemokines (such as CCL5) and interleukins (such as IL15) and to validate further the exact mechanism of how our senescent cells interact with NK cells and whether this can be exploited to promote NK-mediated senescence surveillance.

Several findings in recent literature have reported the significance of SASP activation in mediating immune surveillance of senescent cells (Cuollo et al., 2020; Prieto and Baker, 2019; Saleh et al., 2018). Interestingly, a recent study suggested that $p21^{CIP1}$ overexpression in stressed cells was capable of halting cell cycle progression and orchestrating an immunosurveillance programme through the secretion of chemokines, further emphasising the role of secreted immunomodulatory components in triggering a cytotoxic immune response (Reen and Gil, 2021; Sturmlechner et al., 2021). In line with established literature, we showed that the SASP regulates NK cell recruitment. NK cells did not migrate towards the CM from non-senescent cells but instead were attracted to the CM of senescent fibroblasts.

Furthermore, blocking CXCR2 signalling strongly inhibited the migration of NK cells, highlighting the relevance of the SASP programme for NK cell activity. As we aim to identify novel siRNAs or compounds that can increase the SASP and, in turn, NK-mediated killing of senescent cells, it would be interesting to exploit this NK cell chemotaxis assay to study the effect of potential candidates in regulating NK cell recruitment towards senescent cells.

In line with published reports (Sagiv and Krizhanovsky, 2013; Tasdemir et al., 2016; Xue et al., 2007), we observed that NK cells preferentially targeted and killed senescent cells. We used live cell microscopy to visualise selective NK cell-mediated cytotoxicity, and high throughput analysis to quantify the changes in senescent cell numbers following co-culture with NK cells. Our objective at this stage of the project was to set up an assay to evaluate NK-based senescence surveillance. This assay must have several attributes: a) accuracy to measure NK-mediated killing (i.e. change in senescent cell viability after NK cell co-culture); b) physiologically relevant conditions; c) adequate robustness between replicates; d) amenable to measure changes caused by siRNAs and drugs; e) amenable to perform on a large-scale; f) reproducibility. Several groups have recently performed NK cell co-cultures with senescent cells using distinct protocols to measure NK cell-arbitrated killing. For instance, in co-cultures of irradiated senescent skin fibroblasts with primary NK cells, cytotoxicity was evaluated based on caspase-3 activation (Pereira et al., 2019). Similarly, Ruscetti and colleagues co-cultured NK cells with senescent KRAS mutant lung and pancreatic tumours and measured senescent cell viability through DRAQ7 staining (Ruscetti et al., 2018). Dissimilar to these studies, the challenges we faced when directly calculating cell death was that in our co-culture system, the NK cells were cultured directly in the medium of the target senescent cell as opposed to the NK culture media. Therefore, despite the increased NK cell activity and proliferation, we also observed a minority of NK cells dying, which would otherwise interfere with calculations based on cell death measurements. In another former study by Tasdemir and colleagues, NK cells were co-cultured with TIS IMR90 cells expressing a GFP-linked shRNA. Quantifying NK-mediated cytotoxicity was based on detecting GFP-positive cells (Tasdemir et al., 2016). Analogous to this study, we used NK cell co-cultures with IMR90 ER:RAS cells expressing either cellular turboGFP or nuclear GFP to measure changes in senescent cell counts. Although helpful in visualising and quantifying the senescent-NK cell interaction in a small experimental setting, this

assay would pose a logistical challenge to perform rapidly at a large scale for screening purposes. Several other studies have developed different techniques for measurements of NK-mediated killing of senescent cells, including quantification of crystal violet staining (Sagiv et al., 2016), or the release of lactate dehydrogenase (LDH) from senescent cells (Kim et al., 2022), depending on the senescence inducer, or the NK cell type. We employed a high-throughput system (HTS) that quantifies senescent cells based on DAPI staining. This approach fits the criteria for all the attributes we required of an assay to measure NK-mediated cytotoxicity of senescent cells.

We tested a range of effector-to-target (E:T) ratios to adjust for optimal physiological conditions for NK cell-mediated senescence surveillance. Several lines of evidence have reported the benefits of NK cells as a major senotherapeutic avenue (Kale et al., 2020). However, in many studies, the co-culture conditions may not be fully representative of an internal milieu whereby NK cells are not actively present at high ratios (Pereira et al., 2019; Ruscetti et al., 2018), including some cases whereby E:T ratios of over 80:1 are employed (Iannello et al., 2013). Such high E:T ratios may also conflict with the phenomenon of NK cell serial killing, whereby a single NK cell may be capable of killing more than 10 target cells, depending on the NK cell line (Bhat and Watzl, 2007; Choi and Mitchison, 2013; Navarrete-Galvan et al., 2022). In addition, using high E:T ratios such as those reported in the literature might result in increased NK cell-mediated killing of not only senescent but also normal control cells (Pereira et al., 2019). Finally, co-culture duration may be significant to maximise the effect of NK cell killing. It has been described that IL2-activated NK cells secrete only a tiny fraction of their total cytolytic enzyme reserves after 16 hours (Kim et al., 2022; Vanherberghen et al., 2013). A prolonged co-culture period is also required to allow NK cells to use death receptor-mediated apoptosis and to secrete cytolytic granules (Prager and Watzl, 2019). Therefore, based on these studies, a more physiologically relevant NK-mediated killing assay would use a low E:T ratio for a longer co-culture duration. Here, we demonstrated that the optimal settings for our co-culture system are at a 2:1 E:T ratio for 48 hours. These conditions are presumably physiological and produce a selective NK-mediated killing response in senescent cells, and importantly, do not target non-senescent cells. Furthermore, a 2:1 E:T ratio provides a good dynamic range to measure NK-mediated cytotoxicity that can be modulated.

Throughout this chapter, we have also tested whether NK cell-mediated cytotoxicity can be regulated by the SASP. We used SASP-repressing glucocorticoids which effectively suppressed NK-mediated killing of senescent cells without reducing $p16^{INK4a}$ expression. On the other hand, promoting SASP secretion by using HF or indisulam increased NK cell-mediated cytotoxicity in OIS and TIS cell lines.

Additional mechanisms at play may influence NK cell response, including changes in NK ligand activating and inhibitory signalling. Generally, a single NK cell receptor activation is insufficient to trigger NK cell cytotoxicity; instead, synergistic combinations of multiple activating signals are required (Kwon et al., 2017a). However, inhibitory signalling tends to be more dominant and only requires the engagement of a single class of NK inhibitory receptor. As a result, the outcome of engaging both positive and negative receptor signalling favours NK cell inhibition (Long et al., 2013). In addition, senescent cells have been documented to escape NK-mediated surveillance by regulating NK ligand expression. For example, senescent cells cleave and shed their NKG2D ligands (MICA/B) using MMPs, thereby thwarting an NK-mediated response (Muñoz et al., 2019). Ionising radiation-induced senescent fibroblasts can also evade NK cell surveillance by upregulating inhibitory ligand expression, such as HLA-E, which binds to the NKG2A inhibitory receptors on NK cells (Pereira et al., 2019). With this in mind, we carried out a small-scale pilot screen of siRNAs using genes encoding canonical and non-canonical NK inhibitory ligands. In theory, curtailing the inhibitory signals to NK cells should reinforce the positive signals that senescent cells deliver through the SASP and NK activating ligand expression. Following the transfection of siRNAs in IMR90 ER:RAS cells, we identified several inhibitory ligands whose knockdown promoted NK-mediated killing of senescent cells. More importantly, we validated that our NK cell co-culture and analysis system is easily adaptable and can accurately measure the selective targeting of senescent cells by NK cells.

A limitation of our study is that it does not corroborate senescent cell death being directly NK-cell dependent. As aforementioned, quantifying cell viability based on DRAQ7 staining poses logistical difficulties in segregating the positive signal of senescent cell death away from NK cell death. Therefore, it is essential that alternative strategies are used that ensure NK cells directly induce killing of target senescent cells *in vitro*. For example, NK cells target senescent cells through perforin-mediated

exocytosis of apoptotic granzymes (Sagiv et al., 2013). Thus, quantifying apoptosis of senescent cells via caspase activity can validate NK-mediated killing of senescent cells using time-lapse microscopy. A similar strategy would be to perform immunofluorescence staining of any surviving senescent fibroblasts for cleaved-caspase 3/7 levels following coculture with NK cells to validate apoptosis specifically of senescent cells. On the contrary, treating senescent fibroblasts with pan-caspase inhibitors prior to co-culture, or the treatment of NK cells with chemokine inhibitors to impede NK receptor activity, may nullify NK-mediated killing and validate the role of NK cells in directly targeting senescent cells. Indeed, flow cytometry can also be used to measure the upregulation of the activation marker CD69 and the degranulation marker CD107a on NK cells following co-culture indicative of NK92-MI cell stimulation. In addition, elevated production of interferon-gamma (IFN-γ) in the cell free supernatant following co-culture suggests increased NK cytotoxic activity (Leung et al., 2020). On the other hand, within an *in vivo* setting, NK-mediated killing of senescent cells can be validated by treating mice with anti-NK1.1 depleting antibodies to inhibit NK cell activity (in comparison to isotope control antibodies) (see Chapter 7.2 for discussion of future *in vivo* studies).

Finally, the NK cell line used is an essential determinant for senescence surveillance. Here we use the lymphoma-derived NK92-MI cell line, which can self-produce the IL2 cytokine (Tam et al., 1999). IL2 is critical for the proliferation of resting NK cells and inducing cytotoxic activity. Standard NK cell killing assays, using primary human NK cells derived from peripheral blood mononuclear cells (PBMCs) or tumour infiltrating NK cells may show variable cytotoxic activity depending on the concentrations of IL2 administered. The use of NK92-MI cells ensures NK cells maintain cytotoxic activity through self-activation. In addition, NK92-MI possess a high basal level of expression for the degranulation marker CD107a (Leung et al., 2020) and lack most inhibitory killer cell immunoglobulin-like receptors (KIRs) (Tonn and Becker, 2001) which accounts for their marked cytotoxic activity and may also explain, in part, why inhibiting the KIRs HLA-A, HLA-B, and HLA-C did not strongly promote NK-mediated killing of senescent cells. NK92-MI cells, just as its parental NK92 cell line, are also immortal and can be expanded indefinitely. In contrast, among PBMCs, primary NK cells comprise approximately 5 to 20%, and require isolation, expansion and activation prior to use, and can survive only for two to three weeks (Becker et al., 2016). These criteria make NK92-MI cells widely appealing for *in vitro* high-throughput

co-culture assays as they can more consistently phenocopy NK cell behaviour. Regardless, we also aim to validate any screen candidates we identify that promote NK92-MI-mediated killing of senescent cells using primary NK cells from PBMC with senescent IMR90 ER:RAS cells *in vitro* as well as human patient tissue samples.

In addition, despite the immortal nature of this cell line, we have observed in the lab that the cytotoxic competence of these cells declines with increased passaging in culture, potentially impacting NK cell-mediated killing assays. This may have been evident in our pilot siRNA test on NK inhibitory ligands, whereby senescent cells transfected with the control non-targeting siRNAs showed a relatively higher cell death following co-culture with low-passage NK cells compared with previous tests at the same 2:1 E:T ratio. This indicates the need to utilise lower-passage NK cells for consistency. Indeed, the increased NK cell-mediated killing effect could also result from experimental-specific features such as increased stress of siRNA transfections or the passage status and seeding densities of the target cells. Despite some variability, all assays will comprise a positive and negative control to allow an unbiased comparison of changes in senescent cell killing mediated by NK cells.

Overall, based on our experiments, we have set up a system to quantify NK-dependent killing that can be used to screen for factors that modulate NK-mediated killing of cells undergoing OIS and TIS.

Chapter 4 - Screen for siRNAs potentiating the SASP

4.1 Introduction

Stress-induced premature senescence, such as oncogene-induced senescence, arrests cell proliferation and triggers a complex SASP programme. The SASP is a medium of intercellular communication which allows senescent cells to influence their surrounding microenvironment (Birch and Gil, 2020). For instance, the SASP can promote the recruitment of immune cells, favouring the clearance of senescent cells (Fafián-Labora and O'Loghlen, 2020). We previously reported that the SASP of OIS and TIS IMR90 cells is enriched in NK cell activating factors that incite NK cell recruitment and a potent anti-senescence NK cell surveillance system. However, *in vivo*, the efficacy of NK-mediated cytotoxicity of senescent cells may deteriorate over time for reasons including, but not limited to, age (immunosenescence) or immune evasion mechanisms instigated by senescent cells. Consequently, there is tremendous potential in stimulating NK cell effector functions as a 'natural senolytic' therapy by potentiating SASP expression, for example, to eliminate senescent tumour cells in combination with cytostatic drugs (Ruscetti et al., 2018).

Therefore, in this current chapter, we aim to identify siRNAs increasing the SASP using an unbiased screen. Loss-of-function screens have been extensively used to discover regulators of senescence (Acosta et al., 2008; Herranz et al., 2015; Tordella et al., 2016). In addition, our group has previously screened for repressors of the SASP (Georgilis et al., 2018). However, to our knowledge, no large-scale genetic screens for factors able to potentiate the SASP have been conducted. We theorise that increasing SASP expression would bolster an anti-senescence immune programme. Here, we use RNAi screening to identify new SASP-promoting siRNAs.

4.2 Large-scale siRNA screen to identify SASP reinforcers

To screen for siRNAs that potentiate the SASP, we used the human siGENOME SMARTpool library of siRNAs targeting the druggable genome, including protein kinases, GPCRs, ion channels, proteases, phosphatases, and a subset of ubiquitin conjugation ligases, altogether comprising over 7,500 genes

(Dharmacon). The siRNAs were organised in 96-well plates, thereby facilitating high content analysis of immunofluorescence (IF) SASP staining through our automated high-throughput imaging system. The screen was performed with IMR90 ER:RAS cells and used IL6 and IL8 as SASP readouts. It is important to note that the preliminary optimisation and the initial large-scale siRNA screen for SASP reinforcers were performed by a past postdoctoral researcher from our group, Dr Pia Søgaard. All subsequent analyses on the screen data and all additional screens were conducted by myself.

Before performing the screen, we first needed to set up the screening conditions (e.g., controls, timepoints, and siRNA transfection settings). A previous siRNA screen in our group identified suppressors of the SASP in IMR90 ER:RAS cells (Georgilis et al., 2018). Based on this study, we applied the same transfection conditions for our siRNA screen, using 0.1µL of DharmaFECT^{TM}1 transfection reagent to achieve the highest knockdown (KD) efficiency of target genes compared to wells containing water (mock) or non-targeting control siRNAs (see Methods and Materials, Chapter 2.8). Next, positive control siRNAs that upregulate IL6 and IL8 were selected. The study by Georgilis and colleagues identified 125 genes that suppress the SASP in cells undergoing OIS and 96 genes that increased SASP expression (even if the screen was not optimised to identify siRNAs increasing the SASP) (Georgilis et al., 2018). Using a customised siRNA library (Dharmacon), we tested individual siRNAs against these 96 genes for upregulation of IL6 and IL8 expression in senescent IMR90 ER:RAS cells. The SASP was measured seven days post senescence induction as this timepoint struck the right balance in which the SASP was at a high enough level to be detected by IF, yet sufficiently low to provide a large dynamic range to measure increases in SASP expression using siRNAs. We identified siRNAs against 4 genes, namely LGMN, SIRT1, LPAR2, and EPRS, that potentiated IL6 and/or IL8 expression and would be used as positive controls for our screen.

Based on the optimised settings, we screened the siRNA druggable genome library targeting 7,560 genes to identify novel SASP reinforcers (Figure 4.1A). The library contained 4 pooled siRNAs against each gene. We configured each plate to include a set of controls: non-targeting siRNAs (siNT) as negative controls, and siRNAs against LGMN, SIRT1, LPAR2, and EPRS as positive controls. IMR90 ER:RAS cells were reverse transfected with the siRNAs before being treated with either DMSO or 4OHT

(to induce senescence) the following day, with the treatment lasting up to 7 days (Figure 4.1A). The screen readouts measured the percentage of cells expressing IL6 and IL8 above a set threshold that excludes any background staining stemming from autofluorescence. To mitigate any potential variation in the screen, a plate-median normalisation method was employed, termed the B-score normalisation (Brideau et al., 2003). Each sample well in the plate is assigned a 'B-score' for both IL6 expression and IL8 expression individually, to which an algorithm is applied that makes use of the spatial location of each well in the plate and the cell numbers seeded. The normalised B-scores for all wells from all plates in each replicate experiment were coalesced to produce a normal distribution (Figure 4.1B), whereby the wells containing control non-targeting siRNAs were present along the midpoint, with a normalised value of approximately 0. On the contrary, control siRNAs or any sample siRNAs strongly upregulating (or downregulating) the SASP produced B-scores on the tail end of the distribution plots.

Following normalisation, we next wanted to select siRNAs upregulating the expression of IL6 and IL8. To identify hits in an unbiased manner, we first analysed how each siRNA scored for SASP expression compared to the controls (Figure 4.1C). To select the top siRNAs that potentiate the SASP, we applied a stringent filtering criterion beyond the intersecting B-score of the negative and positive controls (Figure 4.1C). Specifically, the threshold was the B-score corresponding to two standard deviations (SD) above the mean B-score of the senescent non-targeting negative controls for each SASP readout. We performed the analysis individually for IL6 (Figure 4.1D) and classified all genes above the cut-off. We only considered candidates if the siRNAs increased IL6 expression above the threshold in both replicates (Figure 4.1E). Based on this selection, we identified 184 hits increasing IL6 expression. We then repeated this analysis for IL8 expression and discovered 336 hits that passed the criteria (Figure 4.1F & G). To ensure the robustness of the hits to be retested, we shortlisted only those candidates for further analysis that upregulated expression of both IL6 and IL8. Consequently, we selected 156 hits for secondary assays (Figure 4.1H).

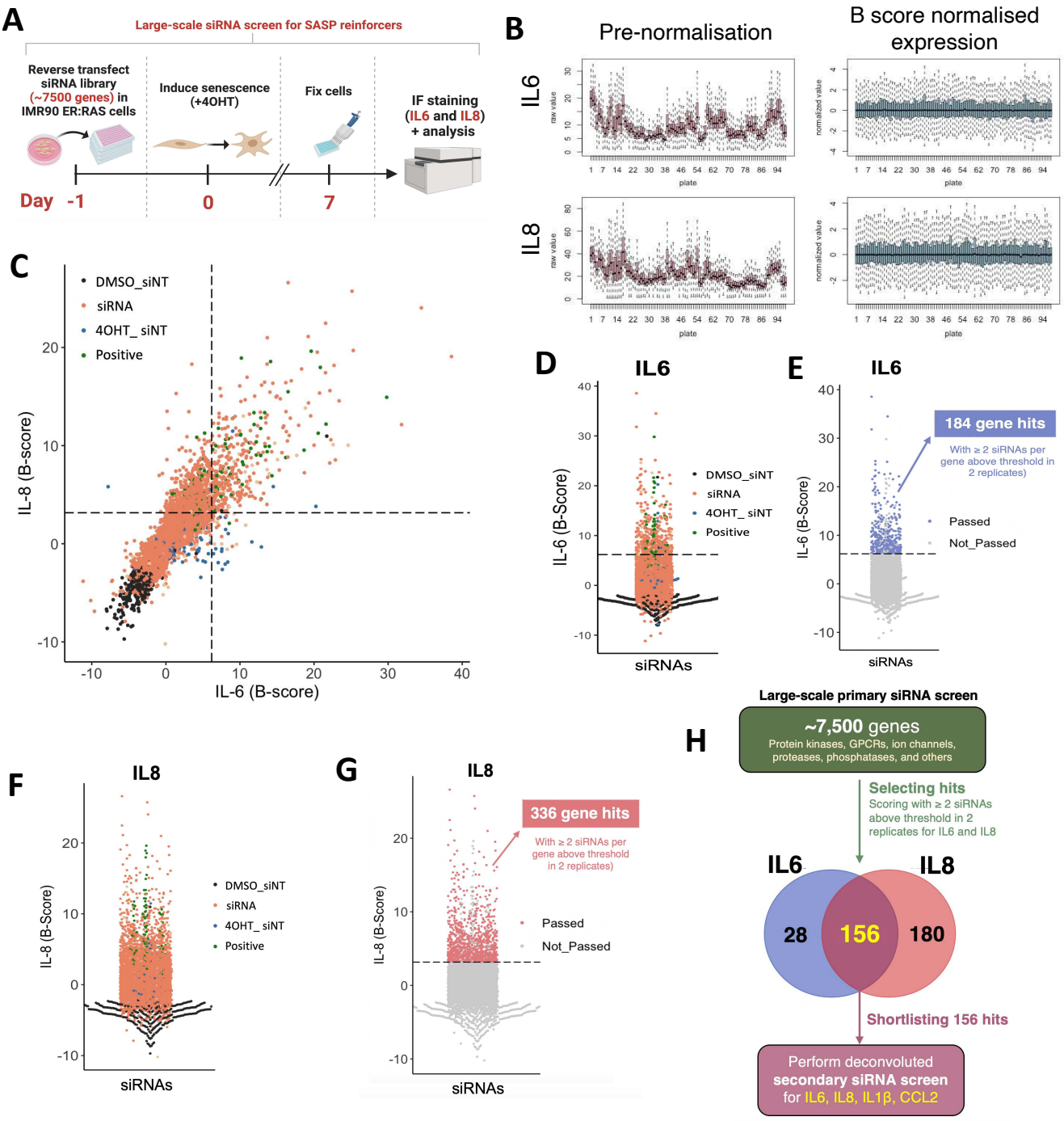


Figure 4.1 Large scale siRNA screen identifies siRNAs enhancing SASP expression

(A) Schematic of the experimental settings for the primary siRNA screen in IMR90 ER:RAS cells to identify reinforcers of the SASP during OIS. Screen comprised of siRNAs against ~7,500 genes from the 'druggable genome' library.

(B) B-score normalisation for IL6 and IL8 from the siRNA screen described in **(A)**. Distribution of the normalisation within each screen plate is displayed as an individual box-and-whisker plot. Left panel shows the raw B-score value prior to normalisation for the expression of IL6 or IL8 for plates containing IMR90 ER:RAS cells transfected with siRNAs. Right panel shows the normalised B-score values for each screened plate. Hit selection based on having a B-score in ≥2 siRNAs for a specific gene in 2 replicates. Displayed are the representative pre- and post-normalisation distributions for 1 biological replicate of the primary screen out of 2 (*n*=2).

(C) Scatter plot of the screen results showing B-score normalised values of IL6 against IL8 for each siRNA sample in the screen. Each dot represents a replicate siRNA. Dashed lines indicate the threshold set at the mean of the senescent non-targeting negative controls + 2 SDs for each of IL6 and IL8. Hits were selected if ≥ 2 siRNAs for a gene scored above the threshold for IL6 or IL8 in 2 replicates (*n*=2).

(D & E) Dot plot of the screen results showing the distribution of B-score normalised values of IL6 for each siRNA across both replicates of the screen **(D)** and selection of hits that enhance IL6 expression **(E)**. Dashed lines indicates the threshold as in **(C).** 184 hits were selected whose knockdown (KD) enhances IL6 expression **(E)** above the threshold with ≥2 siRNAs in 2 replicates (*n*=2).

(F & G) Dot plot of the screen results showing the distribution of B-score normalised values of IL8 for each siRNA across both replicates of the screen **(F)** and selection of hits whose KD enhance IL8 expression **(G)**. Dashed lines indicates the threshold as in **(C).** 336 hits were selected for reinforcing IL8 expression **(G)** in which ≥2 siRNAs scored above the threshold in 2 replicates (*n*=2).

(H) Summary of the large-scale RNAi screen to identify SASP reinforcers. Initially, siRNAs targeting ~7,500 genes were screened in OIS IMR90 ER:RAS cells. KD of 156 hits enhanced both IL6 and IL8 expression. These 156 hits were selected for secondary siRNA screens.

n signifies independent experiments. All error bars represent mean ± SD. *P < 0.05, **P < 0.01, ***P < 0.001, ****P < 0.0001; ns= not significant.

4.3 Secondary siRNA screen to validate hits potentiating SASP expression

To validate the candidates identified from the large-scale screen, we conducted a secondary siRNA screen using a customised siRNA library (Dharmacon) containing 4 individual siRNAs (rather than a pool) targeting each of the 156 hits. We included the same controls as the primary screen and measured not only IL6 and IL8 expression but also IL1β and CCL2. Following the secondary screen, the data was normalised using an alternative control-based plate normalisation method termed the normalised percent activation (NPA) rather than the B-score. B-score normalisation requires all samples to be inactive (i.e., unbiased for the readout) and randomly distributed across plates (Brideau et al., 2003). However, candidates for the secondary screen were selected based on their ability to increase IL6 and IL8 expression upon knockdown, thereby biasing the screen. The NPA method normalised each sample to both the positive and negative controls within each plate to assign an NPA score (see Methods and Materials, Chapter 2.8.2). For our secondary screen, the threshold for hit selection was tailored to the individual SASP readouts as opposed to a broad-spectrum cut-off to allow a more fitted and stringent selection of validated hits.

To identify hits potentiating IL6 expression in senescent cells, a threshold was assigned at an NPA score of ≥ 1, suggesting that any hits selected increase IL6 expression beyond the normalised mean expression of the positive controls. Hits were chosen if at least 2 siRNAs (out of 4) increased the induction of IL6 above the threshold in at least 2 out of 3 replicates (Figure 4.2A). According to these criteria, we identified 39 genes whose knockdown increased IL6 expression in senescent IMR90 ER:RAS cells. To validate these findings, we investigated two randomly selected hits, SSH3 and L3HYPDH, in which at least 2 siRNAs targeting these genes significantly increased IL6 expression relative to the senescent non-targeting control, and even higher than the expression of the positive controls (Figure 4.2B-E). We conducted a similar analysis to identify siRNAs increasing the expression of IL8 (Figure 4.3A). Likewise, we identified a large number of hits (82 genes) for which 2 or more siRNAs were above the threshold in at least 2 out of 3 replicates. Downregulating the expression of RFWD2 or EIF5A, for example, significantly increased the percentage of cells expressing IL8, approximately three to four-fold higher than that of the senescent non-targeting controls (Figure 4.3B-E). To select hits upregulating the expression of IL1β or CCL2, a more rigorous filtering threshold was

assigned at an NPA ≥ 2, implying that any genes classified as hits will increase IL1β or CCL2 levels at least two-fold higher than the mean normalised expression of the positive controls. We identified 55 genes whose knockdown raised the normalised expression of IL1β above the cut-off (with ≥2 siRNAs per gene in ≥2 replicates) (Figure 4.4A). For example, siRNAs targeting KDM5C (Figure 4.4B & C) or IGBP1 (Figure 4.4D & E) showed a significant increase in IL1β expression. From the CCL2 analysis, we selected 46 genes with at least 2 siRNAs that passed the threshold in 2 of 3 replicates (Figure 4.5A). Although CCL2 expression was not increased to the extent of other SASP markers, we still observed a significant increase in CCL2 expression with hits, including siRNAs targeting MYBPP1A (Figure 4.5B & C) and SMARCA4 (Figure 4.5C & D).

Overall, this secondary screen identified 124 hits that increased the expression of at least one of the four SASP readouts (Figure 4.6A). Among these, 68 hits upregulated at least two different SASP factors, and we confirmed three genes that significantly increased the expression of all four SASP readouts (IL6, IL8, IL1β, and CCL2) when knocked down compared to the senescent non-targeting control: FCRL2, IGBP1, and FURIN (Figure 4.6B-G).

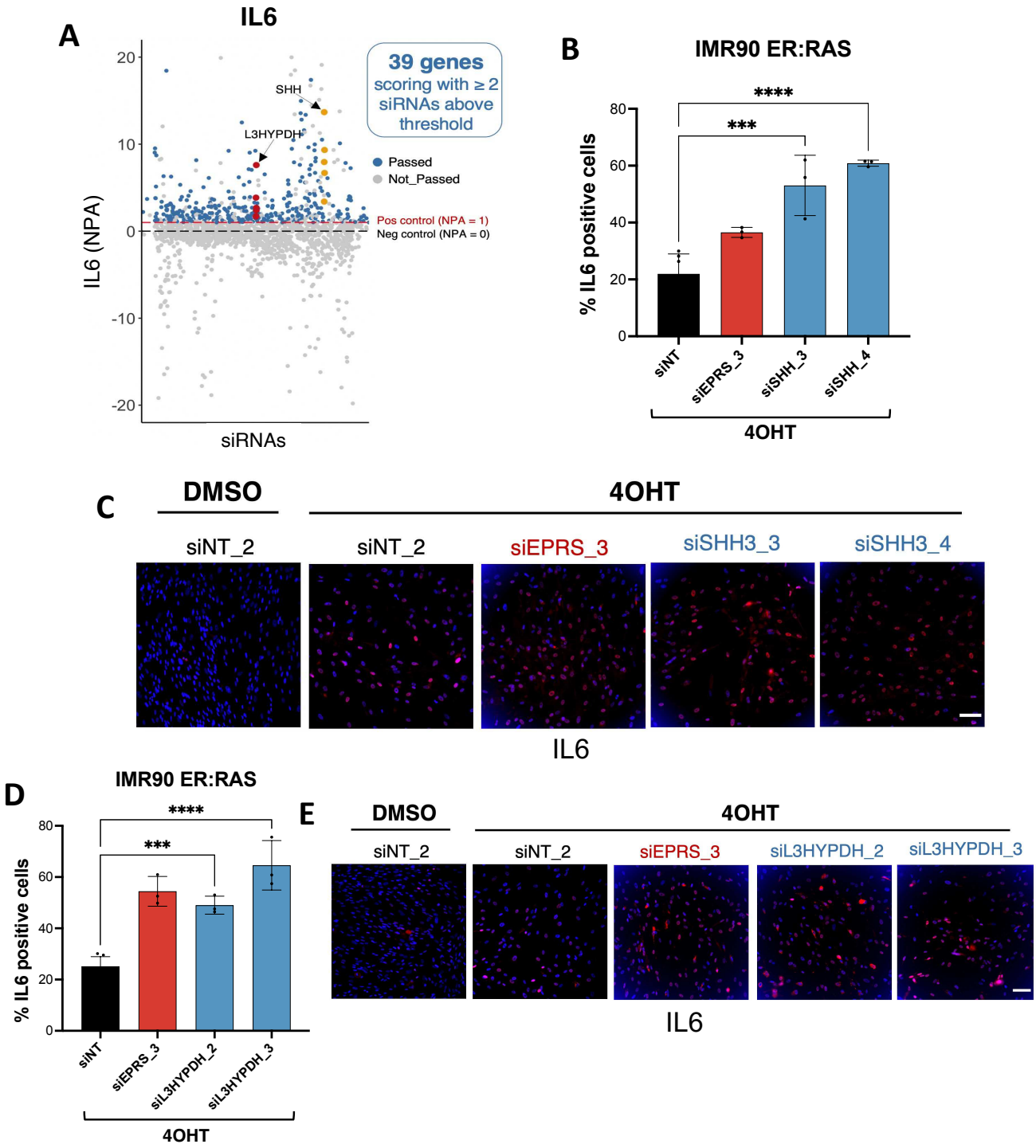


Figure 4.2 Secondary siRNA screen validates hits upregulating IL6

(A) Scatter plot of the secondary siRNA screen results showing NPA (normalised percent activation) values of IL6 for each siRNA sample in the screen. Black dashed lines indicates the mean NPA of the senescent non-targeting negative controls (NPA = 0). Red dashed lines indicates the mean NPA of the senescent siRNA positive controls (NPA = 1). Threshold for the screen was set at NPA ≥ 1. Hit were selected if ≥2 siRNAs per gene were above NPA ≥1 in ≥2 replicates. All hits selected are coloured as indicated. Two hits, SSH3 and L3HYPDH, are highlighted. Overall, 39 genes were selected as hits for IL6 (*n*=3).

(B & C) Quantification of percentage of cells staining positive for IL6 **(B)** and representative IF images **(C)** in OIS IMR90 ER:RAS cells 7 days following transfection of siRNAs targeting SSH3, followed by treatment with DMSO or 4OHT as indicated. For the positive control, siRNAs against EPRS are shown. For the negative control, non-targeting siRNAs were used (*n* = 3). Scale bar, 100µm.

(D & E) Quantification of percentage of cells staining positive for IL6 **(D)** and representative IF images **(E)** in OIS IMR90 ER:RAS cells 7 days following transfection of siRNAs targeting L3HYPDH, followed by treatment with DMSO or 4OHT as indicated. For the positive control, siRNAs against EPRS are shown. For the negative control, non-targeting siRNAs were used (*n* = 3). Scale bar, 100µm.

(B & D) Ordinary one-way ANOVA.

n signifies independent experiments. All error bars represent mean ± SD. *P < 0.05, **P < 0.01, ***P < 0.001, ****P < 0.0001; ns= not significant.

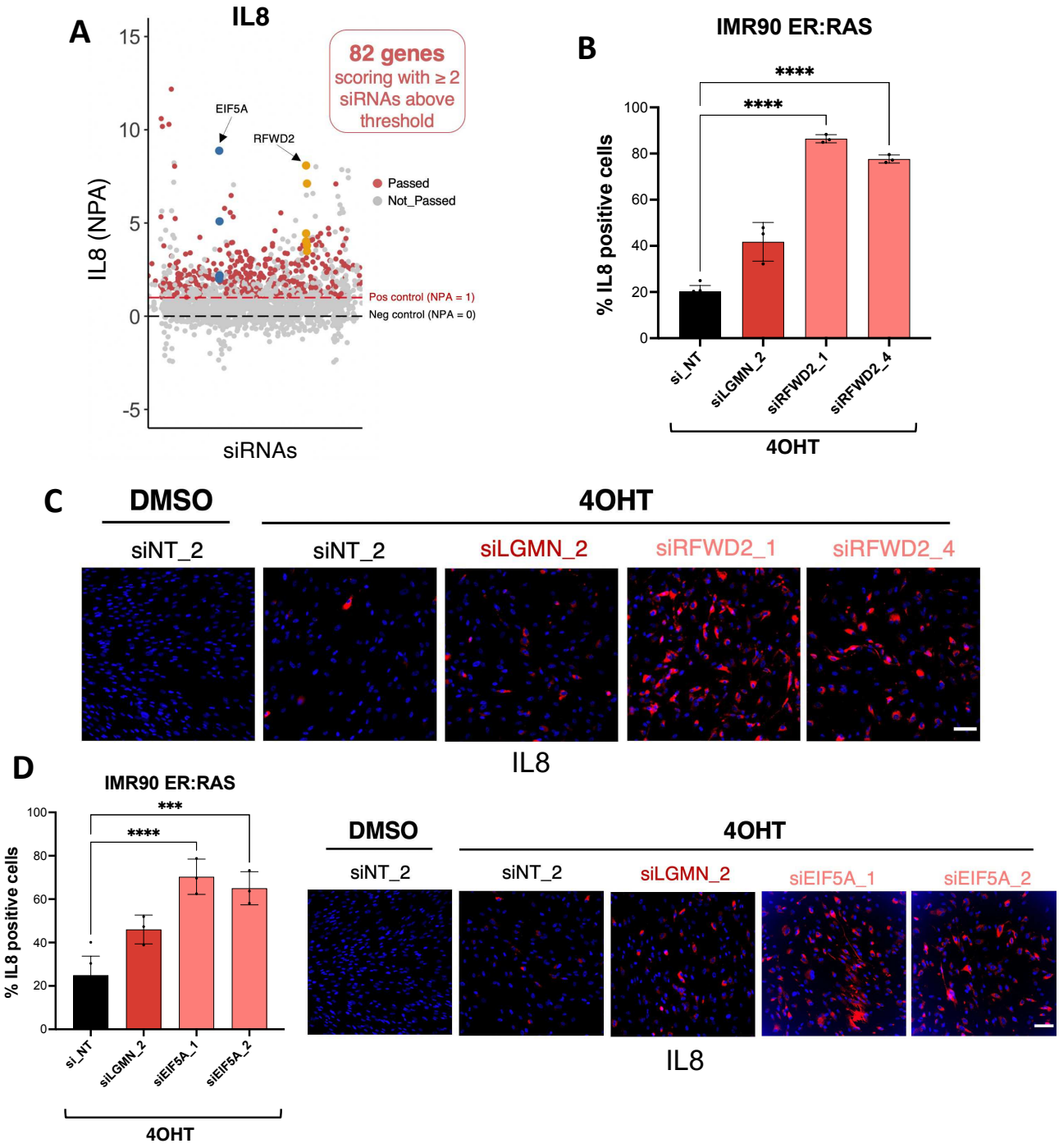


Figure 4.3 Secondary siRNA screen validates hits upregulating IL8

(A) Scatter plot of the secondary siRNA screen results showing NPA values of IL8 for each replicate siRNA sample in the screen. Black dashed lines indicates the mean NPA of the senescent non-targeting siRNA negative controls (NPA = 0). Red dashed lines indicates the mean NPA of the senescent siRNA positive controls (NPA = 1). Threshold for the screen was set at NPA ≥ 1. Hit were selected if ≥2 siRNAs per gene were above NPA ≥1 in ≥2 replicates. All hits selected are coloured as indicated. Two example hits, RFWD2 and EIF5A, are highlighted. Overall, 82 genes were selected as hits for IL8 (*n*=3).

(B & C) Quantification of percentage of cells staining positive for IL8 **(B)** and representative IF images **(C)** in OIS IMR90 ER:RAS cells 7 days following transfection of siRNAs targeting RFWD2, followed by treatment with DMSO or 4OHT as indicated. For the positive control, siRNAs against LGMN are shown. For the negative control, non-targeting siRNAs were used (*n* = 3). Scale bar, 100μm.

(D & E) Quantification of percentage of cells staining positive for IL8 **(D)** and representative IF images **(E)** in OIS IMR90 ER:RAS cells 7 days following transfection of siRNAs targeting EIF5A, followed by treatment with DMSO or 4OHT as indicated. For the positive control, siRNAs against LGMN are shown. For the negative control, non-targeting siRNAs were used (*n* = 3). Scale bar, 100μm.

(B & D) Ordinary one-way ANOVA.

n signifies independent experiments. All error bars represent mean ± SD. *P < 0.05, **P < 0.01, ***P < 0.001, ****P < 0.0001; ns= not significant.

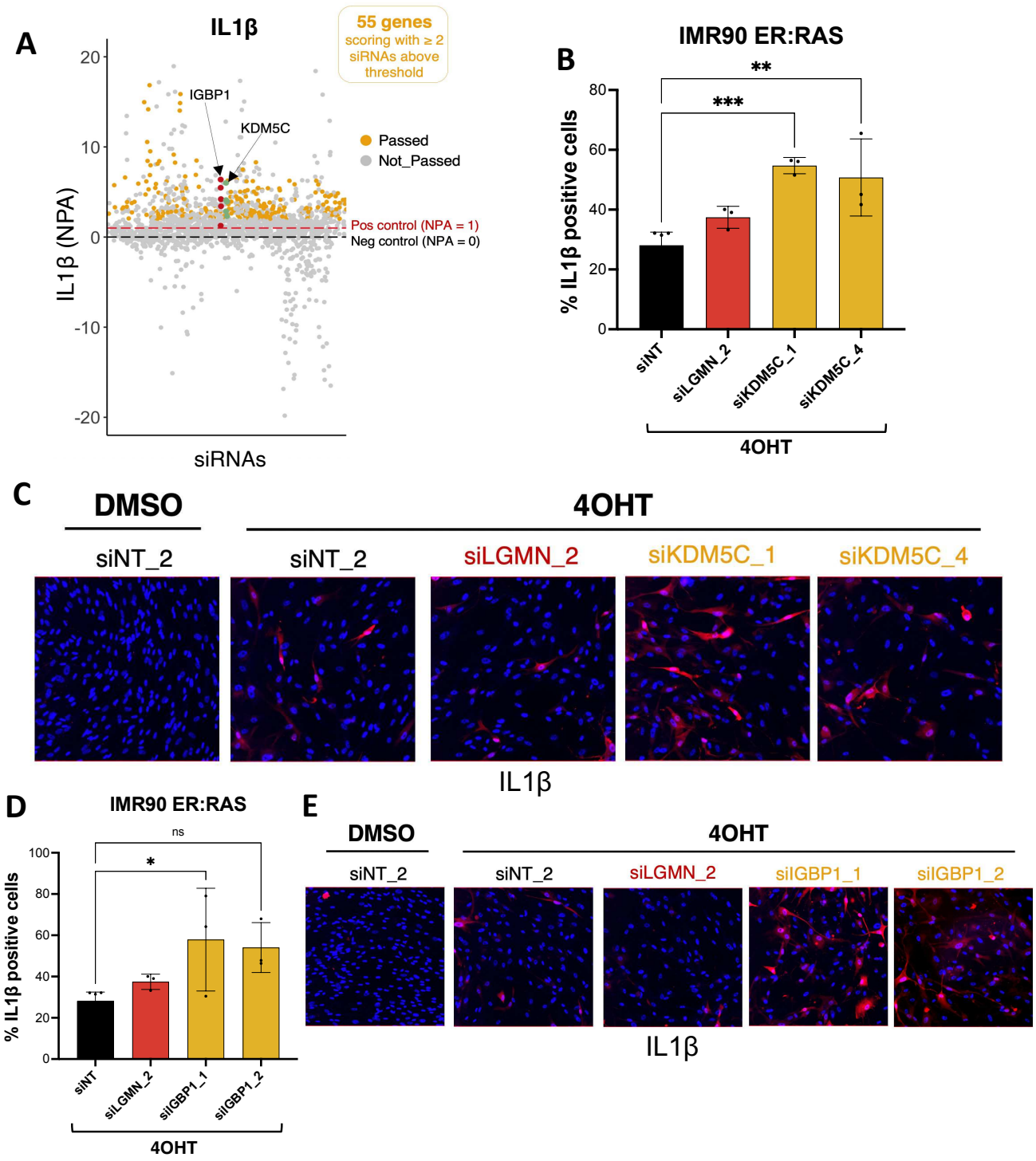


Figure 4.4 Secondary siRNA screen validates hits upregulating IL1β

(A) Scatter plot of the secondary siRNA screen results showing NPA values of IL1β for each replicate siRNA sample in the screen. Black dashed lines indicates the mean NPA of the senescent non-targeting siRNA negative controls (NPA = 0). Red dashed lines indicates the mean NPA of the senescent siRNA positive controls (NPA = 1). Threshold for the screen was set at NPA ≥ 1.5. Hit were selected if ≥2 siRNAs per gene were above NPA ≥1.5 in ≥2 replicates. All hits selected are coloured as indicated. Two example hits, KDM5C and IGBP1, are highlighted. Overall, 55 genes were selected as hits for IL1β (*n*=3).

(B & C) Quantification of percentage of cells staining positive for IL1β **(B)** and representative IF images **(C)** in OIS IMR90 ER:RAS cells 7 days following transfection of siRNAs targeting KDM5C, followed by treatment with DMSO or 4OHT as indicated. For the positive control, siRNAs against LGMN are shown. For the negative control, non-targeting siRNAs were used (*n* = 3). Scale bar, 100μm.

(D & E) Quantification of percentage of cells staining positive for IL1β **(D)** and representative IF images **(E)** in OIS IMR90 ER:RAS cells 7 days following transfection of siRNAs targeting IGBP1, followed by treatment with DMSO or 4OHT as indicated. For the positive control, siRNAs against LGMN are shown. For the negative control, non-targeting siRNAs were used (*n* = 3). Scale bar, 100μm.

(B & D) Ordinary one-way ANOVA.

n signifies independent experiments. All error bars represent mean ± SD. *P < 0.05, **P < 0.01, ***P < 0.001, ****P < 0.0001; ns= not significant.

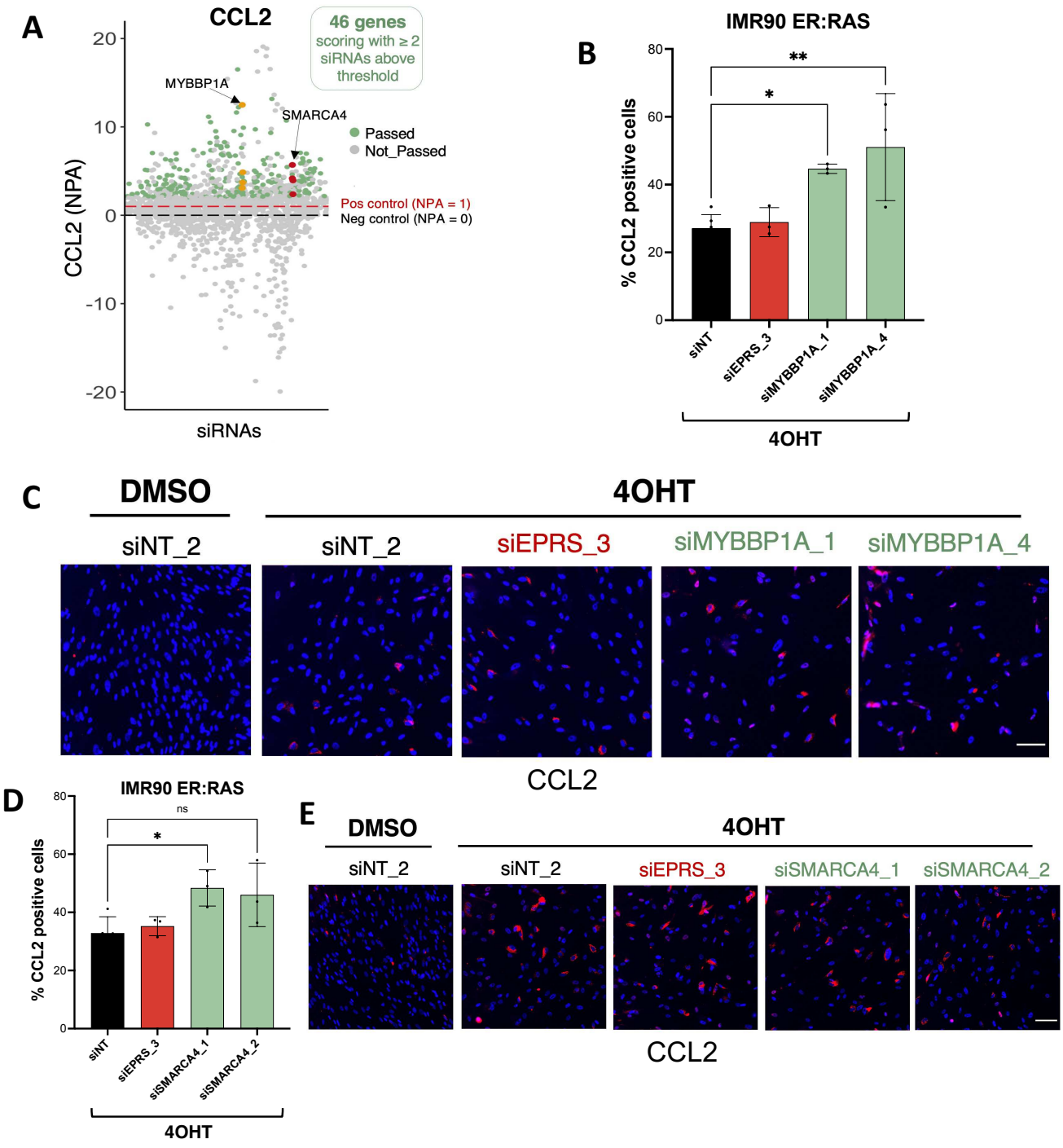


Figure 4.5 Secondary siRNA screen validates hits upregulating CCL2

(A) Scatter plot of the secondary siRNA screen results showing NPA values of CCL2 for each replicate siRNA sample in the screen. Black dashed lines indicates the mean NPA of the senescent non-targeting siRNA negative controls (NPA = 0). Red dashed lines indicates the mean NPA of the senescent siRNA positive controls (NPA = 1). Threshold for the screen was set at NPA ≥ 1.5. Hits were selected if ≥2 siRNAs per gene were above NPA ≥1.5 in ≥2 replicates. All hits selected are coloured as indicated. Two example hits, MYBBP1A and SMARCA4, are highlighted. Overall, 55 genes were selected as hits for CCL2 (*n*=3).

(B & C) Quantification of percentage of cells staining positive for CCL2 **(B)** and representative IF images **(C)** in OIS IMR90 ER:RAS cells 7 days following transfection of siRNAs targeting MYBBP1A, followed by treatment with DMSO or 4OHT as indicated. For the positive control, siRNAs against EPRS are shown. For the negative control, non-targeting siRNAs were used (*n* = 3). Scale bar, 100μm.

(D & E) Quantification of percentage of cells staining positive for CCL2 **(D)** and representative IF images **(E)** in OIS IMR90 ER:RAS cells 7 days following transfection of siRNAs targeting SMARCA4, followed by treatment with DMSO or 4OHT as indicated. For the positive control, siRNAs against EPRS are shown. For the negative control, non-targeting siRNAs were used (*n* = 3). Scale bar, 100μm.

(B & D) Ordinary one-way ANOVA.

n signifies independent experiments. All error bars represent mean ± SD. *P < 0.05, **P < 0.01, ***P < 0.001, ****P < 0.0001; ns= not significant.

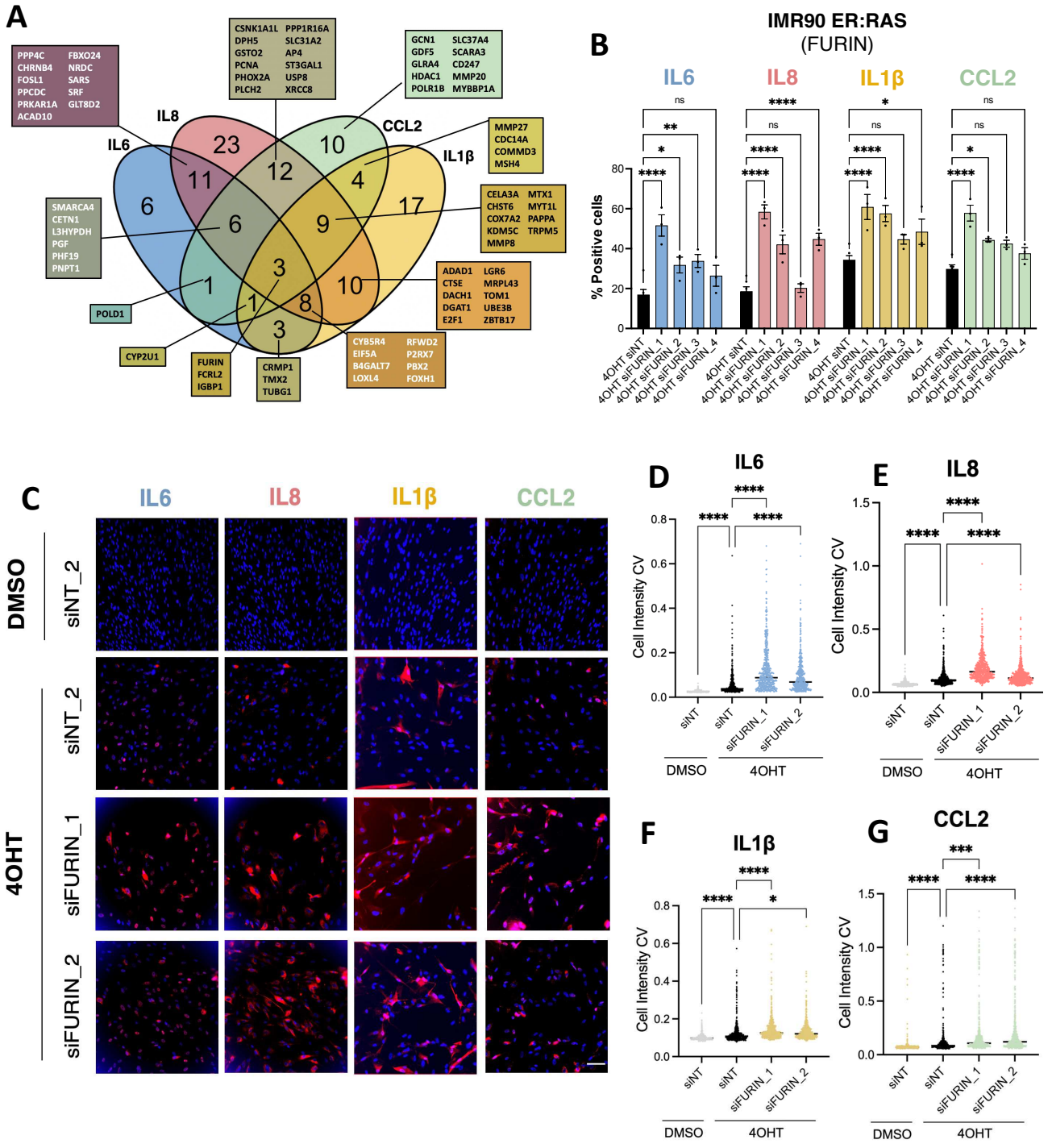


Figure. 4.6 Identifying siRNAs that upregulate the expression of several SASP factors

(A) Venn diagram showing 124 genes selected as hits from the secondary siRNA screen distributed across the 4 SASP readouts. Multiple genes show an upregulation of at least 2 distinct SASP factors upon knockdown in oncogene-induced senescent cells. 3 genes show an increase in all four SASP readouts, including FURIN.

(B) Quantification of the percentage of cells staining positive for the four indicated SASP readouts in OIS IMR90 ER:RAS cells 7 days following transfection of siRNAs against FURIN. Presented are four deconvoluted siRNAs targeting FURIN well as the senescent negative control (n = 3).

(C) Representative images of IF staining for the indicated SASP markers in IMR90 ER:RAS cells transfected with the specified siRNAs and treated with either DMSO or 4OHT, as appropriate for 7 days. siRNAs targeting FURIN strongly potentiate SASP expression in senescent cells relative to the senescent non-targeting control. Scale bar, 100µm.

(D-G) Distribution of 500 arbitrarily selected single cell intensities of each SASP marker within each sample from **(C).**

(B) Two-way ANOVA. **(D-G)** Ordinary one-way ANOVA.

n signifies independent experiments. All error bars represent mean ± SD. *P < 0.05, **P < 0.01, ***P < 0.001, ****P < 0.0001; ns= not significant.

4.4 Summary and discussion

Although prolonged SASP expression is held accountable for the harmful effects associated with senescence, acute SASP facilitates the recruitment of immune cells for senescent cell clearance (Coppé et al., 2010; Faget et al., 2019; Yoshimoto et al., 2013). In the previous chapter, we demonstrated that the SASP is a critical determinant in the recruitment of NK cells and the ensuing NK cell cytolytic activity targeting senescent cells. With this in mind, in the current chapter, we carried out a screen for siRNAs increasing the SASP of cells undergoing OIS. Our rationale was that strategies promoting the SASP may stimulate NK cell-mediated killing of senescent cells. It is important to consider that the total senescent population represents only a minor percentage of all cells within tissues, even with increased age (Biran et al., 2017). Therefore, in a biological context, secretion of immunomodulatory SASP factors would only produce low overall concentrations in the external milieu (Rolt et al., 2019). Consequently, it is even more vital to exogenously and substantially reinforce SASP expression to stimulate an immune response. On top of this, it would be interesting to learn whether any identified hits reinforce the SASP in a broad spectrum of senescence types and in different senescence-elicited pathologies. Of particular relevance is cancer, where we aim to elevate the SASP in tumour cells undergoing therapy-induced senescence to render them vulnerable to NK-mediated killing.

Reinforcing SASP expression to trigger anti-senescence immunity may prove more complex and be context- and tissue-dependent. In past studies, the SASP has been shown to exert an immunosuppressive effect, for instance, through the recruitment of immature myeloid cells that can suppress NK cell activity (Eggert et al., 2016; Di Mitri et al., 2014). Although we plan to examine our hits in NK-mediated killing assays to ensure that any hit promotes NK-mediated killing of senescent cells, whether these effects are relevant in other senescence modes or *in vivo* in the presence of an active immune microenvironment would require examination.

Chronic SASP can cause deleterious effects on the surrounding tissue microenvironment. Persistent proinflammatory SASP secretion (inflammaging) underlies tissue dysfunction and several age-associated disorders (Franceschi and Campisi, 2014). The SASP also induces tumour-promoting

functions, including inciting epithelial-to-mesenchymal transition (EMT) and metastasis (Coppé et al., 2010; Laberge et al., 2012; Takasugi et al., 2022). Therefore, it is no surprise that there are accumulating studies looking into the regulation of the SASP to control its proinflammatory properties (Aird et al., 2016; Herranz et al., 2015; Xu et al., 2015). For example, a study from our lab used an RNAi screen to identify that the KD of PTBP1 (polypyrimidine tract-binding protein 1), a regulator of alternative splicing, suppressed the pro-tumorigenic SASP in pre-cancerous senescent hepatocytes, demonstrating the therapeutic benefits of SASP inhibition to prevent the development of inflammation-driven carcinogenesis (Georgilis et al., 2018). Using a similar screening set-up, here, we instead identified genes that boosted SASP expression to take advantage of the beneficial immunostimulatory properties of an acute SASP. The clearance of senescent cells resulting from the activated immune system should ideally prevent chronic inflammation.

High-throughput screening (HTS) is the cornerstone of modern-day drug discovery and has been widely used in the context of senescence to discover novel regulators (Fuhrmann-Stroissnigg et al., 2017; Guerrero et al., 2019; Herranz et al., 2015; Tordella et al., 2016; Wang et al., 2021; Zhu et al., 2015). Genetic screens, such as those involving siRNAs, shRNAs, and CRISPR, confer many advantages as they can be used to accurately identify pathways associated with a desired therapeutic effect, as well as help better understand the mechanisms of toxicities and resistance associated with drugs (Emmerich et al., 2021). In addition, genetic screens can be used to uncover possible synergistic combination targets by exploiting the synthetic lethal connection between different genes (Kampmann, 2017). Here, we used HTS to carry out a large-scale primary siRNA screen to search for novel inducers of IL6 and IL8 in IMR90 ER:RAS cells undergoing OIS. As described in Chapter 4.2, the initial screen and optimisations were performed by another group member, Dr Pia Søgaard.

Before conducting the primary siRNA screen, we first optimised the screen settings. This involved establishing controls and other conditions of the screen. After several trial experiments, we selected four siRNAs targeting genes that increased IL6 and IL8 expression in senescent cells based on siRNAs previously reported as positive SASP regulators in our lab (Georgilis et al., 2018). These genes included 1) EPRS (an aminoacyl-tRNA synthetase, we have reported the inhibition of EPRS as a potent SASP

inducer); 2) LPAR2 (a receptor for lysophosphatidic acid); 3) LGMN (a cysteine protease, loss of LGMN has recently been reported as an inducer of premature senescence (Wang et al., 2022a); and 4) SIRT1 (a member of the sirtuin family heavily associated with ageing. SIRT1 is well known to suppress SASP activity; therefore, loss of function of SIRT1 is a suitable positive control (Hayakawa et al., 2015). These positive controls were essential to ensure the correct functioning of our screen and for the appropriate normalisation of our data.

To perform the screen, we used a library of pooled siRNAs against 7,560 genes (Dharmacon), targeting the druggable genome. We selected hits based on a strict criterion whereby candidates would only be chosen if they passed the filtering cut-off for IL6 and IL8 expression in both replicates. Naturally, we may have lost some potential candidates. For example, siRNAs for genes that upregulated only one of the two SASP readouts could promote an anti-senescence NK cell response but have been excluded from selection. Nonetheless, the stringent selection ensured we shortlisted the top 156 genes that increase the expression of both IL6 and IL8 cytokines upon knockdown. Whether this knockdown has repercussions on the senescence growth arrest or other cell non-autonomous effects of senescent cells remains to be seen. Similarly, it would be interesting to study whether the silencing of the 156 genes could potentiate a SASP in other forms of senescence.

IL6 and IL8 offer several advantages to be used as screen readouts. Firstly, IL6 and IL8 are highly induced during senescence. Suitable antibodies are available against these factors with high specificities, making these SASP proteins easily detectable by IF. Secondly, IL6 and IL8 are conserved in multiple different senescence types and are robust markers for investigating SASP regulation (Partridge et al., 2020). Thirdly, both IL6 and IL8 have immunomodulatory properties. For example, elevated IL6 levels trigger signal transduction to activate the JAK/STAT3 signalling pathway, eventually resulting in transcriptional activation of STAT3 targets, including a broad range of proinflammatory genes (Heinrich et al., 2003; Kojima et al., 2013). In this manner, IL6 and IL8 secretion from senescent cells may represent a proxy for a broader SASP phenotype. Finally, although other direct immunoregulatory SASP factors exist, such as CCL2 or CXCL10, their detection by IF is more problematic. Therefore, we selected IL6 and IL8 as readouts for our screen.

Due to the scale of the screen, a considerable number of plates were used, meaning that siRNA transfections, as well as the IF staining of the plates, were conducted in batches. Alongside batch effects, high-throughput screening at such a large-scale inadvertently introduces positional effects. These could be the result of 'edge-plate effects' to both the control and sample wells or a technical bias introduced during reverse transfection of seeded cells, giving rise to inter- and intra-plate variability. Hence, the screen relied on automated robotics for acquiring and imaging plates and multichannel pipettes for transfection and staining procedures. It was also fundamental to minimise any sources of variation by applying the B-score normalisation criteria to all plates. The normalisation algorithm assumes that cell counts are similar in all wells, allowing the algorithm to estimate any biases introduced during screening and correct any outlying variables resulting from positional effects or manual handling (for example, during IF staining). To alleviate any additional random errors, the entire screen was repeated under identical experimental conditions, and all data generated from both replicates were collectively normalised and analysed.

Our siRNA screen aimed to identify genes that can strengthen the SASP and provoke an NK-mediated senescence surveillance programme. However, double-stranded siRNAs are recognised as non-self nucleic acids and, as such, can stimulate an immune response (Jackson and Linsley, 2010). As the screen readouts were proinflammatory cytokines, any hit identified could, in theory, have been induced by an immunogenic siRNA transfection, giving rise to false positive hits. To limit this possibility, we selected at least two non-targeting siRNA controls that were transfected into DMSO-treated non-senescent (non-induced) and 4OHT-induced senescent cells (negative control). In addition, the primary screen used an arrayed pool of 4 siRNAs for each gene (as opposed to individual siRNAs) to ensure the screening procedure was not overly cumbersome or intensive. However, siRNA can produce off-target effects, or immunogenic or toxic outcomes, giving rise to false discoveries (Mohr and Perrimon, 2012). Moreover, for such a comprehensive screening analysis, it is logistically challenging to validate the knockdown of each target hit. To address these concerns, we performed a secondary siRNA screen comprised of four deconvoluted siRNAs for each of the 156 shortlisted genes. Using individual siRNAs

to target the same hits during rescreening validates their phenotypic reproducibility and limits the possibility of selecting siRNAs with non-specific targeting.

Although IL6 and IL8 were screen readouts, the SASP comprises hundreds of secreted components. For this reason, our secondary screen examined two additional SASP factors, IL1β and CCL2. IL1β is an important mediator of a proinflammatory SASP and is often secreted from innate immune cells as a signalling mechanism (Lopez-Castejon and Brough, 2011). The latter cytokine, CCL2, is known for its immune-activating properties and plays a crucial role in NK cell recruitment. In a study of RAS-induced hepatocellular carcinoma, CCL2 was shown to be involved in NK cell recruitment (Iannello et al., 2013). These NK cells were then activated by ligands expressed on the tumour to eliminate the senescent cells (Iannello et al., 2013). A later study noted the secretion of CCL2 as a key SASP component in senescent lung tumours to activate an NK cell-mediated cytotoxic response against the tumour (Ruscetti et al., 2018). For our secondary screen, we identified multiple hits that upregulated the expression of IL6, IL8, IL1β, or CCL2. Due to the biased nature of the secondary screen, whereby the hits chosen were already shown to reinforce the SASP, an alternative normalisation method, NPA, was employed rather than the B-score normalisation. NPA normalises all samples based on each plate's positive and negative controls. This posed an issue when identifying hits for the two new screen readouts, IL1β and CCL2, as the positive controls for the screen were optimised for IL6 and IL8. To counterbalance this issue, we applied a rigorous filtering threshold for the IL1β and CCL2 readouts so that the hits selected would significantly reinforce the expression of IL1β and CCL2 beyond the senescent negative control. We ultimately selected only the top hits for each SASP readout, which in theory would be the same, regardless of the controls and normalisation used.

The secondary screening identified 124 hits whose knockdown increased at least one SASP readout, with 68 hits reinforcing multiple SASP factors. Interestingly, the largest proportion of the 68 hits derived from one particular SASP readout: CCL2 (36 genes). This could play to our advantage with the aims of this project. Furthermore, as CCL2 is a crucial NK cell activator, it could also be compelling to investigate hits only upregulating CCL2 expression. Overall, we performed siRNA screens to reveal 68 genes that increase the expression of multiple SASP factors upon knockdown in OIS. Going forward,

we are interested in learning whether silencing these genes can promote NK-mediated killing of senescent cells.

Chapter 5 - Screen for siRNAs potentiating NK-mediated killing of senescent cells

5.1 Introduction

Genetic screenings have been used to identify novel regulators of senescence (Georgilis et al., 2018; Herranz et al., 2015; Tordella et al., 2016; Wang et al., 2017a). Using this approach in the previous chapter, we revealed siRNAs that upregulate the expression of different SASP factors, including immunomodulatory chemokines such as CCL2.

A novel therapeutic strategy proposed for cancer therapy has been the paired administration of a pro-senescence drug to induce a stable growth arrest, promptly followed by a senolytic agent to eradicate any senescent tumour cells, suitably termed the 'one-two punch' approach (Wang and Bernards, 2018). Analogous to this strategy, here we propose to implement a more physiological, immune-dependent one-two punch, whereby the induction of senescence is subsequently combined with strategies that enhance an immunostimulatory SASP to facilitate the immune-mediated clearance of senescent cells. Formerly, we have demonstrated the direct association between the SASP of cells undergoing OIS and the recruitment and cytolytic activity of NK cells. We next wanted to understand whether the SASP-promoting properties of our shortlisted screen candidates can orchestrate an anti-senescence NK cell response.

5.2 siRNA screen of selected SASP reinforcers to enhance NK-mediated killing of senescent cells

In the previous chapter, we identified 124 genes whose knockdown increases SASP expression. To investigate hits that can also evoke NK surveillance of senescent cells, we selected 68 genes that upregulated at least two different SASP factors when silenced. As CCL2 has chemoattractant properties, we selected an additional 8 genes whose knockdown increased CCL2 expression. We also shortlisted siRNAs against 8 genes that have been described to stimulate NK cell surveillance of

leukaemia cells (Pech et al., 2019), resulting in siRNAs against a total of 84 genes for the NK cell co-culture screen (Figure 5.1A).

We designed a customised siRNA library (Dharmacon) comprising four individual siRNAs targeting each of the 84 genes. We adhered to the identical screening conditions and siRNA controls we previously optimised in a pilot assay investigating siRNAs against NK cell inhibitory ligands (see Chapter 3.7). As additional controls, we used indisulam and halofuginone. In total, 1,008 individual datapoints were investigated in the screen, corresponding to all siRNAs across all three replicates (excluding controls) (Figure 5.1A). For the screen, IMR90 ER:RAS cells were reverse transfected with the siRNAs and subsequently treated in the presence or absence of 4OHT for up to 7 days. NK92-MI cells were then added at a 2:1 E:T ratio for 48 hours (Figure 5.1B).

Screen data was normalised using the NPA method to mitigate inter-plate variation. To select siRNAs potentiating NK-mediated killing, we applied a stringent threshold at an NPA value of ≥ 1.5, exceeding the normalised 'Cytotoxicity Score' of the siRNA-positive controls. We identified 295 datapoints that surpassed this cut-off and strongly increased NK-mediated killing of senescent cells (Figure 5.1C). To select candidates, we filtered for those genes with at least 2 out of 4 siRNAs that scored above the threshold in a minimum of 2 out of 3 replicates. We next removed any siRNA outliers that produced highly variable results between the replicates despite high NPA scores. Based on this selection criteria, we identified 22 hits, such as PPP4C and POLR1B, whose knockdown boosted NK-mediated killing of senescent cells but not in the non-senescent condition (Figure 5.1D-F). This screen was performed in parallel with control plates containing siRNA-transfected IMR90 ER:RAS cells that did not undergo NK cell co-culture. In the absence of NK cells, siRNAs targeting the hits did not induce senescent cell death (Figure 5.1E & F).

Given the inherent variability of large-scale screens and the variable nature of NK cells, we conducted a second independent screen following an identical procedure, termed 'Screen 2' (Figure 5.2A). From this screen, we identified 274 siRNA datapoints that enhanced NK-mediated killing of senescent cells above the normalised cut-off score (Figure 5.2B). Among the top siRNAs, we found several repeated

from Screen 1, including siRNAs against PPP4C or FOSL1, in addition to some new candidates, including siRNAs targeting the SWI/SNF chromatin remodelling complex subunit SMARCA4. Following the selection criteria, we identified 10 hits that sensitised senescent cells to NK-mediated cytotoxicity, including 7 new hits (Figure 5.2C). Knockdown of SMARCA4, for example, increased NK-mediated killing exclusively of senescent cells (Figure 5.2D). Similarly, we found silencing of another hit, GLRA4, to promote NK cell-mediated killing of cells undergoing OIS but not growing cells (Figure 5.2E). In all cases, siRNAs targeting the hits did not induce senescent cell death in the absence of NK cells.

To combine the result of both screens, we analysed all data from Screen 1 and 2 together (Figure 5.3A). To maintain consistency of data analysis and hit selection, we averaged the percentage of NK-mediated killing of senescent cells between each replicate from Screen 1 and Screen 2, to produce a total of three mean replicates (rather than 6). Following normalisation, we found 299 datapoints to exceed the cut-off of NPA ≥ 1.5 (Figure 5.3B). The combined screen analysis uncovered 16 hits potentiating NK-mediated cytotoxicity of senescent cells (Figure 5.3C). Among the 16 hits, half had previously been identified from the original screens, with 8 new candidates identified. In total, 37 genes were identified between the different siRNA screens, with 9 genes consistently shared between the different screen analyses (Figure 5.4A). Interestingly, the knockdown of two genes, FURIN and FBXO24, consistently promoted NK cell-mediated clearance of senescent cells in all the screening datasets (Figure 5.4B).

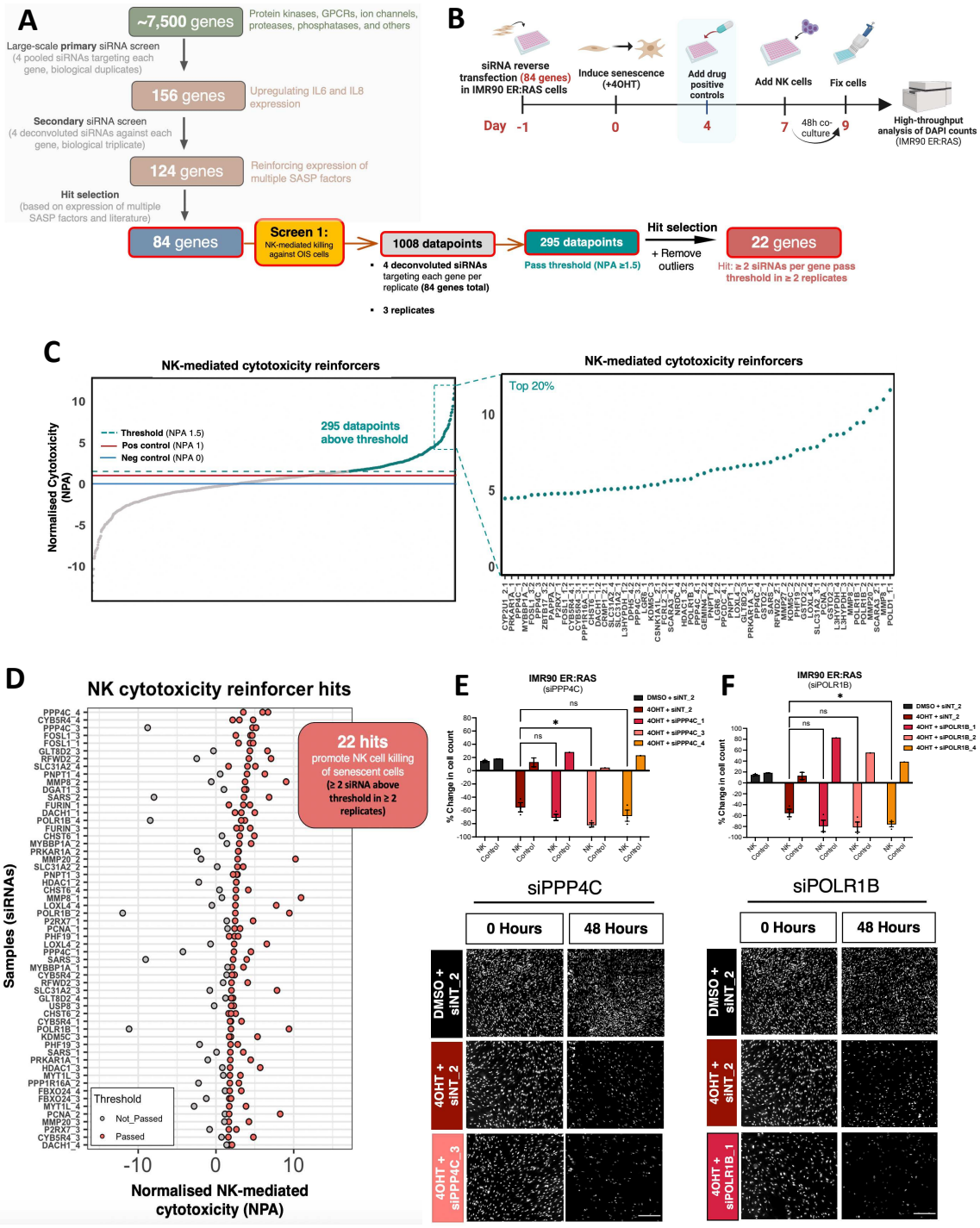


Figure 5.1 RNAi screen 1 identifies 22 targets whose knockdown potentiates NK-mediated killing of senescent cells

(A) Summary of the multiple RNAi screens performed. Initially, a large siRNA screen of over 7,500 genes was performed to identify SASP reinforcers in OIS IMR90 ER:RAS cells and was narrowed down to 84 genes. Here, a deconvoluted siRNA screen based on the 84 candidates is performed to identify novel inducers of an anti-senescence NK cell response (termed Screen 1). We identify 22 gene hits from this screen.

(B) Schematic of the timeline and the experimental settings for the siRNA screen to identify regulators of NK-mediated cytotoxicity

(C) Results from 'Screen 1' portraying the distribution of the individual siRNA datapoints from all replicates arranged ascendingly according to their normalised percent activation (NPA) cytotoxicity scores (NPA scores represent the percentage change in IMR90 ER:RAS cell count following co-culture with NK cells for each siRNA transfection, normalised to the negative and positive siRNA controls in each plate). Left panel displays 1,008 total siRNA datapoints based on the 84 genes in all 3 replicates. Blue line represents the mean normalised negative control (NPA=0). Red line represents the mean normalised positive control (NPA = 1). The threshold for hit selection was placed at NPA ≥1.5 with 295 datapoints scoring above the threshold (i.e.. 295 total siRNAs across 3 replicates). Right panel displays the top 20% scoring datapoints.

(D) Results from 'Screen 1' showing the individual siRNAs for the 22 genes selected as hits. Each dot per row represents a replicate experiment. Hits were considered if ≥2 siRNA for a specific gene had an NPA score above the threshold in ≥2 replicates (n = 3).

(E & F) Quantification of the percentage change in viability in IMR90 ER:RAS cells transfected with siRNAs against two hits from 'Screen 1'. IMR90 ER:RAS cells with siRNAs against PPP4C **(E)** or POLR1B **(F)** showed a larger percentage of senescent cell death relative to the non-targeting control following co-culture with NK cells. Representative images of the co-culture for each hit are also shown (n = 3). Scale bar, 300μm.

(E & F) Ordinary one-way ANOVA.

n signifies independent experiments. All error bars represent mean ± SD. *P < 0.05, **P < 0.01, ***P < 0.001, ****P < 0.0001; ns= not significant.

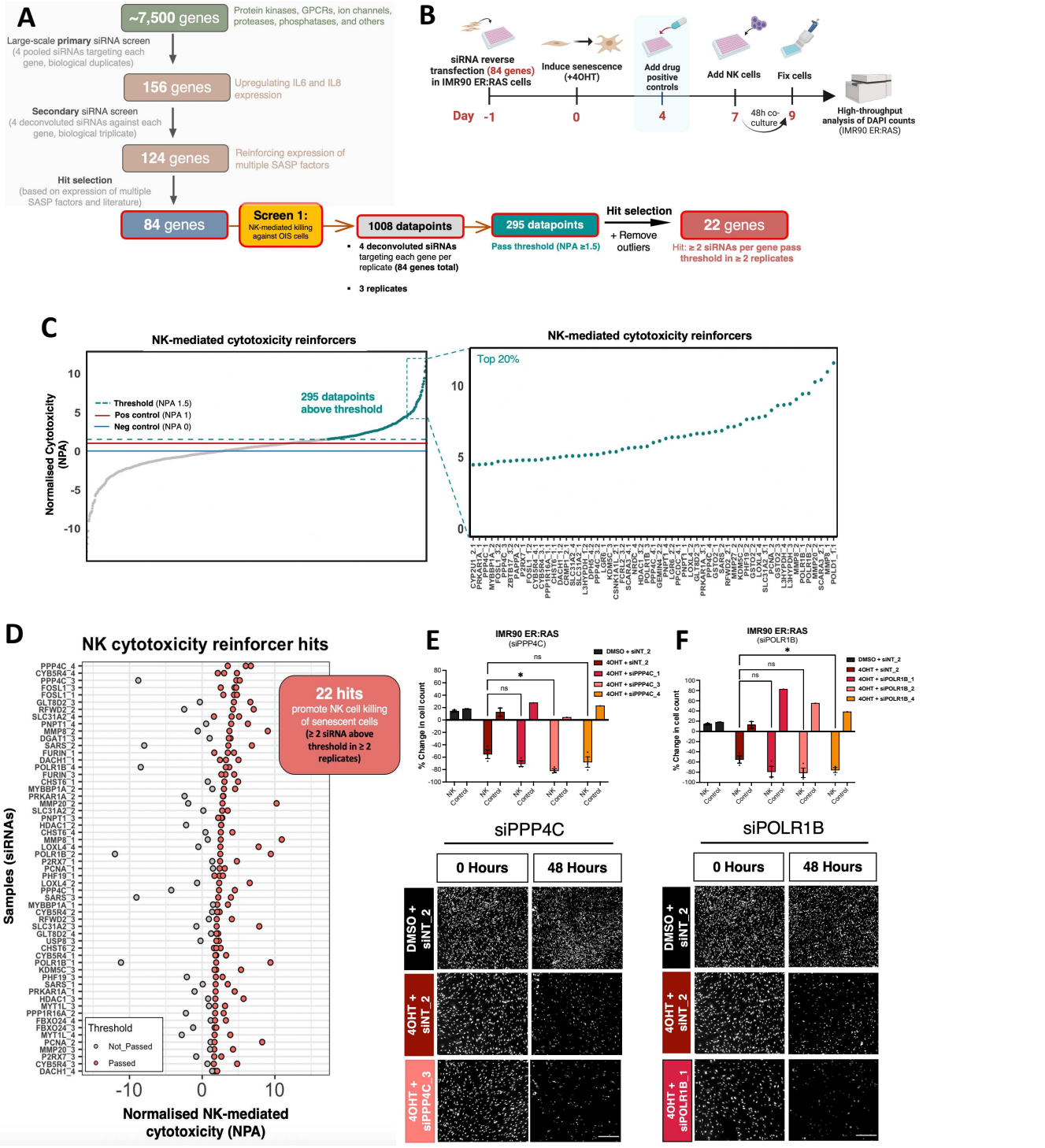


Figure 5.1 RNAi screen 1 identifies 22 targets whose knockdown potentiates NK-mediated killing of senescent cells

(A) Summary of the multiple RNAi screens performed. Initially, a large siRNA screen of over 7,500 genes was performed to identify SASP reinforcers in OIS IMR90 ER:RAS cells and was narrowed down to 84 genes. Here, a deconvoluted siRNA screen based on the 84 candidates is performed to identify novel inducers of an anti-senescence NK cell response (termed Screen 1). We identify 22 gene hits from this screen.

(B) Schematic of the timeline and the experimental settings for the siRNA screen to identify regulators of NK-mediated cytotoxicity

(C) Results from 'Screen 1' portraying the distribution of the individual siRNA datapoints from all replicates arranged ascendingly according to their normalised percent activation (NPA) cytotoxicity scores (NPA scores represent the percentage change in IMR90 ER:RAS cell count following co-culture with NK cells for each siRNA transfection, normalised to the negative and positive siRNA controls in each plate). Left panel displays 1,008 total siRNA datapoints based on the 84 genes in all 3 replicates. Blue line represents the mean normalised negative control (NPA=0). Red line represents the mean normalised positive control (NPA = 1). The threshold for hit selection was placed at NPA ≥1.5 with 295 datapoints scoring above the threshold (i.e.. 295 total siRNAs across 3 replicates). Right panel displays the top 20% scoring datapoints.

(D) Results from 'Screen 1' showing the individual siRNAs for the 22 genes selected as hits. Each dot per row represents a replicate experiment. Hits were considered if ≥2 siRNA for a specific gene had an NPA score above the threshold in ≥2 replicates (*n* = 3).

(E & F) Quantification of the percentage change in viability in IMR90 ER:RAS cells transfected with siRNAs against two hits from 'Screen 1'. IMR90 ER:RAS cells with siRNAs against PPP4C **(E)** or POLR1B **(F)** showed a larger percentage of senescent cell death relative to the non-targeting control following co-culture with NK cells. Representative images of the co-culture for each hit are also shown (*n* = 3). Scale bar, 300μm.

(E & F) Ordinary one-way ANOVA.

n signifies independent experiments. All error bars represent mean ± SD. *P < 0.05, **P < 0.01, ***P < 0.001, ****P < 0.0001; ns= not significant.

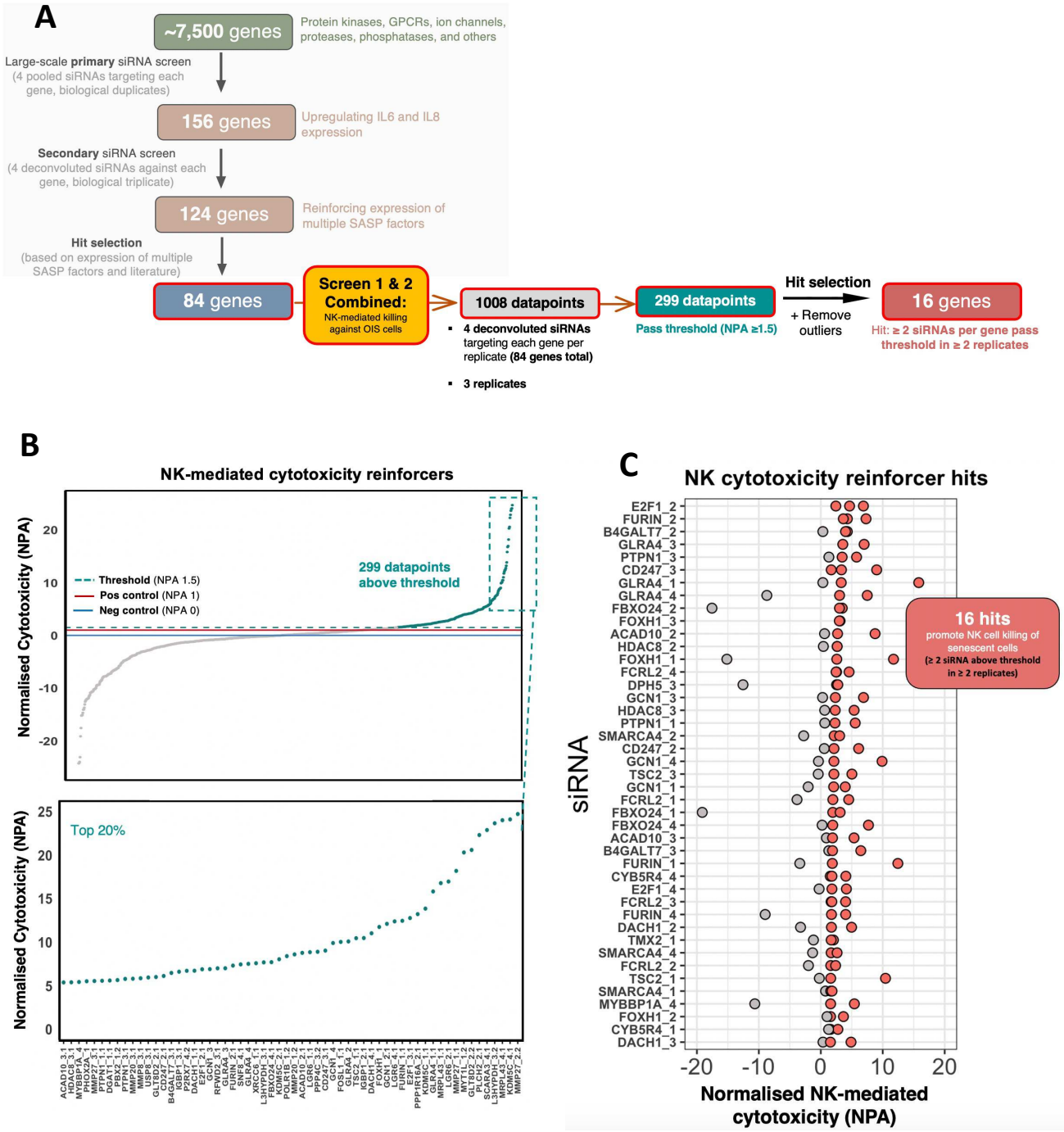


Figure 5.3 Combined analysis of siRNA screens

(A) Summary of the multiple RNAi screens performed. The primary large-scale siRNA screen for SASP reinforcers of over 7,500 genes was performed to identify SASP reinforcers and was narrowed down to 84 genes. Here, combined analysis from screen 1 and screen 2 datasets are performed based on the 84 genes. From this analysis, we identify 16 hits from the combined screens.

(B) Mean results from 'Screen 1' and 'Screen 2' combined analyses. Plot displays the distribution of the individual siRNA datapoints from all replicates arranged ascendingly according to their NPA. Each replicate from Screens 1 and 2 were averaged together. Left panel displays 1,008 total sample siRNA datapoints based on the 84 candidates for 3 mean replicates of both screens. Blue line represents the mean normalised negative control (NPA=0). Red line represents the mean normalised positive control (NPA = 1). The threshold for hit selection was placed at NPA ≥1.5 with 299 datapoints scoring above the threshold (i.e.. 299 total siRNAs across 3 mean replicates from Screens 1 and 2). Right panel displays the top 20% scoring datapoints.

(C) Screen results showing the individual siRNAs for the 16 genes selected as hits for the combined Screen 1 and 2 analyses. Hits were considered if ≥2 siRNA for the gene was above the threshold in ≥2 mean replicates (n = 3)

n signifies independent experiments.

5.3 Validation of candidates that promote NK cell-mediated cytotoxicity of senescent cells

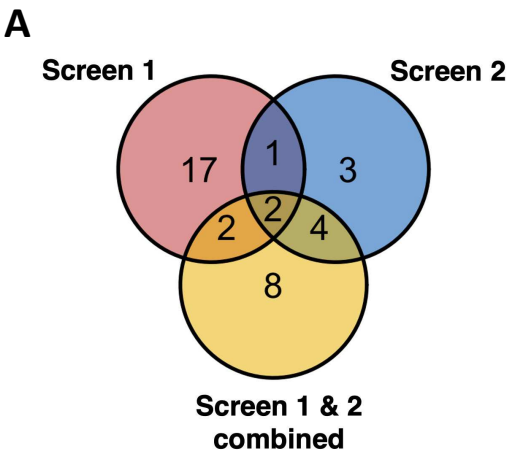
Of the 37 candidates, we shortlisted 12 for validation (Figure 5.4C) based on multiple criteria, including their capacity to potentiate a robust NK cell response, previous literature, the availability of compounds targeting the hits, and how the hits affect SASP expression (Figure 5.4D) (see Summary and Discussion, Chapter 5.4). Any remaining targets would be investigated, if required, in the future.

The experimental conditions and controls for the validation assay were identical to the NK co-culture siRNA screen. IMR90 ER:RAS cells were reverse transfected with 4 siRNAs targeting each of the 12 candidates. To ensure that knockdown of the 12 genes does not render non-senescent cells susceptible to NK-mediated killing, the siRNA validation screen was performed in parallel conditions in both senescent (4OHT-treated) and non-senescent (DMSO-treated) IMR90 ER:RAS cells (Figure 5.5A). In each condition, siRNA-transfected IMR90 ER:RAS cells were treated with DMSO or 4OHT, as appropriate, before being co-cultured with NK92-MI cells for 48 hours. Due to this assay's reduced scale, no HTS-based normalisation was required. The threshold for hit selection was set as the percentage change in IMR90 ER:RAS cell counts after co-culture (i.e. 'Cytotoxicity Score') equal to 1 SD above the 'Cytotoxicity Score' of the negative controls. Only genes with at least 2 out of 4 siRNAs above the threshold in at least 2 out of 3 replicates were selected as hits.

For the senescent (4OHT-treatment) condition, the knockdown of 9 genes were increased NK-mediated selective killing of senescent IMR90 ER:RAS cells, in many cases, beyond the 'Cytotoxicity Score' of the siRNA- and drug-positive controls (Figure 5.5A & B). Importantly, in the absence of NK cells, we found that the knockdown of all hits did not induce the killing of senescent cells, suggesting that this effect is NK-dependent (Figure 5.5C).

In the non-senescent condition, DMSO-treated IMR90 ER:RAS cells transfected with non-targeting siRNAs (siNTs) served as negative controls, whereas 4OHT-treated cells transfected with siNTs were additional controls to ensure NK cells were activated and targeting senescent cells. Remarkably, we found that siRNAs targeting the 12 genes did not cause the NK-mediated killing of non-senescent cells

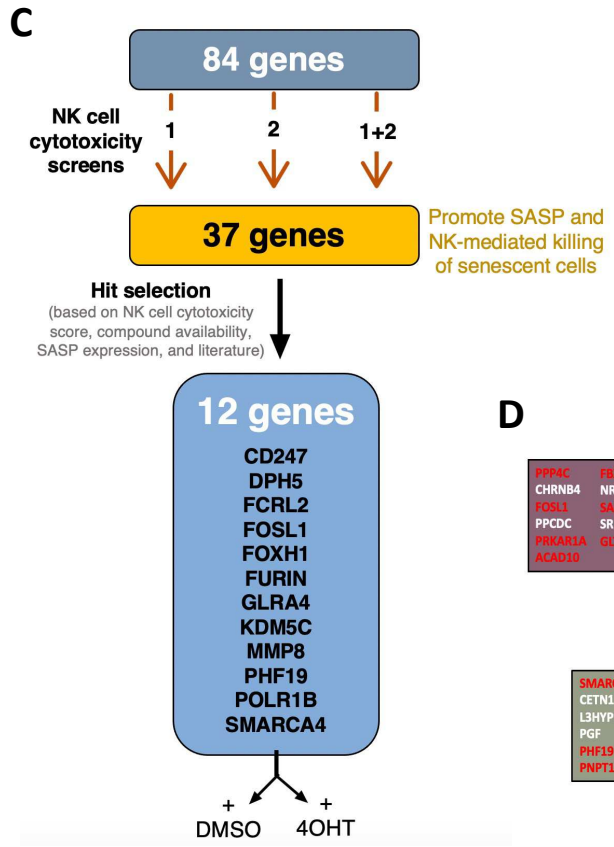
(Figure 5.6A & B). Similarly, in the absence of NK cells, siRNAs did not induce non-senescent cell death (Figure 5.6C). Overall, our findings identify 9 genes whose knockdown promotes NK-mediated killing specifically of senescent cells.



B

37 candidates promoting NK mediated cytotoxicity

Gene	Screen 1 (NPA1.5)	Screen 2 (NPA1.5)	Screen 1 & 2 (NPA1.5)	Total
FBXO24	1	1	1	3
FURIN	1	1	1	3
CYB5R4	1		1	2
DACH1	1		1	2
FCRL2		1	1	2
FOXH1		1	1	2
GLRA4		1	1	2
LOXL4	1	1		2
SMARCA4		1	1	2
ACAD10			1	1
B4GALT7			1	1
CD247			1	1
CHST6	1			1
DPH5		1		1
E2F1			1	1
EIF5A		1		1
FOSL1	1			1
GCN1			1	1
GLT82D	1			1
HDAC1	1			1
HDAC8			1	1
MMP20	1			1
MMP8	1			1
MRPL43		1		1
MYBBP1A	1			1
P2RX7	1			1
PCNA	1			1
PHF19	1			1
PNPT1	1			1
POLR1B	1			1
PPP4C	1			1
PRKAR1A	1			1
PTPN1			1	1
RFWD2	1			1
SARS	1			1
SLC31A2	1			1
TSC2			1	1



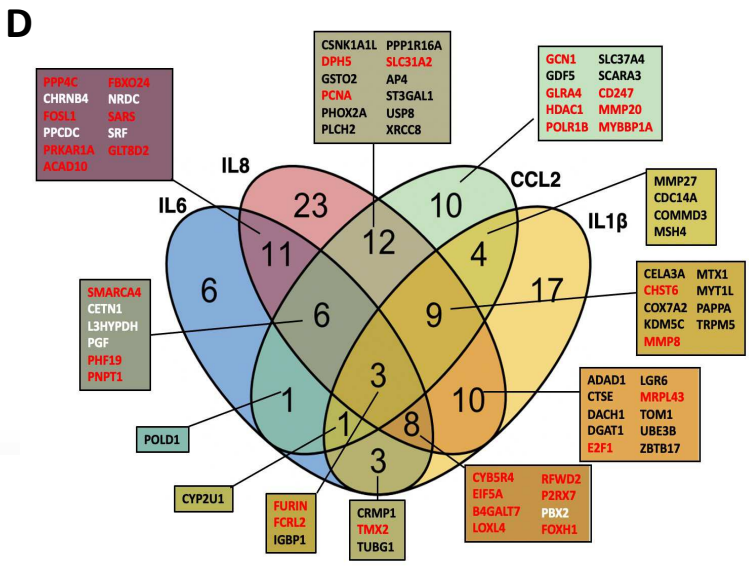


Figure 5.4 RNAi screens discover 37 candidates whose knockdown potentiates NK cell-mediated killing of senescent cells

(A) Venn diagram showing the distribution of the 37 genes selected as hits from siRNA NK cell co-culture screen 1, screen 2, and the combined screen 1 and 2 datasets. 9 hits were shared between the different screens.

(B) Table listing the 37 hits selected from the siRNA NK cell co-culture screens.

(C) Summary workflow of selection of hits from siRNA screens to identify reinforcers of NK cell-mediated killing of senescent cells. From the original 84 candidates that reinforce the SASP, 3 distinct screening analysis were performed to identify 37 genes that promote NK cytotoxic activity against OIS IMR90 ER:RAS cells. From these hits, 12 candidate genes were selected to be investigated further.

(D) Venn diagram of the 124 genes selected as hits from the SASP reinforcer secondary siRNA screen as described in Figure 4.6. Gene names in red signify those genes that were also hits in the NK co-culture screen. 18 out of 37 genes that promote NK cell cytotoxicity against senescent cells also promoted the expression of at least CCL2 in the SASP.

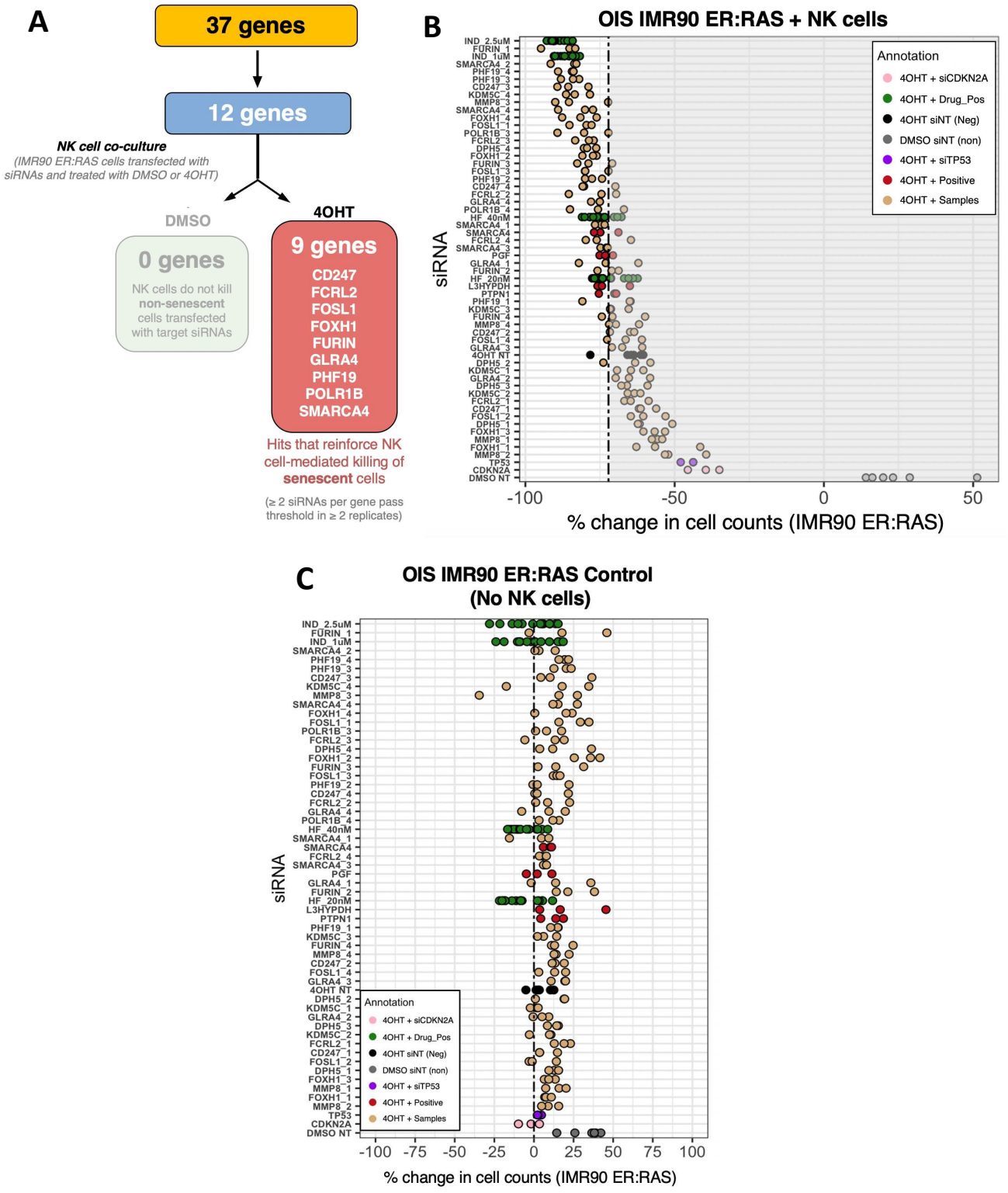


Figure 5.5 siRNAs against 9 genes potentiate NK-mediated killing of senescent cells

(A) Summary of the validation siRNA screens with the shortlisted 12 candidates. Deconvoluted siRNAs against each of the 12 genes were transfected into IMR90 ER:RAS cells which were treated with either DMSO or 4OHT for 7 days prior to co-culture with NK cells. siRNA transfection in non-senescent IMR90 ER:RAS cells treated with DMSO did not affect NK cell activity. However, siRNAs against 9 genes transfected in OIS IMR90 ER:RAS treated with 4OHT strongly promoted NK cell cytotoxicity against the senescent cells.

(B) Plot of the results from NK cell co-culture with senescent (4OHT treated) IMR90 ER:RAS cells transfected with siRNAs against the 12 candidates. Each dot represents one replicate for each individual siRNA and there were four deconvoluted siRNAs per candidate gene. Percentage change in cell count was measured based on the change in nuclei count (DAPI) of IMR90 ER:RAS cells over 48 hours of co-culture. Vertical, black dashed line represents the threshold to select for hits and represents the mean percentage change in IMR90 ER:RAS cell counts of the non-targeting negative controls + 1 SD. Hits were considered if ≥2 siRNAs for a gene scored above this threshold in ≥2 replicates (n = 3).

(C) Plot of the results as in **(B)** for a control experiment in which siRNA transfected senescent IMR90 ER:RAS cells did not undergo co-culture with NK cells. Vertical dashed line lies at 0 percent to indicate change in IMR90 ER:RAS cell death if dots fall below the line. Transfections of most siRNAs alone did not show senolytic or toxic effects in the senescent cells without NK cells present (n = 3).

n signifies independent experiments.

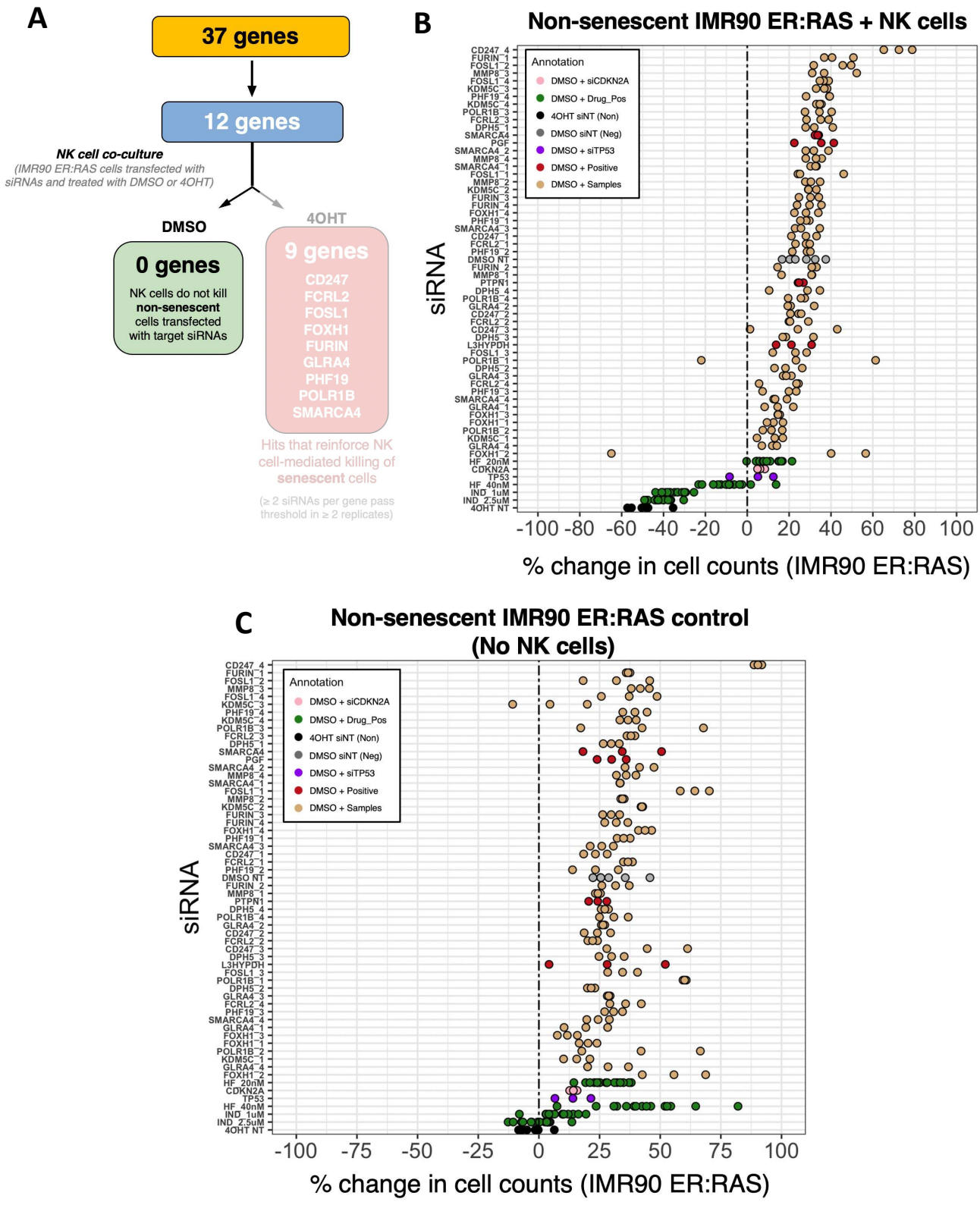


Figure 5.6 siRNAs against candidates do not cause NK-mediated killing of non-senescent cells

(A) Summary of the validation siRNA screens with the shortlisted 12 candidates as in **(Figure 5.5A)**. siRNA transfection in non-senescent (DMSO-treated) IMR90 ER:RAS cells did not promote NK-mediated cytotoxicity.

(B) Plot of the results from NK cell co-culture with non-senescent (DMSO treated) IMR90 ER:RAS cells transfected with siRNAs against the 12 candidates. Each dot represents one replicate for each individual siRNA and there were four deconvoluted siRNAs per candidate gene. Percentage change in cell count was measured based on the change in nuclei count (DAPI) of IMR90 ER:RAS cells over 48 hours of co-culture. Vertical, black dashed line is at 0 percent to indicate change in in IMR90 ER:RAS cell death if dots fall below the line. Hits were considered if ≥2 siRNAs for a gene scored below this line in ≥2 replicates (n = 3).

(B) Plot of the results as in **(A)** for a control experiment in which siRNA transfected non-senescent IMR90 ER:RAS cells did not undergo co-culture with NK cells (n = 3).

n signifies independent experiments.

5.4 Summary and Discussion

By leveraging high-throughput genetic screening together with a robust co-culture system, we wanted to demonstrate that SASP-promoting siRNAs can also promote NK-mediated surveillance of senescent cells. In this chapter, we screened 84 candidates to identify novel inducers of NK cell-mediated anti-senescence immunity, of which several hits may hold therapeutic value.

Taking advantage of our NK cell co-culture screens, we identified 37 genes whose knockdown strongly stimulated NK cell-mediated killing specifically in senescent cells. As an internal validation of the result, we found several hits that have been corroborated in literature to promote immune evasion. The most well-defined example is the matrix metalloproteinase (MMP) family, whose encoded proteins are commonly secreted as part of the SASP and are implicated in the proteolytic shedding of the NKG2D activating ligands on the surface of senescent and tumour cells (Muñoz et al., 2019; Zingoni et al., 2020). MMPs enable senescent cells to evade recognition by NK cells, thereby facilitating their escape from immune surveillance. Our findings revealed that the knockdown of MMP genes promoted NK-mediated recognition and elimination of senescent cells. Likewise, our screens identified HDAC1 and HDAC8, members of the histone deacetylase protein family known to regulate the expression of NKG2D ligands on NK cells and inhibit anti-tumour immunity, respectively (Yang et al., 2021; Zhu et al., 2015). Another candidate, LOXL4, an amine oxidase involved in catalysing collagen cross-link formation in the extracellular matrix, contributes to immune evasion in hepatocellular carcinoma (HCC) tissues (Tan et al., 2021). We found that in our senescent cells, knocking down LOXL4 also suppressed NK cell evasion.

Many of the 37 hits encoded subunits for proteins required for diverse biological processes. For example, FOSL1, an AP1 transcription factor subunit, is an essential component of the senescence enhancer landscape programme (Martínez-Zamudio et al., 2020). Outside of senescence, inhibition of FOSL1 strongly increases vulnerabilities in KRAS mutant lung and pancreatic tumours (Vallejo et al., 2017), suggesting a potential avenue to explore vulnerabilities of senescent cells from FOSL1 silencing. In addition, the RNA polymerase 1 subunit B (POLR1B) and the protein phosphatase catalytic subunit (PPP4C) both substantially increase NK cell surveillance of senescent cells (Figure 5.1E & F). It is

important to note that the screen analysis showed that the statistical significance was either low or non-significant for some hits. This was due to our screen hit selection process being based on 2 out of 3 replicates with high concordance rates beyond an arbitrary threshold. As such, we intend to perform additional validation experiments on any candidates shortlisted from this siRNA screen and not only depend on the findings from these screens before we investigate target genes in vivo.

Due to the scale of the NK cell co-culture siRNA screen, several variabilities can arise (as described in Chapter 4). In addition, the nature of NK cell behaviour in co-culture is conditional on numerous parameters including, but not limited to, the passage numbers and seeding densities of the IMR90 ER:RAS cells, the strength of senescence and SASP induction, the dispersal of NK cells within wells, as well as the concentrations of any transfection reagents and compounds used during the screen, all of which could be subject of technical bias. This, in turn, may curb the dynamic range of senescent cell death within the negative control wells resulting in the omission of potential hits. Given such variabilities, we repeated the screen. To ensure we do not initially disregard any interesting candidates, we also combined all the hits from each screen (rather than only selecting hits shared between the different replicate screens). Indeed, the number of candidates selected greatly depended on the threshold we set up. Due to the arbitrary cut-off at an NPA ≥ 1.5, we identified 37 hits, of which approximately 25% were shared between the screens. One explanation for this low percentage is related to siRNA outliers. In many cases, siRNAs with abnormally high NPA scores (for example, siRNAs against POLR1B from Screen 2) were manually discarded as outliers, which would otherwise have been designated as shared hits. Another reason was due to the selection cut-off applied. Reducing the threshold would substantially increase both the total number of hits, as well as shared hits between the screen, as multiple siRNAs for candidate genes narrowly missed the cut-off in both Screen 1 and Screen 2.

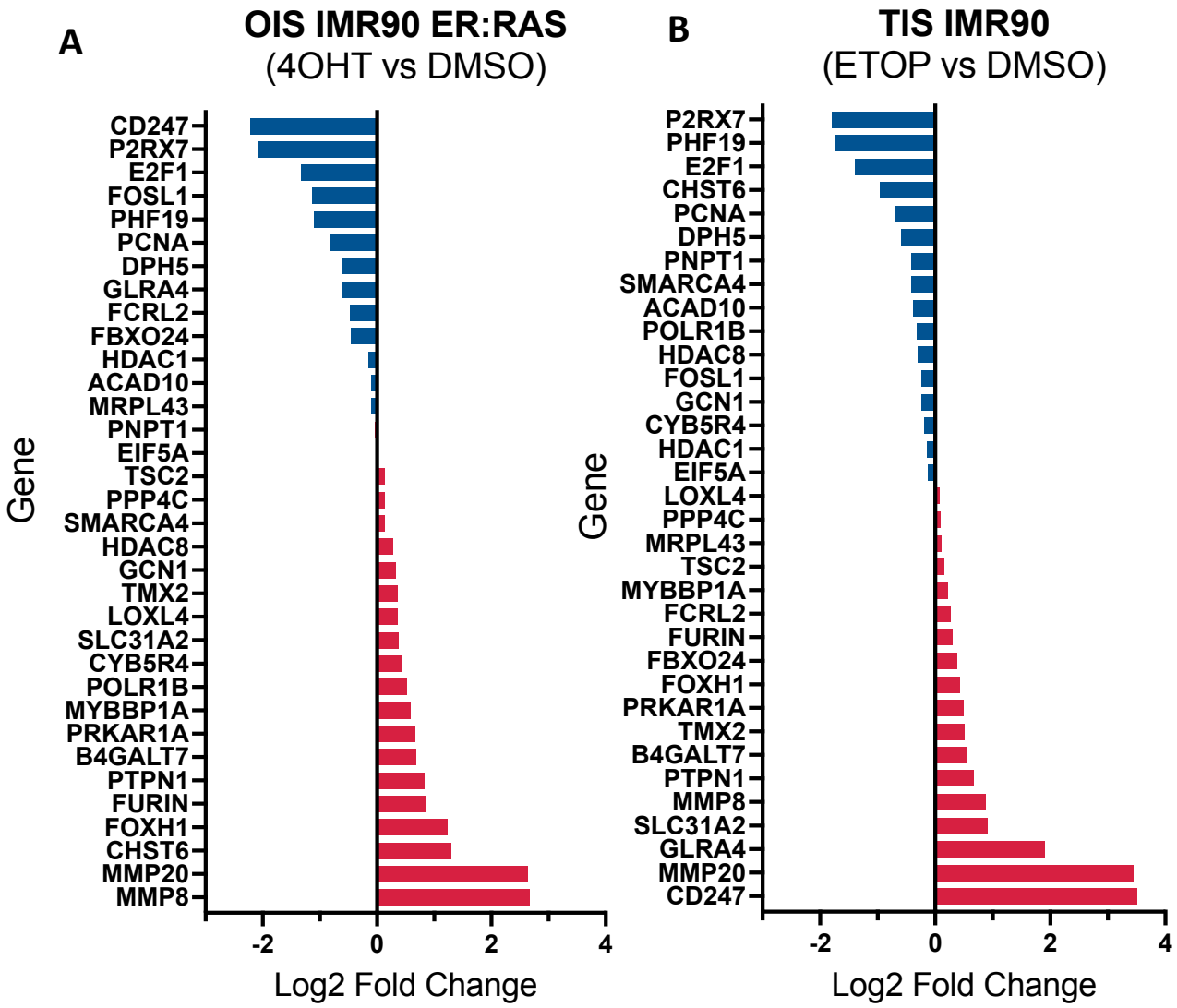
Validation assays are essential to examine any identified lead candidates following the initial screen. Therefore, we retested our siRNAs against a reduced list of 12 genes to narrow down potential targets. Many factors were considered in parallel for the selection of these 12 candidates. Firstly, candidates from Screen 1, Screen 2, and the combined Screen 1 & 2 datasets were selected based on their NPA scores. For instance, SMARCA4 or DPH5 knockdown strongly reinforced NK-mediated killing of

senescent cells in Screen 2, whereas FOSL1, POLR1B, and the MMP genes ranked among the highest in Screen 1. Secondly, many candidates were shortlisted based on the availability of chemical compounds that target the genes, including SMARCA4, POLR1B, FURIN and PHF19. Thirdly, as CCL2 is a vital NK-activating cytokine, we considered candidates whose knockdown reinforced CCL2 expression. Knockdown of 9 out of the 12 selected candidates upregulated CCL2 in senescent cells (Figure 5.4C & D). Fourthly, to understand potential vulnerabilities in different types of senescence, we analysed the expression of the 37 genes in IMR90 cells undergoing OIS or TIS (Supplementary Figure S5.1). Genes such as FOXH1, MMP8, and FURIN were strongly upregulated in IMR90 ER:RAS cells undergoing OIS, whereas genes including CD247 or GLRA4 showed increased expression in cells undergoing TIS. Therefore, candidates were shortlisted based on their expression in different senescence types. In addition, FURIN was selected as a candidate as its knockdown not only increased the expression of IL6, IL8, IL1β, and CCL2 (Figure 4.6B & C) but also reinforced NK-mediated killing in all three screen datasets (Figure 5.4B). Finally, to facilitate our candidate selection process, we explored published literature. Several hits were excluded if they had been characterised as NK activators in past publications, for example, PTPN1 (Pech et al., 2019). On the other hand, the hit KDM5C was narrowly filtered out from the original 37 genes yet selected among the 12 candidates based on published reports suggesting that the KDM5 family members help promote immune evasion (Zhang et al., 2021b). Overall, based on these criteria, we selected 12 candidates for further validation. Of course, the excluded 25 genes will remain of interest for future studies.

Testing siRNAs against these 12 genes identified 9 hits whose knockdown increased NK-mediated clearance of senescent cells. Furthermore, these selected hits did not induce NK-mediated killing of non-senescent cells. To corroborate these findings, we could examine the effect of NK cells in co-cultures of siRNA-transfected non-senescent and senescent cells. In addition, we will need to directly evaluate NK-mediated response against senescent cells *in vivo*.

Overall, in this chapter, we characterised 9 genes whose knockdown enhances NK-mediated killing of cells undergoing OIS. Whether inhibiting these hits using drugs provokes a similar anti-senescence NK

cell response and whether this can be translated to other modalities of senescence could be of considerable therapeutic interest and warrants investigation.



Supplementary Figure S5.1 Expression of the 37 hits from RNAi screens during senescence.
(A & B) Results from the differential gene expression analysis of the 37 candidates identified as hits from the NK cell-mediated cytotoxicity RNAi screens in OIS IMR90 ER:RAS cells **(A)** or therapy-induced senescence **(B)**. Original RNA-Seq experiment for **(A)** performed by Verena Wagner, unpublished data. For **(B)** RNA-Seq data was retrieved from Casella et al., 2019.

Chapter 6 – FURIN, SMARCA4, and POLR1B can be targeted to potentiate NK-mediated killing of senescent cells

6.1 Introduction

Over the last two decades, an improved understanding of senescence has accomplished significant breakthroughs in senotherapies. Senotherapeutics to suppress the proinflammatory SASP (senomorphics) or to induce senescent cell death (senolytics) have been proposed as treatment for age-associated disorders, and some are undergoing clinical trials (Raffaele and Vinciguerra, 2022). Immunotherapy is another strategy that holds tremendous promise in the clearance of senescent cells. For instance, during chronic liver damage, senescent hepatic stellate cells (HSCs) secrete a range of SASP factors that attract macrophages to kill senescent cells, thereby averting the development of liver cirrhosis (Lujambio et al., 2013). Similarly, CD4+ T cells mediate senescence surveillance by promoting the elimination of pre-cancerous senescent hepatocytes (Kang et al., 2011). As reported throughout this thesis, NK cells are an appealing choice for anti-senescence immunotherapy for their ability to function where other immune populations, such as cytotoxic T cells, may stall. Furthermore, NK cells share effector functions with CD8+ T cells and have broad cytotoxicity against stressed and tumour cells without the requirement of prior antigen activation (Abel et al., 2018). Therefore, it is no surprise that NK cells can eliminate senescent cells, for example, removing senescent HSCs to suppress the liver fibrotic response (Krizhanovsky et al., 2008; Ogrodnik et al., 2017). In the context of cancer, drug combinations (e.g. palbociclib + trametinib) can promote NK cell responses against senescent lung cancer cells, invoke tumour regression, and prolong survival (Ruscetti et al., 2018). Similarly, we have characterised how senescent cells upregulate the SASP and the expression of NK activating ligands to promote their NK-mediated elimination.

In the previous chapter, we identified 9 genes whose knockdown specifically potentiate the SASP and NK-mediated cytotoxicity of senescent cells, but not that of non-senescent cells. In this chapter, we are interested in characterising the therapeutic potential of these hits.

6.2 Candidate drugs that promote NK-mediated killing of senescent cells

Using RNAi screens, we identified 9 genes whose knockdown promote the SASP and NK-mediated killing of cells undergoing OID (Figure 6.1A). These genes have diverse functions, with many encoding proteins for transcription factors or epigenetic regulators. Over-representation analysis (ORA) of the 9 candidates revealed an enrichment in KEGG pathways associated with IL-17 cytokine signalling and T cell receptor activity, corroborating our findings that the selected candidates may be involved in SASP modulation and immune regulation (Figure 6.2A). More importantly, we also found an enrichment in the NK cell-mediated cytotoxicity pathway (Figure 6.2A). In part, due to the small number of genes input, the ORA results show a high FDR value; nonetheless, the findings suggest an interplay between our screen hits and NK cell effector function.

As the knockdown of our 9 candidate genes promoted the elimination of senescent cells but not non-senescent cells, we wanted to understand why these genes exclusively induced vulnerabilities during senescence. To address this question, we investigated the expression of our hits in different senescent datasets using RNA-Seq analysis. Differential expression analysis revealed an upregulation of 4 of the 9 candidates in IMR90 ER:RAS cells undergoing OIS. Among these included POLR1B, FURIN and SMARCA4, suggesting a correlation between their expression in cells undergoing OIS and their NK cytotoxicity-promoting properties (Figure 6.2B). Likewise, the same 4 genes were upregulated in WI-38 fibroblasts undergoing OIS, analysed from datasets available in published literature (Figure 6.2C) (Casella et al., 2019). We also examined the expression of the hits in IMR90 datasets undergoing therapy-induced senescence (Figure 6.2D; Supplementary Figure S6.1A & B), where we observed different genes upregulated, including CD247 and GLRA4. As CD247 and GLRA4 expression was downregulated in OIS datasets, these results suggest that the expression of the genes during senescence may not necessarily be the only factor in determining their immunogenic properties.

We next wanted to find drugs against our 9 hits to test in a therapeutic setting. Compounds offer a more straightforward approach to inhibit our hits both in culture and *in vivo* models. We found 5 (of the 9) candidates with available inhibitors that directly target our candidates or a related pathway (Figure

6.2E). We selected 8 different inhibitors against 5 of our hits (FURIN, SMARCA4, POLR1B, FOSL1, PHF19) (Figure 6.2E) to investigate their effect on NK-mediated killing of senescent cells.

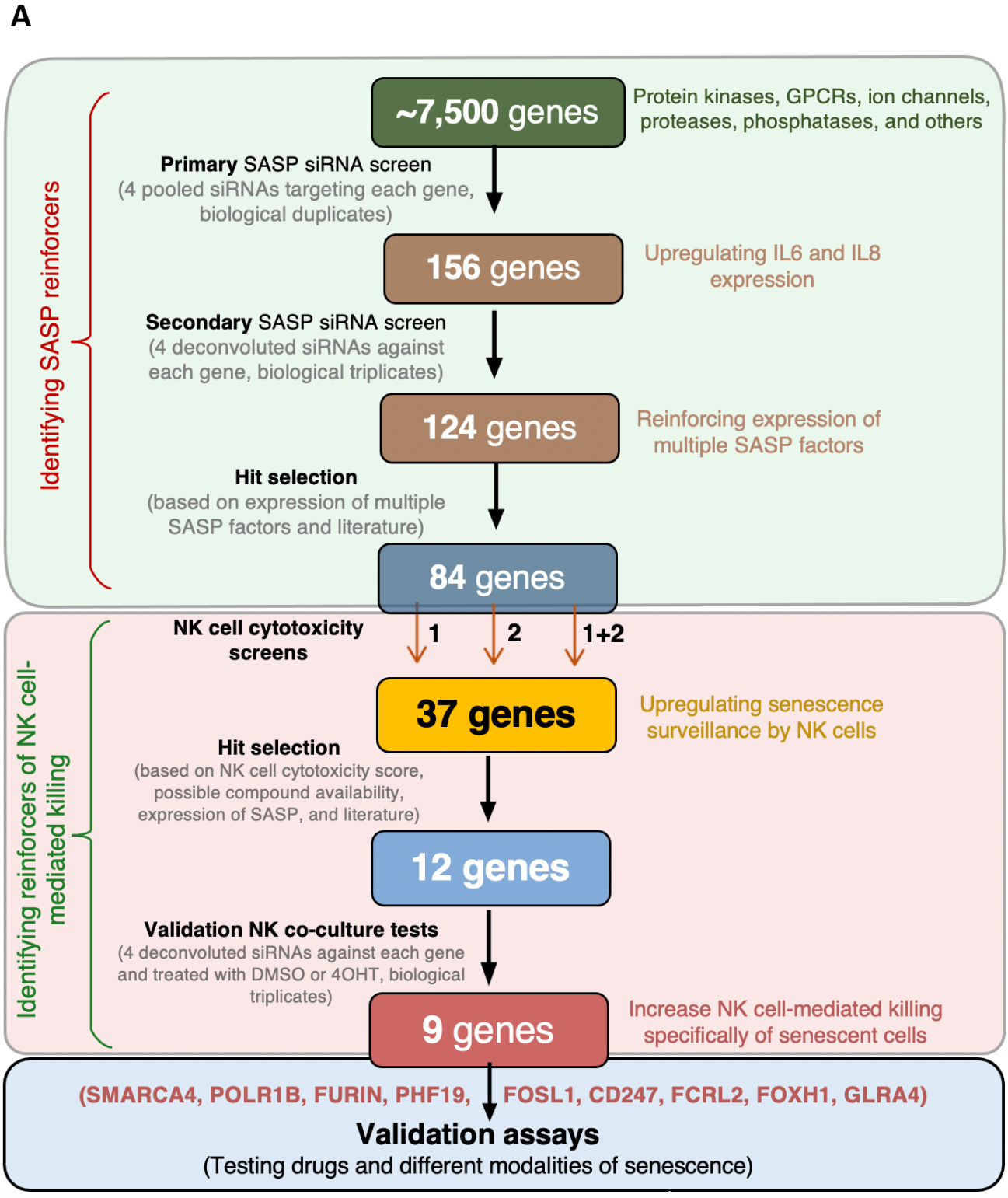
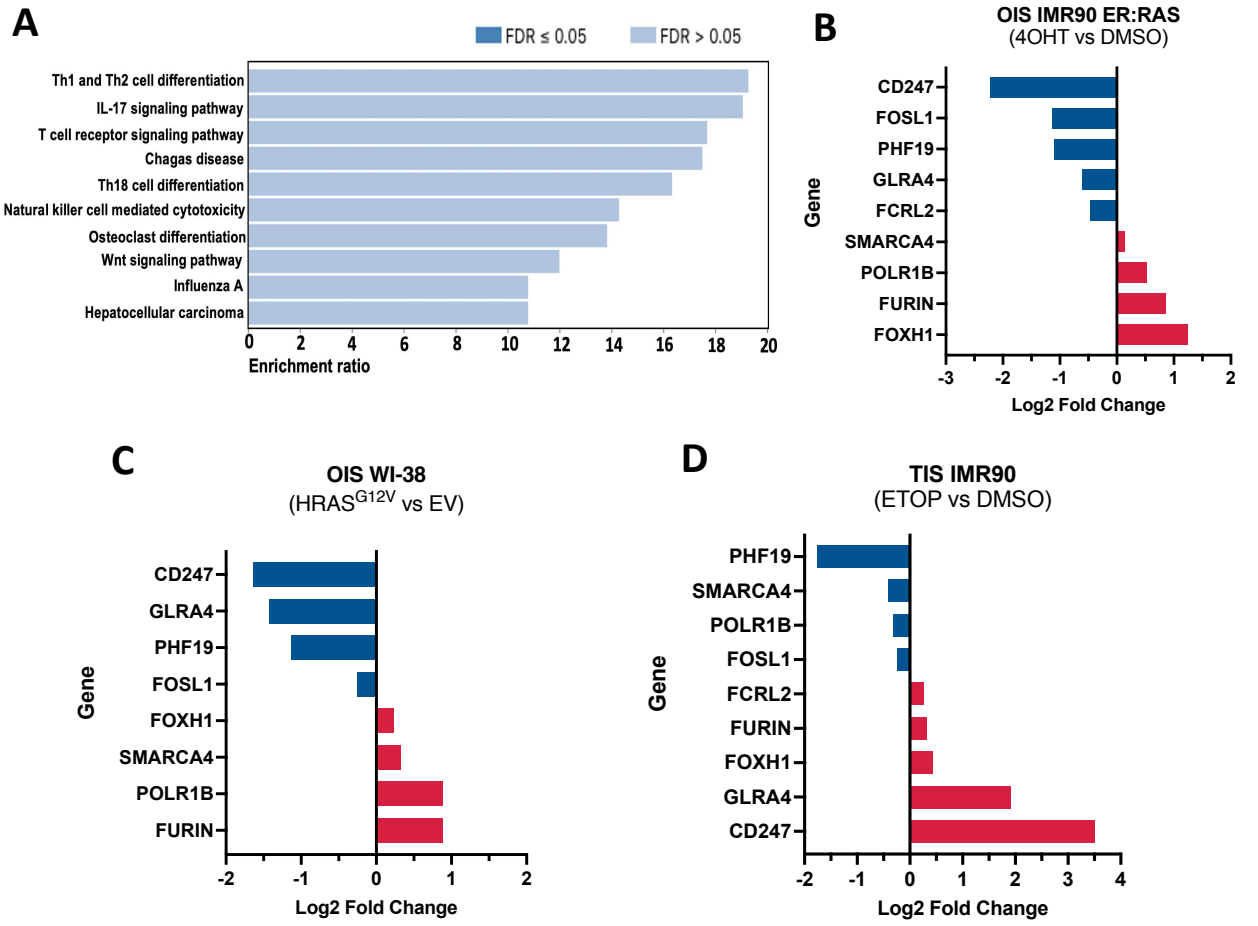


Figure 6.1 Workflow summary of hit identification from multiple RNAi screens
(A) Summary of all RNAi screens performed. Based on the SASP reinforcer siRNA screens and NK cell-mediated cytotoxicity screens in IMR90 ER:RAS cells, we narrowed down our candidate selection to 12 genes. Additional RNAi-based validation of the 12 genes in OIS cells in co-culture with NK cells revealed 9 hits that strongly reinforced NK cell mediated killing of senescent cells.



E

9 Hits

SMARCA4
POLR1B
FURIN
PHF19
FOSL1
CD247
FCRL2
FOXH1
GLRA4

Gene Hit	Inhibitor	Target
SMARCA4	**SGC-SMARCA-BRDVIII**	**SMARCA2/4, PB1(5)**
POLR1B	**BMH-21**	**RNA Polymerase I**
	CX-5461	**RNA Polymerase I**
FURIN	**SSM 3 trifluoroacetate**	**FURIN**
	Hexa-D-arginine	**FURIN**
PHF19	Tazemetostat	EZH2
	GSK126	EHZ2
FOSL1	T5224	C-Fos/AP-1

Figure 6.2. FURIN, SMARCA4, and POLR1B show increased expression in cells undergoing OIS
(A) Over representation analysis results of the Top 10 KEGG biological pathways enriched from our 12 candidate genes reported in **Figure 5.4C** and **Figure 6.1A**. Enrichment in pathways associated with NK cell-mediated cytotoxicity, cytokine signalling and T cell response are observed. Due to the low number of genes input the enrichment scores are not significant (FDR > 0.05), however the findings provide an overview of the processes associated with our screen hits.
(B-D) Results from differential gene expression analysis of the 12 genes from **(A)** in oncogene-induced senescent IMR90 ER:RAS **(B)** or WI-38 **(C)** fibroblasts, or in therapy-induced senescent IMR90 cells **(D)**. For **(B)** and **(D)**, RNA extraction for RNA-sequencing performed by Verena Wagner, unpublished data. For **(C)**, constitutive $HRAS^{G12V}$ vector expression was compared to an empty vector (EV) and the raw RNA-Sequencing data was obtained from Casella et al., 2019.
(E) Table representing details of the 8 inhibitor compounds tested against 5 of the 9 total hits reported in **(A)**. Inhibitors for hits highlighted in the bold and black typeface produced a strong and significant NK cell mediated killing response against OIS cells.

6.3 Characterising effect of inhibiting FURIN on NK-mediated killing of senescent cells

To understand if targeting the protease FURIN potentiates NK-mediated killing of senescent cells, we first tested the effect of silencing FURIN expression in IMR90 cells undergoing OIS. siRNAs against FURIN significantly promoted NK-mediated cytotoxicity of senescent cells (Figure 6.3A) but did not induce senescent cell death in the absence of NK cells. As expected, knockdown of FURIN did not promote NK-mediated killing in non-senescent IMR90 ER:RAS cells (Figure 6.3B). To ensure that these effects were due to the suppression of FURIN, we validated its knockdown in IMR90 ER:RAS cells. siRNAs targeting FURIN significantly reduced the levels of FURIN in senescent cells compared to the control cells (Figure 6.3C).

To investigate if pharmacological inhibition of FURIN can potentiate NK-mediated killing of senescent cells, we took advantage of two distinct FURIN inhibitors: Hexa-D-arginine (from herein, Hex-D) and SSM 3 trifluoroacetate (from herein, SSM3) (Figure 6.4A). Analogous to the siRNA screen results, treatment with either FURIN inhibitor significantly increased NK-mediated killing of senescent but not of non-senescent cells (Figure 6.4B & C). In the absence of NK cells, treatment with Hex-D or SSM3 did not enhance the killing of cells undergoing OIS. These findings suggest that genetic of pharmacological inhibition of FURIN promotes senescent clearance by NK cells.

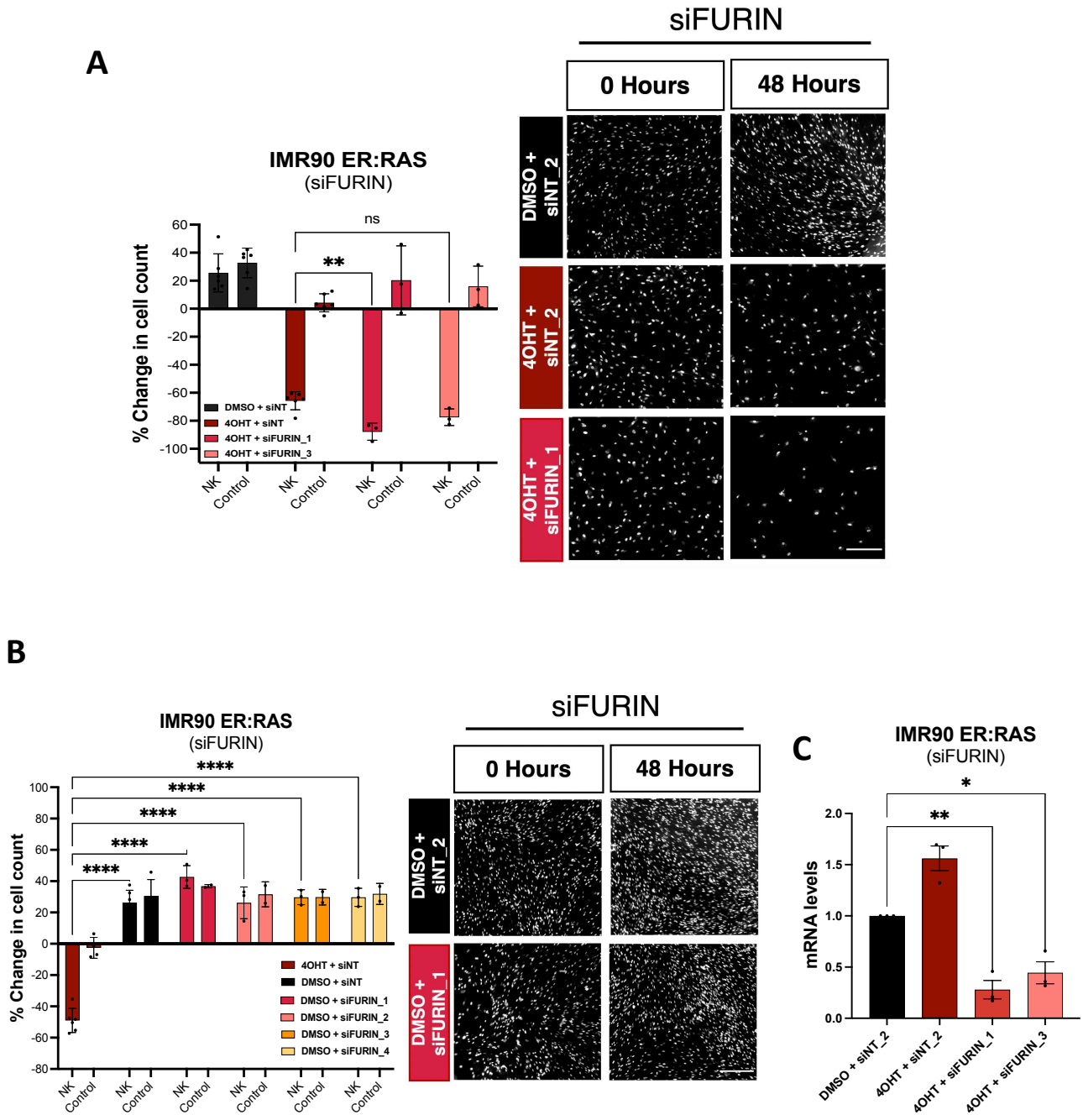


Figure 6.3 siRNAs against FURIN specifically enhance NK-mediated killing of cells undergoing OIS
(A) Quantification of the percentage change in senescent (4OHT-treated) IMR90 ER:RAS cell counts transfected with siRNAs against non-targeting controls or against FURIN following co-culture with NK92-MI cells. Representative images of the co-culture for each hit are also shown (*n* = 3). Scale bar, 300μm.
(B) Quantification of the percentage change in non-senescent (DMSO-treated) IMR90 ER:RAS counts transfected with siRNAs against non-targeting controls or against FURIN following co-culture with NK92-MI cells. siRNA transfection of FURIN did not promote NK cell activity against non-senescent cells. Representative images of the co-culture for each hit are also shown (*n* = 3). Scale bar, 300μm.
(C) qRT-PCR analysis showing the mRNA expression of FURIN in IMR90 ER:RAS cells transfected with two selected siRNAs against FURIN (*n* = 3).
(A-C) Ordinary one-way ANOVA.
n signifies independent experiments. All error bars represent mean ± SEM. *P < 0.05, **P < 0.01, ***P < 0.001, ****P < 0.0001; ns= not significant.

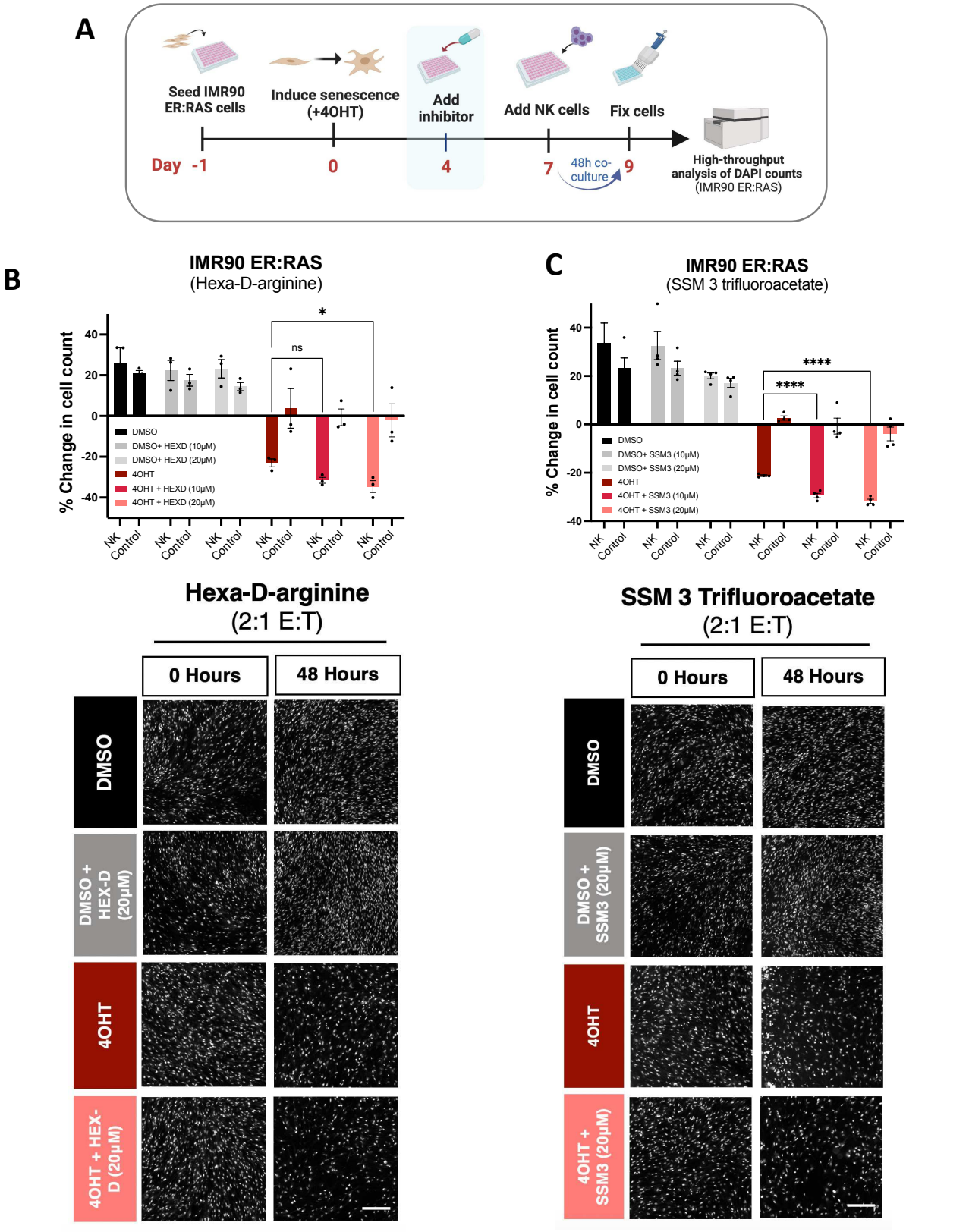


Figure 6.4 Inhibitors of FURIN increase NK-mediated killing of cells undergoing OIS
(A) Schematic of the protocol timeline to investigate the effect of inhibitor administration on NK mediated killing of OIS cells.
(B & C) Top panel depicts quantification of NK-mediated cytotoxicity of IMR90 ER:RAS cells following treatment with either DMSO or 4OHT alone or in combination with Hexa-D-arginine (Hex-D) **(A)** or SSM 3 trifluoroacetate (SSM3) **(B)** at 10μM and 20μM. Inhibitors of FURIN (FURINi) were added 4 days following DMSO/4OHT administration. Experimental co-culture wells contained treated IMR90 ER:RAS cells co-cultured with NK92-MI cells at a 2:1 E:T ratio for 48 hours. NK-mediated cytotoxicity was measured as the percentage change in nuclei count (DAPI) of IMR90 ER:RAS cells over 48 hours of co-culture. Control wells contained treated IMR90 ER:RAS in the absence of NK cells. Bottom panel for **(A & B)** show representative images before and after co-culture (*n* = 3). Scale bar, 300μm.
(B & C) Ordinary one-way ANOVA.
n signifies independent experiments. All error bars represent mean ± SEM. *P < 0.05, **P < 0.01, ***P < 0.001, ****P < 0.0001; ns= not significant.

6.4 Characterising effect of inhibiting SMARCA4 on NK-mediated killing of senescent cells

We next investigated how the downregulation of the SWI/SNF complex subunit SMARCA4 affects NK-mediated senescence surveillance. Knockdown of SMARCA4 selectively enhanced NK-mediated killing of senescent IMR90 ER:RAS cells (Figure 6.5A) but not that of non-senescent cells (Figure 6.5B). We validated the effect on NK cytotoxic activity to be dependent on SMARCA4 knockdown as siRNAs targeting SMARCA4 significantly reduced SMARCA4 expression (Figure 6.5C).

Next, we explored the pharmacological inhibition of SMARCA4 by testing multiple concentrations of the SMARCA4 inhibitor, SCG-SMARCA-BRDVIII (from hereafter, SMARCA4i). We found that increasing concentration of SMARCA4i resulted in increased NK-mediated killing of senescent but not of non-senescent cells (Figure 6.6A). Treatment with 20μM or 40μM SMARCA4i in cells undergoing OIS significantly potentiated NK-mediated killing up to almost two-fold relative to control senescent cells (Figure 6.6B). The increase in NK-mediated killing of senescent cells observed following SMARCA4 inhibition was similar at both the 2:1 and 1:1 E:T ratios during NK cell co-culture (Figure 6.6B; Supplementary Figure S6.2A), and more potent than that observed using FURIN inhibitors.

Next, we explored whether the immunostimulatory effects from SMARCA4 inhibition was restricted only to cells undergoing OIS. Previously, we characterised a model of therapy-induced senescence in IMR90 fibroblasts following etoposide treatment (see Chapter 3.6; Figure 3.13). Furthermore, we demonstrated that IMR90 cells undergoing OIS or TIS treated with HF or indisulam potentiated NK-mediated cytotoxicity in different modalities of senescence (see Chapter 3.6; Figure 3.14). Taking advantage of the TIS system, we combined etoposide treatment in IMR90 cells with SMARCA4i. We found that the combination of SMARCA4i and etoposide potentiated NK-mediated killing of senescent cells, compared to monotherapy with either etoposide or SMARCA4i (Figure 6.7A). NK cytotoxic activity was selective towards cells undergoing TIS as non-senescent control cells treated with SMARCA4i were not killed by NK cells.

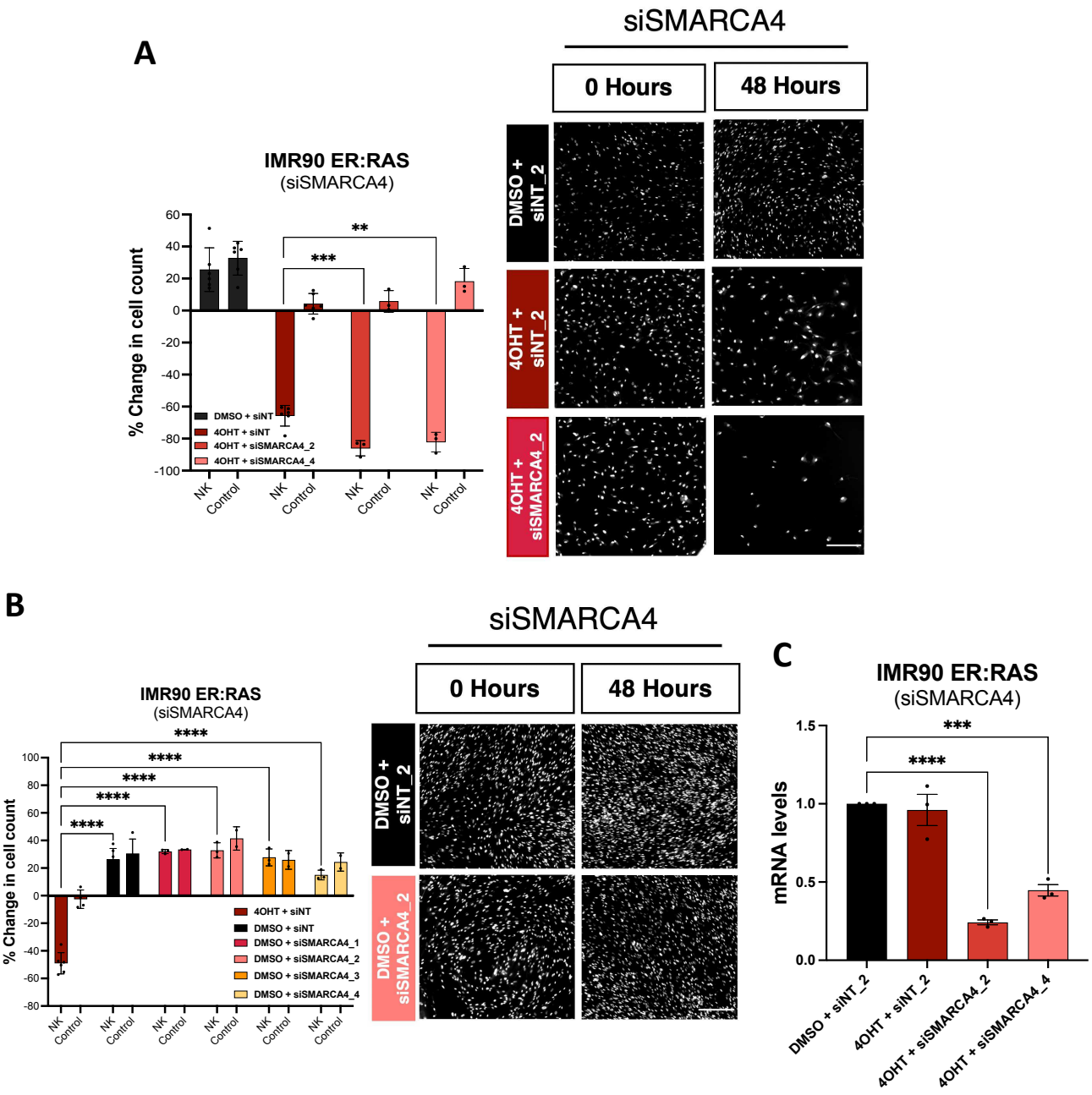


Figure 6.5 siRNAs against SMARCA4 selectively enhance NK-mediated killing exclusively of cells undergoing OIS
(A) Quantification of the percentage change in senescent (4OHT-treated) IMR90 ER:RAS cell counts transfected with siRNAs against non-targeting controls or against SMARCA4 following co-culture with NK92-MI cells. Representative images of the co-culture for each hit are also shown (n = 3). Scale bar, 300µm.
(B) Quantification of the percentage change in non-senescent (DMSO-treated) IMR90 ER:RAS counts transfected with siRNAs against non-targeting controls or against SMARCA4 following co-culture with NK92-MI cells. siRNA transfection of SMARCA4 did not promote NK cell activity against non-senescent cells. Representative images of the co-culture for each hit are also shown (n = 3). Scale bar, 300µm.
(C) qRT-PCR analysis showing the mRNA expression of SMARCA4 in IMR90 ER:RAS cells transfected with two selected siRNAs against SMARCA4 (n = 3).
(A-C) Ordinary one-way ANOVA.
n signifies independent experiments. All error bars represent mean ± SEM. *P < 0.05, **P < 0.01, ***P < 0.001, ****P < 0.0001; ns= not significant.

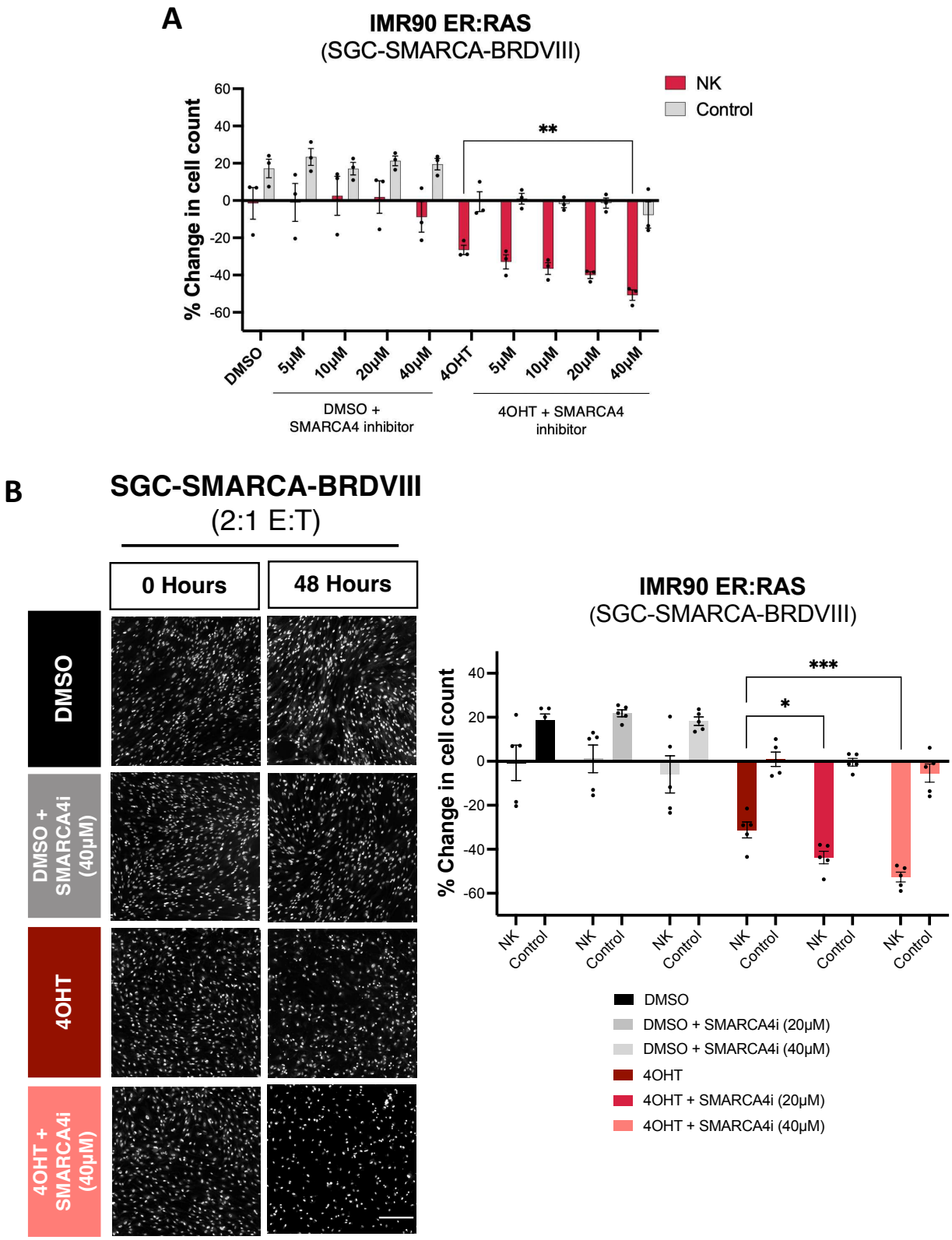


Figure 6.6 A SMARCA4 inhibitor enhances NK-mediated killing of cells undergoing OIS

(A) Quantification of NK cell-mediated cytotoxicity of IMR90 ER:RAS cells following treatment with either DMSO or 4OHT alone or in combination with different concentrations of the compound SGC-SMARCA-BRDVIII (SMARCA4i). SMARCA4i was added 4 days following DMSO/4OHT administration. Experimental NK wells contained treated IMR90 ER:RAS cells co-cultured with NK92-MI cells at a 2:1 E:T ratio for 48 hours. NK-mediated cytotoxicity was measured as the percentage change in nuclei count (DAPI) of IMR90 ER:RAS cells over 48 hours of co-culture. Control wells contained treated IMR90 ER:RAS in the absence of NK cells (*n* = 3).

(B) Left panel shows representative images of IMR90 ER:RAS cells treated with DMSO or 4OHT alone and in combination with SMARCA4i (40μM) before and after co-culture with NK cells at a 2:1 E:T ratio. Right panel shows quantification of NK cell-mediated cytotoxicity as described in **(A)**, focusing only on 2 concentrations of SMARCA4i (20μM and 40μM) (*n* = 5). Scale bar, 300μm.

(A & B) Ordinary one-way ANOVA.

n signifies independent experiments. All error bars represent mean ± SEM. *P < 0.05, **P < 0.01, ***P < 0.001, ****P < 0.0001; ns= not significant.

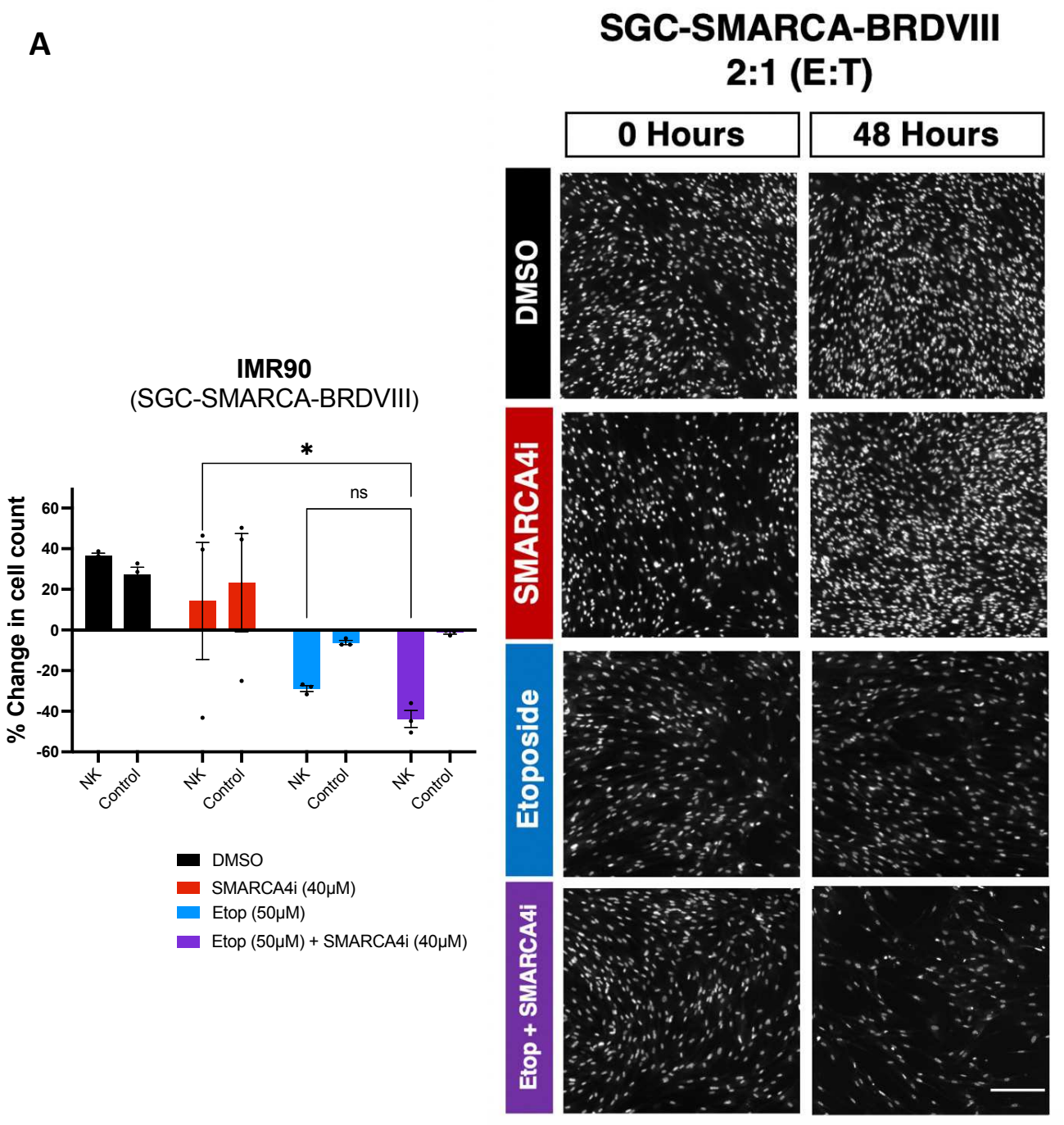


Fig. 6.7 Inhibitor of SMARCA4 enhances NK-mediated killing of cells undergoing TIS

(A) Quantification representative images of NK cell-mediated cytotoxicity of IMR90 cells 7 days following initial administration of either DMSO or etoposide. The SMARCA4 inhibitor SGC-SMARCA-BRDVIII **(C)** was added 4 days after DMSO/etoposide induction. Experimental wells contained treated IMR90 cells co-cultured with NK92-MI cells at a 2:1 E:T ratio. Control wells contained treated IMR90 in the absence of NK cells Percentage change in cell count was measured based on the change in nuclei count (DAPI) of IMR90 cells over 48 hours of co-culture (*n* = 3). Scale bar, 300μm.

Two-way ANOVA.

n signifies independent experiments. All error bars represent mean ± SD. *P < 0.05, **P < 0.01, ***P < 0.001, ****P < 0.0001; ns= not significant.

6.5 Characterising effect of inhibiting POLR1B on NK-mediated killing of senescent cells

The RNA Pol I subunit B, POLR1B, is a component of the RNA polymerase I (RNA Pol I) complex (Goodfellow and Zomerdijk, 2013). Similar to FURIN and SMARCA4, the knockdown of POLR1B significantly potentiated NK-mediated killing of senescent IMR90 ER:RAS cells (Figure 6.8A) without inducing the killing of non-senescent cells (Figure 6.8B). siRNAs strongly reduced POLR1B expression compared to non-targeting control siRNAs, confirming that POLR1B knockdown was responsible for the increased anti-senescence NK-mediated cytotoxicity observed (Figure 6.8C).

Having previously demonstrated POLR1B expression to be upregulated during OIS (Figure 6.2B), we speculated whether inhibiting POLR1B expression using drugs would selectively target cells undergoing OIS. We investigated two drugs inhibiting RNA Pol I, BMH-21 and CX-5461. We first tested different concentrations of BMH-21, a DNA intercalator frequently used as a potent inhibitor of RNA Pol I. Treatment with low concentrations of this inhibitor (625nM) potentiated NK mediated killing of senescent cells at both a 2:1 and 1:1 E:T ratio, whereas increasing BMH-21 concentration (to 1.25μM) more than doubled the NK-mediated senescence clearance (Figure 6.9A; Supplementary Figure S6.2B). An alternative RNA Pol I inhibitor, CX-5461, also enhanced the NK-mediated elimination of senescent cells at both E:T ratios assessed (Figure 6.9B; Supplementary Figure S6.2C). Although we have also investigated the NK-modulating effects of compounds that inhibit pathways related to either PHF19 or FOSL1, our remaining hits, we only observed a modest increase in NK-mediated killing of senescent cells compared to SMARCA4 or POLR1B inhibition (Supplementary Figure S6.3A-C).

Finally, we investigated changes to NK-mediated senescence surveillance using RNA Pol I inhibitors in cells undergoing TIS. Similar to our findings with HF, indisulam, and SMARCA4i, we found that the combined administration of BMH-21 or CX-5461 following etoposide treatment prompted a rapid and substantial elimination of senescent cells by NK92-MI cells compared to treatment with either drug alone (Figure 6.10A & B). Non-senescent (DMSO-treated) control cells did not undergo NK-mediated cell death. Taken together, these co-culture assays have revealed that genetic or pharmacological inhibition of our FURIN, SMARCA4, or RNA Pol I, can stimulate an anti-senescence NK-cell response.

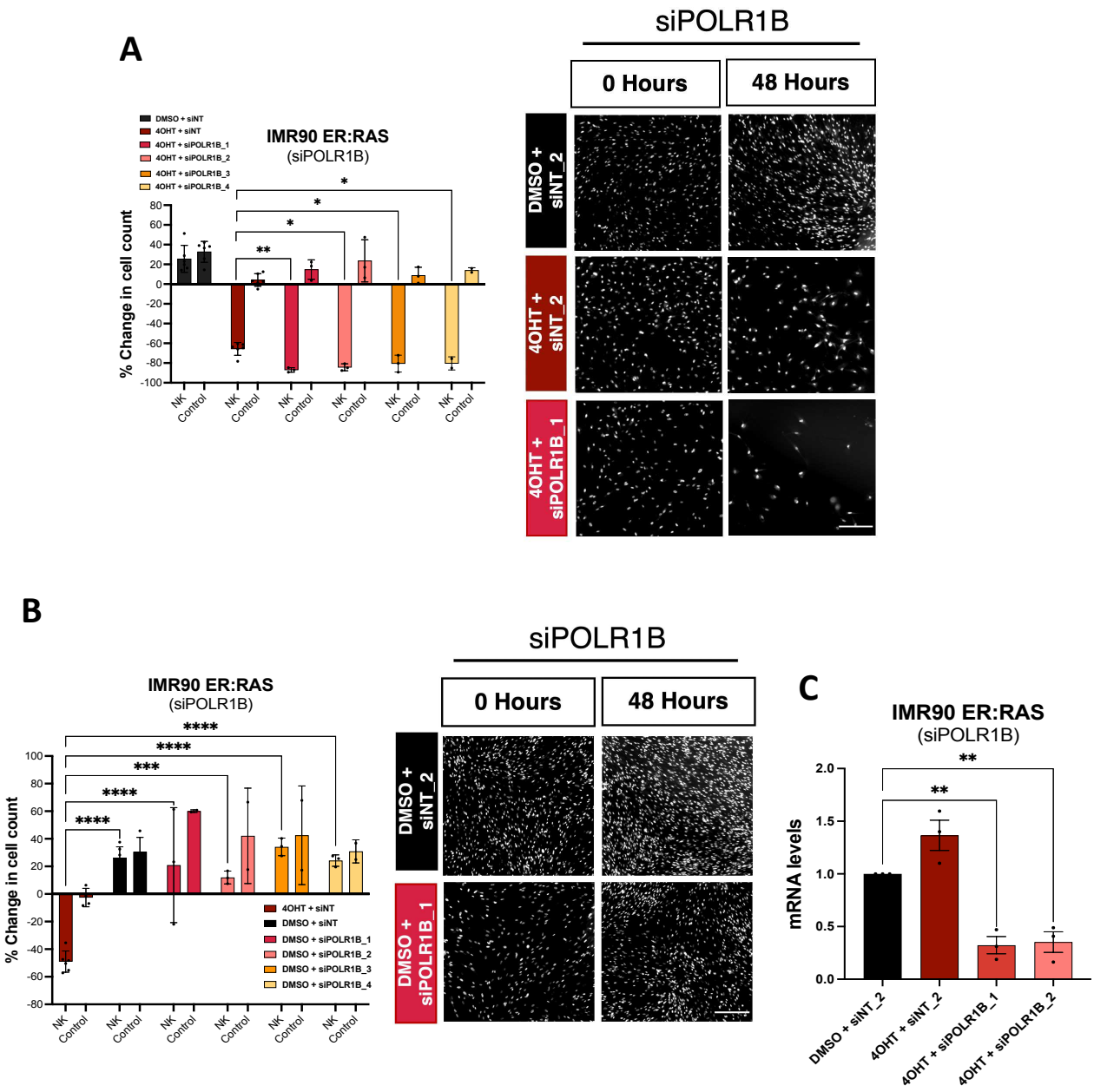


Figure 6.8 siRNAs against POLR1B selectively promote NK-mediated killing of senescent cells

(A) Quantification of the percentage change in senescent (4OHT-treated) IMR90 ER:RAS cell counts transfected with siRNAs against non-targeting controls or against POLR1B following co-culture with NK92-MI cells. Representative images of the co-culture for each hit are also shown (*n* = 3). Scale bar, 300μm.

(B) Quantification of the percentage change in non-senescent (DMSO-treated) IMR90 ER:RAS counts transfected with siRNAs against non-targeting controls or against POLR1B following co-culture with NK92-MI cells. siRNA transfection of POLR1B did not promote NK cell activity against non-senescent cells. Representative images of the co-culture for each hit are also shown (*n* = 3). Scale bar, 300μm.

(C) qRT-PCR analysis showing the mRNA expression of POLR1B in IMR90 ER:RAS cells transfected with two selected siRNAs against POLR1B (*n* = 3).

(A-C) Ordinary one-way ANOVA.

n signifies independent experiments. All error bars represent mean ± SEM. *P < 0.05, **P < 0.01, ***P < 0.001, ****P < 0.0001; ns= not significant.

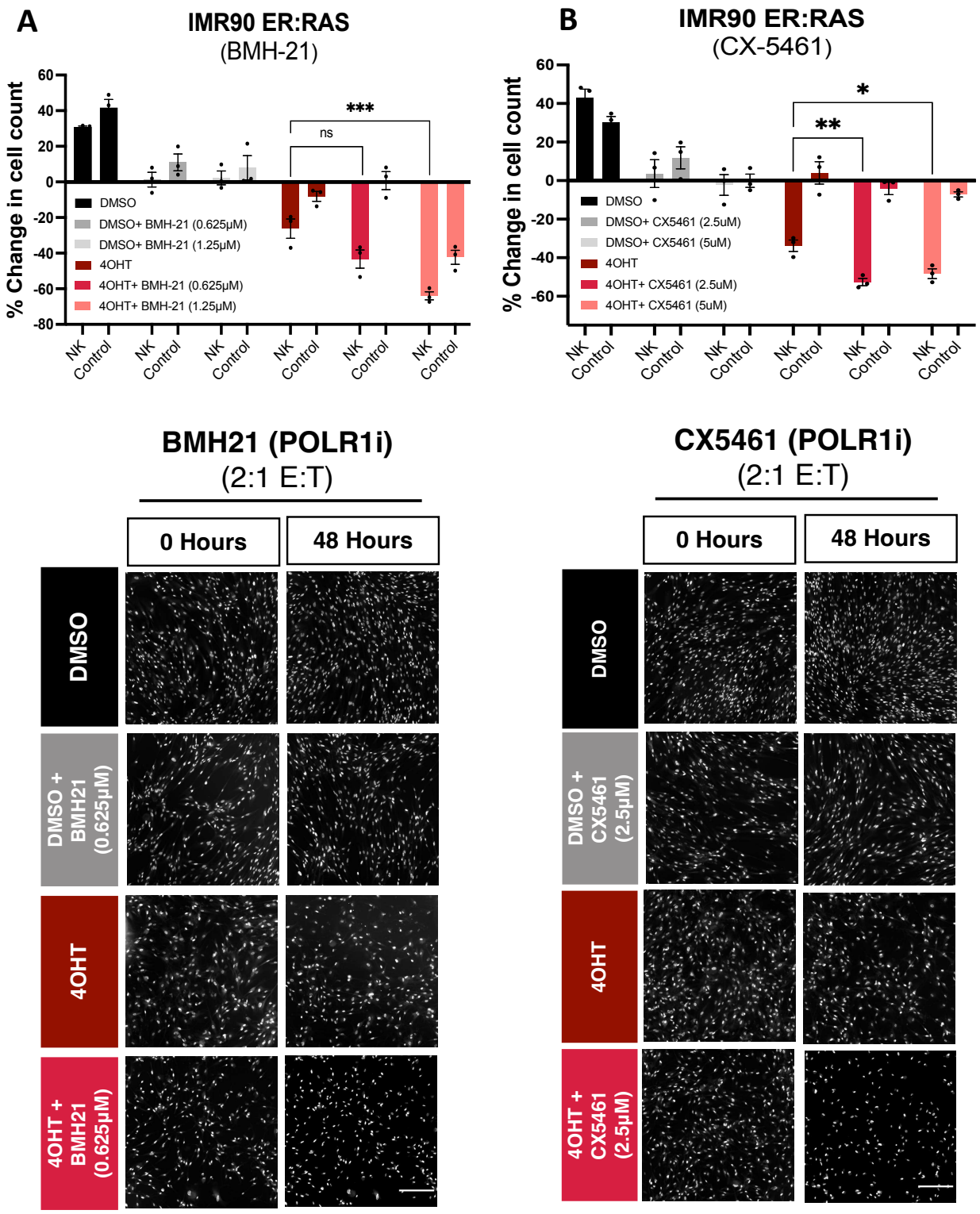


Figure 6.9 RNA Pol I inhibitors enhance NK-mediated killing of cells undergoing OIS

(A & B) Top panel depicts quantification of NK cytotoxicity of IMR90 ER:RAS cells following treatment with either DMSO or 4OHT alone or in combination with BMH-21 (0.625μM & 1.25μM) **(A)** or CX-5461 (2.5μM & 5μM) **(B)**. Inhibitors of RNA Pol I (POLR1i) were added 4 days following DMSO/4OHT administration. Experimental NK wells contained treated IMR90 ER:RAS cells co-cultured with NK92-MI cells at a 2:1 E:T ratio for 48 hours. NK-mediated cytotoxicity was measured as the percentage change in nuclei count (DAPI) of IMR90 ER:RAS cells over 48 hours of co-culture. Control wells contained treated IMR90 ER:RAS in the absence of NK cells. Bottom panel for **(A & B)** show representative images before and after co-culture (*n* = 3). Scale bar, 300μm.
(A & B) Ordinary one-way ANOVA.
n signifies independent experiments. All error bars represent mean ± SEM. *P < 0.05, **P < 0.01, ***P < 0.001, ****P < 0.0001; ns= not significant.

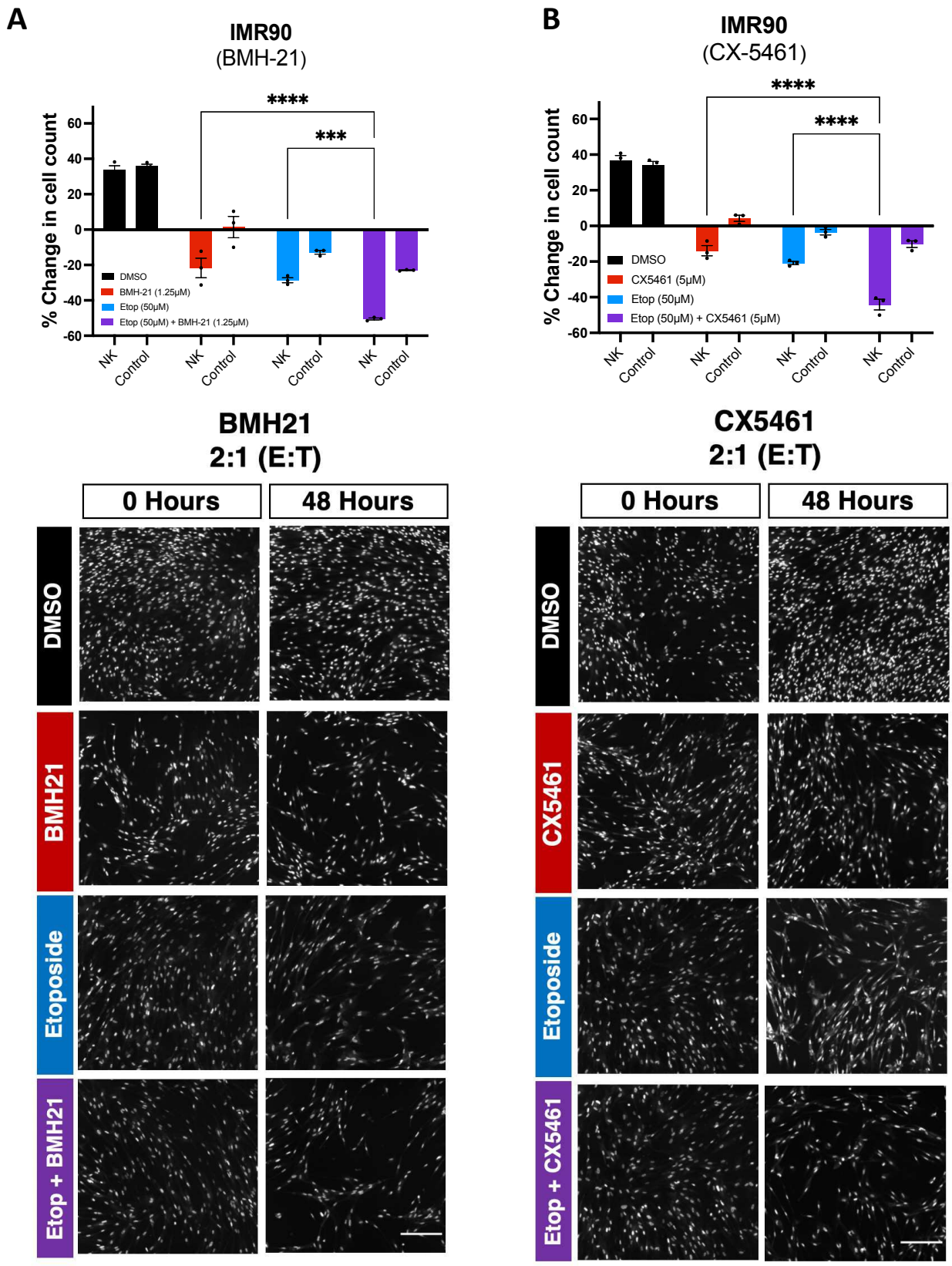


Figure 6.10 Inhibitors of RNA Pol I enhance NK-mediated killing of cells undergoing TIS

(A & B) Quantification representative images of NK cell-mediated cytotoxicity of IMR90 cells 7 days following initial administration of either DMSO or etoposide. RNA Pol I inhibitors BMH-21 **(A)** or CX-541 **(B)** were added 4 days after DMSO/etoposide induction. Experimental wells contained treated IMR90 cells co-cultured with NK92-MI cells at a 2:1 E:T ratio. Control wells contained treated IMR90 in the absence of NK cells Percentage change in cell count was measured based on the change in nuclei count (DAPI) of IMR90 cells over 48 hours of co-culture (*n* = 3). Scale bar, 300μm.

(A & B) Two-way ANOVA.

n signifies independent experiments. All error bars represent mean ± SD. *P < 0.05, **P < 0.01, ***P < 0.001, ****P < 0.0001; ns= not significant.

6.6 Summary and Discussion

From a therapeutic standpoint, triggering senescence clearance by NK cells can expedite wound repair and the resolution of fibrosis, promote rejuvenation and maintain homeostasis of the endometrium, as well as induce durable tumour regressions for both solid and liquid tumours (Brighton et al., 2017; Krizhanovsky et al., 2008; Ruscetti et al., 2018; Soriani et al., 2009; Walle et al., 2022). A rising number of studies have proposed the use of molecularly targeted therapies to sensitise senescent cells to NK-based immunotherapy (Kale et al., 2020). However, given the limited number of senescence markers shared between different cell types, and the fact that even fewer of them can be targeted to induce immunogenic vulnerabilities in senescent cells, the challenge lies in identifying compounds that promote an anti-senescence immune response. With this in mind, in this chapter, we wanted to characterise whether inhibitors targeting the hits identified in our screen can promote NK cell-mediated cytotoxicity in different senescence types.

In the previous chapter, we shortlisted 9 candidates from our screen that promote senescence surveillance by NK cells when silenced. Pathway analysis revealed our candidates to be associated with NK cell-mediated cytotoxicity as well as SASP and T cell signalling, validating our hit selection criteria. Although these 9 candidates were selected from a 'druggable genome' library, only a limited number of small molecule inhibitors have currently been developed that target these hits. As a result, we identified drugs inhibiting only 5 of the 9 candidates, namely SMARCA4, POLR1B, FURIN, PHF19, and FOSL1 (thereby excluding CD247, FCRL2, FOXH1, GLRA4).

Our initial siRNA screens entailed siRNA transfections in IMR90 ER:RAS cells prior to senescence induction. To mimic a more pathological context, however, we investigated the effect of the selected drugs after senescence induction. In this manner, we found 3 hits whose inhibition produced a robust NK-mediated cytotoxic response against senescent cells: FURIN, SMARCA4, and POLR1B. These candidates merit further studies both to understand their mechanism of action and to evaluate to their therapeutic value.

FURIN is a ubiquitously expressed proprotein convertase that catalyses the processing and maturation of protein precursors from the trans-Golgi network (TGN) to the cell surface as part of the secretory pathway (Braun and Sauter, 2019). Increased expression of deregulated FURIN is associated with various malignancies and can operate as a prognostic biomarker (Jaaks and Bernasconi, 2017). Due to its role in regulating the proteolysis of proproteins during secretion, it can be deduced that FURIN is associated with the secretory phenotype of senescent cells. In fact, knockdown of FURIN in our siRNA screens promoted the expression of IL6, IL8, IL1β, and CCL2. In addition, FURIN has been described as a regulator of innate and adaptive immune responses (Rose et al., 2021). For instance, through its proteolytic activities, FURIN can modify the immunosuppressive properties of T regulatory cells or promote PD-1 expression in CD8+ T cells to restrict their function in colorectal cancers (Tome et al., 2019). Furthermore, FURIN activity is generally negatively correlated with tumour immune infiltration, and inhibiting FURIN can activate immune response across various cancer types (Zhou and Gao, 2021). Correspondingly in senescence, we also discovered that inhibiting FURIN expression through the treatment with Hex-D and SSM3 enhanced NK cell-mediated cytotoxicity of senescent cells, albeit to a lower degree relative to SMARCA4 or POLR1B inhibition.

SMARCA4 encodes the protein BRG1, an essential ATPase subunit of the SWI/SNF chromatin remodelling complex. The complex regulates the transcriptional activation of genes associated with DNA repair, cell differentiation, and cell division by reconfiguring the chromatin structure (Mardinian et al., 2021). Through these processes, SMARCA4, alongside other concomitant subunits, including SMARCA2 and SMARCB1, act as tumour suppressors (Mardinian et al., 2021). In general, SMARCA4 alterations occur in most cancer types. Expression of SMARCA4 is associated with tumour immune evasion leading to a poor prognosis and survival (Peng et al., 2021). Interestingly, despite the poor clinical outcomes, multiple SMARCA4-deficient tumours are sensitive to immunotherapies, including immune checkpoint inhibitors (ICI), as the SWI/SNF-mutant alterations to the chromatin structure can incite the transcription of interferon-stimulated genes (ISGs) whose protein products initiate the recruitment and activation different immune cells through non-cell autonomous mechanisms (Schoenfeld et al., 2021; Takada et al., 2019; Tischkowitz et al., 2020). Moreover, ISGs can self-reinforce the interferon signalling pathway, which may rationalise the upregulation of SASP we

observed following SMARCA4 silencing (see Chapter 4.3). Indeed, the knockdown of SMARCA4 has previously been shown to enhance immunostimulatory ISGs and the innate immune response in hypercalcaemic small cell carcinoma of the ovary (Hu et al., 2020). Similarly, increased sensitivity to ICI therapy in SMARCA4-mutant tumours suggests the possibility that SMARCA4 inhibition in senescent cells can produce a cytotoxic T cell response, which would warrant further investigation. Here, we showed that the SMARCA4 knockdown induced immunogenic vulnerabilities within senescent cells. Drug-mediated inhibition of SMARCA4 promoted NK-mediated killing of senescent cells, and this effect was positively correlated with SMARCA4i concentration. In future experiments, exploring SMARCA4 inhibition to target senescent tumours would be of interest.

Despite the enhanced NK-mediated clearance of senescent cells invoked by the SMARCA4 inhibitor, the concentrations of SMARCA4i used were high (20-40μM). Although these high dosages are relevant for treatment in culture, they may not be physiologically feasible or lead to off-target effects. SGC-SMARCA-BRDVIII is an inhibitor of both SMARCA2 and SMARCA4 ATPases and the SWI/SNF subunit PB1(5), which all function with mutually exclusive transcriptional behaviour (Raab et al., 2017). As a result, a mechanistic characterisation of the inhibitor is required to validate the specific effects mediated by SMARCA4 inhibition. In addition, a recent study reported the development of a novel proteolysis-targeting chimera (PROTAC) degrader of SMARCA2/4, AU-15330, which potently inhibited prostate cancer growth in mice models (Xiao et al., 2022). Although investigating the immune response following AU-15330 treatment was not considered, the study signifies the importance of targeting both SMARCA2 and SMARCA4 for maximising therapeutic potential. In addition, the concentrations of the PROTAC used were lower (~1μM) compared to those we use of SGC-SMARCA-BRDVIII, and thus represents a promising compound that we can use to investigate SMARCA4 suppression in future studies, particularly *in vivo*.

POLR1B encodes the B subunit as part of a core protein complex that constitutes RNA polymerase (Pol) I. As RNA Pol I is essential for the transcription of ribosomal RNAs and ribosomal biogenesis (Goodfellow and Zomerdijk, 2013), human cancers display an increased Pol I-dependent transcription that is necessary for their proliferation. POLR1B expression is often upregulated in tumours (Ferreira

et al., 2020). Similarly, increased rRNA transcription can be driven by cellular stress, such as oncogenic stress. This might be related to increased POLR1B expression observed during OIS from our RNA-seq analysis. On the other hand, various chemotherapeutic agents that drive senescence in tumours have been described to have non-selective inhibitory effects on RNA Pol I, including doxorubicin, etoposide, and cisplatin, which could explain the downregulation of POLR1B expression observed in our etoposide-induced senescence RNA-Seq datasets (Bruno et al., 2017; Pommier et al., 2016).

A few features of RNA Pol I activity are shared between tumours and senescent cells, which makes its inhibition an attractive therapeutic target. 1) Firstly, almost all cancers show increased expression of RNA Pol I components to meet the demands of rapid cell division (Ferreira et al., 2020). Similarly, we found cells undergoing OIS to show an upregulation of POLR1B. 2) Secondly, normal cells express lower levels of RNA Pol I, making them less susceptible to the effects of RNA Pol I inhibition. 3) RNA Pol I is solely responsible for transcribing the single pre-RNA transcript of 47S rRNA, which is subsequently processed into alternative rRNAs. Therefore, in theory, targeting RNA Pol I can be highly selective, minimising off-target effects that may otherwise interfere with the actions of RNA Pols II and III. Considering these factors, inhibiting RNA Pol I in tumours can promote cancer cell death (Bywater et al., 2012; Peltonen et al., 2015). Here, we report that inhibiting RNA Pol I increased senescent cell death by activating an NK cell surveillance programme. Furthermore, inhibition of RNA Pol I has shown to induce the DNA damage response (DDR) and the activation of the STING pathway in ovarian carcinomas, a pathway known to mediate an innate immune response (Cornelison et al., 2021; Sanij et al., 2020). Whether RNA Pol I inhibition recapitulates this effect in senescent cells requires further examination.

We tested two RNA Pol I inhibitors, BMH-21 and CX-5461. BMH-21 treatment in cells undergoing OIS and TIS and found an increase in NK-mediated killing of senescent cells . Surprisingly, increasing BMH-21 concentration promoted senescent cell death even in the absence of NK cells, but not in non-senescent cells, implicating BMH-21 as both an immunostimulatory and a potential senolytic candidate. The small molecule CX-5461 selectively inhibits RNA Pol I by targeting rRNA biosynthesis and is currently in early phase clinical trials for both haematological and breast tumours (Drygin et al., 2011;

Ferreira et al., 2020). In ovarian cancers, CX-5461 treatment has shown to induce the DDR pathway and produce an accumulation of cytosolic DNA, leading to cGAS-STING pathway activation and the production of proinflammatory and immunomodulatory cytokines (Cornelison et al., 2021). Here, we showed that CX-5461 administration enhanced NK cell-mediated killing of senescent cells but not in growing cells. Unlike BMH-21, treatment with CX-5461 did not induce the killing of senescent cells without the presence of NK cells. Finally, as these NK-stimulatory effects were dependent on RNA Pol I inhibition, the level at which these effects were explicitly mediated through POLR1B inhibition requires dissecting.

Although inhibition of SMARCA4, POLR1B, and FURIN in IMR90 ER:RAS cells undergoing OIS produced a potent NK cell cytotoxic response, there are other hits from our screen which may potentiate NK-mediated cytotoxicity in different senescence and cell types.

PHF19 is a core component of the polycomb repressive complex 2 (PRC2), a transcriptional repressor involved in fundamental biological processes, including differentiation and cell proliferation. We tested inhibitors of the methyltransferase EZH2, the catalytic subunit of PRC2 that promotes heterochromatin formation repressing the *INK4A* locus and SASP genes in non-senescent cells (Gil and Peters, 2006; Hoare et al., 2016). To inhibit EZH2, we used the drugs GSK126 and Tazemetostat, both of which have entered clinical trials for the treatment of various tumour types (Li et al., 2021a). We found that both inhibitors only modestly promoted NK-mediated cytotoxicity in IMR90 ER:RAS cells undergoing OIS (Supplementary Figure S6.3A & B). However, current evidence has shown that EZH2 inhibition potentiates cytokine secretion and NK-mediated killing of hepatocellular carcinomas (HCCs) (Bugide et al., 2021). This was corroborated in high-grade serous ovarian carcinomas (HGSOCs), whereby the combined inhibition of the histone methyltransferases EZH2 and G9A not only synergistically induced chemokine secretion and the recruitment of NK cells but also decreased the population of the immunosuppressive CD4+ T regulatory cells, promoting tumour burden reduction (Spiliopoulou et al., 2022). Remarkably, a recent report described that the pharmacological inhibition of EZH2, in combination with the senescence-inducing cytostatic drugs palbociclib and trametinib, generated a durable SASP and led to NK cell infiltration and widespread tumour regressions in senescent pancreatic

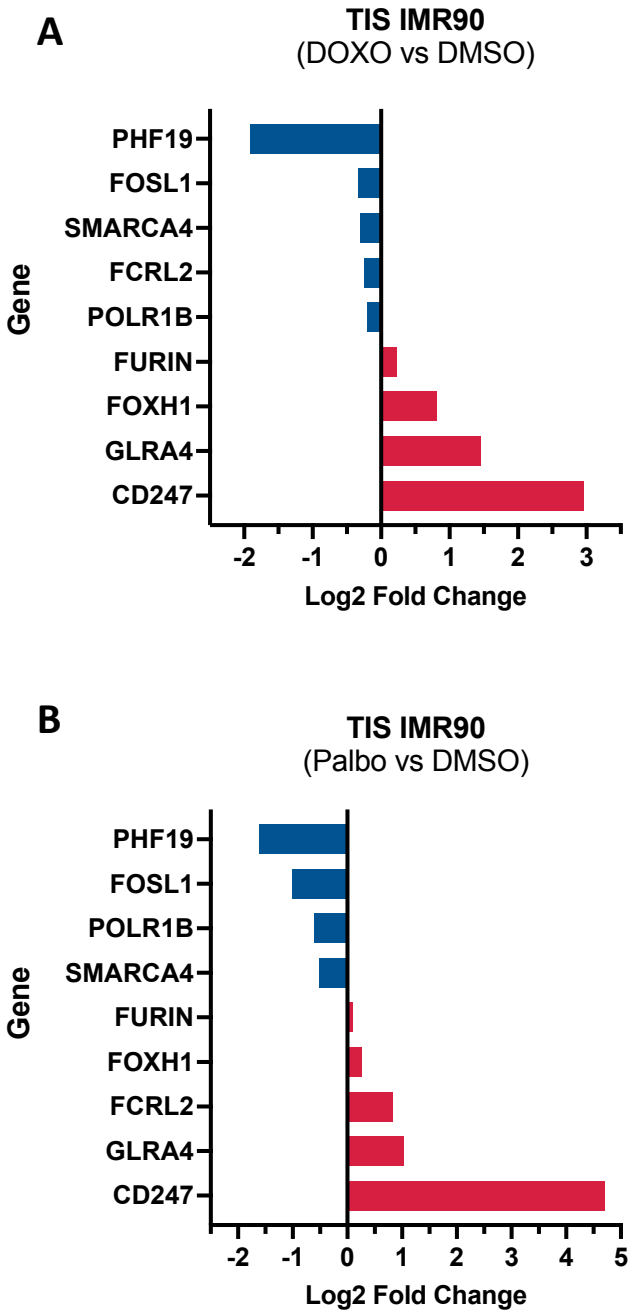
ductal adenocarcinomas (PDACs), a tumour type previously reported to suppress NK cell surveillance (Chibaya et al., 2022b; Ruscetti et al., 2020). The latter study not only shared a similar therapeutic objective to our project but also advocated the need to investigate the inhibition of different targets from our screen in other senescence models.

CD247 and FCRL2. Both genes encode proteins associated with transmembrane receptors but serve distinct functions. CD247 constitutes part of the T cell receptor CD3 complex, a co-receptor that regulates activation of both CD4+ and CD8+ T cells. For this reason, CD247 deficiency is reported to impair an immune response through defective T cell receptor engagement. For example, in ovarian tumours, low CD247 expression in the peripheral blood lymphocytes reduces the population of tumour infiltrating lymphocytes (TILs) and is associated with a poor prognosis (Ye et al., 2019). Similarly, low CD247 expression levels in the blood and lung tissue samples of patients with idiopathic pulmonary fibrosis (IPF) correlate with declining lung function (Li et al., 2021b). Surprisingly, we found CD247 expressed highly in cells undergoing TIS, and its knockdown enhanced a cytotoxic immune response against senescent IMR90 ER:RAS cells. Monoclonal antibodies against CD247 provide a promising route to decipher the precise mode of action which links CD247 to senescence and NK cell activity. Indeed, antibody depletion of a senescence-associated disialylated ganglioside, GD3, was recently described to switch an immune checkpoint from NK cell tolerance to NK cell surveillance in various senescent cells, emphasising the practicality of the assay (Iltis et al., 2021). Likewise, FCRL2, encoding an FC receptor-like protein and member of the immunoglobulin superfamily, could be inhibited by monoclonal blocking antibodies. Like FURIN, knockdown of FCRL2 during OIS upregulated the expression of multiple SASP readouts during our initial siRNA screen.

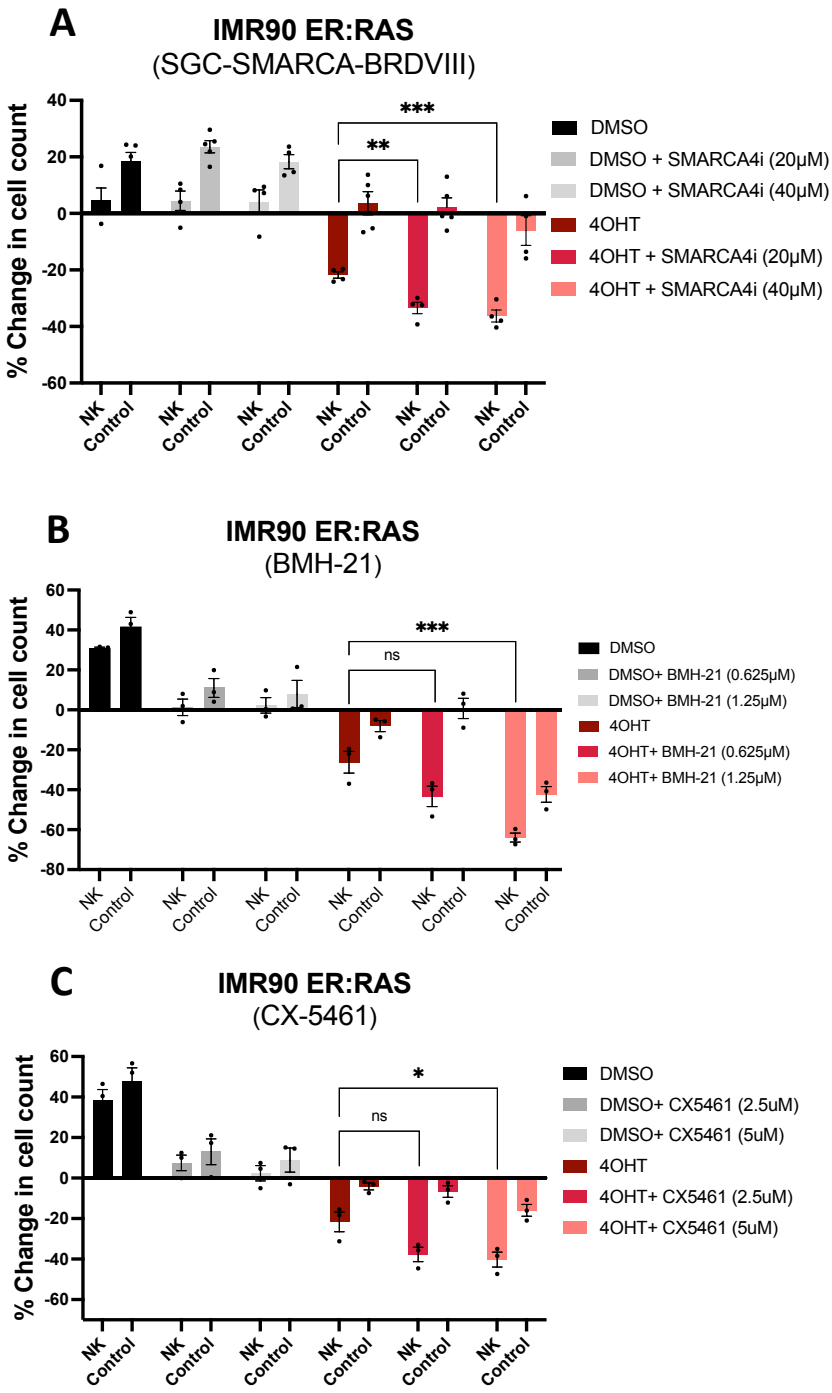
The forkhead box protein H1 **(FOXH1)** is a FOX transcription factor family member. FOXH1 was shown to be upregulated in cells undergoing OIS or TIS based on our RNA-Seq analysis. Clinically, FOXH1 activity is persistently upregulated in various cancers, and FOXH1 suppression has been reported to activate the Wnt/β-catenin signalling in lung tumours, a pathway well known to promote immunological tolerance (Pai et al., 2017; Zhang et al., 2021a). In addition, FOXH1 canonical interaction with SMAD2/3

drives TGF-β-mediated immune suppression (Attisano et al., 2001). Considering these factors, FOXH1 is an interesting target to inhibit to promote senescence immunosurveillance.

As described here, several of our screen candidates could be targeted to potentiate an anti-senescence immune response. Overall, by combining our co-culture assay with inhibitors targeting FURIN, SMARCA4, or RNA Pol I, we have identified new strategies to strengthen NK-mediated killing of senescent cells. This could provide therapeutic benefits in different senescence-related disorders. For example, inhibiting SMARCA4 or POLR1B may facilitate fibrosis resolution or be used as an anti-cancer therapy. Going forward, we aim to explore how these compounds potentiate NK-mediated killing of tumour cells in combination with therapy-induced senescence.

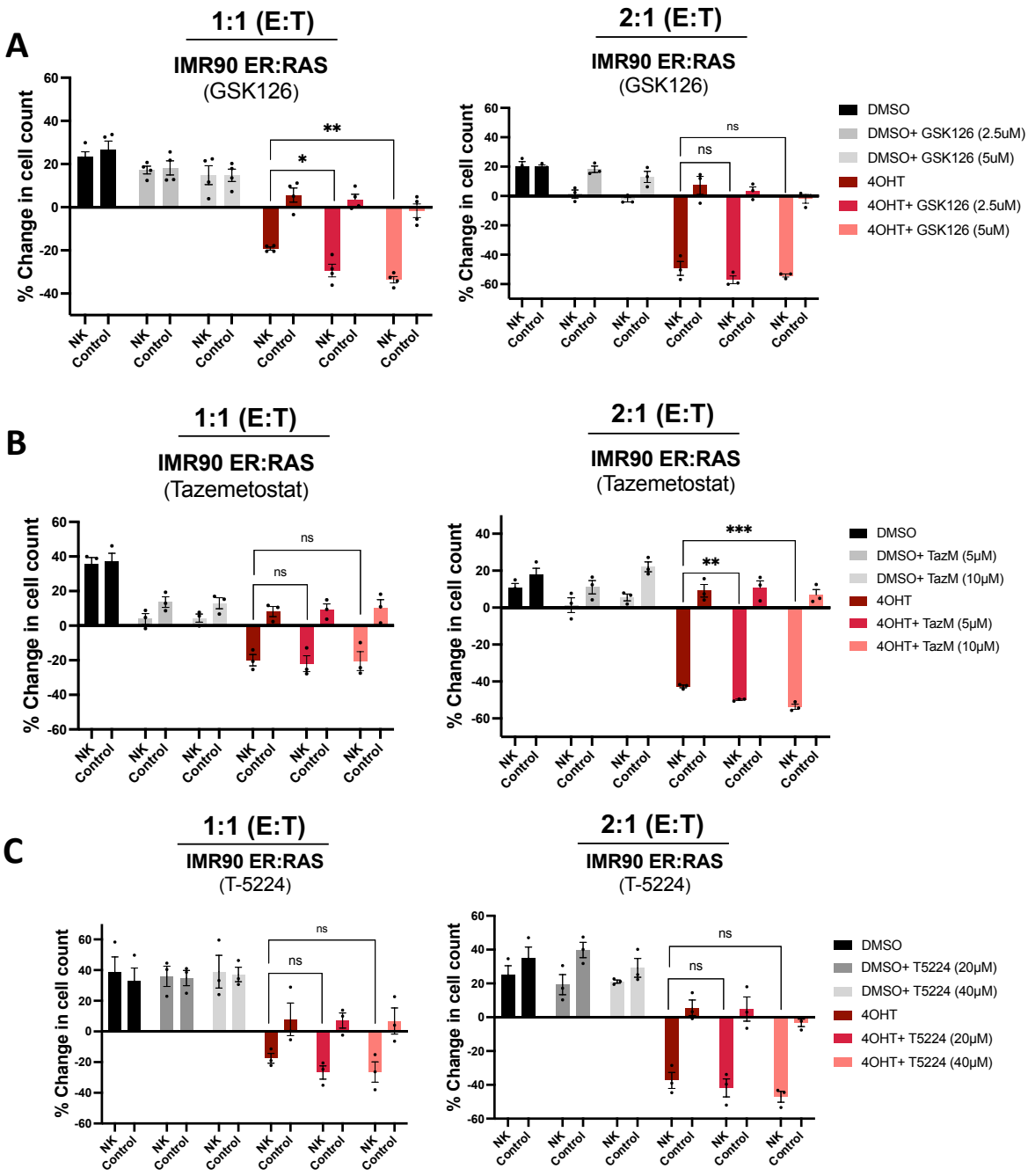


Supplementary Figure S6.1 Expression of the candidate genes in therapy-induced senescence.
(A & B) Results from differential gene expression analysis of the 9 genes in TIS IMR90 cells following treatment with Doxorubicin **(A)** or Palbociclib **(B)**. Original RNA-sequencing performed by Verena Wagner, unpublished data.



Supplementary Figure S6.2 SMARCA4 and RNA Pol I inhibitors enhance NK-mediated killing of cells undergoing OIS at low E:T ratios

(A) Quantification of NK cell-mediated cytotoxicity of IMR90 ER:RAS cells as **Figure 6.3C** using a 1:1 E:T ratio for NK cell co-culture.
(B) Quantification of NK cell-mediated cytotoxicity of IMR90 ER:RAS cells as **Figure 6.4A** using a 1:1 E:T ratio for NK cell co-culture.
(C) Quantification of NK cell-mediated cytotoxicity of IMR90 ER:RAS cells as **Figure 6.4B** using a 1:1 E:T ratio for NK cell co-culture.
(A-C) Ordinary one-way ANOVA.
n signifies independent experiments. All error bars represent mean ± SEM. *P < 0.05, **P < 0.01, ***P < 0.001, ****P < 0.0001; ns= not significant.



Supplementary Figure S6.3 Inhibitors against EZH2 and FOSL1 modestly increase NK-mediated killing of cells undergoing OIS

(A-C) Quantification of NK cell-mediated cytotoxicity of IMR90 ER:RAS cells following treatment with either DMSO or 4OHT alone or in combination with either the EZH2 inhibitors GSK126 **(A)** or Tazemetostat **(B)** or the C-Fos/AP-1 inhibitor T-5224 **(C)**. Inhibitors were added 4 days following DMSO/4OHT administration. Experimental NK wells contained treated IMR90 ER:RAS cells co-cultured with NK92-MI cells at either a 1:1 or 2:1 E:T ratio for 48 hours. Cytotoxicity was measured as the percentage change in IMR90 ER:RAS nuclei count (DAPI) during co-culture. Control wells contained treated IMR90 ER:RAS in the absence of NK cells (*n* = 3).

(A-C) Ordinary one-way ANOVA.

n signifies independent experiments. All error bars represent mean ± SEM. *P < 0.05, **P < 0.01, ***P < 0.001, ****P < 0.0001; ns= not significant.

Chapter 7 - General Discussion

7.1. Overall summary and discussion of current work

Acute senescence induction provides a protective barrier against tumour development, can limit the extent of fibrosis, and can promote wound healing. The key to these effects is the transient presence of senescent cells within tissues which are eventually cleared by the immune system. However, with age, or if the nature of the senescence or damage is chronic, the immune response may decline, and recent evidence has revealed that senescent cells are also capable of evading immune surveillance (Muñoz et al., 2019; Ovadya et al., 2018; Pereira et al., 2019). This results in a chronic inflammatory senescent phenotype that exacerbates tissue aberrations and contributes to age-related pathologies and tumour progression. Consequently, therapeutic interventions have primarily focused on using senolytic compounds to selectively kill senescent cells, which, although promising in pre-clinical trials, have raised concerns regarding their side effects in clinical use (Kirkland and Tchkonia, 2017). Alternative strategies include targeting the SASP of senescent cells to inhibit their proinflammatory effects or, paradoxically, to potentiate the immunomodulatory SASP to reactivate immune-mediated clearance. In this study, we used genetic and pharmacological inhibition to identify genes that enhance the SASP and subsequently sensitise senescent cells to elimination by NK cells. We discovered novel therapeutic targets that, when inhibited, potentiate NK cell-mediated killing of senescent cells without killing non-senescent cells.

Both innate and adaptive immune cells are implicated in the surveillance of senescent cells (Kale et al., 2020). The specific immune response triggered may vary depending on the senescence inducer and target cell. NK cells have previously been described to clear senescent cells in a variety of pathological contexts (Chaturvedi et al., 2022; Iannello et al., 2013; Jin et al., 2021; Krizhanovsky et al., 2008; Ruscetti et al., 2018; Xue et al., 2007) and mediate cytolytic functions by deploying perforin-mediated granule exocytosis (Sagiv et al., 2013). As NK cell activation can bypass antigen recognition or co-receptor engagement, these cells confer a superior advantage over antigen-specific T cell surveillance. Instead, NK cells are governed by the direct interaction of their activating receptors with a broad range of senescent cell types (Sagiv et al., 2016) or through the stimulation of

secreted cytokines (Zwirner and Domaica, 2010). Therefore, strategies that modulate the SASP could enhance NK-mediated surveillance. Activated NK cells can also rapidly release proinflammatory cytokines that stimulate further NK cell activation and may provoke adaptive immune surveillance, which therapeutically could be coordinated using existing T-cell immunotherapy. With this in mind, we set out to perform RNAi screens to identify genetic perturbations that enhance the NK-mediated killing of senescent cells via the hyperinduction of the SASP.

Using a model of oncogene-induced senescence (OIS) in IMR90 ER:RAS fibroblasts, we first characterised the interplay between the SASP and NK cell activity. The SASP is frequently cited as a 'double-edged sword' and can exert deleterious proinflammatory effects on the surrounding microenvironment, but in the proper context can also promote immune cell recruitment (Birch and Gil, 2020). We found that cells undergoing OIS produced a strong SASP phenotype enriched in immunostimulatory cytokines, including CCL2 and CXCL10. Furthermore, we used a chemotaxis assay to show that the senescent secretome attracted NK cells.

To investigate the NK-mediated killing of senescent cells, we developed a NK cell co-culture system that is amenable to large-scale RNAi and drug screens. At a 2:1 E:T ratio of NK cells to senescent cells, NK cells aggregated and selectively killed senescent cells after 48 hours in co-culture, whereas non-senescent cells continued to proliferate despite NK cell presence. Indeed, the level of NK-mediated cytotoxicity of senescent cells may vary depending on senescent cell confluency, among many factors discussed in Chapter 5.4. Regardless, given the low E:T ratio, we observed a highly efficient NK-mediated killing response under physiologically relevant settings. However, despite the preferential killing of senescent cells by NK cells, most senescent cells were not eradicated, suggesting that this immune surveillance is susceptible to improvement. In pathological contexts, senescence immune surveillance may be impaired, particularly in cancer and other age-related diseases, whereby the immune response is dysfunctional or senescent cells have undergone immune tolerance. Our set-up provides an extensive dynamic range to improve NK-mediated killing through modulation of the SASP rather than resorting to external approaches such as adoptive NK cell transfer. To explore this potential, we took advantage of the EPRS inhibitor halofuginone (HF) and the

anticancer agent indisulam. HF had been characterised in our lab to promote the SASP, whereas indisulam has been described to increase an anti-tumour NK cell response (Pech et al., 2019). Interestingly, recent work has demonstrated that indisulam could be a senolytic agent (Pogacar et al., 2021). Here, we showed that both HF and indisulam amplified the SASP programme and substantially promoted NK cell cytotoxic activity against cells undergoing OIS. On the contrary, downregulating the SASP through glucocorticoid administration significantly restricted NK cell effector functions, highlighting the importance of the SASP response.

In light of our findings, we carried out a large-scale siRNA screen to uncover critical reinforcers of the SASP (see discussion in Chapter 4.4). Our primary screen comprised siRNAs targeting over 7,500 genes, and the proinflammatory SASP proteins IL6 and IL8 served as the screen readouts. Secondary screens explored two additional SASP components, IL1β and CCL2. Ultimately, we identified 124 candidates whose knockdown upregulated at least one SASP factor. Of these, 68 genes enhanced at least two SASP readouts when silenced. We postulated that at least a fraction of these 68 candidates may induce a pro-immunogenic response to sensitise senescent cells to NK cell surveillance. However, it must be noted that the SASP can also promote immunosuppression in specific contexts (Faget et al., 2019). For instance, senescent preneoplastic hepatocytes can recruit immature myeloid cells through their SASP, suppressing NK cell activity and triggering tumour growth (Eggert et al., 2016). Whether the net effect of the SASP is immunostimulatory or immunosuppressive is context dependent and can vary according to several factors including the cytokine milieu present in the tissue microenvironment, as well as the cell type or senescence inducer. Therefore, it is essential that we test our selected candidates *in vivo* where a complete immune microenvironment is present to determine the net changes in SASP expression and immune response.

Although a plethora of evidence supports the role of the SASP in immune surveillance, it is, by no means, the only method to promote NK cell-mediated killing of senescent cells. For instance, our study demonstrated that IMR90 ER:RAS cells undergoing OIS contradictorily upregulate both NK activating and inhibitory ligands. Knockdown of individual inhibitory ligands resulted in the enhancement of NK-mediated elimination of senescent cells. siRNA-mediated silencing of five NK

inhibitory ligands particularly stood out, including HLA-E, which has been documented to inhibit NK and cytotoxic T lymphocyte responses (Pereira et al., 2019). Interestingly, the study by Pereira et al. employed an autologous NK cell co-culture system using senescent primary human skin fibroblasts transfected with siRNAs against HLA-E. However, they found only ~10% of the senescent cells were killed despite the use of an E:T ratio of 10:1. Although we utilised a different co-culture system, we also found the repression of NK inhibitory ligands produced a relatively low increase of NK-mediated cytotoxicity compared to control senescent cells. Alternatively, targeting the SASP as a medium for NK cell activation confers several advantages over NK inhibitory ligands.

Firstly, the SASP can recruit cells from various immune populations, including macrophages, neutrophils, and T cells, in addition to NK cells to eliminate senescent cells, depending on the SASP composition. However, suppressing NK inhibitory ligands may only affect NK cells and highly differentiated CD8+ T cells (Kale et al., 2020). Here, we have shown that cells undergoing OIS upregulate CCL2 and CXCL10, among other immunomodulatory SASP factors associated. Although our focus is on characterising NK-mediated killing of senescent cells, the activation of additional immune surveillance programmes could be beneficial in augmenting senescent cell death or transforming immunologically cold senescent tumours into hot.

Secondly, although frequently overexpressed in tumours and some senescent cells, NK inhibitory ligands are also expressed in normal cells to promote self-immune tolerance, and targeting these ligands may induce undesired effects.

Moreover, an emerging concern of senescent cells is that they can evolve mechanisms to evade the immune response. For example, senescent cells can shed NKG2D activating ligands from their surface, facilitating senescent cell accumulation through immune evasion (see Introduction Chapter 1.7.4) (Muñoz et al., 2019; Zhang et al., 2022). As the complex balance of NK activating and inhibitory receptor signalling tends to favour inhibition (Long et al., 2013), it may suggest that despite the targeted silencing of inhibitory ligand expression on senescent cells, the effect may be counteracted by the simultaneous shedding of activating ligands, once again resulting in immune evasion.

Resolving these issues could require the inhibition of multiple NK inhibitory ligands. However, potentiating the SASP overcomes the reliance on NK ligand-receptor interactions to achieve a selective NK cell-mediated senescence surveillance programme.

By leveraging our NK cell co-culture system, we next searched for targets whose knockdown promotes NK-mediated killing of cells undergoing OIS (for discussion of NK co-culture, see Chapter 3.8; for discussion of NK siRNA screens, see Chapter 5.4). Through multiple validation siRNA screens, we narrowed our selection to 9 candidates whose downregulation enhanced NK-mediated elimination of senescent cells. Ideally, the knockdown of any candidates selected should pose minimal adverse effects on normal cells. To address whether the stimulated NK cytotoxic activity was restricted to senescent cells, we silenced the expression of the 9 candidates in proliferating healthy IMR90 ER:RAS cells prior to co-culture with NK cells. Remarkably, despite using potent NK92-MI cells, the knockdown of our hits did not induce NK-mediated killing of proliferating cells. Senescent cells, however, were actively targeted and killed by NK cells verifying that the NK cell effector response was selective for senescence. Similarly, it would be interesting to investigate whether our candidates could induce effector functions in NK cells isolated from fresh PBMCs as opposed to the NK92-MI cell line.

To ensure that our identified hits can be targeted therapeutically, we next examined whether pharmaceutical inhibition of our hits potentiated NK-mediated killing of senescent cells. We identified drugs inhibiting the expression of five of our hits (for detailed discussion, see Chapter 6.5). Among those, we focused on inhibitors of two leading screen candidates, the SWI/SNF complex component SMARCA4 and the RNA Pol I subunit POLR1B, to promote senescence immunogenicity. Aberrant expression of both SMARCA4 and RNA Pol I has been observed in multiple tumour types, and the downregulation of SMARCA4 is positively correlated with immune checkpoint inhibitor treatment (Ferreira et al., 2020; Peng et al., 2021; Takada et al., 2019). Here, we showed that the drug-mediated inhibition of SMARCA4 or the RNA Pol I complex enhanced NK cell-mediated killing of senescent cells compared to control senescent cells. In contrast to the knockdown of POLR1B, we

found that inhibiting RNA Pol I by the compound BMH-21 killed senescent cells even in the absence of NK cells (albeit at a lower level), suggesting its potential senolytic properties.

Although both the genetic and pharmaceutical inhibition of SMARCA4 and POLR1B promoted NK cell activation, we found siRNA knockdown of both hits to produce more specific and potent effects relative to small molecule inhibition. In fact, the knockdown of these two candidates was previously shown to potentiate the SASP phenotype, likely contributing to the enhanced NK cell effector functions. Therefore, it is also essential that we validate SASP expression following inhibitor treatment which may help to understand the efficacy of these compounds and fine-tune the administration of the drugs. More importantly, we noticed drug inhibition of our hits to marginally induce NK-mediated killing of non-senescent cells, which was not observed with genetic knockdowns. However, these effects in growing cells were mitigated when we used a lower E:T ratio of 1:1 rather than 2:1 whilst retaining an equivalent ratio of senescent cell death. Overall, these findings suggest that targeted suppression of SMARCA4 and RNA Pol I leads to increased NK-mediated senescence surveillance. However, additional modifications to the treatment regimen may be needed to improve the therapeutic index of these inhibitors.

Ideally, compounds would promote anti-senescence immunity regardless of how senescence is induced. Here, using the chemotherapeutic agent etoposide, we demonstrated that the sequential combination of etoposide followed by SMARCA4 or RNA Pol I inhibitors triggered the cooperated killing of senescent cells by NK cells. Although, up to now, we have only looked into the immunostimulatory effects mediated by these drugs, it would be interesting to learn whether compounds targeting other screen candidates could also augment NK cell surveillance in therapy-induced senescence (TIS). Regardless, our findings have revealed that the pharmaceutical inhibition of SMARCA4 and RNA Pol I can be functionally translated with different senescence inducers. In future studies, we aim to characterise these targeted therapies in senescent cancer models to promote anti-tumour immunity.

HF and indisulam have been used as controls throughout our study. While indisulam is well known to sensitise tumour or senescent cells to NK-mediated killing or senolytic activity, respectively, few studies have explored the role of HF in senescence or immune surveillance. HF has been described to limit fibrosis in the gastrointestinal tract and inhibit the immunosuppressive TGF-β signalling pathway (Pines, 2014), and may be indirectly associated with senescence and the SASP. Here, we found that HF treatment not only reinforces the SASP and NK-mediated cytotoxicity in cells undergoing OIS but also TIS. In fact, HF treatment did not induce NK-mediated killing of non-senescent cells. Although HF was not discovered as part of our screens, we may have unexpectedly characterised an additional therapeutic target whose effects warrant further studies in senescence-associated diseases.

One drawback of our current study is that we did not examine how our inhibitors may affect the senescence growth arrest. From a clinical perspective, the drugs would be administered following the onset of senescence; therefore, we must address this issue in future experiments. Finally, it is essential to remember that despite the benefits reported here from senescent cell elimination, the outcome may not always be positive depending on the tissue type or pathology. For instance, NK-mediated clearance of senescent neuroblasts in the brain has been shown to promote neurogenesis and impair cognition (Jin et al., 2021). Therefore, for future *in vivo* studies, in addition to characterising the mechanism of our selected inhibitors on NK cell cytotoxicity, it is important that we investigate potential harmful consequences to the surrounding tissue microenvironment.

7.2 Future perspectives

From our RNAi screens, we selected 9 genes which, upon silencing, upregulated SASP production leading to increased NK-mediated killing of senescent cells. Among these, we concentrated on 2 candidates: SMARCA4 and POLR1B, whose altered expressions are frequently correlated with increased tumour burden (see Chapter 6.5). Small-molecule inhibition of these candidates promoted NK-mediated killing of fibroblasts undergoing either oncogene- or therapy-induced senescence. This was a significant finding as it opens up the investigation of these genes in a therapeutic context, for

example, in treating fibrosis or various age-associated diseases (see Introduction, Table 1). In particular, we are interested in characterising the immunomodulatory effects of SMARCA4 and POLR1B inhibition in cancer. However, it is also important to keep in mind that there are 7 other candidates that merit exploration in TIS, specifically those with available inhibitors that would expedite future studies in mice models.

To investigate the NK-mediated clearance of tumours, we aimed to implement an immunogenic 'one-two punch' approach, whereby cancer cells would be treated with pro-senescence drugs to induce growth arrest, followed by the treatment with SMARCA4 or RNA Pol I inhibitors to potentiate an NK-stimulatory SASP. As preliminary work, we first want to understand which cancer models we can use to characterise senescence and examine an NK cell surveillance programme.

7.2.1 Investigating NK-mediated surveillance in KRAS mutant lung tumours

We investigated two different models of cancer. The first is a model of KRAS-mutant lung cancer, which has been described to undergo clearance by NK cells following TIS (Ruscetti et al., 2018). In an intriguing study by Ruscetti and colleagues, it was reported that inhibition of CDK4/6 and MEK1/2 by the small molecule inhibitors palbociclib and trametinib, respectively, induced a senescence phenotype in *KRAS*-mutant tumours. *KRAS* mutations are among the most frequent aberrations in human cancers and have often been cited as 'undruggable' (Papke and Der, 2017). Ruscetti et al. demonstrated that palbociclib can synergise with trametinib to invoke an immunostimulatory SASP in A549 lung cancer cells capable of driving NK-mediated cytotoxicity of senescent cancer cells and instigating tumour regressions *in vivo* (Ruscetti et al., 2018).

Based on this study, we first intended to recapitulate these findings. Complementary to the results reported by Ruscetti et al., we found that the combined cytostatic drug inhibition (palbociclib and trametinib) in A549 lung cancer cells was considerably more effective at impairing tumour growth and inducing senescence than treatment with either drug alone (Figure 7.1A-C). In fact, this combination treatment promoted SASP expression (Figure 7.1D), and this secretome was enriched in

immunomodulatory factors capable of recruiting NK cells (Figure 7.2A & B). Using our co-culture system, we also found that this drug combination strongly potentiated NK-mediated killing of senescent lung cancer cells but not in proliferating cells (Figure 7.2C). Interestingly, the 2:1 E:T ratio employed during the 48-hour co-culture period potentiated NK-mediated cytotoxicity in the cancer cells, despite being lower than the E:T ratios described in the study by Ruscetti et al. (which ranged between 10:1 to 20:1). More importantly, we established a working model of NK-mediated killing of senescent cells in lung cancer.

These findings demonstrated novel strategies to potentiate NK-mediated killing of senescent tumour cells. However, the combination of palbociclib and trametinib may not translate in different tumour types or if cancer cells develop resistance. Therefore, additional targets that induce immunogenic vulnerabilities in senescent tumours are required. CDK4/6 inhibitors are among the foremost cytostatic drugs undergoing clinical trials for multiple cancer types (Wagner and Gil, 2020). As we observed, although palbociclib treatment alone can reduce tumour growth, it does not drive a robust SASP response and therefore cannot promote senescence surveillance and durable tumour regressions when used as a single agent. With this in mind, in future experiments, we aim to use this model of A549 cells to test whether SMARCA4 or RNA Pol I inhibitors can be combined with palbociclib to promote NK-mediated killing of the tumour cells.

To reach this stage, we have begun testing our drug-positive controls halofuginone (HF) or indisulam in NK cell co-culture assays in combination with palbociclib in A549 cells. Previously, we have shown that HF or indisulam can potentiate NK-mediated killing of fibroblasts undergoing OIS or TIS. Furthermore, in a tumour setting, we found that HF (Figure 7.3A & B) and indisulam (Figure 7.4A & B) treatment substantially enhanced NK-mediated clearance of lung cancer cells when combined with palbociclib. From these experiments, we concluded that our lung cancer model is adequate to investigate changes in NK-mediated surveillance. Therefore, we plan to explore SMARCA4 and RNA Pol I inhibitors *in vitro* before investigating the immunomodulatory effect of these inhibitors *in vivo*, using the *Kras*$^{G12D/+;}$*Trp53*$^{-/-}$ (KP) lung tumour mice model (reported in Ruscetti et al., 2018). Finally, as mentioned in Chapter 7.1, given the ability of HF treatment to promote the SASP and NK cytotoxic

activity against fibroblasts undergoing OIS and TIS, as well as lung cancer cells undergoing TIS, HF could serve as a potential alternative candidate.

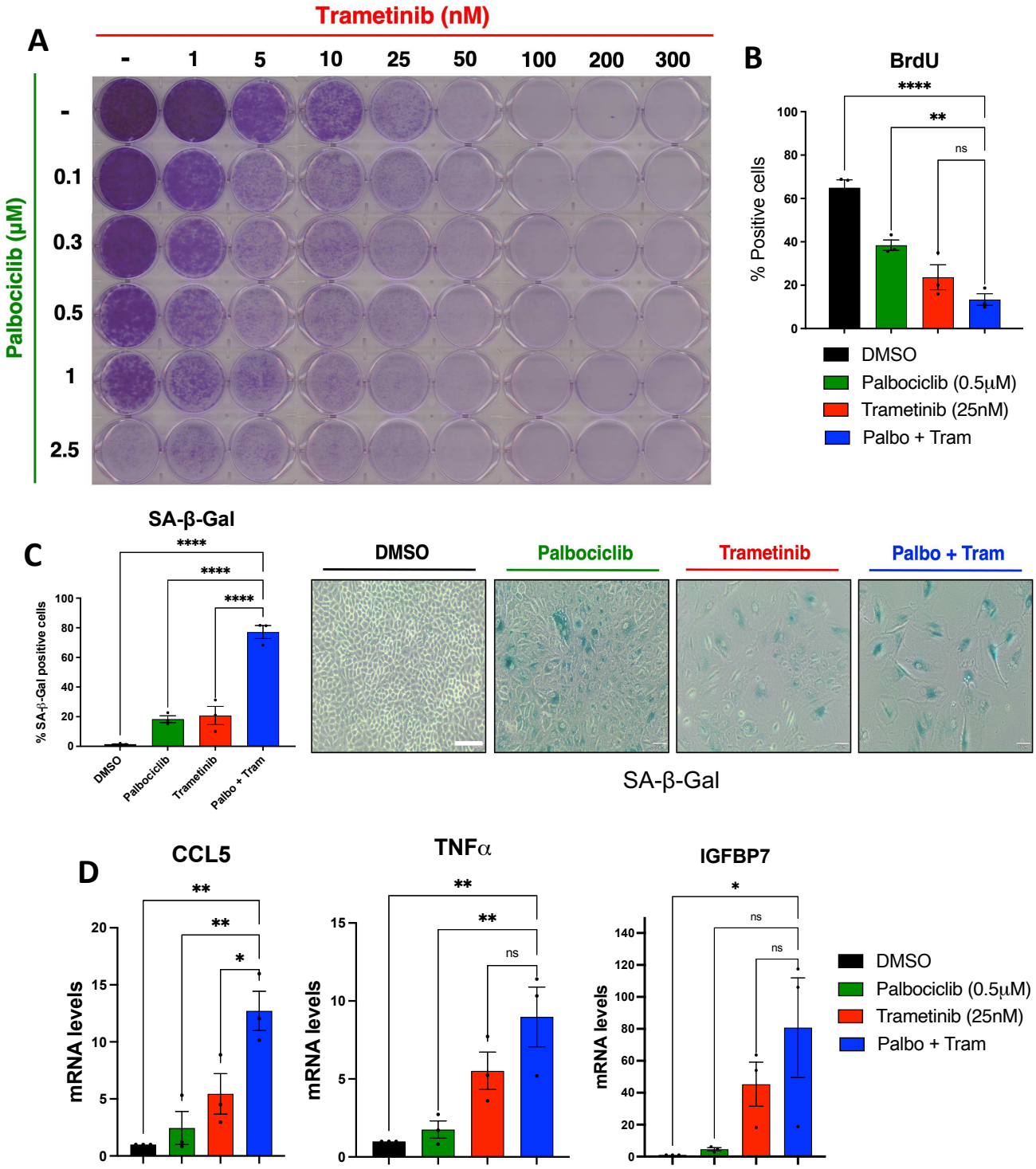


Figure 7.1 Palbociclib synergises with trametinib to induce senescence in lung cancer cells

(A) Clonogenic assay of A549 lung cancer cells treated with palbociclib and trametinib, either independently or in combination at the indicated concentrations. Shown are representative images out of two independent experiments

(B) Quantification of BrdU incorporation performed at day 8 in A549 cells. Cells were treated with either palbociclib (0.5μM), trametinib (25nM), or in combination (*n* = 3).

(C) Quantification and representative images of SA-β-gal staining (blue) performed on A549 cells fixed at Day 8 post treatment with either palbociclib (0.5μM), trametinib (25nM), or in combination (*n* = 3). Scale bar, 50μm.

(D) qRT-PCR analysis of the indicated SASP markers in A549 cells following 8-day treatment with palbociclib (0.5μM), trametinib (25nM), or in combination (*n* = 3).

(B-D) Ordinary one-way ANOVA.

n signifies independent experiments. All error bars represent mean ± SEM. *P < 0.05, **P < 0.01, ***P < 0.001, ****P < 0.0001; ns= not significant.

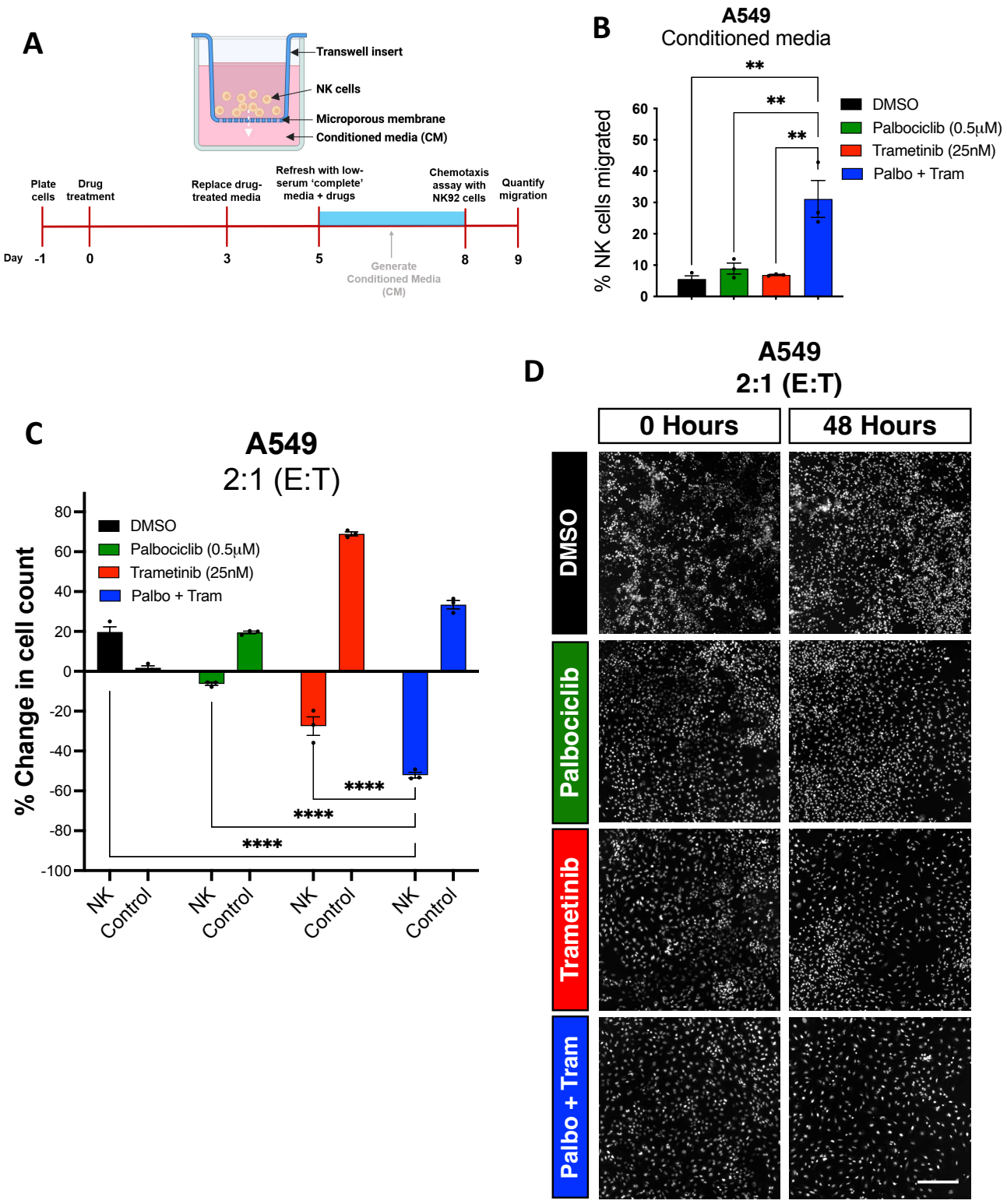


Figure 7.2 Palbociclib and trametinib combination promotes NK cell surveillance of senescent lung cancer cells
(A) Schematic of the chemotaxis assay experimental setting.
(B) Quantification of the percentage of NK92-MI cells migrating of the lower chamber of the transwell insert after 21 hours of the chemotaxis assay. Lower chamber comprised of raw conditioned media (CM) generated from A549 cells treated with either palbociclib (0.5μM), trametinib (25nM), or in combination (*n* = 3).
(C) Quantification of NK cell-mediated cytotoxicity of A549 cells after treatment with either palbociclib (0.5μM), trametinib (25nM), or in combination for 7 days and co-cultured with NK92-MI cells at a 2:1 effector-to-target (E:T) ratio for 48 hours. % change represents the percentage change in A549 cell count before and after co-culture with NK cells. Control wells comprised pre-treated A549 cells in the absence of NK cells (*n* = 3).
(D) Representative images of A549 cells before and after co-culture with NK cells as described and quantified in **(C)**. Scale bar, 300μm.
(B & C) Ordinary one-way ANOVA.
n signifies independent experiments. All error bars represent mean ± SEM. *P < 0.05, **P < 0.01, ***P < 0.001, ****P < 0.0001; ns= not significant.

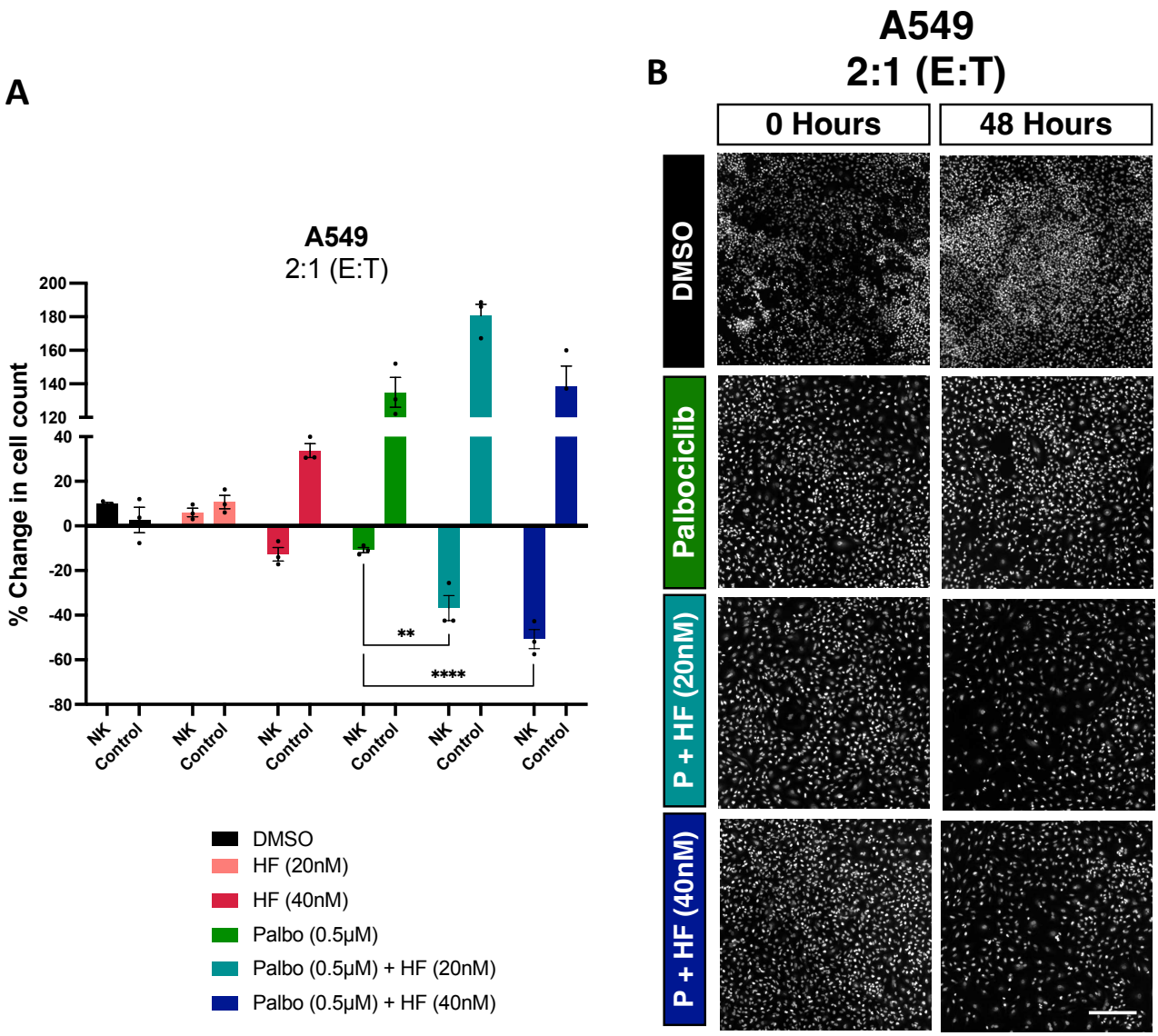


Figure 7.3 Combined palbociclib and halofuginone treatment promotes NK cell-mediated killing of lung cancer cells

(A) Quantification of NK cell-mediated cytotoxicity of A549 cells after treatment with the indicated drugs, either individually or in combination. A549 cells were pre-treated with palbociclib (0.5μM) for a total of 7 days whereas halofuginone (HF) (20nM or 40nM) was added 4 days following the induction of palbociclib for a total of 3 days. Co-cultures with NK92-MI cells were performed at 7 days following the induction of palbociclib treatment at a 2:1 effector-to-target (E:T) ratio for 48 hours. % change represents the percentage change in A549 cell count before and after co-culture with NK cells. Control wells comprised pre-treated A549 cells in the absence of NK cells (*n* = 3).

(B) Representative images of A549 cells before and after co-culture with NK cells as described and quantified in **(A)**. Scale bar, 300μm.

(A) Ordinary one-way ANOVA.

n signifies independent experiments. All error bars represent mean ± SEM. *P < 0.05, **P < 0.01, ***P < 0.001, ****P < 0.0001; ns= not significant.

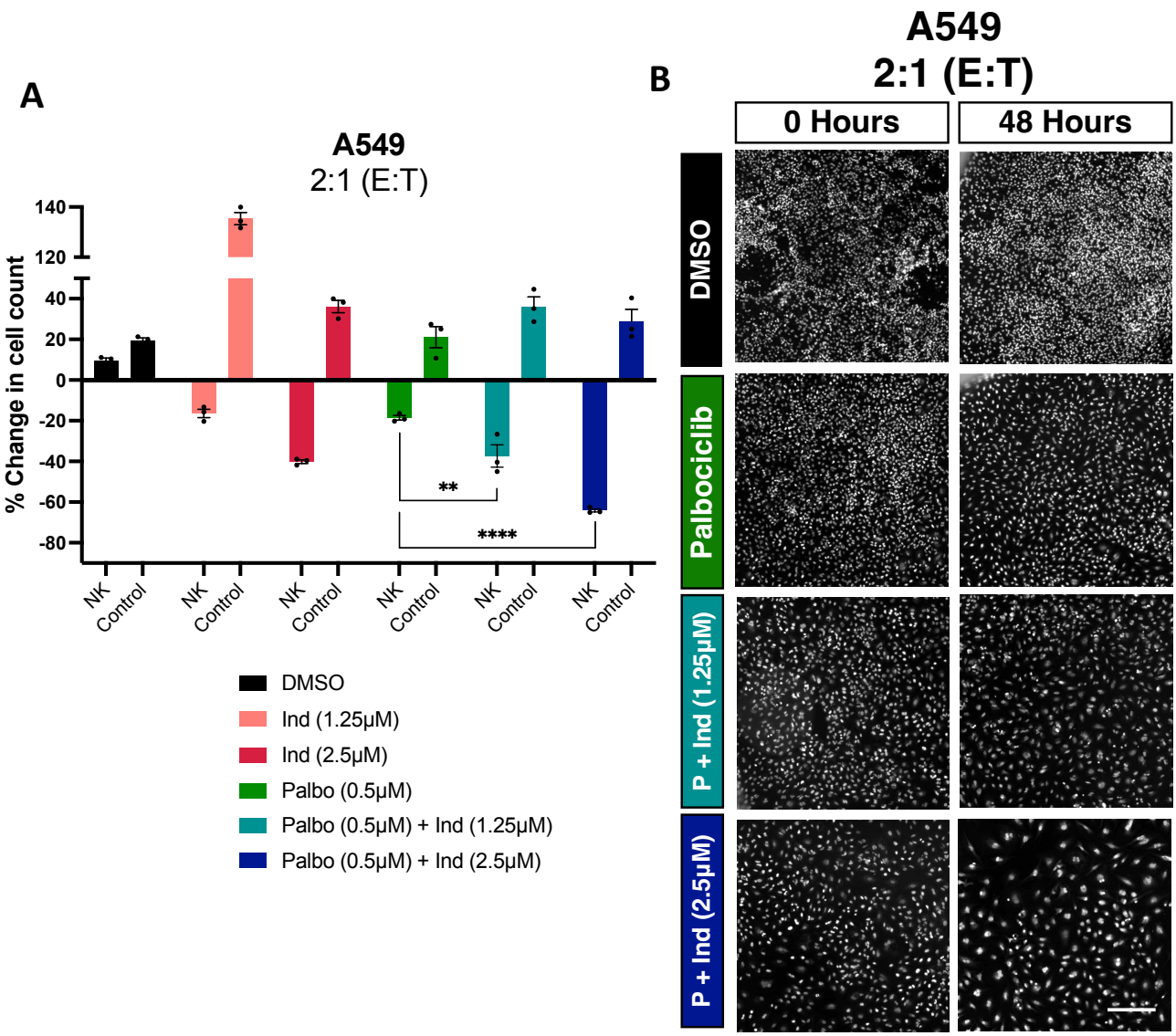


Figure 7.4 Combined palbociclib and indisulam treatment promotes NK cell-mediated killing of lung cancer cells
(A) Quantification of NK cell-mediated cytotoxicity of A549 cells after treatment with the indicated drugs, either individually or in combination. A549 cells were pre-treated with palbociclib (0.5μM) for a total of 7 days whereas indisulam (Ind) (1.25μM or 2.5μM) was added 4 days following the induction of palbociclib for a total of 3 days. Co-cultures with NK92-MI cells were performed at 7 days following the induction of palbociclib treatment at a 2:1 effector-to-target (E:T) ratio for 48 hours. % change represents the percentage change in A549 cell count before and after co-culture with NK cells. Control wells comprised pre-treated A549 cells in the absence of NK cells (*n* = 3).
(B) Representative images of A549 cells before and after co-culture with NK cells as described and quantified in **(A)**. Scale bar, 300μm.
(A) Ordinary one-way ANOVA.
n signifies independent experiments. All error bars represent mean ± SEM. *P < 0.05, **P < 0.01, ***P < 0.001, ****P < 0.0001; ns= not significant.

7.2.2 Investigating NK-mediated surveillance in ID8 ovarian cancer

Another model that may be relevant for promoting anti-tumour NK-mediated killing is ovarian cancer. Ovarian high-grade serous carcinoma (HGSC) is the dominant subtype and accounts for approximately 75% of ovarian cancer deaths (Bowtell et al., 2015). The standard first-line treatment for advanced HGSC usually comprises surgical cytoreduction followed by platinum-based chemotherapy, which can induce remission; however, such treatments frequently result in therapy resistance and patient relapse (Kandalaft et al., 2020). Furthermore, as ovarian cancers are immunoreactive tumours, the clinical outcome positively correlates with increased tumour immune infiltration (Sato et al., 2005). It is, therefore, logical that treatments attempt to potentiate the infiltration of cytotoxic lymphocytes to eradicate the tumour. In fact, in a recent study, Paffenholz and colleagues found homologous recombination (HR)-deficient HGSC to undergo senescence following cisplatin treatment and induce a SASP-dependent infiltration of CD8+ T cell and NK cells to the tumour microenvironment, thereby improving ICI treatment response (Paffenholz et al., 2022). Therefore, in future experiments, we want to investigate whether we can combine our SMARCA4 and RNA Pol I inhibitors with cisplatin to potentiate the SASP and anti-tumour NK surveillance in HGSCs.

Before we test our candidate inhibitors, we first needed to characterise the senescence response to cisplatin treatment in p53-null HR-proficient and HR-deficient (*Brca1*$^{-/-}$) ID8 ovarian cancer cells (Figure 7.5A & Figure 7.7A). Cisplatin administration (1μM) reduced the growth of HR-proficient *Trp53*$^{-/-}$ ID8 cells (Figure 7.5B-D) and produced a phenotype resembling senescence (Figure 7.5C & D). We also observed a substantial upregulation in the expression of several immunomodulatory cytokines, particularly CCL2, CCL5, and CXCL10 (Figure 7.6A) that was augmented further when cisplatin treatment was combined with either HF or indisulam (Figure 7.6B-E). Remarkably, the expression of NK cell activating ligands was also upregulated in the ovarian tumour cells following cisplatin treatment, suggesting these cells are susceptible to NK-mediated activity (Figure 7.6F). As expected, *Trp53*$^{-/-}$*;Brca1*$^{-/-}$ ID8 cells showed higher sensitivity to cisplatin treatment than their HR-proficient counterpart and induced a senescent phenotype at a lower cisplatin concentration (375nM) (Figure 7.7B-E). This low cisplatin dosage was sufficient to upregulate the SASP (Figure 7.8A) and NK activating ligand

expression (Figure 7.8F). Combining HF or indisulam treatment with cisplatin promoted the expression of multiple immunostimulatory cytokines in the *Trp53*$^{-/-}$*;Brca1*$^{-/-}$ ID8 cells (Figure 7.8B-E).

Regardless of the varying sensitivities to cisplatin treatment, both *Trp53*$^{-/-}$ and *Trp53*$^{-/-}$*;Brca1*$^{-/-}$ ID8 cells upregulated SASP and NK activating ligand expression indicating the potential to generate an NK cell response to eliminate senescent ovarian cancer. However, until future experiments using NK cell co-cultures with senescent ID8 cells are performed, we cannot state with certainty whether cisplatin-induced senescence promotes tumour immunogenicity. Interestingly, we found that cisplatin treatment produced a prominent SASP expression in both ID8 cell lines, limiting the dynamic range to enhance the SASP further with additional drugs. It is important to note that despite the enhanced SASP, cisplatin monotherapy may be inadequate for overcoming drug resistance associated with HGSCs (Damia and Broggini, 2019; Kandalaft et al., 2020). Similarly, despite successful reports of combining cisplatin with ICB treatment of HR-deficient ovarian tumours, these results may not translate to the more common HR-proficient HGSCs, whereby tumour immune infiltration may still be hindered (Matulonis et al., 2019). Therefore, combining cisplatin treatment with inhibitors of SMARCA4 or RNA Pol I may provide a solution to overcome chemoresistance and directly promote NK-mediated elimination of ovarian cancer cells.

Targeting RNA Pol I has previously been reported to alter the tumour immune microenvironment and contribute to reduced tumour burden in ovarian cancer (Cornelison et al., 2021). In this study, the administration of CX-5461 (an RNA Pol I inhibitor that we have demonstrated to enhance NK-mediated senescence surveillance) was reported to activate cGAS-STING signalling in serous ovarian carcinomas, resulting in a type I interferon response and increasing the transcription of immunostimulatory cytokines. In an similar study, Sanij et al. demonstrated that CX-5461 treatment promoted cell death across various ovarian cancer cell lines and prolonged the survival of HGSC-PDX mice (Sanij et al., 2020). Importantly, ovarian cancer cells with higher Pol I expression showed greater susceptibility to CX-5461 treatment. Based on these studies and our experimental findings, we postulate that the small-molecule inhibition of RNA Pol I following cisplatin treatment can enhance HGSC immunogenicity. Therefore, going forward, we plan to investigate the inhibition of POLR1B and

SMARCA4, as well as other screen hits to potentiate NK-mediated cytotoxicity of senescent ovarian tumour cells *in vitro,* before exploring the *in vivo* immune response using the syngeneic *Trp53*$^{-/-}$ and *Trp53*$^{-/-}$*;Brca1*$^{-/-}$ ID8 murine model (described in (Walton et al., 2016, 2017)).

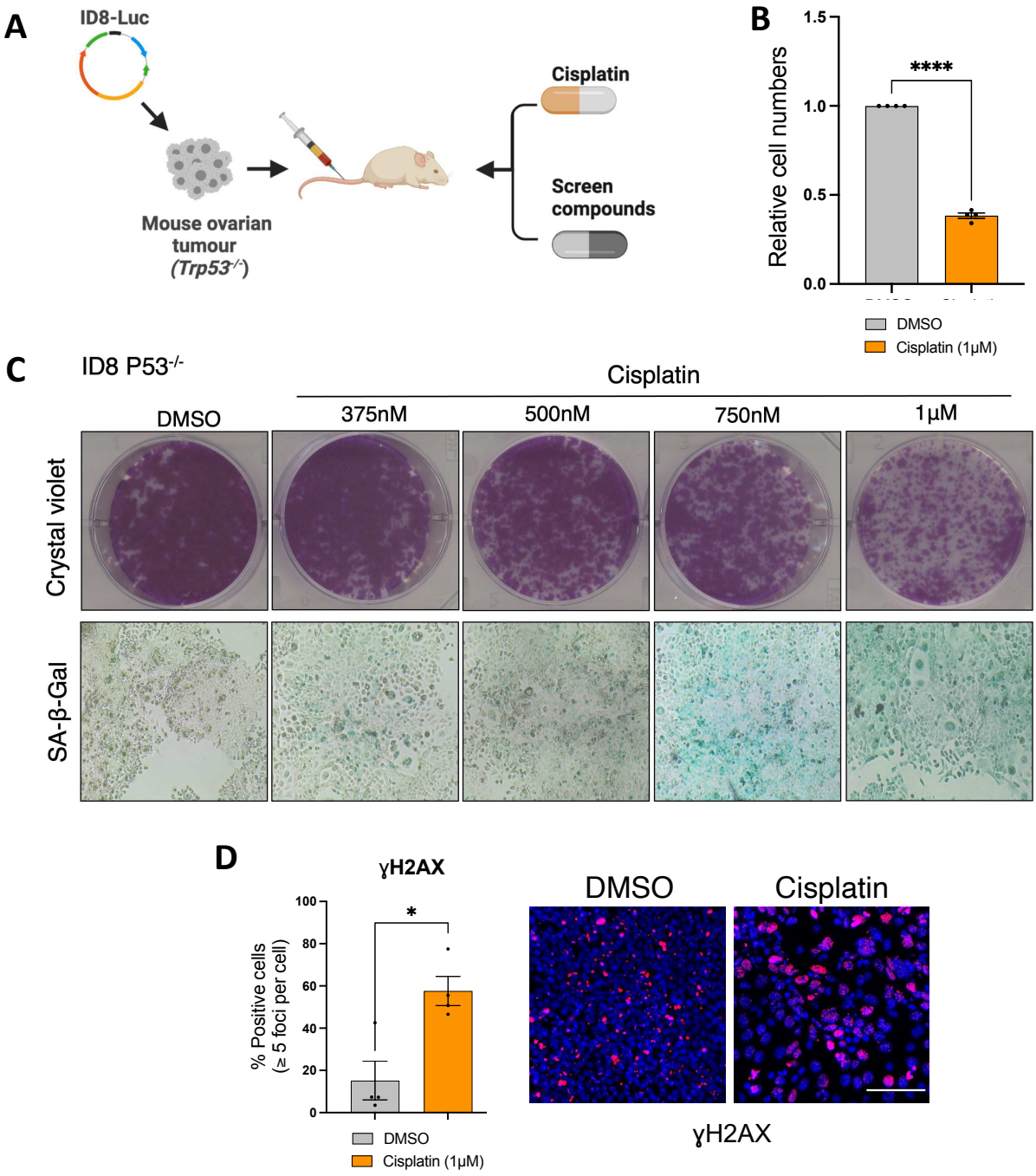


Figure 7.5 Cisplatin treatment induces senescence in p53-null ID8 mouse ovarian cancer cells

(A) Schematic of the planned *in vivo* experiments with *Trp53*$^{-/-}$ ID8 mouse ovarian cancer cell lines. Cells will be treated with cisplatin to induce senescence in combination with inhibitors of our screened candidates to evaluate the anti-tumour immune response.
(B) Quantification of the normalised cell count in *Trp53*$^{-/-}$ ID8 cells 6 days following administration of DMSO or cisplatin (1μM) (*n* = 4).
(C) Cisplatin treatment induces a senescence phenotype in *Trp53*$^{-/-}$ ID8 cells. Clonogenic assay (top panel) and SA-β-gal staining (bottom panel) of *Trp53*$^{-/-}$ ID8 cells 5 days following treatment with the indicated concentrations of cisplatin. Images for SA-β-gal taken at a 4x magnification. All images are representative of three independent experiments.
(D) Quantification of fold change and representative IF images for γH2AX accumulation in *Trp53*$^{-/-}$ ID8 cells, 6 days following treatment with DMSO or cisplatin (1μM) (*n* = 4). Scale bar, 100μm.
(B & D) Unpaired two-tailed Student's *t*-tests.
n signifies independent experiments. All error bars represent mean ± SEM. *P < 0.05, **P < 0.01, ***P < 0.001, ****P < 0.0001; ns= not significant.

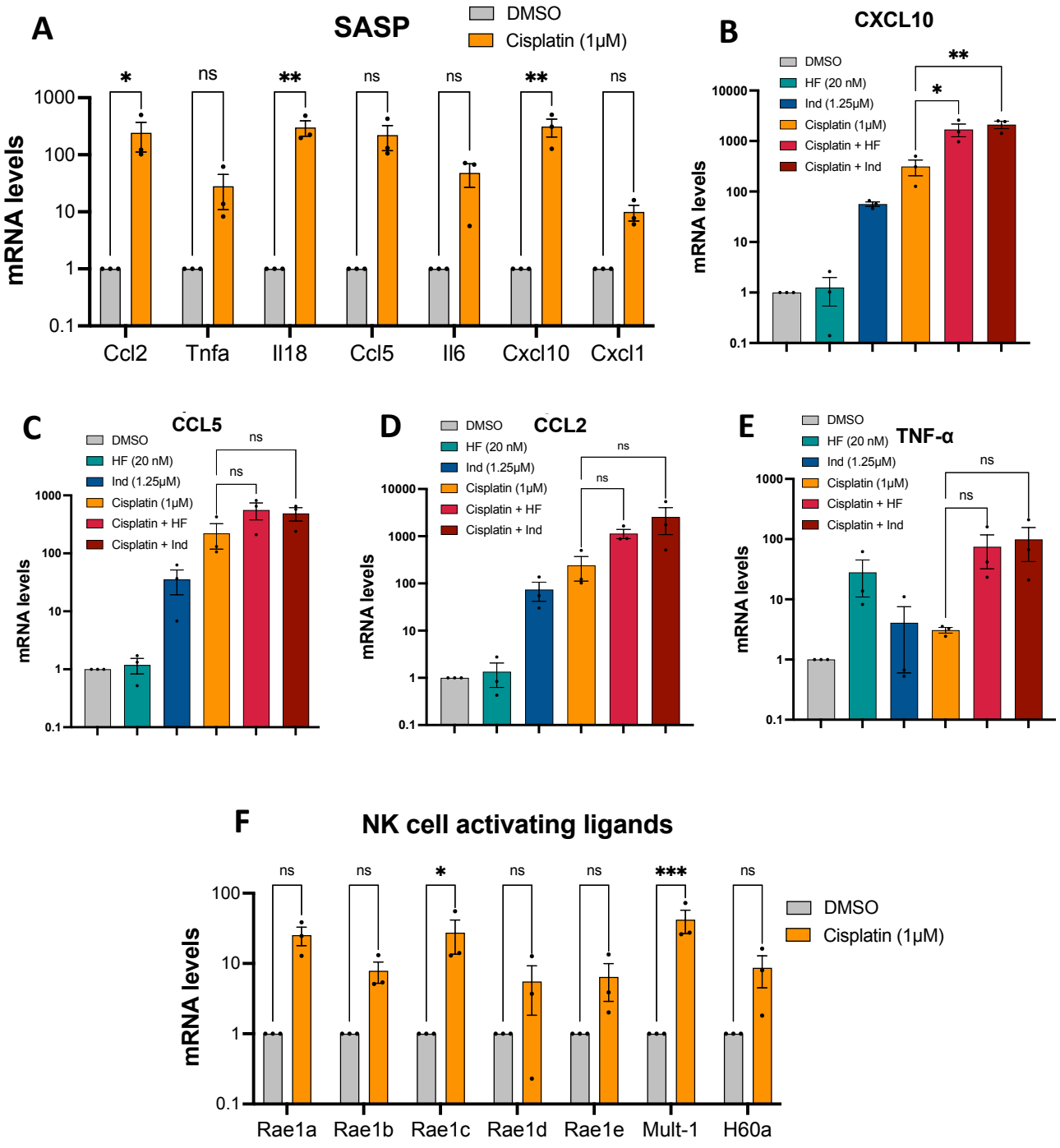


Figure 7.6 Cisplatin treatment upregulates SASP and NK activating ligands in p53-null ID8 cells
(A) qRT-PCR analysis of indicated SASP markers in *Trp53*$^{-/-}$ ID8 cells, 6 days following treatment with DMSO or cisplatin (1μM) (*n* = 3).
(B-E) qRT-PCR analysis of indicated SASP markers in *Trp53*$^{-/-}$ ID8 cells, pre-treated for 7 days with either cisplatin (1μM), halofuginone (HF) (20nM), indisulam (Ind) (1.25μM), or the specified combinations (*n* = 3).
(F) qRT-PCR analysis of indicated NK activating ligands in *Trp53*$^{-/-}$ ID8 cells, 6 days following treatment with DMSO or cisplatin (1μM) (*n* = 3).
(A & F) Two-way ANOVA. **(B-E)** Ordinary one-way ANOVA.
n signifies independent experiments. All error bars represent mean ± SEM. *P < 0.05, **P < 0.01, ***P < 0.001, ****P < 0.0001; ns= not significant.

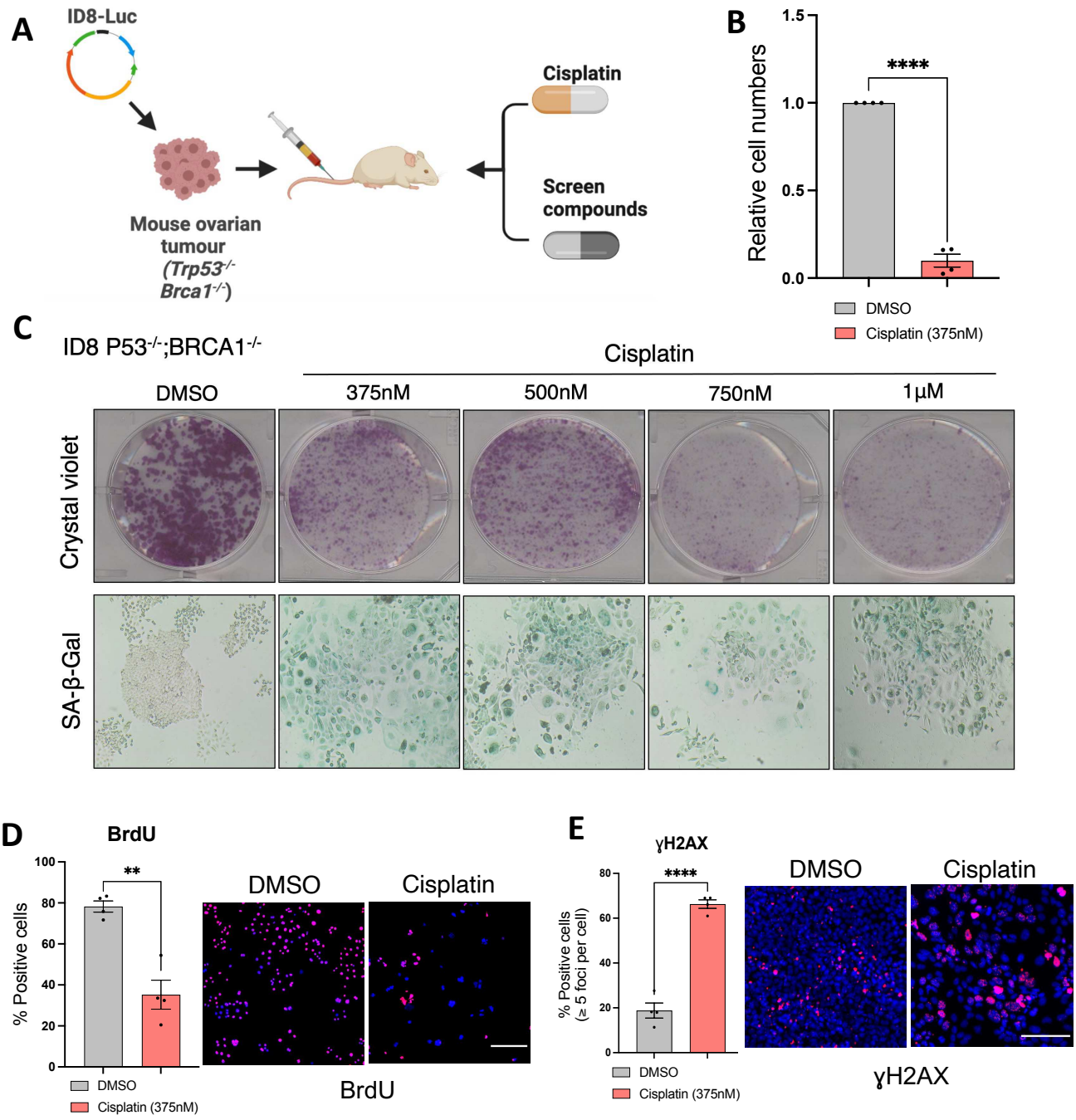


Figure 7.7 Cisplatin treatment induces senescence in p53-null HR-deficient ID8 cells

(A) Schematic of the planned *in vivo* experiments with *Trp53*$^{-/-}$;*Brca1*$^{-/-}$ ID8 mouse ovarian cancer cell lines. Cells will be treated with cisplatin to induce senescence in combination with inhibitors of our screened candidates to evaluate the anti-tumour immune response.

(B) Quantification of the normalised cell count in *Trp53*$^{-/-}$;*Brca1*$^{-/-}$ ID8 cells 6 days following administration of DMSO or cisplatin (375nM) (*n* = 4).

(C) Cisplatin treatment induces senescence in *Trp53*$^{-/-}$;*Brca1*$^{-/-}$ ID8 cells. Clonogenic assay (top panel) and SA-β-gal staining (bottom panel) of *Trp53*$^{-/-}$;*Brca1*$^{-/-}$ ID8 cells 5 days following treatment with the indicated concentrations of cisplatin. Images for SA-β-gal taken at a 4x magnification. All images are representative of three independent experiments.

(D) Quantification and representative images of IF staining for BrdU incorporation in *Trp53*$^{-/-}$;*Brca1*$^{-/-}$ ID8 cells. BrdU incorporation was measured 6 days after administration of DMSO or cisplatin (375nM) (*n* = 4). Scale bar, 100μm.

(E) Quantification of fold change and representative IF images for γH2AX accumulation in *Trp53*$^{-/-}$;*Brca1*$^{-/-}$ ID8 cells, 6 days following treatment with DMSO or cisplatin (375nM) (*n* = 4). Scale bar, 100μm.

(B, D & E) Unpaired two-tailed Student's *t*-tests.

n signifies independent experiments. All error bars represent mean ± SEM. *P < 0.05, **P < 0.01, ***P < 0.001, ****P < 0.0001; ns= not significant.

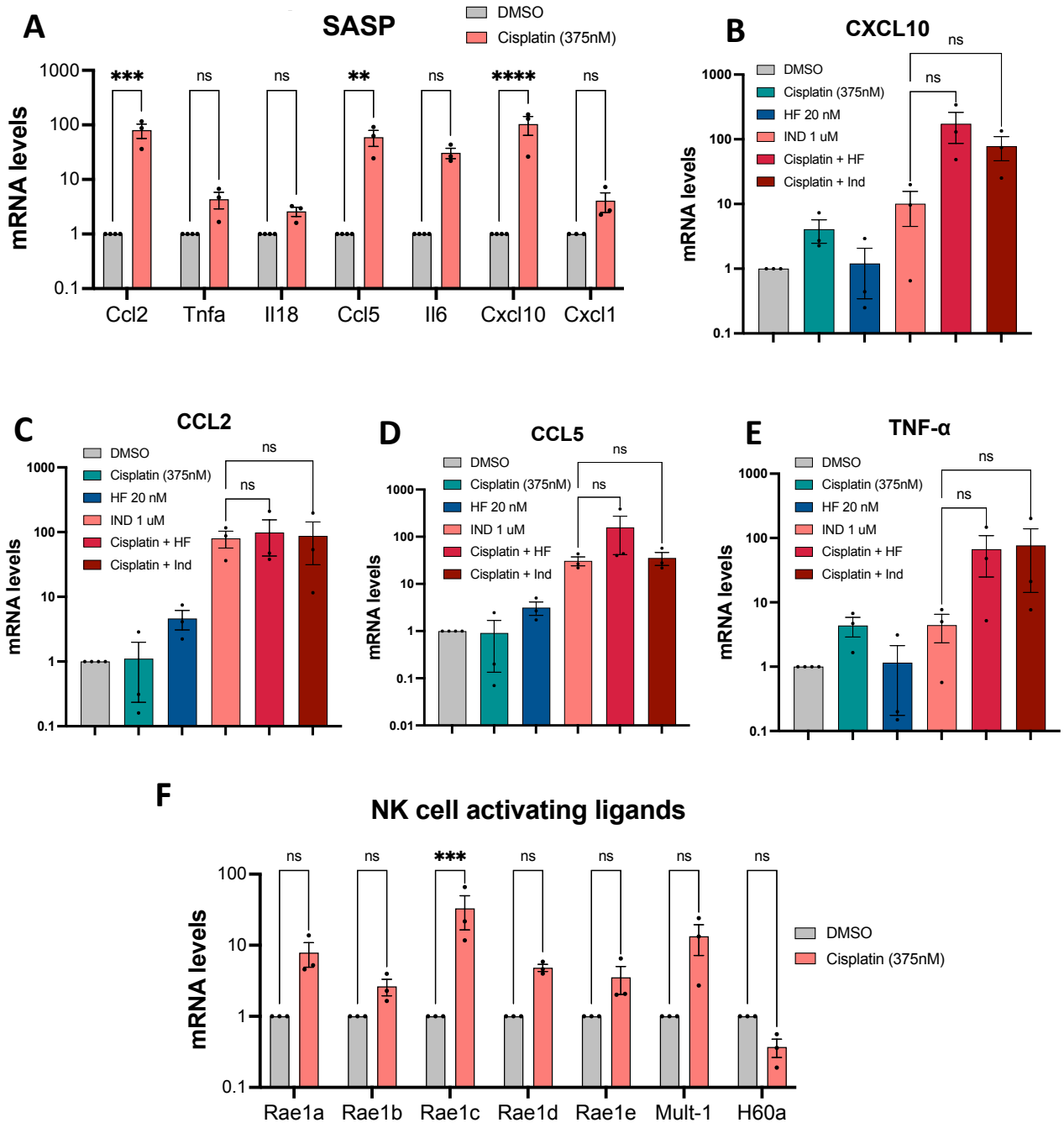


Figure 7.8 Low dosage cisplatin treatment sufficiently upregulates SASP and NK activating ligands in p53-null HR-deficient ID8 cancer cells

(A) qRT-PCR analysis of indicated SASP markers in *Trp53*$^{-/-}$;*Brca1*$^{-/-}$ ID8 cells, 6 days following treatment with DMSO or cisplatin (1μM) (*n* = 3).

(B-E) qRT-PCR analysis of indicated SASP markers in *Trp53*$^{-/-}$;*Brca1*$^{-/-}$ ID8 cells, pre-treated for 7 days with either cisplatin (1μM), halofuginone (HF) (20nM), indisulam (Ind) (1.25μM), or the specified combinations (*n* = 3).

(F) qRT-PCR analysis of indicated NK activating ligands in *Trp53*$^{-/-}$;*Brca1*$^{-/-}$ ID8 cells, 6 days following treatment with DMSO or cisplatin (1μM) (*n* = 3).

(A & F) Two-way ANOVA. **(B-E)** Ordinary one-way ANOVA.

n signifies independent experiments. All error bars represent mean ± SEM. *P < 0.05, **P < 0.01, ***P < 0.001, ****P < 0.0001; ns= not significant.

8. Concluding remarks

Our findings reveal that manipulating the SASP can modulate NK-mediated clearance of senescent cells, and we identified novel strategies that exploit this phenomenon for therapeutic purposes.

We took a two-step approach. First, we searched for perturbations that enhance SASP expression through a large-scale genetic screen. Secondly, we explored different strategies to potentiate NK-mediated senescence surveillance based on the screen hits. Engaging an immunomodulatory SASP eliminates the need for alternative cytokine therapies and facilitates the direct targeting of senescent cells. Although chronic SASP expression can generate undesired tissue inflammation, inhibiting our screen hits can enhance NK-mediated killing of senescent cells in a timely manner before the onset of any deleterious effects.

Recently, there has been a surge of studies that have shown the benefits of using NK cells in combating cancer and senescence-related diseases, from CAR-NK cell therapy to the development of immunotherapeutic bifunctional protein complexes as well as NK-dependent oncolytic viruses and cancer vaccinations (Badrinath et al., 2022; Chaturvedi et al., 2022; Leung et al., 2020; Di Vito et al., 2019a; Xie et al., 2020). From our RNAi screens, we identified 9 genes that robustly induce immunogenic vulnerabilities in senescent cells upon knockdown and may represent additional munitions in the arsenal of NK-dependent senescence therapy. In particular, we focused on two targets, SMARCA4 and POLR1B, whose repression are associated with improved anti-tumour immune response (see Chapter 6.5).

Here we provided additional evidence that the pharmacological inhibition of SMARCA4 and RNA Pol I can enhance NK-mediated cytotoxicity of cells undergoing oncogene- or therapy-induced senescence. These hits may represent ‘natural senolytic’ targets that trigger NK-dependent clearance of different senescent cells and settings. A major objective of this thesis has been to investigate these hits to promote NK-mediated killing in the context of cancer. In this setting, we aim to perform a one-two punch-like combination using pro-senescence cancer therapy followed by the drug-mediated inhibition of SMARCA4 or RNA Pol I to trigger an anti-tumour NK cell response. Besides cancer, NK cells have also

shown to clear senescent cells in other diseases, including fibrosis (Krizhanovsky et al., 2008). Indeed, accumulation of senescent cells has been shown to contribute to fibrosis and the elimination of these cells using senolytics has been shown to improve this phenotype (Ogrodnik et al., 2017; Schafer et al., 2017). Within a fibrosis setting, we aim to potentiate NK-mediated killing of senescent cells through immunotherapy using our identified candidates alone, without the need for prior pro-senescence drugs.

By identifying several hits through our screens, such as FURIN, SMARCA4, and POLR1B, among others, we have discovered a catalogue of tools that target different pathways and may be more suitable to kill different types of senescent cells. For example, SMARCA4 is often mutated in cancer, with high SMARCA4 expression linked with tumour immune evasion (Peng et al., 2021). Loss of SMARCA4 sensitises tumours to immunotherapy (Schoenfeld et al., 2021; Takada et al., 2019) suggesting that targeting this gene in SMARCA4-high senescent tumour cells may promote an anti-tumour NK cell response. Therefore, depending on the type of senescent cells being targeted (cancer or fibrosis), it may be relevant to investigate the expression of our target genes in order to select the most suitable candidate for the disease model (see Box 1 for further outstanding questions). Indeed, additional experiments are pending, both *in vitro* and in murine tumour and fibrosis models, to validate the candidates' efficacy in senescence associated diseases and to understand the mechanisms behind the effect.

In summary, we have identified 9 candidates with different cellular functions that can each be targeted to promote NK-mediated killing of senescent cells in a context-dependent manner. Specifically, we have shown that inhibiting SMARCA4 and POLR1B using genetic and pharmacological approaches can strengthen immune surveillance of senescent cells, and may represent novel senotherapeutic strategies for various senescence-related pathologies such as lung and ovarian cancer and fibrosis.

Box 1. Outstanding questions from our study

Senescence and SASP:

- Can changes to the SASP composition following SMARCA4 or RNA Pol I inhibition generate an immunosuppressive or pro-tumorigenic microenvironment?
- Does inhibiting SMARCA4 or RNA Pol I influence the senescence phenotype beyond the SASP?
- Can SMARCA4 or RNA Pol I inhibition promote paracrine senescence?

NK cell surveillance:

- How do SMARCA4 and RNA Pol I inhibitors promote NK cell recruitment and activity? What mechanisms are at play *in vitro* and *in vivo*?
- Can senescent cells subdue or escape NK surveillance following SMARCA4 or RNA Pol I inhibition?
- Can SMARCA4 or RNA Pol I inhibition promote NK-mediated clearance in models of fibrosis? And in other age-associated disease models?
- Do NK cells eliminate bystander senescent tumour cells following SMARCA4 or RNA Pol I inhibition?
- To what extent do alternative immune populations mediate the killing of senescent cells following SMARCA4 or RNA Pol I inhibition?
- Can the pharmacological inhibition of other screen candidates promote NK-mediated clearance of senescent tumour cells?

Bibliography

Abel, A.M., Yang, C., Thakar, M.S., and Malarkannan, S. (2018). Natural killer cells: Development, maturation, and clinical utilization. Front. Immunol. *9*, 1–23.

Acosta, J.C., O'Loghlen, A., Banito, A., Guijarro, M. V., Augert, A., Raguz, S., Fumagalli, M., Da Costa, M., Brown, C., Popov, N., et al. (2008). Chemokine Signaling via the CXCR2 Receptor Reinforces Senescence. Cell *133*, 1006–1018.

Acosta, J.C., Banito, A., Wuestefeld, T., Georgilis, A., Janich, P., Morton, J.P., Athineos, D., Kang, T.W., Lasitschka, F., Andrulis, M., et al. (2013). A complex secretory program orchestrated by the inflammasome controls paracrine senescence. Nat. Cell Biol. *15*, 978–990.

Adams, P.D. (2007). Remodeling of chromatin structure in senescent cells and its potential impact on tumor suppression and aging. Gene *397*, 84–93.

Aghajanian, H., Kimura, T., Rurik, J.G., Hancock, A.S., Leibowitz, M.S., Li, L., Scholler, J., Monslow, J., Lo, A., Han, W., et al. (2019). Targeting cardiac fibrosis with engineered T cells. Nature *573*, 430–433.

Aird, K.M., Iwasaki, O., Kossenkov, A. V., Tanizawa, H., Fatkhutdinov, N., Bitler, B.G., Le, L., Alicea, G., Yang, T.L., Johnson, F.B., et al. (2016). HMGB2 orchestrates the chromatin landscape of senescence-associated secretory phenotype gene loci. J. Cell Biol. *215*, 325–334.

Akbar, A.N., Henson, S.M., and Lanna, A. (2016). Senescence of T Lymphocytes: Implications for Enhancing Human Immunity. Trends Immunol. *37*, 866–876.

Algarra, I., García-Lora, A., Cabrera, T., Ruiz-Cabello, F., and Garrido, F. (2004). The selection of tumor variants with altered expression of classical and nonclassical MHC class I molecules: Implications for tumor immune escape. Cancer Immunol. Immunother. *53*, 904–910.

Althubiti, M., Lezina, L., Carrera, S., Jukes-Jones, R., Giblett, S.M., Antonov, A., Barlev, N., Saldanha, G.S., Pritchard, C.A., Cain, K., et al. (2014). Characterization of novel markers of senescence and their prognostic potential in cancer. Cell Death Dis. *5*, 1–10.

Amor, C., Feucht, J., Leibold, J., Ho, Y.J., Zhu, C., Alonso-Curbelo, D., Mansilla-Soto, J., Boyer, J.A., Li, X., Giavridis, T., et al. (2020). Senolytic CAR T cells reverse senescence-associated pathologies. Nature *583*, 127–132.

André, P., Denis, C., Soulas, C., Bourbon-Caillet, C., Lopez, J., Arnoux, T., Bléry, M., Bonnafous, C., Gauthier, L., Morel, A., et al. (2018). Anti-NKG2A mAb Is a Checkpoint Inhibitor that Promotes Anti-tumor Immunity by Unleashing Both T and NK Cells. Cell *175*, 1731-1743.e13.

Anisimov, V.N., Berstein, L.M., Popovich, I.G., Zabezhinski, M.A., Egormin, P.A., Piskunova, T.S., Semenchenko, A. V., Tyndyk, M.L., Yurova, M.N., Kovalenko, I.G., et al. (2011). If started early in life, metformin treatment increases life span and postpones tumors in female SHR mice. Aging (Albany. NY). *3*, 148–157.

Antonangeli, F., Zingoni, A., Soriani, A., and Santoni, A. (2019). Senescent cells: Living or dying is a matter of NK cells. J. Leukoc. Biol. *105*, 1275–1283.

Arora, S., Thompson, P.J., Wang, Y., Bhattacharyya, A., Apostolopoulou, H., Hatano, R., Naikawadi, R.P., Shah, A., Wolters, P.J., Koliwad, S., et al. (2021). Invariant natural killer T cells coordinate removal of senescent cells. Med *2*, 938-950.e8.

Attisano, L., Silvestri, C., Izzi, L., and Labbe, E. (2001). Foxh1.Pdf. *180*, 3–11.

Aw, D., Silva, A.B., and Palmer, D.B. (2007). Immunosenescence: Emerging challenges for an ageing population. Immunology *120*, 435–446.

Baar, M.P., Brandt, R.M.C., Putavet, D.A., Klein, J.D.D., Derks, K.W.J., Bourgeois, B.R.M., Stryeck, S., Rijksen, Y., van Willigenburg, H., Feijtel, D.A., et al. (2017). Targeted Apoptosis of Senescent Cells Restores Tissue Homeostasis in Response to Chemotoxicity and Aging. Cell *169*, 132-147.e16.

Badrinath, S., Dellacherie, M.O., Li, A., Zheng, S., Zhang, X., Sobral, M., Pyrdol, J.W., Smith, K.L., Lu, Y., Haag, S., et al. (2022). A vaccine targeting resistant tumours by dual T cell plus NK cell attack. Nature.

Baker, D.J., Wijshake, T., Tchkonia, T., Lebrasseur, N.K., Childs, B.G., Van De Sluis, B., Kirkland, J.L., and Van Deursen, J.M. (2011). Clearance of p16 Ink4a-positive senescent cells delays ageing-associated disorders. Nature *479*, 232–236.

Baker, D.J., Childs, B.G., Durik, M., Wijers, M.E., Sieben, C.J., Zhong, J., A. Saltness, R., Jeganathan, K.B., Verzosa, G.C., Pezeshki, A., et al. (2016). Naturally occurring p16 Ink4a-positive cells shorten healthy lifespan. Nature *530*, 184–189.

Barradas, M., Anderton, E., Acosta, J.C., Li, S. De, Banito, A., Rodriguez-Niedenführ, M., Maertens, G., Banck,

M., Zhou, M.M., Walsh, M.J., et al. (2009). Histone demethylase JMJD3 contributes to epigenetic control of INK4a/ARF by oncogenic RAS. Genes Dev. *23*, 1177–1182.

Bartkova, J., Rezaei, N., Liontos, M., Karakaidos, P., Kletsas, D., Issaeva, N., Vassiliou, L.V.F., Kolettas, E., Niforou, K., Zoumpourlis, V.C., et al. (2006). Oncogene-induced senescence is part of the tumorigenesis barrier imposed by DNA damage checkpoints. Nature *444*, 633–637.

Bavik, C., Coleman, I., Dean, J.P., Knudsen, B., Plymate, S., and Nelson, P.S. (2006). The gene expression program of prostate fibroblast senescence modulates neoplastic epithelial cell proliferation through paracrine mechanisms. Cancer Res. *66*, 794–802.

Beauséjour, C.M., Krtolica, A., Galimi, F., Narita, M., Lowe, S.W., Yaswen, P., and Campisi, J. (2003). Reversal of human cellular senescence: Roles of the p53 and p16 pathways. EMBO J. *22*, 4212–4222.

Becker, P.S.A., Suck, G., Nowakowska, P., Ullrich, E., Seifried, E., Bader, P., Tonn, T., and Seidl, C. (2016). Selection and expansion of natural killer cells for NK cell-based immunotherapy. Cancer Immunol. Immunother. *65*, 477–484.

Ben-Porath, I., and Weinberg, R.A. (2005). The signals and pathways activating cellular senescence. Int. J. Biochem. Cell Biol. *37*, 961–976.

Bhat, R., and Watzl, C. (2007). Serial killing of tumor cells by human natural killer cells - Enhancement by therapeutic antibodies. PLoS One *2*.

Biran, A., Perelmutter, M., Gal, H., G.A. Burton, D., Ovadya, Y., Vadai, E., Geiger, T., and Krizhanovsky, V. (2015). Senescent cells communicate via intercellular protein transfer. Genes Dev. *29*, 791–802.

Biran, A., Zada, L., Abou Karam, P., Vadai, E., Roitman, L., Ovadya, Y., Porat, Z., and Krizhanovsky, V. (2017). Quantitative identification of senescent cells in aging and disease. Aging Cell *16*, 661–671.

Birch, J., and Gil, J. (2020). Senescence and the SASP: Many therapeutic avenues. Genes Dev. *34*, 1565–1576.

Bird, T.G., M ller, M., Boulter, L., Vincent, D.F., Ridgway, R.A., Lopez-Guadamillas, E., Lu, W.Y., Jamieson, T., Govaere, O., Campbell, A.D., et al. (2018). TGFβ inhibition restores a regenerative response in acute liver injury by suppressing paracrine senescence. Sci. Transl. Med. *10*, 1–15.

Boutros, M., Brás, L.P., and Huber, W. (2006). Analysis of cell-based RNAi screens. Genome Biol. *7*.

Bowtell, D.D., Böhm, S., Ahmed, A.A., Aspuria, P.J., Bast, R.C., Beral, V., Berek, J.S., Birrer, M.J., Blagden, S., Bookman, M.A., et al. (2015). Rethinking ovarian cancer II: Reducing mortality from high-grade serous ovarian cancer. Nat. Rev. Cancer *15*, 668–679.

Bracken, A.P., Kleine-Kohlbrecher, D., Dietrich, N., Pasini, D., Gargiulo, G., Beekman, C., Theilgaard-Mönch, K., Minucci, S., Porse, B.T., Marine, J.C., et al. (2007). The Polycomb group proteins bind throughout the INK4A-ARF locus and are disassociated in senescent cells. Genes Dev. *21*, 525–530.

Braig, M., Lee, S., Loddenkemper, C., Rudolph, C., Peters, A.H.F.M., Schlegelberger, B., Stein, H., Dörken, B., Jenuwein, T., and Schmitt, C.A. (2005). Oncogene-induced senescence as an initial barrier in lymphoma development. Nature *436*, 660–665.

Braumüller, H., Wieder, T., Brenner, E., Aßmann, S., Hahn, M., Alkhaled, M., Schilbach, K., Essmann, F., Kneilling, M., Griessinger, C., et al. (2013). T-helper-1-cell cytokines drive cancer into senescence. Nature *494*, 361–365.

Braun, E., and Sauter, D. (2019). Furin-mediated protein processing in infectious diseases and cancer. Clin. Transl. Immunol. *8*, 1–19.

Brideau, C., Gunter, B., Pikounis, B., and Liaw, A. (2003). Improved statistical methods for hit selection in high-throughput screening. J. Biomol. Screen. *8*, 634–647.

Brighton, P.J., Maruyama, Y., Fishwick, K., Vrljicak, P., Tewary, S., Fujihara, R., Muter, J., Lucas, E.S., Yamada, T., Woods, L., et al. (2017). Clearance of senescent decidual cells by uterine natural killer cells in cycling human endometrium. Elife *6*, 1–23.

Bruno, P.M., Liu, Y., Park, G.Y., Murai, J., Koch, C.E., Eisen, T.J., Pritchard, J.R., Pommier, Y., Lippard, S.J., and Hemann, M.T. (2017). A subset of platinum-containing chemotherapeutic agents kills cells by inducing ribosome biogenesis stress. Nat. Med. *23*, 461–471.

Bugide, S., Gupta, R., Green, M.R., and Wajapeyee, N. (2021). EZH2 inhibits NK cell–mediated antitumor immunity by suppressing CXCL10 expression in an HDAC10-dependent manner. Proc. Natl. Acad. Sci. U. S. A. *118*.

Burd, C.E., Sorrentino, J.A., Clark, K.S., Darr, D.B., Krishnamurthy, J., Deal, A.M., Bardeesy, N., Castrillon, D.H., Beach, D.H., and Sharpless, N.E. (2013). Monitoring tumorigenesis and senescence in vivo with a p16 INK4a-luciferase model. Cell *152*, 340–351.

Burton, D.G.A., and Stolzing, A. (2018). Cellular senescence: Immunosurveillance and future immunotherapy. Ageing Res. Rev. *43*, 17–25.

Bussian, T.J., Aziz, A., Meyer, C.F., Swenson, B.L., van Deursen, J.M., and Baker, D.J. (2018). Clearance of senescent glial cells prevents tau-dependent pathology and cognitive decline. Nature *562*, 578–582.

Bussiere, D.E., Xie, L., Srinivas, H., Shu, W., Burke, A., Be, C., Zhao, J., Godbole, A., King, D., Karki, R.G., et al. (2020). Structural basis of indisulam-mediated RBM39 recruitment to DCAF15 E3 ligase complex. Nat. Chem. Biol. *16*, 15–23.

Bywater, M.J., Poortinga, G., Sanij, E., Hein, N., Peck, A., Cullinane, C., Wall, M., Cluse, L., Drygin, D., Anderes, K., et al. (2012). Inhibition of RNA Polymerase I as a Therapeutic Strategy to Promote Cancer-Specific Activation of p53. Cancer Cell *22*, 51–65.

Cahu, J., Bustany, S., and Sola, B. (2012). Senescence-associated secretory phenotype favors the emergence of cancer stem-like cells. Cell Death Dis. *3*, 1–8.

Campisi, J. (2005). Senescent cells, tumor suppression, and organismal aging: Good citizens, bad neighbors. Cell *120*, 513–522.

Camps, J., Erdos, M.R., and Ried, T. (2015). The role of lamin BI for the maintenance of nuclear structure and function. Nucleus *6*, 8–14.

Canino, C., Mori, F., Cambria, A., Diamantini, A., Germoni, S., Alessandrini, G., Borsellino, G., Galati, R.Z., Battistini, L., Blandino, R., et al. (2012). SASP mediates chemoresistance and tumor-initiating-activity of mesothelioma cells. Oncogene *31*, 3148–3163.

Casella, G., Munk, R., Kim, K.M., Piao, Y., De, S., Abdelmohsen, K., and Gorospe, M. (2019). Transcriptome signature of cellular senescence. Nucleic Acids Res. *47*, 7294–7305.

Chaib, S., Tchkonia, T., and Kirkland, J.L. (2022). Cellular senescence and senolytics: the path to the clinic. Nat. Med. *28*, 1556–1568.

Chan, C.J., Smyth, M.J., and Martinet, L. (2014). Molecular mechanisms of natural killer cell activation in response to cellular stress. Cell Death Differ. *21*, 5–14.

Chandeck, C., and Mooi, W.J. (2010). Oncogene-induced cellular senescence. Adv. Anat. Pathol. *17*, 42–48.

Chandra, T., and Narita, M. (2013). High-order chromatin structure and the epigenome in SAHFs. Nucl. (United States) *4*, 23–28.

Chang, J., Wang, Y., Shao, L., Laberge, R.M., Demaria, M., Campisi, J., Janakiraman, K., Sharpless, N.E., Ding, S., Feng, W., et al. (2016). Clearance of senescent cells by ABT263 rejuvenates aged hematopoietic stem cells in mice. Nat. Med. *22*, 78–83.

Chaturvedi, P., George, V., Shrestha, N., Wang, M., Dee, M.J., Zhu, X., Liu, B., Egan, J., D'Eramo, F., Spanoudis, C., et al. (2022). Immunotherapeutic HCW9218 augments anti-tumor activity of chemotherapy via NK cell-mediated reduction of therapy-induced senescent cells. Mol. Ther. *30*, 1171–1187.

Chen, Z., Trotman, L.C., Shaffer, D., Lin, H.K., Dotan, Z.A., Niki, M., Koutcher, J.A., Scher, H.I., Ludwig, T., Gerald, W., et al. (2005). Crucial role of p53-dependent cellular senescence in suppression of Pten-deficient tumorigenesis. Nature *436*, 725–730.

Chibaya, L., Snyder, J., and Ruscetti, M. (2022a). Senescence and the tumor-immune landscape: Implications for cancer immunotherapy. Semin. Cancer Biol.

Chibaya, L., Murphy, K.C., Lopez-Diaz, Y., DeMarco, K.D., Liu, H., Gopalan, S., Faulkner, M., Li, J., Morris, J.P., Ho, Y., et al. (2022b). EZH2 inhibition remodels the inflammatory senescence-associated secretory phenotype to potentiate pancreatic cancer immune surveillance. BioRxiv 2022.06.21.495523.

Chien, Y., Scuoppo, C., Wang, X., Fang, X., Balgley, B., Bolden, J.E., Premsrirut, P., Luo, W., Chicas, A., Lee, C.S., et al. (2011). Control of the senescence-associated secretory phenotype by NF-κB promotes senescence and enhances chemosensitivity. Genes Dev. *25*, 2125–2136.

Childs, B.G., Baker, D.J., Wijshake, T., Conover, C.A., Campisi, J., and Van Deursen, J.M. (2016). Senescent intimal foam cells are deleterious at all stages of atherosclerosis. Science (80-.). *354*, 472–477.

Childs, B.G., Gluscevic, M., Baker, D.J., Laberge, R.M., Marquess, D., Dananberg, J., and Van Deursen, J.M. (2017). Senescent cells: An emerging target for diseases of ageing. Nat. Rev. Drug Discov. *16*, 718–735.

Chinta, S.J., Woods, G., Demaria, M., Rane, A., Zou, Y., McQuade, A., Rajagopalan, S., Limbad, C., Madden, D.T., Campisi, J., et al. (2018). Cellular Senescence Is Induced by the Environmental Neurotoxin Paraquat and Contributes to Neuropathology Linked to Parkinson's Disease. Cell Rep. *22*, 930–940.

Choi, P.J., and Mitchison, T.J. (2013). Imaging burst kinetics and spatial coordination during serial killing by single natural killer cells. Proc. Natl. Acad. Sci. U. S. A. *110*, 6488–6493.

Chong, M., Yin, T., Chen, R., Xiang, H., Yuan, L., Ding, Y., Pan, C.C., Tang, Z., Alexander, P.B., Li, Q., et al. (2018). CD 36 initiates the secretory phenotype during the establishment of cellular senescence . EMBO Rep. *19*, 1–13.

Collins, C.J., and Sedivy, J.M. (2003). Involvement of the INK4a/Arf gene locus in senescence. Aging Cell *2*, 145–150.

Coppe, J.P., Kauser, K., Campisi, J., and Beauséjour, C.M. (2006). Secretion of vascular endothelial growth factor by primary human fibroblasts at senescence. J. Biol. Chem. *281*, 29568–29574.

Coppé, J.-P., Desprez, P.-Y., Krtolica, A., and Campisi, J. (2010). The Senescence-Associated Secretory Phenotype: The Dark Side of Tumor Suppression. Annu. Rev. Pathol. Mech. Dis. *5*, 99–118.

Coppé, J.P., Patil, C.K., Rodier, F., Sun, Y., Muñoz, D.P., Goldstein, J., Nelson, P.S., Desprez, P.Y., and Campisi, J. (2008). Senescence-associated secretory phenotypes reveal cell-nonautonomous functions of oncogenic RAS and the p53 tumor suppressor. PLoS Biol. *6*.

Coppola, D., Balducci, L., Chen, D.T., Loboda, A., Nebozhyn, M., Staller, A., Fulp, W.J., Dalton, W., Yeatman, T., and Brem, S. (2014). Senescence-associated-gene signature identifies genes linked to age, prognosis, and progression of human gliomas. J. Geriatr. Oncol. *5*, 389–399.

Cornelison, R., Biswas, K., Llaneza, D.C., Harris, A.R., Sosale, N.G., Lazzara, M.J., and Landen, C.N. (2021). Cx-5461 treatment leads to cytosolic dna-mediated sting activation in ovarian cancer. Cancers (Basel). *13*, 1–11.

Crouch, J., Shvedova, M., Thanapaul, R.J.R.S., Botchkarev, V., and Roh, D. (2022). Epigenetic Regulation of Cellular Senescence. Cells *11*, 1–16.

Cui, H., Kong, Y., Xu, M., and Zhang, H. (2013). Notch3 functions as a tumor suppressor by controlling cellular senescence. Cancer Res. *73*, 3451–3459.

Cuollo, L., Antonangeli, F., Santoni, A., and Soriani, A. (2020). The senescence-associated secretory phenotype (Sasp) in the challenging future of cancer therapy and age-related diseases. Biology (Basel). *9*, 1–16.

D'Adda Di Fagagna, F., Reaper, P.M., Clay-Farrace, L., Fiegler, H., Carr, P., Von Zglinicki, T., Saretzki, G., Carter, N.P., and Jackson, S.P. (2003). A DNA damage checkpoint response in telomere-initiated senescence. Nature *426*, 194–198.

Dai, C.Y., and Enders, G.H. (2000). p16(INK4a) can initiate an autonomous senescence program. Oncogene *19*, 1613–1622.

Damia, G., and Broggini, M. (2019). Platinum resistance in ovarian cancer: Role of DNA repair. Cancers (Basel). *11*, 1–15.

Debacq-Chainiaux, F., Boilan, E., Le Moutier, J.D., Weemaels, G., and Toussaint, O. (2010). P38MAPK in the senescence of human and murine fibroblasts. Adv. Exp. Med. Biol. *694*, 126–137.

Demaria, M., Ohtani, N., Youssef, S.A., Rodier, F., Toussaint, W., Mitchell, J.R., Laberge, R.M., Vijg, J., VanSteeg, H., Dollé, M.E.T., et al. (2014). An essential role for senescent cells in optimal wound healing through secretion of PDGF-AA. Dev. Cell *31*, 722–733.

Demaria, M., O'Leary, M.N., Chang, J., Shao, L., Liu, S., Alimirah, F., Koenig, K., Le, C., Mitin, N., Deal, A.M., et al. (2017). Cellular senescence promotes adverse effects of chemotherapy and cancer relapse. Cancer Discov. *7*, 165–176.

Van Deursen, J.M. (2014). The role of senescent cells in ageing. Nature *509*, 439–446.

Dhomen, N., Reis-Filho, J.S., da Rocha Dias, S., Hayward, R., Savage, K., Delmas, V., Larue, L., Pritchard, C., and Marais, R. (2009). Oncogenic Braf Induces Melanocyte Senescence and Melanoma in Mice. Cancer Cell *15*, 294–303.

Dimri, G.P., Lee, X., Basile, G., Acosta, M., Scott, G., Roskelley, C., Medrano, E.E., Linskens, M., Rubelj, I., Pereira-Smith, O., et al. (1995). A biomarker that identifies senescent human cells in culture and in aging skin in vivo. Proc. Natl. Acad. Sci. U. S. A. *92*, 9363–9367.

Dolgin, E. (2020). Send in the senolytics. Nat. Biotechnol. *38*.

Dou, Z., Ghosh, K., Vizioli, M.G., Zhu, J., Sen, P., Wangensteen, K.J., Simithy, J., Lan, Y., Lin, Y., Zhou, Z., et al. (2017). Cytoplasmic chromatin triggers inflammation in senescence and cancer. Nature *550*, 402–406.

Drygin, D., Lin, A., Bliesath, J., Ho, C.B., O'Brien, S.E., Proffitt, C., Omori, M., Haddach, M., Schwaebe, M.K., Siddiqui-Jain, A., et al. (2011). Targeting RNA polymerase I with an oral small molecule CX-5461 inhibits ribosomal RNA synthesis and solid tumor growth. Cancer Res. *71*, 1418–1430.

Efeyan, A., and Serrano, M. (2007). p53: Guardian of the genome and policeman of the oncogenes. Cell Cycle

6, 1006–1010.

Eggert, T., Wolter, K., Ji, J., Ma, C., Yevsa, T., Klotz, S., Medina-Echeverz, J., Longerich, T., Forgues, M., Reisinger, F., et al. (2016). Distinct Functions of Senescence-Associated Immune Responses in Liver Tumor Surveillance and Tumor Progression. Cancer Cell *30*, 533–547.

Emery, P., Keystone, E., Tony, H.P., Cantagrel, A., Van Vollenhoven, R., Sanchez, A., Alecock, E., Lee, J., and Kremer, J. (2008). IL-6 receptor inhibition with tocilizumab improves treatment outcomes in patients with rheumatoid arthritis refractory to anti-tumour necrosis factor biologicals: Results from a 24-week multicentre randomised placebo-controlled trial. Ann. Rheum. Dis. *67*, 1516–1523.

Emmerich, C.H., Gamboa, L.M., Hofmann, M.C.J., Bonin-Andresen, M., Arbach, O., Schendel, P., Gerlach, B., Hempel, K., Bespalov, A., Dirnagl, U., et al. (2021). Improving target assessment in biomedical research: the GOT-IT recommendations. Nat. Rev. Drug Discov. *20*, 64–81.

Engeland, K. (2022). Cell cycle regulation: p53-p21-RB signaling. Cell Death Differ. *29*, 946–960.

Ewald, J.A., Desotelle, J.A., Wilding, G., and Jarrard, D.F. (2010). Therapy-induced senescence in cancer. J. Natl. Cancer Inst. *102*, 1536–1546.

Fafián-Labora, J.A., and O'Loghlen, A. (2020). Classical and Nonclassical Intercellular Communication in Senescence and Ageing. Trends Cell Biol. *30*, 628–639.

Faget, D. V., Ren, Q., and Stewart, S.A. (2019). Unmasking senescence: context-dependent effects of SASP in cancer. Nat. Rev. Cancer *19*, 439–453.

Falci, C., Gianesin, K., Sergi, G., Giunco, S., De Ronch, I., Valpione, S., Soldà, C., Fiduccia, P., Lonardi, S., Zanchetta, M., et al. (2013). Immune senescence and cancer in elderly patients: Results from an exploratory study. Exp. Gerontol. *48*, 1436–1442.

Farr, J.N., Xu, M., Weivoda, M.M., Monroe, D.G., Fraser, D.G., Onken, J.L., Negley, B.A., Sfeir, J.G., Ogrodnik, M.B., Hachfeld, C.M., et al. (2017). Targeting cellular senescence prevents age-related bone loss in mice. Nat. Med. *23*, 1072–1079.

Ferreira, R., Schneekloth, J.S., Panov, K.I., Hannan, K.M., and Hannan, R.D. (2020). Targeting the RNA Polymerase I Transcription for Cancer Therapy Comes of Age. Cells *9*, 1–23.

Finn, R.S., Crown, J.P., Lang, I., Boer, K., Bondarenko, I.M., Kulyk, S.O., Ettl, J., Patel, R., Pinter, T., Schmidt, M., et al. (2015). The cyclin-dependent kinase 4/6 inhibitor palbociclib in combination with letrozole versus letrozole alone as first-line treatment of oestrogen receptor-positive, HER2-negative, advanced breast cancer (PALOMA-1/TRIO-18): A randomised phase 2 study. Lancet Oncol. *16*, 25–35.

Finn, R.S., Martin, M., Rugo, H.S., Jones, S., Im, S.A., Gelmon, K., Harbeck, N., Lipatov, O.N., Walshe, J.M., Moulder, S., et al. (2016). Palbociclib and letrozole in advanced breast cancer. N. Engl. J. Med. *375*, 1925–1936.

Flores, I., Benetti, R., and Blasco, M.A. (2006). Telomerase regulation and stem cell behaviour. Curr. Opin. Cell Biol. *18*, 254–260.

Franceschi, C., and Campisi, J. (2014). Chronic inflammation (Inflammaging) and its potential contribution to age-associated diseases. Journals Gerontol. - Ser. A Biol. Sci. Med. Sci. *69*, S4–S9.

Frescas, D., Roux, C.M., Aygun-Sunar, S., Gleiberman, A.S., Krasnov, P., Kurnasov, O. V., Strom, E., Virtuoso, L.P., Wrobel, M., Osterman, A.L., et al. (2017). Senescent cells expose and secrete an oxidized form of membrane-bound vimentin as revealed by a natural polyreactive antibody. Proc. Natl. Acad. Sci. U. S. A. *114*, E1668–E1677.

Freund, A., Orjalo, A. V., Desprez, P.Y., and Campisi, J. (2010). Inflammatory networks during cellular senescence: causes and consequences. Trends Mol. Med. *16*, 238–246.

Freund, A., Patil, C.K., and Campisi, J. (2011). P38MAPK is a novel DNA damage response-independent regulator of the senescence-associated secretory phenotype. EMBO J. *30*, 1536–1548.

Freund, A., Laberge, R.M., Demaria, M., and Campisi, J. (2012). Lamin B1 loss is a senescence-associated biomarker. Mol. Biol. Cell *23*, 2066–2075.

Fuhrmann-Stroissnigg, H., Ling, Y.Y., Zhao, J., McGowan, S.J., Zhu, Y., Brooks, R.W., Grassi, D., Gregg, S.Q., Stripay, J.L., Dorronsoro, A., et al. (2017). Identification of HSP90 inhibitors as a novel class of senolytics. Nat. Commun. *8*.

Fumagalli, M., Rossiello, F., Clerici, M., Barozzi, S., Cittaro, D., Kaplunov, J.M., Bucci, G., Dobreva, M., Matti, V., Beausejour, C.M., et al. (2012). Telomeric DNA damage is irreparable and causes persistent DNA-damage-response activation. Nat. Cell Biol. *14*, 355–365.

Fyhrquist, F., Saijonmaa, O., and Strandberg, T. (2013). The roles of senescence and telomere shortening in cardiovascular disease. Nat. Rev. Cardiol. *10*, 274–283.

Georgakilas, A.G., Martin, O.A., and Bonner, W.M. (2017). p21: A Two-Faced Genome Guardian. Trends Mol. Med. *23*, 310–319.

Georgilis, A., Klotz, S., Hanley, C.J., Herranz, N., Weirich, B., Morancho, B., Leote, A.C., D'Artista, L., Gallage, S., Seehawer, M., et al. (2018). PTBP1-Mediated Alternative Splicing Regulates the Inflammatory Secretome and the Pro-tumorigenic Effects of Senescent Cells. Cancer Cell *34*, 85-102.e9.

Gewirtz, D.A., Holt, S.E., and Elmore, L.W. (2008). Accelerated senescence: An emerging role in tumor cell response to chemotherapy and radiation. Biochem. Pharmacol. *76*, 947–957.

Giglia-Mari, G., Zotter, A., and Vermeulen, W. (2011). DNA damage response. Cold Spring Harb. Perspect. Biol. *3*, 1–19.

Gil, J., and Peters, G. (2006). Regulation of the INK4b-ARF-INK4a tumour suppressor locus: All for one or one for all. Nat. Rev. Mol. Cell Biol. *7*, 667–677.

Goel, S., Decristo, M.J., Watt, A.C., Brinjones, H., Sceneay, J., Li, B.B., Khan, N., Ubellacker, J.M., Xie, S., Metzger-Filho, O., et al. (2017). CDK4/6 inhibition triggers anti-tumour immunity. Nature *548*, 471–475.

Gonzalez, H., Hagerling, C., and Werb, Z. (2018). Roles of the immune system in cancer: From tumor initiation to metastatic progression. Genes Dev. *32*, 1267–1284.

Goodfellow, S.., and Zomerdijk, J.. (2013). Basic Mechanisms in RNA Polymerase I Transcription of the Ribosomal RNA Genes. Epigenetics Dev. Dis. *61*, 211–236.

Gorgoulis, V., Adams, P.D., Alimonti, A., Bennett, D.C., Bischof, O., Bishop, C., Campisi, J., Collado, M., Evangelou, K., Ferbeyre, G., et al. (2019). Cellular Senescence: Defining a Path Forward. Cell *179*, 813–827.

Gravett, A.M., Dalgleish, A.G., and Copier, J. (2019). In vitro culture with gemcitabine augments death receptor and NKG2D ligand expression on tumour cells. Sci. Rep. *9*, 1–9.

Grosse, L., Wagner, N., Emelyanov, A., Molina, C., Lacas-Gervais, S., Wagner, K.D., and Bulavin, D. V. (2020). Defined p16High Senescent Cell Types Are Indispensable for Mouse Healthspan. Cell Metab. *32*, 87-99.e6.

Guerrero, A., Herranz, N., Sun, B., Wagner, V., Gallage, S., Guiho, R., Wolter, K., Pombo, J., Irvine, E.E., Innes, A.J., et al. (2019). Cardiac glycosides are broad-spectrum senolytics. Nat. Metab. *1*, 1074–1088.

Guillon, J., Petit, C., Toutain, B., Guette, C., Lelièvre, E., and Coqueret, O. (2019). Chemotherapy-induced senescence, an adaptive mechanism driving resistance and tumor heterogeneity. Cell Cycle *18*, 2385–2397.

Hanahan, D., and Weinberg, R.A. (2011). Hallmarks of cancer: The next generation. Cell *144*, 646–674.

Harley, C.B., Futcher, A.B., and Greider, C.W. (1990). Telomeres shorten during ageing of human fibroblasts. Nature *345*, 458–460.

Hayakawa, T., Iwai, M., Aoki, S., Takimoto, K., Maruyama, M., Maruyama, W., and Motoyama, N. (2015). SIRT1 suppresses the senescence-associated secretory phenotype through epigenetic gene regulation. PLoS One *10*, 1–16.

Hayflick, L. (1965). The limited in vitro lifetime of human diploid cell strains. Exp. Cell Res. *37*, 614–636.

Hayflick, L., and Moorhead, P.S. (1961). The serial cultivation of human diploid cell strains. Exp. Cell Res. *25*, 585–621.

He, S., and Sharpless, N.E. (2017). Senescence in Health and Disease. Cell *169*, 1000–1011.

Heinrich, P.C., Behrmann, I., Haan, S., Hermanns, H.M., Müller-Newen, G., and Schaper, F. (2003). Principles of interleukin (IL)-6-type cytokine signalling and its regulation. Biochem. J. *374*, 1–20.

Helman, A., Klochendler, A., Azazmeh, N., Gabai, Y., Horwitz, E., Anzi, S., Swisa, A., Condiotti, R., Granit, R.Z., Nevo, Y., et al. (2016). p16 Ink4a-induced senescence of pancreatic beta cells enhances insulin secretion. Nat. Med. *22*, 412–420.

Herbig, U., Ferreira, M., Condel, L., Carey, D., and Sedivy, J.M. (2006). Cellular senescence in aging primates. Science (80-.). *311*, 1257.

Herman, J.G., Lapidus, R.G., Issa, J.P.J., Davidson, N.E., Sidransky, D., Baylin, S.B., Merlo, A., and Mao, L. (1995). Inactivation of the CDKN2/pl6/MTS1 Gene Is Frequently Associated with Aberrant DNA Methylation in All Common Human Cancers. Cancer Res. *55*, 4525–4530.

Hernandez-Segura, A., Nehme, J., and Demaria, M. (2018). Hallmarks of Cellular Senescence. Trends Cell Biol. *28*, 436–453.

Herranz, N., Gallage, S., Mellone, M., Wuestefeld, T., Klotz, S., Hanley, C.J., Raguz, S., Acosta, J.C., Innes, A.J., Banito, A., et al. (2015). mTOR regulates MAPKAPK2 translation to control the senescence-associated secretory phenotype. Nat. Cell Biol. *17*, 1205–1217.

Herranz, N., Gil, J., Herranz, N., and Gil, J. (2018). Mechanisms and functions of cellular senescence Find the

latest version : Mechanisms and functions of cellular senescence. JCI J. Clin. Investig. *128*, 1238–1246.

Hills, S.A., and Diffley, J.F.X. (2014). DNA replication and oncogene-induced replicative stress. Curr. Biol. *24*, R435–R444.

Hoare, M., Ito, Y., Kang, T.W., Weekes, M.P., Matheson, N.J., Patten, D.A., Shetty, S., Parry, A.J., Menon, S., Salama, R., et al. (2016). NOTCH1 mediates a switch between two distinct secretomes during senescence. Nat. Cell Biol. *18*, 979–992.

Hoffman, H.M., Throne, M.L., Amar, N.J., Sebai, M., Kivitz, A.J., Kavanaugh, A., Weinstein, S.P., Belomestnov, P., Yancopoulos, G.D., Stahl, N., et al. (2008). Efficacy and safety of rilonacept (Interleukin-1 Trap) in patients with cryopyrin-associated periodic syndromes: Results from two sequential placebo-controlled studies. Arthritis Rheum. *58*, 2443–2452.

Hu, B., Lin, J.Z., Yang, X.B., and Sang, X.T. (2020). The roles of mutated SWI/SNF complexes in the initiation and development of hepatocellular carcinoma and its regulatory effect on the immune system: A review. Cell Prolif. *53*, 1–15.

Iannello, A., Thompson, T.W., Ardolino, M., Lowe, S.W., and Raulet, D.H. (2013). p53-dependent chemokine production by senescent tumor cells supports NKG2D-dependent tumor elimination by natural killer cells. J. Exp. Med. *210*, 2057–2069.

Iltis, C., Seguin, L., Cervera, L., Duret, L., Hamidouche, T., Kunz, S., Croce, O., Delannoy, C., Gueŕardel, Y., Allain, F., et al. (2021). A ganglioside-based senescence-associated immune checkpoint. BioRxiv 2021.04.23.440408.

Innes, A.J., and Gil, J. (2019). IMR90 ER:RAS: A cell model of oncogene-induced senescence. Methods Mol. Biol. *1896*, 83–92.

Irvine, K.M., Skoien, R., Bokil, N.J., Melino, M., Thomas, G.P., Loo, D., Gabrielli, B., Hill, M.M., Sweet, M.J., Clouston, A.D., et al. (2014). Senescent human hepatocytes express a unique secretory phenotype and promote macrophage migration. World J. Gastroenterol. *20*, 17851–17862.

Jaaks, P., and Bernasconi, M. (2017). The proprotein convertase furin in tumour progression. Int. J. Cancer *141*, 654–663.

Jackson, A.L., and Linsley, P.S. (2010). Recognizing and avoiding siRNA off-target effects for target identification and therapeutic application. Nat. Rev. Drug Discov. *9*, 57–67.

Jacobs, J.J.L., and de Lange, T. (2004). Significant Role for p16INK4a in p53-Independent Telomere-Directed Senescence. Curr. Biol. *14*, 2302–2308.

Janzen, V., Forkert, R., Fleming, H.E., Saito, Y., Waring, M.T., Dombkowski, D.M., Cheng, T., DePinho, R.A., Sharpless, N.E., and Scadden, D.T. (2006). Stem-cell ageing modified by the cyclin-dependent kinase inhibitor p16 INK4a. Nature *443*, 421–426.

Jeon, O.H., Kim, C., Laberge, R.M., Demaria, M., Rathod, S., Vasserot, A.P., Chung, J.W., Kim, D.H., Poon, Y., David, N., et al. (2017). Local clearance of senescent cells attenuates the development of post-traumatic osteoarthritis and creates a pro-regenerative environment. Nat. Med. *23*, 775–781.

Jerby-Arnon, L., Shah, P., Cuoco, M.S., Rodman, C., Su, M.J., Melms, J.C., Leeson, R., Kanodia, A., Mei, S., Lin, J.R., et al. (2018). A Cancer Cell Program Promotes T Cell Exclusion and Resistance to Checkpoint Blockade. Cell *175*, 984-997.e24.

Jin, W.N., Shi, K., He, W., Sun, J.H., Van Kaer, L., Shi, F.D., and Liu, Q. (2021). Neuroblast senescence in the aged brain augments natural killer cell cytotoxicity leading to impaired neurogenesis and cognition. Nat. Neurosci. *24*, 61–73.

Jun, J. Il, and Lau, L.F. (2010). Cellular senescence controls fibrosis in wound healing. Aging (Albany. NY). *2*, 627–631.

Jurk, D., Wilson, C., Passos, J.F., Oakley, F., Correia-Melo, C., Greaves, L., Saretzki, G., Fox, C., Lawless, C., Anderson, R., et al. (2014). Chronic inflammation induces telomere dysfunction and accelerates ageing in mice. Nat. Commun. *2*.

Kaefer, A., Yang, J., Noertersheuser, P., Mensing, S., Humerickhouse, R., Awni, W., and Xiong, H. (2014). Mechanism-based pharmacokinetic/pharmacodynamic meta-analysis of navitoclax (ABT-263) induced thrombocytopenia. Cancer Chemother. Pharmacol. *74*, 593–602.

Kale, A., Sharma, A., Stolzing, A., Stolzing, A., Desprez, P.Y., Desprez, P.Y., Campisi, J., and Campisi, J. (2020). Role of immune cells in the removal of deleterious senescent cells. Immun. Ageing *17*, 1–9.

Kampmann, M. (2017). Elucidating drug targets and mechanisms of action by genetic screens in mammalian cells. Chem. Commun. *53*, 7162–7167.

Kandalaft, L.E., Odunsi, K., and Coukos, G. (2020). Immune Therapy Opportunities in Ovarian Cancer. Am.

Soc. Clin. Oncol. Educ. B. *3*, e228–e240.

Kang, T.W., Yevsa, T., Woller, N., Hoenicke, L., Wuestefeld, T., Dauch, D., Hohmeyer, A., Gereke, M., Rudalska, R., Potapova, A., et al. (2011). Senescence surveillance of pre-malignant hepatocytes limits liver cancer development. Nature *479*, 547–551.

Kansara, M., Leong, H.S., Lin, D.M., Popkiss, S., Pang, P., Garsed, D.W., Walkley, C.R., Cullinane, C., Ellul, J., Haynes, N.M., et al. (2013). Immune response to rb1-Regulated senescence limits radiation-Induced osteosarcoma formation. J. Clin. Invest. *123*, 5351–5360.

Katlinskaya, Y. V., Carbone, C.J., Yu, Q., and Fuchs, S.Y. (2015). Type 1 interferons contribute to the clearance of senescent cell. Cancer Biol. Ther. *16*, 1214–1219.

Kaur, A., Webster, M.R., Marchbank, K., Behera, R., Ndoye, A., Kugel, C.H., Dang, V.M., Appleton, J., O'Connell, M.P., Cheng, P., et al. (2016). SFRP2 in the aged microenvironment drives melanoma metastasis and therapy resistance. Nature *532*, 250–254.

Kessenbrock, K., Plaks, V., and Werb, Z. (2010). Matrix Metalloproteinases: Regulators of the Tumor Microenvironment. Cell *141*, 52–67.

Kim, W.Y., and Sharpless, N.E. (2006). The Regulation of INK4/ARF in Cancer and Aging. Cell *127*, 265–275.

Kim, K., Admasu, T.D., Stolzing, A., and Sharma, A. (2022). co-culture and enrichment of h-NKs. *14*, 2131–2147.

Kim, K.M., Noh, J.H., Bodogai, M., Martindale, J.L., Yang, X., Indig, F.E., Basu, S.K., Ohnuma, K., Morimoto, C., Johnson, P.F., et al. (2017). Identification of senescent cell surface targetable protein DPP4. Genes Dev. *31*, 1529–1534.

Kim, K.M., Noh, J.H., Bodogai, M., Martindale, J.L., Pandey, P.R., Yang, X., Biragyn, A., Abdelmohsen, K., and Gorospe, M. (2018). SCAMP4 enhances the senescent cell secretome. Genes Dev. *32*, 909–914.

Kirkland, J.L., and Tchkonia, T. (2017). Cellular Senescence: A Translational Perspective. EBioMedicine *21*, 21–28.

Klareskog, L., Van Der Heijde, D., De Jager, J.P., Gough, A., Kalden, J., Malaise, M., Martín Mola, E., Pavelka, K., Sany, J., Settas, L., et al. (2004). Therapeutic effect of the combination of etanercept and methotrexate compared with each treatment alone in patients with rheumatoid arthritis: Double-blind randomised controlled trial. Lancet *363*, 675–681.

Kojima, H., Inoue, T., Kunimoto, H., and Nakajima, K. (2013). IL-6-STAT3 signaling and premature senescence. Jak-Stat *2*, e25763.

Kong, X., Feng, D., Wang, H., Hong, F., Bertola, A., Wang, F.S., and Gao, B. (2012). Interleukin-22 induces hepatic stellate cell senescence and restricts liver fibrosis in mice. Hepatology *56*, 1150–1159.

Kortlever, R.M., Higgins, P.J., and Bernards, R. (2006). Plasminogen activator inhibitor-1 is a critical downstream target of p53 in the induction of replicative senescence. Nat. Cell Biol. *8*, 878–884.

Kotake, Y., Naemura, M., Murasaki, C., Inoue, Y., and Okamoto, H. (2015). Transcriptional regulation of the p16 tumor suppressor gene. Anticancer Res. *35*, 4397–4402.

Krishnamurthy, J., Torrice, C., Ramsey, M.R., Kovalev, G.I., Al-Regaiey, K., Su, L., and Sharpless, N.E. (2004). Ink4a/Arf expression is a biomarker of aging. J. Clin. Invest. *114*, 1299–1307.

Krizhanovsky, V., Yon, M., Dickins, R.A., Hearn, S., Simon, J., Miething, C., Yee, H., Zender, L., and Lowe, S.W. (2008). Senescence of Activated Stellate Cells Limits Liver Fibrosis. Cell *134*, 657–667.

Krtolica, A., Parrinello, S., Lockett, S., Desprez, P.Y., and Campisi, J. (2001). Senescent fibroblasts promote epithelial cell growth and tumorigenesis: A link between cancer and aging. Proc. Natl. Acad. Sci. U. S. A. *98*, 12072–12077.

de Kruijf, E.M., Sajet, A., van Nes, J.G.H., Natanov, R., Putter, H., Smit, V.T.H.B.M., Liefers, G.J., van den Elsen, P.J., van de Velde, C.J.H., and Kuppen, P.J.K. (2010). HLA-E and HLA-G Expression in Classical HLA Class I-Negative Tumors Is of Prognostic Value for Clinical Outcome of Early Breast Cancer Patients. J. Immunol. *185*, 7452–7459.

Kuilman, T., and Peeper, D.S. (2009). Senescence-messaging secretome: SMS-ing cellular stress. Nat. Rev. Cancer *9*, 81–94.

Kuilman, T., Michaloglou, C., Vredeveld, L.C.W., Douma, S., van Doorn, R., Desmet, C.J., Aarden, L.A., Mooi, W.J., and Peeper, D.S. (2008). Oncogene-Induced Senescence Relayed by an Interleukin-Dependent Inflammatory Network. Cell *133*, 1019–1031.

Kuilman, T., Michaloglou, C., Mooi, W.J., and Peeper, D.S. (2010). The essence of senescence. Genes Dev. *24*, 2463–2479.

Kumar, S. (2018). Natural killer cell cytotoxicity and its regulation by inhibitory receptors. Immunology *154*, 383–393.

Kumari, R., and Jat, P. (2021). Mechanisms of Cellular Senescence: Cell Cycle Arrest and Senescence Associated Secretory Phenotype. Front. Cell Dev. Biol. *9*, 1–24.

Kurz, D.J., Decary, S., Hong, Y., and Erusalimsky, J.D. (2000). Senescence-associated β-galactosidase reflects an increase in lysosomal mass during replicative ageing of human endothelial cells. J. Cell Sci. *113*, 3613–3622.

Kwon, H.J., Kim, N., and Kim, H.S. (2017a). Molecular checkpoints controlling natural killer cell activation and their modulation for cancer immunotherapy. Exp. Mol. Med. *49*, 1–11.

Kwon, Y., Kim, J.W., Jeoung, J.A., Kim, M.S., and Kang, C. (2017b). Autophagy is pro-senescence when seen in close-up, but anti-senescence in long-shot. Mol. Cells *40*, 607–612.

Laberge, R.M., Awad, P., Campisi, J., and Desprez, P.Y. (2012). Epithelial-mesenchymal transition induced by senescent fibroblasts. Cancer Microenviron. *5*, 39–44.

Laberge, R.M., Sun, Y., Orjalo, A. V., Patil, C.K., Freund, A., Zhou, L., Curran, S.C., Davalos, A.R., Wilson-Edell, K.A., Liu, S., et al. (2015). MTOR regulates the pro-tumorigenic senescence-associated secretory phenotype by promoting IL1A translation. Nat. Cell Biol. *17*, 1049–1061.

Lakin, N.D., and Jackson, S.P. (1999). Regulation of p53 in response to DNA damage. Oncogene *18*, 7644–7655.

Lamarche, B.J., Orazio, N.I., and Weitzman, M.D. (2010). The MRN complex in double-strand break repair and telomere maintenance. FEBS Lett. *584*, 3682–3695.

Lane, D.P. (1992). p53, guardian of the genome. Nature *358*, 15–16.

De Lange, T. (2005). Shelterin: The protein complex that shapes and safeguards human telomeres. Genes Dev. *19*, 2100–2110.

Lanier, L.L. (2005). NK cell recognition. Annu. Rev. Immunol. *23*, 225–274.

Lanna, A., Henson, S.M., Escors, D., and Akbar, A.N. (2014). The kinase p38 activated by the metabolic regulator AMPK and scaffold TAB1 drives the senescence of human T cells. Nat. Immunol. *15*, 965–972.

Latchman, Y., Wood, C.R., Chernova, T., Chaudhary, D., Borde, M., Chernova, I., Iwai, Y., Long, A.J., Brown, J.A., Nunes, R., et al. (2001). PD-L2 is a second ligand for PD-1 and inhibits T cell activation. Nat. Immunol. *2*, 261–268.

Le, O.N.L., Rodier, F., Fontaine, F., Coppe, J.P., Campisi, J., DeGregori, J., Laverdière, C., Kokta, V., Haddad, E., and Beauséjour, C.M. (2010). Ionizing radiation-induced long-term expression of senescence markers in mice is independent of p53 and immune status. Aging Cell *9*, 398–409.

Lee, S., and Schmitt, C. (2019). The dynamic nature of senescence in cancer. Nat. Cell Biol. *21*.

Leung, E.Y.L., Ennis, D.P., Kennedy, P.R., Hansell, C., Dowson, S., Farquharson, M., Spiliopoulou, P., Nautiyal, J., McNamara, S., Carlin, L.M., et al. (2020). NK Cells Augment Oncolytic Adenovirus Cytotoxicity in Ovarian Cancer. Mol. Ther. - Oncolytics *16*, 289–301.

Li, C., Wang, Y., Gong, Y., Zhang, T., Huang, J., Tan, Z., and Xue, L. (2021a). Finding an easy way to harmonize: a review of advances in clinical research and combination strategies of EZH2 inhibitors. Clin. Epigenetics *13*, 1–12.

Li, S., Balmain, A., and Counter, C.M. (2018). A model for RAS mutation patterns in cancers: finding the sweet spot. Nat. Rev. Cancer *18*, 767–777.

Li, Y., Nichols, M.A., Shay, J.W., and Yue Xiong (1994). Transcriptional Repression of the D-Type Cyclin-dependent Kinase Inhibitor pl6 by the Retinoblastoma Susceptibility Gene Product pRb. Cancer Res. *54*, 6078–6082.

Li, Y., Chen, S., Li, X., Wang, X., Li, H., Ning, S., and Chen, H. (2021b). CD247, a Potential T Cell–Derived Disease Severity and Prognostic Biomarker in Patients With Idiopathic Pulmonary Fibrosis. Front. Immunol. *12*, 1–15.

Liu, E., Marin, D., Banerjee, P., Macapinlac, H.A., Thompson, P., Basar, R., Nassif Kerbauy, L., Overman, B., Thall, P., Kaplan, M., et al. (2020). Use of CAR-Transduced Natural Killer Cells in CD19-Positive Lymphoid Tumors. N. Engl. J. Med. *382*, 545–553.

Liu, Y., Hawkins, O.E., Su, Y., Vilgelm, A.E., Sobolik, T., Thu, Y.M., Kantrow, S., Splittgerber, R.C., Short, S., Amiri, K.I., et al. (2013). Targeting aurora kinases limits tumour growth through DNA damage-mediated senescence and blockade of NF-κB impairs this drug-induced senescence. EMBO Mol. Med. *5*, 149–166.

Long, E.O., Sik Kim, H., Liu, D., Peterson, M.E., and Rajagopalan, S. (2013). Controlling natural killer cell

responses: Integration of signals for activation and inhibition. Annu. Rev. Immunol. *31*, 227–258.

Lopes-Paciencia, S., Saint-Germain, E., Rowell, M.C., Ruiz, A.F., Kalegari, P., and Ferbeyre, G. (2019). The senescence-associated secretory phenotype and its regulation. Cytokine *117*, 15–22.

López-Botet, M., Llano, M., Navarro, F., and Bellon, T. (2000). NK cell recognition of non-classical HLA class I molecules. Semin. Immunol. *12*, 109–119.

Lopez-Castejon, G., and Brough, D. (2011). Understanding the mechanism of IL-1β secretion. Cytokine Growth Factor Rev. *22*, 189–195.

Lujambio, A. (2016). To clear, or not to clear (senescent cells)? That is the question. Insid. Cell *1*, 87–95.

Lujambio, A., and Villanueva, A. (2015). The usual SASPects of liver cancer. Aging (Albany. NY). *7*, 348–349.

Lujambio, A., Akkari, L., Simon, J., Grace, D., Tschaharganeh, D.F., Bolden, J.E., Zhao, Z., Thapar, V., Joyce, J.A., Krizhanovsky, V., et al. (2013). Non-cell-autonomous tumor suppression by p53. Cell *153*, 449–460.

Maciejowski, J., and De Lange, T. (2017). Telomeres in cancer: Tumour suppression and genome instability. Nat. Rev. Mol. Cell Biol. *18*, 175–186.

Maiuri, M.C., Galluzzi, L., Morselli, E., Kepp, O., Malik, S.A., and Kroemer, G. (2010). Autophagy regulation by p53. Curr. Opin. Cell Biol. *22*, 181–185.

Mallette, F.A., Gaumont-Leclerc, M.F., and Ferbeyre, G. (2007). The DNA damage signaling pathway is a critical mediator of oncogene-induced senescence. Genes Dev. *21*, 43–48.

Mardinian, K., Adashek, J.J., Botta, G.P., Kato, S., and Kurzrock, R. (2021). SMARCA4: Implications of an altered chromatin-remodeling gene for cancer development and therapy. Mol. Cancer Ther. *20*, 2341–2351.

Martínez-Zamudio, R.I., Roux, P.F., de Freitas, J.A.N.L.F., Robinson, L., Doré, G., Sun, B., Belenki, D., Milanovic, M., Herbig, U., Schmitt, C.A., et al. (2020). AP-1 imprints a reversible transcriptional programme of senescent cells. Nat. Cell Biol. *22*, 842–855.

Di Martino, S., Amoreo, C.A., Nuvoli, B., Galati, R., Strano, S., Facciolo, F., Alessandrini, G., Pass, H.I., Ciliberto, G., Blandino, G., et al. (2018). HSP90 inhibition alters the chemotherapy-driven rearrangement of the oncogenic secretome. Oncogene *37*, 1369–1385.

Matulonis, U.A., Shapira-Frommer, R., Santin, A.D., Lisyanskaya, A.S., Pignata, S., Vergote, I., Raspagliesi, F., Sonke, G.S., Birrer, M., Provencher, D.M., et al. (2019). Antitumor activity and safety of pembrolizumab in patients with advanced recurrent ovarian cancer: results from the phase II KEYNOTE-100 study. Ann. Oncol. *30*, 1080–1087.

Meyer, K., Hodwin, B., Ramanujam, D., Engelhardt, S., and Sarikas, A. (2016). Essential Role for Premature Senescence of Myofibroblasts in Myocardial Fibrosis. J. Am. Coll. Cardiol. *67*, 2018–2028.

Di Micco, R., Krizhanovsky, V., Baker, D., and d'Adda di Fagagna, F. (2021). Cellular senescence in ageing: from mechanisms to therapeutic opportunities. Nat. Rev. Mol. Cell Biol. *22*, 75–95.

Michaloglou, C., Vredeveld, L.C.W., Soengas, M.S., Denoyelle, C., Kuilman, T., Van Der Horst, C.M.A.M., Majoor, D.M., Shay, J.W., Mooi, W.J., and Peeper, D.S. (2005). BRAFE600-associated senescence-like cell cycle arrest of human naevi. Nature *436*, 720–724.

Milanovic, M., Yu, Y., and Schmitt, C.A. (2018). The Senescence–Stemness Alliance – A Cancer-Hijacked Regeneration Principle. Trends Cell Biol. *28*, 1049–1061.

Milczarek, M. (2020). The premature senescence in breast cancer treatment strategy. Cancers (Basel). *12*, 1–22.

Di Mitri, D., Toso, A., Chen, J.J., Sarti, M., Pinton, S., Jost, T.R., D'Antuono, R., Montani, E., Garcia-Escudero, R., Guccini, I., et al. (2014). Tumour-infiltrating Gr-1 + myeloid cells antagonize senescence in cancer. Nature *515*, 134–137.

Miwa, S., Kashyap, S., Chini, E., and von Zglinicki, T. (2022). Mitochondrial dysfunction in cell senescence and aging. J. Clin. Invest. *132*, 1–9.

Mohr, S.E., and Perrimon, N. (2012). RNAi screening: New approaches, understandings, and organisms. Wiley Interdiscip. Rev. RNA *3*, 145–158.

Moiseeva, O., Deschênes-Simard, X., St-Germain, E., Igelmann, S., Huot, G., Cadar, A.E., Bourdeau, V., Pollak, M.N., and Ferbeyre, G. (2013). Metformin inhibits the senescence-associated secretory phenotype by interfering with IKK/NF-κB activation. Aging Cell *12*, 489–498.

van Montfoort, N., Borst, L., Korrer, M.J., Sluijter, M., Marijt, K.A., Santegoets, S.J., van Ham, V.J., Ehsan, I., Charoentong, P., André, P., et al. (2018). NKG2A Blockade Potentiates CD8 T Cell Immunity Induced by Cancer Vaccines. Cell *175*, 1744-1755.e15.

Morvan, M.G., and Lanier, L.L. (2016). NK cells and cancer: You can teach innate cells new tricks. Nat. Rev.

Cancer *16*, 7–19.

Mosteiro, L., Pantoja, C., Alcazar, N., Marión, R.M., Chondronasiou, D., Rovira, M., Fernandez-Marcos, P.J., Muñoz-Martin, M., Blanco-Aparicio, C., Pastor, J., et al. (2016). Tissue damage and senescence provide critical signals for cellular reprogramming in vivo. Science (80-.). *354*.

Mosteiro, L., Pantoja, C., de Martino, A., and Serrano, M. (2018). Senescence promotes in vivo reprogramming through p16 INK4a and IL-6. Aging Cell *17*.

Mota, M.B.S., Carvalho, M.A., Monteiro, A.N.A., and Mesquita, R.D. (2019). DNA damage response and repair in perspective: Aedes aegypti, Drosophila melanogaster and Homo sapiens. Parasites and Vectors *12*, 1–20.

Muñoz-Espín, D., Cañamero, M., Maraver, A., Gómez-López, G., Contreras, J., Murillo-Cuesta, S., Rodríguez-Baeza, A., Varela-Nieto, I., Ruberte, J., Collado, M., et al. (2013). XProgrammed cell senescence during mammalian embryonic development. Cell *155*, 1104.

Muñoz, D.P., Yannone, S.M., Daemen, A., Sun, Y., Vakar-Lopez, F., Kawahara, M., Freund, A.M., Rodier, F., Wu, J.D., Desprez, P.Y., et al. (2019). Targetable mechanisms driving immunoevasion of persistent senescent cells link chemotherapy-resistant cancer to aging. JCI Insight *4*, 1–22.

Narita, M., Nũnez, S., Heard, E., Narita, M., Lin, A.W., Hearn, S.A., Spector, D.L., Hannon, G.J., and Lowe, S.W. (2003). Rb-mediated heterochromatin formation and silencing of E2F target genes during cellular senescence. Cell *113*, 703–716.

Narita, M., Narita, M., Krizhanovsky, V., Nuñez, S., Chicas, A., Hearn, S.A., Myers, M.P., and Lowe, S.W. (2006). A Novel Role for High-Mobility Group A Proteins in Cellular Senescence and Heterochromatin Formation. Cell *126*, 503–514.

Navarrete-Galvan, L., Guglielmo, M., Cruz Amaya, J., Smith-Gagen, J., Lombardi, V.C., Merica, R., and Hudig, D. (2022). Optimizing NK-92 serial killers: gamma irradiation, CD95/Fas-ligation, and NK or LAK attack limit cytotoxic efficacy. J. Transl. Med. *20*, 1–13.

Nelson, G., Kucheryavenko, O., Wordsworth, J., and von Zglinicki, T. (2018). The senescent bystander effect is caused by ROS-activated NF-κB signalling. Mech. Ageing Dev. *170*, 30–36.

Novais, E.J., Tran, V.A., Johnston, S.N., Darris, K.R., Roupas, A.J., Sessions, G.A., Shapiro, I.M., Diekman, B.O., and Risbud, M. V. (2021). Long-term treatment with senolytic drugs Dasatinib and Quercetin ameliorates age-dependent intervertebral disc degeneration in mice. Nat. Commun. *12*, 1–17.

Ogrodnik, M., Miwa, S., Tchkonia, T., Tiniakos, D., Wilson, C.L., Lahat, A., Day, C.P., Burt, A., Palmer, A., Anstee, Q.M., et al. (2017). Cellular senescence drives age-dependent hepatic steatosis. Nat. Commun. *8*.

Ohanna, M., Giuliano, S., Bonet, C., Imbert, V., Hofman, V., Zangari, J., Bille, K., Robert, C., Bressac-de Paillerets, B., Hofman, P., et al. (2011). Senescent cells develop a parp-1 and nuclear factor-κB-associated secretome (PNAS). Genes Dev. *25*, 1245–1261.

Okita, R., Yukawa, T., Nojima, Y., Maeda, A., Saisho, S., Shimizu, K., and Nakata, M. (2016). MHC class I chain-related molecule A and B expression is upregulated by cisplatin and associated with good prognosis in patients with non-small cell lung cancer. Cancer Immunol. Immunother. *65*, 499–509.

Olivier, M., Hollstein, M., and Hainaut, P. (2010). TP53 mutations in human cancers: origins, consequences, and clinical use. Cold Spring Harb. Perspect. Biol. *2*, 1–18.

Omori, S., Wang, T.W., Johmura, Y., Kanai, T., Nakano, Y., Kido, T., Susaki, E.A., Nakajima, T., Shichino, S., Ueha, S., et al. (2020). Generation of a p16 Reporter Mouse and Its Use to Characterize and Target p16high Cells In Vivo. Cell Metab. *32*, 814-828.e6.

Orjalo, A. V., Bhaumik, D., Gengler, B.K., Scott, G.K., and Campisi, J. (2009). Cell surface-bound IL-1α is an upstream regulator of the senescence-associated IL-6/IL-8 cytokine network. Proc. Natl. Acad. Sci. U. S. A. *106*, 17031–17036.

Ou, H.L., Hoffmann, R., González-López, C., Doherty, G.J., Korkola, J.E., and Muñoz-Espín, D. (2021). Cellular senescence in cancer: from mechanisms to detection. Mol. Oncol. *15*, 2634–2671.

Ovadya, Y., Landsberger, T., Leins, H., Vadai, E., Gal, H., Biran, A., Yosef, R., Sagiv, A., Agrawal, A., Shapira, A., et al. (2018). Impaired immune surveillance accelerates accumulation of senescent cells and aging. Nat. Commun. *9*.

Owens, W.A., Walaszczyk, A., Spyridopoulos, I., Dookun, E., and Richardson, G.D. (2021). Senescence and senolytics in cardiovascular disease: Promise and potential pitfalls. Mech. Ageing Dev. *198*, 111540.

Paffenholz, S. V., Salvagno, C., Ho, Y.J., Limjoco, M., Baslan, T., Tian, S., Kulick, A., de Stanchina, E., Wilkinson, J.E., Barriga, F.M., et al. (2022). Senescence induction dictates response to chemo- and immunotherapy in preclinical models of ovarian cancer. Proc. Natl. Acad. Sci. U. S. A. *119*.

Pai, S.G., Carneiro, B.A., Mota, J.M., Costa, R., Leite, C.A., Barroso-Sousa, R., Kaplan, J.B., Chae, Y.K., and

Giles, F.J. (2017). Wnt/beta-catenin pathway: Modulating anticancer immune response. J. Hematol. Oncol. *10*, 1–12.

Papke, B., and Der, C.J. (2017). Drugging RAS: Know the enemy. Science (80-.). *355*, 1158–1163.

Paramos-de-Carvalho, D., Jacinto, A., and Saúde, L. (2021). The right time for senescence. Elife *10*, 139–141.

Pare, R., Shin, J.S., and Lee, C.S. (2016). Increased expression of senescence markers p14ARF and p16INK4a in breast cancer is associated with an increased risk of disease recurrence and poor survival outcome. Histopathology *69*, 479–491.

Parrinello, S., Coppe, J.P., Krtolica, A., and Campisi, J. (2005). Stromal-epithelial interactions in aging and cancer: Senescent fibroblasts alter epithelial cell differentiation. J. Cell Sci. *118*, 485–496.

Partridge, L., Fuentealba, M., and Kennedy, B.K. (2020). The quest to slow ageing through drug discovery. Nat. Rev. Drug Discov. *19*, 513–532.

Passos, J.F., Nelson, G., Wang, C., Richter, T., Simillion, C., Proctor, C.J., Miwa, S., Olijslagers, S., Hallinan, J., Wipat, A., et al. (2010). Feedback between p21 and reactive oxygen production is necessary for cell senescence. Mol. Syst. Biol. *6*, 1–14.

Pech, M.F., Fong, L.E., Villalta, J.E., Chan, L.J.G., Kharbanda, S., O'brien, J.J., McAllister, F.E., Firestone, A.J., Jan, C.H., and Settleman, J. (2019). Systematic identification of cancer cell vulnerabilities to natural killer cell-mediated immune surveillance. Elife *8*, 1–31.

Peltonen, K., Colis, L., Liu, H., Trivedi, R., Moubarek, M.S., Moore, M., Bai, B., Rudek, M.A., Bieberich, C.J., and Laiho, M. (2015). NIH Public Access. *25*, 77–90.

Peng, L., Li, J., Wu, J., Xu, B., Wang, Z., Giamas, G., Stebbing, J., and Yu, Z. (2021). A Pan-Cancer Analysis of SMARCA4 Alterations in Human Cancers. Front. Immunol. *12*, 1–15.

Pereira, B.I., Devine, O.P., Vukmanovic-Stejic, M., Chambers, E.S., Subramanian, P., Patel, N., Virasami, A., Sebire, N.J., Kinsler, V., Valdovinos, A., et al. (2019). Senescent cells evade immune clearance via HLA-E-mediated NK and CD8+ T cell inhibition. Nat. Commun. *10*.

Pines, M. (2014). Halofuginone for fibrosis, regeneration and cancer in the gastrointestinal tract. World J. Gastroenterol. *20*, 14778–14786.

Pogacar, Z., L. Johnson, J., Krenning, L., De Conti, G., Lieftink, C., Velds, A., Wardak, L., Jochems, F., Groot, K., Schepers, A., et al. (2021). Indisulam Synergizes With Palbociclib to Induce Senescence Through Inhibition of CDK2 Kinase Activity. SSRN Electron. J.

Poggi, A., Catellani, S., Garuti, A., Pierri, I., Gobbi, M., and Zocchi, M.R. (2009). Effective in vivo induction of NKG2D ligands in acute myeloid leukaemias by all-trans-retinoic acid or sodium valproate. Leukemia *23*, 641–648.

Pole, A., Dimri, M., and P. Dimri, G. (2016). Oxidative stress, cellular senescence and ageing. AIMS Mol. Sci. *3*, 300–324.

Polk, A., Kolmos, I.L., Kümler, I., and Nielsen, D.L. (2016). Specific CDK4/6 inhibition in breast cancer: A systematic review of current clinical evidence. ESMO Open *1*, 1–11.

Pommier, Y., Sun, Y., Huang, S.Y.N., and Nitiss, J.L. (2016). Roles of eukaryotic topoisomerases in transcription, replication and genomic stability. Nat. Rev. Mol. Cell Biol. *17*, 703–721.

Prager, I., and Watzl, C. (2019). Mechanisms of natural killer cell-mediated cellular cytotoxicity. J. Leukoc. Biol. *105*, 1319–1329.

Prasanna, P.G., Citrin, D.E., Hildesheim, J., Ahmed, M.M., Venkatachalam, S., Riscuta, G., Xi, D., Zheng, G., Deursen, J. van, Goronzy, J., et al. (2021). Therapy-Induced Senescence: Opportunities to Improve Anticancer Therapy. J. Natl. Cancer Inst. *113*, 1285–1298.

Prata, L.G.P.L., Ovsyannikova, I.G., Tchkonia, T., and Kirkland, J.L. (2019). Senescent cell clearance by the immune system: Emerging therapeutic opportunities. Semin. Immunol. *40*, 101275.

Prieto, L.I., and Baker, D.J. (2019). Cellular Senescence and the Immune System in Cancer. Gerontology *65*, 505–512.

Raab, J.R., Runge, J.S., Spear, C.C., and Magnuson, T. (2017). Co-regulation of transcription by BRG1 and BRM, two mutually exclusive SWI/SNF ATPase subunits. Epigenetics and Chromatin *10*, 1–15.

Raffaele, M., and Vinciguerra, M. (2022). The costs and benefits of senotherapeutics for human health. Lancet Heal. Longev. *3*, e67–e77.

Rakhra, K., Bachireddy, P., Zabuawala, T., Zeiser, R., Xu, L., Kopelman, A., Fan, A.C., Yang, Q., Braunstein, L., Crosby, E., et al. (2010). CD4+ T Cells contribute to the remodeling of the microenvironment required for sustained tumor regression upon oncogene inactivation. Cancer Cell *18*, 485–498.

Rayess, H., Wang, M.B., and Srivatsan, E.S. (2012). Cellular senescence and tumor suppressor gene p16. Int. J. Cancer *130*, 1715–1725.

Reen, V., and Gil, J. (2021). Clearing stressed cells. Science (80-.). *374*, 534–535.

Ritschka, B., Storer, M., Mas, A., Heinzmann, F., Ortells, M.C., Morton, J.P., Sansom, O.J., Zender, L., and Keyes, W.M. (2017). The senescence-associated secretory phenotype induces cellular plasticity and tissue regeneration. Genes Dev. *31*, 172–183.

Rodier, F., and Campisi, J. (2011). Four faces of cellular senescence. J. Cell Biol. *192*, 547–556.

Rodier, F., Coppé, J.P., Patil, C.K., Hoeijmakers, W.A.M., Muñoz, D.P., Raza, S.R., Freund, A., Campeau, E., Davalos, A.R., and Campisi, J. (2009). Persistent DNA damage signalling triggers senescence-associated inflammatory cytokine secretion. Nat. Cell Biol. *11*, 973–979.

Rodier, F., Muñoz, D.P., Teachenor, R., Chu, V., Le, O., Bhaumik, D., Coppé, J.P., Campeau, E., Beauséjour, C.M., Kim, S.H., et al. (2011). DNA-SCARS: Distinct nuclear structures that sustain damage-induced senescence growth arrest and inflammatory cytokine secretion. J. Cell Sci. *124*, 68–81.

Rolt, A., Nair, A., and Cox, L.S. (2019). Optimisation of a screening platform for determining IL-6 inflammatory signalling in the senescence-associated secretory phenotype (SASP). Biogerontology *20*, 359–371.

Rose, M., Duhamel, M., Rodet, F., and Salzet, M. (2021). The Role of Proprotein Convertases in the Regulation of the Function of Immune Cells in the Oncoimmune Response. Front. Immunol. *12*, 1–10.

Rudin, C.M., Hann, C.L., Garon, E.B., Ribeiro De Oliveira, M., Bonomi, P.D., Camidge, D.R., Chu, Q., Giaccone, G., Khaira, D., Ramalingam, S.S., et al. (2012). Phase II study of single-agent navitoclax (ABT-263) and biomarker correlates in patients with relapsed small cell lung cancer. Clin. Cancer Res. *18*, 3163–3169.

Rufini, A., Tucci, P., Celardo, I., and Melino, G. (2013). Senescence and aging: The critical roles of p53. Oncogene *32*, 5129–5143.

Ruscetti, M., Leibold, J., Bott, M.J., Fennell, M., Kulick, A., Salgado, N.R., Chen, C.C., Ho, Y. jui, Sanchez-Rivera, F.J., Feucht, J., et al. (2018). NK cell–mediated cytotoxicity contributes to tumor control by a cytostatic drug combination. Science (80-.). *362*, 1416–1422.

Ruscetti, M., Morris, J.P., Mezzadra, R., Russell, J., Leibold, J., Romesser, P.B., Simon, J., Kulick, A., Ho, Y., Fennell, M., et al. (2020). Senescence-Induced Vascular Remodeling Creates Therapeutic Vulnerabilities in Pancreas Cancer. Cell 1–18.

Ryu, S.J., Oh, Y.S., and Park, S.C. (2007). Failure of stress-induced downregulation of Bcl-2 contributes to apoptosis resistance in senescent human diploid fibroblasts. Cell Death Differ. *14*, 1020–1028.

Sabbatinelli, J., Prattichizzo, F., Olivieri, F., Procopio, A.D., Rippo, M.R., and Giuliani, A. (2019). Where Metabolism Meets Senescence: Focus on Endothelial Cells. Front. Physiol. *10*, 1–17.

Sagiv, A., and Krizhanovsky, V. (2013). Immunosurveillance of senescent cells: The bright side of the senescence program. Biogerontology *14*, 617–628.

Sagiv, A., Biran, A., Yon, M., Simon, J., Lowe, S.W., and Krizhanovsky, V. (2013). Granule exocytosis mediates immune surveillance of senescent cells. Oncogene *32*, 1971–1977.

Sagiv, A., Burton, D.G.A., Moshayev, Z., Vadai, E., Wensveen, F., Ben-Dor, S., Golani, O., Polic, B., and Krizhanovsky, V. (2016). NKG2D ligands mediate immunosurveillance of senescent cells. Aging (Albany. NY). *8*, 328–344.

Saito, Y., Chikenji, T.S., Matsumura, T., Nakano, M., and Fujimiya, M. (2020). Exercise enhances skeletal muscle regeneration by promoting senescence in fibro-adipogenic progenitors. Nat. Commun. *11*, 1–16.

Salama, R., Sadaie, M., Hoare, M., and Narita, M. (2014). Cellular senescence and its effector programs. Genes Dev. *28*, 99–114.

Saleh, T., Tyutynuk-Massey, L., Cudjoe, E.K., Idowu, M.O., Landry, J.W., and Gewirtz, D.A. (2018). Non-cell autonomous effects of the senescence-associated secretory phenotype in cancer therapy. Front. Oncol. *8*, 1–14.

Saleh, T., Carpenter, V.J., Tyutyunyk-Massey, L., Murray, G., Leverson, J.D., Souers, A.J., Alotaibi, M.R., Faber, A.C., Reed, J., Harada, H., et al. (2020). Clearance of therapy-induced senescent tumor cells by the senolytic ABT-263 via interference with BCL-XL–BAX interaction. Mol. Oncol. *14*, 2504–2519.

Salminen, A., Kauppinen, A., and Kaarniranta, K. (2012). Emerging role of NF-κB signaling in the induction of senescence-associated secretory phenotype (SASP). Cell. Signal. *24*, 835–845.

Sanij, E., Hannan, K.M., Xuan, J., Yan, S., Ahern, J.E., Trigos, A.S., Brajanovski, N., Son, J., Chan, K.T., Kondrashova, O., et al. (2020). CX-5461 activates the DNA damage response and demonstrates therapeutic efficacy in high-grade serous ovarian cancer. Nat. Commun. *11*.

Sarkisian, C.J., Keister, B.A., Stairs, D.B., Boxer, R.B., Moody, S.E., and Chodosh, L.A. (2007). Dose-dependent oncogene-induced senescence in vivo and its evasion during mammary tumorigenesis. Nat. Cell Biol. *9*, 493–505.

Sasaki, M., Kumazaki, T., Takano, H., Nishiyama, M., and Mitsui, Y. (2001). Senescent cells are resistant to death despite low Bcl-2 level. Mech. Ageing Dev. *122*, 1695–1706.

Sato, E., Olson, S.H., Ahn, J., Bundy, B., Nishikawa, H., Qian, F., Jungbluth, A.A., Frosina, D., Gnjatic, S., Ambrosone, C., et al. (2005). Intraepithelial CD8+ tumor-infiltrating lymphocytes and a high CD8+/regulatory T cell ratio are associated with favorable prognosis in ovarian cancer. Proc. Natl. Acad. Sci. U. S. A. *102*, 18538–18543.

Schafer, M.J., White, T.A., Iijima, K., Haak, A.J., Ligresti, G., Atkinson, E.J., Oberg, A.L., Birch, J., Salmonowicz, H., Zhu, Y., et al. (2017). Cellular senescence mediates fibrotic pulmonary disease. Nat. Commun. *8*.

Schmitt, C.A., Fridman, J.S., Yang, M., Lee, S., Baranov, E., Hoffman, R.M., and Lowe, S.W. (2002). A senescence program controlled by p53 and p16INK4a contributes to the outcome of cancer therapy. Cell *109*, 335–346.

Schoenfeld, A.J., Bandlamudi, C., Lavery, J.A., Montecalvo, J., Namakydoust, A., Rizvi, H., Egger, J., Concepcion, C.P., Paul, S., Arcila, M.E., et al. (2021). The Genomic Landscape of SMARCA4 Alterations and Associations with Outcomes in Patients with Lung Cancer Adam. *26*, 5701–5708.

Sen, P., Shah, P.P., Nativio, R., and Berger, S.L. (2016). Epigenetic Mechanisms of Longevity and Aging. Cell *166*, 822–839.

Serrano, M., Lin, A.W., McCurrach, M.E., Beach, D., and Lowe, S.W. (1997). Oncogenic ras provokes premature cell senescence associated with accumulation of p53 and p16(INK4a). Cell *88*, 593–602.

Sfeir, A., and De Lange, T. (2012). Removal of shelterin reveals the telomere end-protection problem. Science (80-.). *336*, 593–597.

Shahbandi, A., Rao, S.G., Anderson, A.Y., Frey, W.D., Olayiwola, J.O., Ungerleider, N.A., and Jackson, J.G. (2020). BH3 mimetics selectively eliminate chemotherapy-induced senescent cells and improve response in TP53 wild-type breast cancer. Cell Death Differ. *27*, 3097–3116.

Sherr, C.J., and McCormick, F. (2002). The RB and p53 pathways in cancer. Cancer Cell *2*, 103–112.

Shimizu, I., and Minamino, T. (2019). Cellular senescence in cardiac diseases. J. Cardiol. *74*, 313–319.

Song, P., An, J., and Zou, M.H. (2020). Immune Clearance of Senescent Cells to Combat Ageing and Chronic Diseases. Cells *9*.

Soriani, A., Zingoni, A., Cerboni, C., Lannitto, M.L., Ricciardi, M.R., Gialleonardo, V. Di, Cippitelli, M., Fionda, C., Petrucci, M.T., Guarini, A., et al. (2009). ATM-ATR-dependent up-regulation of DNAM-1 and NKG2D ligands on multiple myeloma cells by therapeutic agents results in enhanced NK-cell susceptibility and is associated with a senescent phenotype. Blood *113*, 3503–3511.

Spiliopoulou, P., Spear, S., Mirza, H., Garner, I., McGarry, L., Grundland-Freile, F., Cheng, Z., Ennis, D.P., Iyer, N., McNamara, S., et al. (2022). Dual G9A/EZH2 Inhibition Stimulates Antitumor Immune Response in Ovarian High-Grade Serous Carcinoma. Mol. Cancer Ther. *21*, 522–534.

Storer, M., Mas, A., Robert-Moreno, A., Pecoraro, M., Ortells, M.C., Di Giacomo, V., Yosef, R., Pilpel, N., Krizhanovsky, V., Sharpe, J., et al. (2013). XSenescence is a developmental mechanism that contributes to embryonic growth and patterning. Cell *155*, 1119.

Sturmlechner, I., Zhang, C., Sine, C.C., van Deursen, E.J., Jeganathan, K.B., Hamada, N., Grasic, J., Friedman, D., Stutchman, J.T., Can, I., et al. (2021). P21 Produces a Bioactive Secretome That Places Stressed Cells Under Immunosurveillance. Science (80-.). *374*.

Subramanian, A., Tamayo, P., Mootha, V.K., Mukherjee, S., Ebert, B.L., Gillette, M.A., Paulovich, A., Pomeroy, S.L., Golub, T.R., Lander, E.S., et al. (2005). Gene set enrichment analysis: A knowledge-based approach for interpreting genome-wide expression profiles. Proc. Natl. Acad. Sci. U. S. A. *102*, 15545–15550.

Sun, Y., Coppé, J.P., and Lam, E.W.F. (2018). Cellular Senescence: The Sought or the Unwanted? Trends Mol. Med. *24*, 871–885.

Suram, A., Kaplunov, J., Patel, P.L., Ruan, H., Cerutti, A., Boccardi, V., Fumagalli, M., Di Micco, R., Mirani, N., Gurung, R.L., et al. (2012). Oncogene-induced telomere dysfunction enforces cellular senescence in human cancer precursor lesions. EMBO J. *31*, 2839–2851.

Takada, K., Sugita, S., Murase, K., Kikuchi, T., Oomori, G., Ito, R., Hayasaka, N., Miyanishi, K., Iyama, S., Ikeda, H., et al. (2019). Exceptionally rapid response to pembrolizumab in a SMARCA4-deficient thoracic sarcoma overexpressing PD-L1: A case report. Thorac. Cancer *10*, 2312–2315.

Takahashi, A., Imai, Y., Yamakoshi, K., Kuninaka, S., Ohtani, N., Yoshimoto, S., Hori, S., Tachibana, M.,

Anderton, E., Takeuchi, T., et al. (2012). DNA damage signaling triggers degradation of histone methyltransferases through APC/C Cdh1 in senescent cells. Mol. Cell *45*, 123–131.

Takasugi, M. (2018). Emerging roles of extracellular vesicles in cellular senescence and aging. Aging Cell *17*, 1–8.

Takasugi, M., Okada, R., Takahashi, A., Virya Chen, D., Watanabe, S., and Hara, E. (2017). Small extracellular vesicles secreted from senescent cells promote cancer cell proliferation through EphA2. Nat. Commun. *8*, 1–11.

Takasugi, M., Yoshida, Y., Hara, E., and Ohtani, N. (2022). The role of cellular senescence and SASP in tumour microenvironment. FEBS J. 1–14.

Tam, Y.K., Maki, G., Miyagawa, B., Hennemann, B., Tonn, T., and Klingemann, H.G. (1999). Characterization of genetically altered, interleukin 2-independent natural killer cell lines suitable for adoptive cellular immunotherapy. Hum. Gene Ther. *10*, 1359–1373.

Tan, H.Y., Wang, N., Zhang, C., Chan, Y.T., Yuen, M.F., and Feng, Y. (2021). Lysyl Oxidase-Like 4 Fosters an Immunosuppressive Microenvironment During Hepatocarcinogenesis. Hepatology *73*, 2326–2341.

Tasdemir, N., Banito, A., Roe, J.S., Alonso-Curbelo, D., Camiolo, M., Tschaharganeh, D.F., Huang, C.H., Aksoy, O., Bolden, J.E., Chen, C.C., et al. (2016). BRD4 connects enhancer remodeling to senescence immune surveillance. Cancer Discov. *6*, 613–629.

Thompson, P.J., Shah, A., Ntranos, V., Van Gool, F., Atkinson, M., and Bhushan, A. (2019). Targeted Elimination of Senescent Beta Cells Prevents Type 1 Diabetes. Cell Metab. *29*, 1045-1060.e10.

Tischkowitz, M., Huang, S., Banerjee, S., Hague, J., Hendricks, W.P.D., Huntsman, D.G., Lang, J.D., Orlando, K.A., Oza, A.M., Pautier, P., et al. (2020). Small-Cell Carcinoma of the Ovary, Hypercalcemic Type–Genetics, New Treatment Targets, and Current Management Guidelines. Clin. Cancer Res. *26*, 3908–3917.

Tome, M., Pappalardo, A., Soulet, F., Lopez, J.J., Olaizola, J., Leger, Y., Dubreuil, M., Mouchard, A., Fessart, D., Delom, F. eric, et al. (2019). Inactivation of proprotein convertases in T cells inhibits PD-1 expression and creates a favorable immune microenvironment in colorectal cancer. Cancer Res. *79*, 5008–5021.

Tominaga, K. (2015). The emerging role of senescent cells in tissue homeostasis and pathophysiology. Pathobiol. Aging Age-Related Dis. *5*, 27743.

Tominaga, K., and Suzuki, H.I. (2019). TGF-β signaling in cellular senescence and aging-related pathology. Int. J. Mol. Sci. *20*.

Tonn, T., and Becker, S. (2001). Natural Killer Cell Line NK-92. J. Hematother. Stem Cell Res. *544*, 535–544.

Toogood, P.L., Harvey, P.J., Repine, J.T., Sheehan, D.J., VanderWel, S.N., Zhou, H., Keller, P.R., McNamara, D.J., Sherry, D., Zhu, T., et al. (2005). Discovery of a potent and selective inhibitor of cyclin-dependent kinase 4/6. J. Med. Chem. *48*, 2388–2406.

Tordella, L., Khan, S., Hohmeyer, A., Banito, A., Klotz, S., Raguz, S., Martin, N., Dhamarlingam, G., Carroll, T., González Meljem, J.M., et al. (2016). SWI/SNF regulates a transcriptional program that induces senescence to prevent liver cancer. Genes Dev. *30*, 2187–2198.

Toso, A., Revandkar, A., DiMitri, D., Guccini, I., Proietti, M., Sarti, M., Pinton, S., Zhang, J., Kalathur, M., Civenni, G., et al. (2014). Enhancing chemotherapy efficacy in pten-deficient prostate tumors by activating the senescence-associated antitumor immunity. Cell Rep. *9*, 75–89.

Triana-martínez, F., Picallos-rabina, P., Silva-álvarez, S. Da, Pietrocola, F., Llanos, S., Rodilla, V., Soprano, E., Pedrosa, P., Ferreirós, A., Barradas, M., et al. (2019). Identi fi cation and characterization of Cardiac Glycosides as senolytic compounds. Nat. Commun. 1–12.

Tsuchida, T., and Friedman, S.L. (2017). Mechanisms of hepatic stellate cell activation. Nat. Rev. Gastroenterol. Hepatol. *14*, 397–411.

van Tuyn, J., Jaber-Hijazi, F., MacKenzie, D., Cole, J.J., Mann, E., Pawlikowski, J.S., Rai, T.S., Nelson, D.M., McBryan, T., Ivanov, A., et al. (2017). Oncogene-Expressing Senescent Melanocytes Up-Regulate MHC Class II, a Candidate Melanoma Suppressor Function. J. Invest. Dermatol. *137*, 2197–2207.

Vanherberghen, B., Olofsson, P.E., Forslund, E., Sternberg-Simon, M., Khorshidi, M.A., Pacouret, S., Guldevall, K., Enqvist, M., Malmberg, K.J., Mehr, R., et al. (2013). Classification of human natural killer cells based on migration behavior and cytotoxic response. Blood *121*, 1326–1334.

Vilgelm, A.E., Pawlikowski, J.S., Liu, Y., Hawkins, O.E., Davis, T.A., Smith, J., Weller, K.P., Horton, L.W., McClain, C.M., Ayers, G.D., et al. (2015). Mdm2 and aurora kinase A inhibitors synergize to block melanoma growth by driving apoptosis and immune clearance of tumor cells. Cancer Res. *75*, 181–193.

Di Vito, C., Mikulak, J., Zaghi, E., Pesce, S., Marcenaro, E., and Mavilio, D. (2019a). NK cells to cure cancer. Semin. Immunol. *41*, 101272.

Di Vito, C., Mikulak, J., and Mavilio, D. (2019b). On the way to become a natural killer cell. Front. Immunol. *10*, 1–15.

Wagner, V., and Gil, J. (2020). Senescence as a therapeutically relevant response to CDK4/6 inhibitors. Oncogene *39*, 5165–5176.

Wajapeyee, N., Serra, R.W., Zhu, X., Mahalingam, M., and Green, M.R. (2008). Oncogenic BRAF Induces Senescence and Apoptosis through Pathways Mediated by the Secreted Protein IGFBP7. Cell *132*, 363–374.

Walle, T., Kraske, J.A., Liao, B., Lenoir, B., Timke, C., Von Bohlen und Halbach, E., Tran, F., Griebel, P., Albrecht, D., Ahmed, A., et al. (2022). Radiotherapy orchestrates natural killer cell dependent antitumor immune responses through CXCL8. Sci. Adv. *8*.

Wallis, R., Mizen, H., and Bishop, C.L. (2020). The bright and dark side of extracellular vesicles in the senescence-associated secretory phenotype. Mech. Ageing Dev. *189*, 111263.

Walton, J., Blagih, J., Ennis, D., Leung, E., Dowson, S., Farquharson, M., Tookman, L.A., Orange, C., Athineos, D., Mason, S., et al. (2016). CRISPR/Cas9-mediated Trp53 and Brca2 knockout to generate improved murine models of ovarian high-grade serous carcinoma. Cancer Res. *76*, 6118–6129.

Walton, J.B., Farquharson, M., Mason, S., Port, J., Kruspig, B., Dowson, S., Stevenson, D., Murphy, D., Matzuk, M., Kim, J., et al. (2017). CRISPR/Cas9-derived models of ovarian high grade serous carcinoma targeting Brca1, Pten and Nf1, and correlation with platinum sensitivity. Sci. Rep. *7*, 1–11.

Wang, L., and Bernards, R. (2018). Taking advantage of drug resistance, a new approach in the war on cancer. Front. Med. *12*, 490–495.

Wang, D., Kang, L., Chen, C., Guo, J., Du, L., Zhou, D., Li, G., Zhang, Y., Mi, X., Zhang, M., et al. (2022a). Loss of legumain induces premature senescence and mediates aging-related renal fibrosis. Aging Cell *21*, 1–18.

Wang, L., Leite de Oliveira, R., Wang, C., Fernandes Neto, J.M., Mainardi, S., Evers, B., Lieftink, C., Morris, B., Jochems, F., Willemsen, L., et al. (2017a). High-Throughput Functional Genetic and Compound Screens Identify Targets for Senescence Induction in Cancer. Cell Rep. *21*, 773–783.

Wang, L., Lankhorst, L., and Bernards, R. (2022b). Exploiting senescence for the treatment of cancer. Nat. Rev. Cancer *22*, 340–355.

Wang, W., Zheng, Y., Sun, S., Li, W., Song, M., Ji, Q., Wu, Z., Liu, Z., Fan, Y., Liu, F., et al. (2021). A genome-wide CRISPR-based screen identifies KAT7 as a driver of cellular senescence. Sci. Transl. Med. *13*.

Wang, Z.N., Liu, D., Yin, B., Ju, W.Y., Qiu, H.Z., Xiao, Y., Chen, Y.J., Peng, X.Z., and Lu, C.M. (2017b). High expression of PTBP1 promote invasion of colorectal cancer by alternative splicing of cortactin. Oncotarget *8*, 36185–36202.

Watanabe, S., Kawamoto, S., Ohtani, N., and Hara, E. (2017). Impact of senescence-associated secretory phenotype and its potential as a therapeutic target for senescence-associated diseases. Cancer Sci. *108*, 563–569.

Wentzensen, I.M., Mirabello, L., Pfeiffer, R.M., and Savage, S.A. (2011). The association of telomere length and cancer: A meta-analysis. Cancer Epidemiol. Biomarkers Prev. *20*, 1238–1250.

Whittle, J.R., Vaillant, F., Surgenor, E., Policheni, A.N., Giner, G., Capaldo, B.D., Chen, H.R., Liu, H.K., Dekkers, J.F., Sachs, N., et al. (2020). Dual Targeting of CDK4/6 and BCL2 Pathways Augments Tumor Response in Estrogen Receptor–Positive Breast Cancer. Clin. Cancer Res. *26*, 4120–4134.

Widmann, T.A., Herrmann, M., Taha, N., König, J., and Pfreundschuh, M. (2007). Short telomeres in aggressive non-Hodgkin's lymphoma as a risk factor in lymphomagenesis. Exp. Hematol. *35*, 939–946.

Wiley, C.D., and Campisi, J. (2016). From Ancient Pathways to Aging Cells - Connecting Metabolism and Cellular Senescence. Cell Metab. *23*, 1013–1021.

Wiley, C.D., Flynn, J.M., Morrissey, C., Lebofsky, R., Shuga, J., Dong, X., Unger, M.A., Vijg, J., Melov, S., and Campisi, J. (2017). Analysis of individual cells identifies cell-to-cell variability following induction of cellular senescence. Aging Cell *16*, 1043–1050.

Wilkinson, H.N., and Hardman, M.J. (2020). Senescence in Wound Repair: Emerging Strategies to Target Chronic Healing Wounds. Front. Cell Dev. Biol. *8*, 1–13.

Witkiewicz, A.K., Knudsen, K.E., Dicker, A.P., and Knudsen, E.S. (2011). The meaning of p16ink4a expression in tumors: Functional significance, clinical associations and future developments. Cell Cycle *10*, 2497–2503.

Wu, C.H., Van Riggelen, J., Yetil, A., Fan, A.C., Bachireddy, P., and Felsher, D.W. (2007). Cellular senescence is an important mechanism of tumor regression upon c-Myc inactivation. Proc. Natl. Acad. Sci. U. S. A. *104*, 13028–13033.

Wyld, L., Bellantuono, I., Tchkonia, T., Morgan, J., Turner, O., Foss, F., George, J., Danson, S., and Kirkland,

J.L. (2020). Senescence and cancer: A review of clinical implications of senescence and senotherapies. Cancers (Basel). *12*, 1–20.

Xiao, L., Parolia, A., Qiao, Y., Bawa, P., Eyunni, S., Mannan, R., Carson, S.E., Chang, Y., Wang, X., Zhang, Y., et al. (2022). Targeting SWI/SNF ATPases in enhancer-addicted prostate cancer. Nature *601*, 434–439.

Xie, G., Dong, H., Liang, Y., Ham, J.D., Rizwan, R., and Chen, J. (2020). CAR-NK cells: A promising cellular immunotherapy for cancer. EBioMedicine *59*.

Xu, M., Tchkonia, T., Ding, H., Ogrodnik, M., Lubbers, E.R., Pirtskhalava, T., White, T.A., Johnson, K.O., Stout, M.B., Mezera, V., et al. (2015). JAK inhibition alleviates the cellular senescence-associated secretory phenotype and frailty in old age. Proc. Natl. Acad. Sci. U. S. A. *112*, E6301–E6310.

Xu, M., Pirtskhalava, T., Farr, J.N., Weigand, B.M., Palmer, A.K., Weivoda, M.M., Inman, C.L., Ogrodnik, M.B., Hachfeld, C.M., Fraser, D.G., et al. (2018). Senolytics improve physical function and increase lifespan in old age. Nat. Med. *24*, 1246–1256.

Xu, Y., Li, N., Xiang, R., and Sun, P. (2014). Emerging roles of the p38 MAPK and PI3K/AKT/mTOR pathways in oncogene-induced senescence. Trends Biochem. Sci. *39*, 268–276.

Xue, W., Zender, L., Miething, C., Dickins, R.A., Hernando, E., Krizhanovsky, V., Cordon-Cardo, C., and Lowe, S.W. (2007). Senescence and tumour clearance is triggered by p53 restoration in murine liver carcinomas. Nature *445*, 656–660.

Yamakoshi, K., Takahashi, A., Hirota, F., Nakayama, R., Ishimaru, N., Kubo, Y., Mann, D.J., Ohmura, M., Hirao, A., Saya, H., et al. (2009). Real-time in vivo imaging of p16Ink4a reveals cross talk with p53. J. Cell Biol. *186*, 393–407.

Yang, H., Wang, H., Ren, U., Chen, Q., and Chena, Z.J. (2017). CGAS is essential for cellular senescence. Proc. Natl. Acad. Sci. U. S. A. *114*, E4612–E4620.

Yang, W., Feng, Y., Zhou, J., Cheung, O.K.W., Cao, J., Wang, J., Tang, W., Tu, Y., Xu, L., Wu, F., et al. (2021). A selective HDAC8 inhibitor potentiates antitumor immunity and efficacy of immune checkpoint blockade in hepatocellular carcinoma. Sci. Transl. Med. *13*.

Ye, J., Ma, C., Hsueh, E.C., Eickhoff, C.S., Zhang, Y., Varvares, M.A., Hoft, D.F., and Peng, G. (2013). Tumor-Derived γδ Regulatory T Cells Suppress Innate and Adaptive Immunity through the Induction of Immunosenescence. J. Immunol. *190*, 2403–2414.

Ye, W., Zhou, Y., Xu, B., Zhu, D., Rui, X., Xu, M., Shi, L., Zhang, D., and Jiang, J. (2019). CD247 expression is associated with differentiation and classification in ovarian cancer. Med. (United States) *98*.

Yosef, R., Pilpel, N., Tokarsky-Amiel, R., Biran, A., Ovadya, Y., Cohen, S., Vadai, E., Dassa, L., Shahar, E., Condiotti, R., et al. (2016). Directed elimination of senescent cells by inhibition of BCL-W and BCL-XL. Nat. Commun. *7*.

Yoshimoto, S., Loo, T.M., Atarashi, K., Kanda, H., Sato, S., Oyadomari, S., Iwakura, Y., Oshima, K., Morita, H., Hattori, M., et al. (2013). Obesity-induced gut microbial metabolite promotes liver cancer through senescence secretome. Nature *499*, 97–101.

Young, A.P., Schisio, S., Minamishima, Y.A., Zhang, Q., Li, L., Grisanzio, C., Signoretti, S., and Kaelin, W.G. (2008). VHL loss actuates a HIF-independent senescence programme mediated by Rb and p400. Nat. Cell Biol. *10*, 361–369.

Young, A.R.J., Narita, M., Ferreira, M., Kirschner, K., Sadaie, M., Darot, J.F.J., Tavaré, S., Arakawa, S., Shimizu, S., Watt, F.M., et al. (2009). Autophagy mediates the mitotic senescence transition. Genes Dev. *23*, 798–803.

Yousefzadeh, M.J., Flores, R.R., Zhu, Y., Schmiechen, Z.C., Brooks, R.W., Trussoni, C.E., Cui, Y., Angelini, L., Lee, K.A., McGowan, S.J., et al. (2021). An aged immune system drives senescence and ageing of solid organs.

Zhang, B., Fu, D., Xu, Q., Cong, X., Wu, C., Zhong, X., Ma, Y., Lv, Z., Chen, F., Han, L., et al. (2018). The senescence-associated secretory phenotype is potentiated by feedforward regulatory mechanisms involving Zscan4 and TAK1. Nat. Commun. *9*.

Zhang, J., Zhang, X., Yang, S., Bao, Y., Xu, D., and Liu, L. (2021a). FOXH1 promotes lung cancer progression by activating the Wnt/β-catenin signaling pathway. Cancer Cell Int. *21*, 1–13.

Zhang, R., Chen, W., and Adams, P.D. (2007). Molecular Dissection of Formation of Senescence-Associated Heterochromatin Foci. Mol. Cell. Biol. *27*, 2343–2358.

Zhang, S.M., Cai, W.L., Liu, X., Thakral, D., Luo, J., Chan, L.H., McGeary, M.K., Song, E., Blenman, K.R.M., Micevic, G., et al. (2021b). KDM5B promotes immune evasion by recruiting SETDB1 to silence retroelements. Nature *598*, 682–687.

Zhang, Y., Hu, R., Xi, B., Nie, D., Xu, H., and Liu, A. (2022). Mechanisms of Senescence-Related NKG2D Ligands Release and Immune Escape Induced by Chemotherapy in Neuroblastoma Cells. Front. Cell Dev. Biol. *10*, 1–11.

Zhou, B., and Gao, S. (2021). Pan-Cancer Analysis of FURIN as a Potential Prognostic and Immunological Biomarker. Front. Mol. Biosci. *8*, 1–15.

Zhu, W., Zhou, B. lun, Rong, L. juan, Ye, L., Xu, H. juan, Zhou, Y., Yan, X. jun, Liu, W. dong, Zhu, B., Wang, L., et al. (2020). Roles of PTBP1 in alternative splicing, glycolysis, and oncogensis. J. Zhejiang Univ. Sci. B *21*, 122–136.

Zhu, Y., Tchkonia, T., Pirtskhalava, T., Gower, A.C., Ding, H., Giorgadze, N., Palmer, A.K., Ikeno, Y., Hubbard, G.B., Lenburg, M., et al. (2015). The Achilles' heel of senescent cells: from transcriptome to senolytic drugs. Aging Cell *14*, 644–658.

Zindy, F., Quelle, D.E., Roussel, M.F., and Sherr, C.J. (1997). Expression of the p16INK4a tumor suppressor versus other INK4 family members during mouse development and aging. Oncogene *15*, 203–211.

Zingoni, A., Cecere, F., Vulpis, E., Fionda, C., Molfetta, R., Soriani, A., Petrucci, M.T., Ricciardi, M.R., Fuerst, D., Amendola, M.G., et al. (2015). Genotoxic Stress Induces Senescence-Associated ADAM10-Dependent Release of NKG2D MIC Ligands in Multiple Myeloma Cells. J. Immunol. *195*, 736–748.

Zingoni, A., Vulpis, E., Loconte, L., and Santoni, A. (2020). NKG2D Ligand Shedding in Response to Stress: Role of ADAM10. Front. Immunol. *11*, 1–8.

Zwirner, N.W., and Domaica, C.I. (2010). Cytokine regulation of natural killer cell effector functions. BioFactors *36*, 274–288.

Appendix

			Antibiotic resistance	
Vector backbone	**Insert name**	**Infection**	**Bacterial**	**Mammalian**
pLNC	ER:RAS	Retroviral	Ampicillin	Neomycin
pLXSN	Empty vector (EV)	Retroviral	Ampicillin	Neomycin
pGIPZ	TurboGFP/ shRNA	Lentiviral	Ampicillin & Zeocin™	Puromycin
FUGW	H2B-GFP (Histone 2B - GFP)	Lentiviral	Ampicillin	Puromycin

Table A1. Plasmids

Antibiotic	**Manufacturer**	**Selection concentration**	**Working concentration**
Neomycin (Geneticin)	Gibco	400µg/ml	200µg/ml
Puromycin	InvivoGen	1µg/ml	0.5µg/ml
Ampicillin	Sigma	100mg/ml	100mg/ml
Zeocin™	InvivoGen	25mg/ml	25mg/ml

Table A2. Antibiotics

Target gene	Forward primer	Reverse primer
RPS14	CTGCGAGTGCTGTCAGAGG	TCACCGCCCTACACATCAAACT
P21^{CIP1}	CGTGTCACTGTCTTGTACCCT	GCGTTTGGAGTGGTAGAAATCT
p16^{INK4a}	CGGTCGGAGGCCGATCCAG	GCGCCGTGGAGCAGCAGCAGCT
PLAUR	CCACTCAGAGAAGACCAACAGG	GTAACGGCTTCGGGAATAGGTG
LMNB1	GAGAGCAACATGATGCCCAAGTG	GTTCTTCCCTGGCACTGTTGAC
IL1α	AGTGCTGCTGAAGGAGATGCCTGA	CCCCTGCCAAGCACACCCAGTA
IL1β	TGCACGCTCCGGGACTCACA	CATGGAGAACACCACTTGTTGCTCC
IL6	CCAGGAGCCCAGCTATGAAC	CCCAGGGAGAAGGCAACTG
IL8	GAGTGGACCACACTGCGCCA	TCCACAACCCTCTGCACCCAGT
CXCL10	GGTGAGAAGAGATGTCTGAATCC	GTCCATCCTTGGAAGCACTGCA
TNF-α	CTCTTCTGCCTGCTGCACTTTG	ATGGGCTACAGGCTTGTCACTC
IGFBP7	GCCATCACCCAGGTCAGCAAG	GGATTCCGATGACCTCACAGCT
CCL5	CCTGCTGCTTTGCCTACATTGC	ACACACTTGGCGGTTCTTTCGG
MICA	CCACCAGGATTTGCCAAGGAGA	CTGCCAATGACTCTGAAGCACC
MICB	GGAATGGAACCTACCAGACCTG	CTGTCCGTTGACTCTGAAGCAC
ULBP1	CTGCTTGACATTCAAGTGGAGAAT	CTGTCCATTGAAGAGGAACTGCC
ULBP2	GAGCAACTGCGTGACATTCAGC	GCCCATCGAAACTGAACTGCCA
ULBP3	CAGACTGGAACTGGCTGACACT	GGAGGAACTTCCGTCCATCGAA
ULBP4	GGTATATGCCACCAGCACTTGG	TCTCGACTTGCAGAGTGGAAGG
ICAM1	AGCGGCTGACGTGTGCAGTAAT	TCTGAGACCTCTGGCTTCGTCA
HLA-A	AGATACACCTGCCATGTGCAGC	GATCACAGCTCCAAGGAGAACC
HLA-B	CTGCTGTGATGTGTAGGAGGAAG	GCTGTGAGAGACACATCAGAGC
HLA-C	GGAGACACAGAAGTACAAGCGC	ACATCCTCTGGAGGGTGTGAGA
HLA-E	CGGCTACTACAATCAGAGCGAG	AATCCTTGCCGTCGTAGGCGAA
NECTIN2	GAGCAGATGGTGTCACGGTCAC	GAGATGGACACTTCAGGAGGGT
CLEC2D	CACCAAAAGGATCTAGTTCTGTAG	AGCCTCTTGGTCAGTCATCCAG
SLC35A1	GCTGTATTGTGCTCAGGATTTGC	GCTCCATCTGACAAGTAGACGC
PDCD1LG2	CTCGTTCCACATACCTCAAGTCC	CTGGAACCTTTAGGATGTGAGTG
PVR	CACTGTCACCAGCCTCTGGATA	TCATAGCCAGAGATGGATACCTC

Table A3. RT-qPCR Primers (Human)

Target gene	Forward primer	Reverse primer
Gapdh	AACTTTGGCATTGTGGAAGG	ACACATTGGGGGTAGGAACA
Il6	TGATTGTATGAACAACGATGATGC	GGACTCTGGCTTTGTCTTTCTTGT
Mcp1/ Ccl2	CATCCACGTGTTGGCTCA	GATCATCTTGCTGGTGAATGAGT
Tnf-α	GGTGCCTATGTCTCAGCCTCTT	GCCATAGAACTGATGAGAGGGAG
Ccl5	CTGCTGCTTTGCCTACCTCT	CGAGTGACAAACACGACTGC
Cxcl10	ATCATCCCTGCGAGCCTATCCT	GACCTTTTTTGGCTAAACGCTTTC
Cxcl1	CTGGGATTCACCTCAAGAACATC	CAGGGTCAAGGCAAGCCTC
Il18	GACAGCCTGTGTTCGAGGATATG	TGTTCTTACAGGAGAGGGTAGAC
Raet1a	GACAGCAAATGCCACTGAAGTGG	GCTTTGCAGATAAATCATGGTGAC
Raet1b	CCAAAGTGGACACTCACAAGACC	GAATTCCCAGGTGGCACTAGGA
Raet1c	GACGGCAAATGCCACTGAAGTG	GCCCTGGCTTTGCGGATAAATC
Raet1d	CCAAAGTGGACACTCACAAGACC	GCTCATAATCTCTGTGTAGAAGGT
Raet1e	CCTCTGAACGATTTGTGCCAGG	GCCCTGGCTTTGCGGATAAATC
Mult-1	GTGCAGGAGACTAACACAACCG	TGCCAGTGCTTGTGTCAACACG
H60a	GGTCTGAGTGTCACCTGGATTG	TTTTCTTCAGCATACACCAAGCGA

Table A4. PRT-qPCR Primers (Mouse)

Table A5. Primary immunofluorescence antibodies

Target	Clone	Manufacturer	Catalogue number	Dilution
53BP1	Polyclonal	Novus Biologicals	NB100-304	1:1000
γ-H2AX	JWB301	Millipore	05-636	1:100
BrdU	3D4	BD Biosciences	555627	1:1000
CCL2	Polyclonal	R&D Systems	AF-279-NA	1:250
IL1α	4414	R&D Systems	MAB-200	1:250
IL1β	8516	R&D Systems	MAB-201	1:250
IL6	Polyclonal	R&D Systems	AF-206-NA	1:250
IL8/CXCL8	6217	R&D Systems	MAB-208	1:250
$p16^{INK4a}$	JC8	CRUK	-	1:1000
$p21^{CIP1}$	M-19	Santa Cruz	Sc-471	1:2000

Table A6. Secondary immunofluorescence antibodies

Target	Clone / Conjugate	Manufacturer	Catalogue number	Dilution
Goat IgG (H+L)	Polyclonal / AlexaFluor® 594	Invitrogen	A-11058	1:2000
Goat IgG (H+L)	Polyclonal / AlexaFluor® 488	Invitrogen	A-11055	1:2000
Mouse IgG (H+L)	Polyclonal / AlexaFluor® 594	Invitrogen	A-11032	1:2000
Mouse IgG (H+L)	Polyclonal / AlexaFluor® 488	Invitrogen	A-11059	1:2000
Rabbit IgG (H+L)	Polyclonal / AlexaFluor® 594	Invitrogen	A-11037	1:2000
Rabbit IgG (H+L)	Polyclonal / AlexaFluor® 488	Invitrogen	**A-11008**	1:2000

Table A7. Chemical compounds

Chemical compounds	CAS Number	Supplier	Catalogue number
4-OHT	68392-35-8	Sigma-Aldrich	H7904
Beclomethasone dipropionate	4419-39-0	Selleckchem	S3078
BMH-21	896705-16-1	Selleckchem	S7718
CX-5461 (Pidnarulex)	1138549-36-6	Selleckchem	S2684
Etoposide	33419-42-0	Sigma-Aldrich	E1383
GSK126	1346574-57-9	Selleckchem	S7061
Halofuginone	55837-20-2	Selleckchem	S8144
Hexa-D-arginine	673202-67-0	Tocris	47112
Indisulam	165668-41-7	Sigma-Aldrich	SML1225
Palbociclib HCL	827022-32-2	Selleckchem	S1116
SGC-SMARCA-BRDVIII	1997319-84-2	Sigma-Aldrich	SML3094
SSM 3 trifluoroacetate	2320930-10-5	Tocris	5253
T-5224	530141-72-1	ApexBio	B4664
Tazemetostat	1403254-99-8	Selleckchem	S7128
Trametinib	871700-17-3	Selleckchem	S2673
Triamcinolone	124-94-7	Selleckchem	S1933

Table A8. siRNA sequences

Gene Target	siRNA_ID	Sequence	Catalogue number (Horizons Discovery)
Non-targeting Control	2	UAAGGCUAUGAAGAGAUAC	D-001210-02
	4	AUGAACGUGAAUUGCUCAA	D-001210-04
CDKN2A	1	AAACUUAGAUCAUCAGUCA	D-011007-24
TP53	4	GCUUCGAGAUGUUCCGAGA	D-003329-26
L3HYPDH	3	GAAGAUGACGACCCAUUGA	D-010373-03
PGF	4	CGUCAGAGGUGGAAGUGGU	D-016246-04
PTPN1	3	CUGAAGAUAUCAAGUCAUA	D-003529-04
EPRS	3	GAAGAGGGAUGACAGUUGA	D-008245-03
SIRT1	3	GCGAUUGGGUACCGAGAUA	D-003540-07
LGMN	2	GAACAGAUCGUUGUGAUGA	D-005924-02
LPAR2	1	UCUACUACCUGCUCGGCAA	D-004602-21
FOSL1	1	GCUCAUCGCAAGAGUAGCA	D-004341-23
	2	GGACACAGGCAGUACCAGU	D-004341-24
	3	AGCGAGAGAUUGAGGAGCU	D-004341-25
	4	GCAGGCGGAGACUGACAAA	D-004341-26
KDM5C	1	GAGCGGAGGUUUCCUAAUA	D-010097-01
	2	GUGGACAACUUCAGGUUUA	D-010097-02
	3	GCAAGGAUAUGCCUAAGGU	D-010097-03
	4	GAGUGAAACUGAACUACUU	D-010097-04
MMP8	1	GCACUAAUGUGAUCGUUGA	D-005969-01
	2	CCAAGGAUAUAUCAAACUA	D-005969-02
	3	GAGAAGGCAUCCUCAGCUA	D-005969-03
	4	AGAAAGAGCUAUCAAGGAU	D-005969-04
PHF19	1	CCUCGUGACUUUCGAAGAU	D-026200-03
	2	GGAAGUGUGGCCUGGGUUA	D-026200-20
	3	GGUCAGCAGCUCUAAGCAA	D-026200-21
	4	GAUCCAGGGACUCGGGACU	D-026200-22
POLR1B	1	UCAUAGGAGUGGUUUAUUA	D-013391-02

	2	GAACCCAACUAUCGGAGAU	D-013391-03
	3	ACCAAUGCCAGAUGGGUAA	D-013391-17
	4	CCUUAACUACCUAGGUGAA	D-013391-18
SMARCA4	1	GAAAGGAGCUGCCCGAGUA	D-010431-01
	2	CCAAGGAUUUCAAGGAAUA	D-010431-02
	3	GAAAGUGGCUCAGAAGAAG	D-010431-03
	4	AGACAGCCCUCAAUGCUAA	D-010431-04
CD247	1	GGAAUCCUCUUCAUCUAUG	D-004257-01
	2	GAAGAGAGGAGUACGAUGU	D-004257-02
	3	ACAGUGAGAUUGGGAUGAA	D-004257-04
	4	AGGAAGGCCUGUACAAUGA	D-004257-05
DPH5	1	GGAAUUCCUUAUAGAGUUA	D-020926-01
	2	GUAUAUGAGUGUAAACCAA	D-020926-02
	3	ACAGUGAUCUUGUUCUAAG	D-020926-03
	4	ACGCUGCAGUCGAGUGUAU	D-020926-04
FCRL2	1	CCUGAUGGCUAUAGAAGAG	D-016490-01
	2	CCUCAUGACAGCUGGAGUU	D-016490-02
	3	CCCAAUCUUGUACCAAUUU	D-016490-03
	4	GUCCUUGGUUUCACUGGUG	D-016490-04
FOXH1	1	CCACGAGAGUGGAGGGGGA	D-008636-01
	2	AGAAGAGGUACCUGCGACA	D-008636-02
	3	GGAAAGACUCCAUUCGCCA	D-008636-03
	4	CCAAUGUGGUAAUGCCCUU	D-008636-04
FURIN	1	GGACUAAACGGGACGUGUA	D-005882-01
	2	GGACUUGGCAGGCAAUUAU	D-005882-02
	3	GCAGAUGGGUUUAAUGACU	D-005882-03
	4	GGGCUGGGCUCCAUCUUUG	D-005882-04
GLRA4	1	UGAAAGACCUCGUGUUUGA	D-034258-05
	2	GCGAACAUCUGGAUAUGAU	D-034258-06
	3	GACCACGGACAACAAGUUA	D-034258-07
	4	CGCCUGUCCUACCGAGAAU	D-034258-09